21 December 2007 | S10

Science

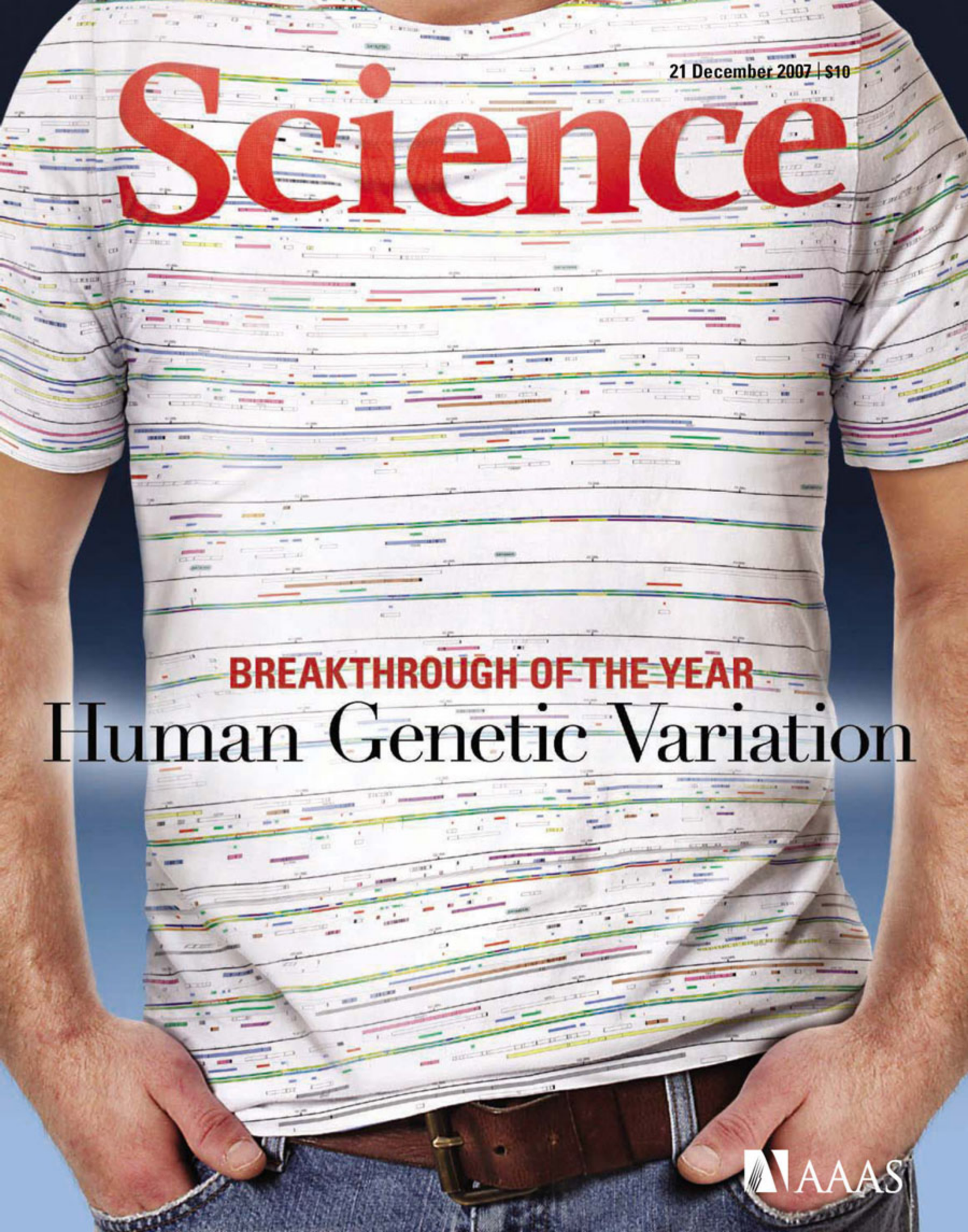

BREAKTHROUGH OF THE YEAR

Human Genetic Variation

AAAS

Volume 318, Issue 5858

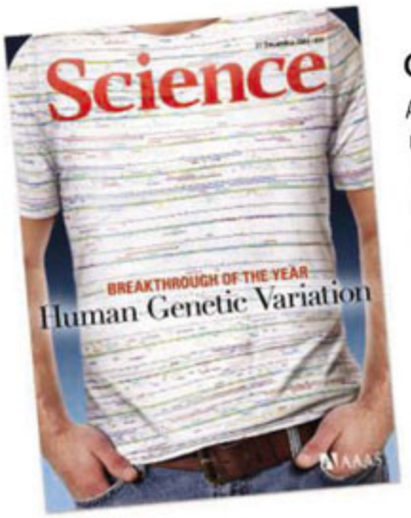

COVER

A T-shirt bearing an annotated gene-sequence map of human chromosome 1 symbolizes the Breakthrough of the Year for 2007—the realization that DNA differs from person to person much more than researchers had suspected. This conceptual advance, driven by results from several fields, may transform medicine but could also threaten personal privacy. See the special section beginning on page 1842.

Photo illustration: Joe Zeff Design Inc.

DEPARTMENTS

EDITORIAL

SPECIAL SECTION

Breakthrough of the Year

WINNER

RUNNERS-UP

OTHER FEATURES

>> Editorial p. 1833; for online content, including related Web resources and multimedia features, go to www.sciencemag.org/sciext/btoy2007/

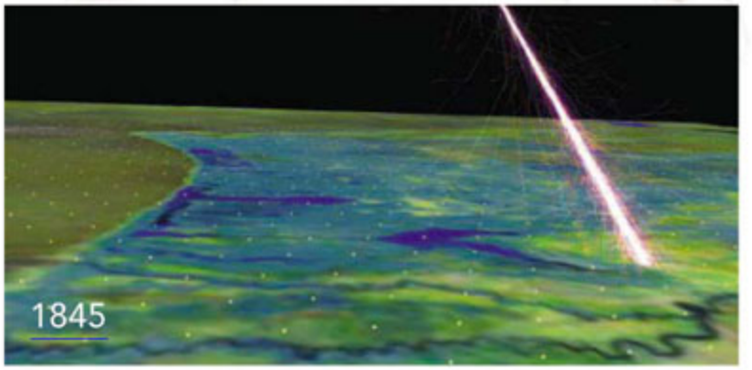

NEWS OF THE WEEK

NEWS FOCUS

CONTENTS continued >>

Science

SCIENCE EXPRESS

www.sciencexpress.org

PHYSICS

Time-Resolved Observation and Control of Superexchange Interactions with Ultracold Atoms in Optical Lattices
S. Trotzky et al.
Ultracold atoms trapped at optical lattice sites are used to investigate the superexchange interaction between neighboring spins.
10.1126/science.1150841

APPLIED PHYSICS

GaN Photonic-Crystal Surface-Emitting Laser at Blue-Violet Wavelengths
H. Matsubara, S. Yoshimoto, H. Saito, Y. Jianglin, Y. Tanaka, S. Noda
Surface-emitting lasers fabricated with photonic crystal structures can now emit at technologically relevant blue-violet wavelengths.
10.1126/science.1150413

LETTERS

BOOKS *ET AL.*

EDUCATION FORUM

POLICY FORUM


1880

PERSPECTIVES

REVIEW

BREVIA

REPORTS

CONTENTS continued >>

Science

REPORTS *CONTINUED...*

MEDICINE

Treatment of Sickle Cell Anemia Mouse Model with iPS Cells Generated from Autologous Skin 1920

J. Hanna et al.

Skin cells from a mouse with sickle cell anemia can be genetically reprogrammed to be pluripotent stem cells, then differentiated and used to treat the diseased mouse. *>> Perspective p. 1879*

AAAS

ADVANCING SCIENCE, SERVING SOCIETY

SCIENCE (ISSN 0036-8075) is published weekly on Friday, except the last week in December, by the American Association for the Advancement of Science, 1200 New York Avenue, NW, Washington, DC 20005. Periodicals Mail postage (publication No. 484460) paid at Washington, DC, and additional mailing offices.

Domestic individual membership and subscription (51 issues): $142 ($74 allocated to subscription). Domestic institutional subscription (51 issues): $710; Foreign postage extra: Mexico, Caribbean (surface mail) $55; other countries (air assist delivery) $85. First class, airmail, student, and emeritus rates on request. Canadian rates with GST available upon request, GST #1254 88122. Publications Mail Agreement Number 1069624. SCIENCE is printed on 30 percent post-consumer recycled paper. **Printed in the U.S.A.**

Change of address: Allow 4 weeks, giving old and new addresses and 8-digit account number. **Postmaster:** Send change of address to AAAS, P.O. Box 96178, Washington, DC 20090–6178. **Single-copy sales:** $10.00 current issue, $15.00 back issue prepaid includes surface postage; bulk rates on request.

The identification code for *Science* is 0036-8075. *Science* is indexed in the *Reader's Guide to Periodical Literature* and in several specialized indexes.

Printed on 30% post-consumer recycled paper.

CONTENTS continued >>

Deep diver.

SCIENCE**NOW**

www.sciencenow.org DAILY NEWS COVERAGE

Why Do Whales Get the Bends?
Shallow dives in response to naval sonar testing may harm cetaceans.

A 40-Hour Laptop Battery?
Silicon whiskers could improve rechargeable battery capacity by a factor of 10.

Why Seniors Say "When" Too Soon
Brain glitch may explain why the elderly drink less water than they should.

Highlights from ASCB in DC.

SCIENCE'S **STKE**

www.stke.org SIGNAL TRANSDUCTION KNOWLEDGE ENVIRONMENT

FORUM: Highlights from ASCB Symposium II
N. R. Gough
The "Architecture of Signaling Systems" session included a discussion of the practical applications of synthetic biology.

FORUM: Highlights from ASCB Symposium V
J. F. Foley
The "Geography of Signaling" session included an interesting talk about communication between yeast and bacteria in the formation of biofilms.

EVENTS
Plan to attend a cell signaling conference.

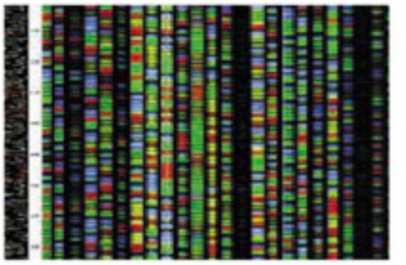

Recognition for young geneticists.

SCIENCE **CAREERS**

www.sciencecareers.org CAREER RESOURCES FOR SCIENTISTS

GLOBAL: Young Geneticists Making a Difference
E. Pain
The search for genetic variations between individuals offered young scientists with varied backgrounds a chance to make a difference.

GLOBAL: Mastering Your Ph.D.—Writing Your Thesis With Style
P. Gosling and B. Noordam
Careful planning and outlining can make writing your thesis less daunting.

US: Tooling Up—Three Categories of Rules
D. Jensen
The rules for success in industry are different from the ones you learned in grad school.

US: From the Archives—Dr. Bridget's New Year's Resolutions
K. Arney
For Dr. Bridget, a New Year engenders a surge of pointless enthusiasm.

SCIENCE**PODCAST**

Listen to the 21 December *Science* Podcast for a review of some of the biggest and most noticed science stories of 2007.
www.sciencemag.org/about/podcast.dtl

CREDITS: (SCIENCE NOW) NATACHA AGUILAR DE SOTO/UNIV. OF LA LAGUNA, SPAIN; (*SCIENCE CAREERS*) GERALD BABER, VIRGINIA TECH/COURTESY NATIONAL SCIENCE FOUNDATION

Separate individual or institutional subscriptions to these products may be required for full-text access.

EDITED BY STELLA HURTLEY AND PHIL SZUROMI

CREDITS (TOP TO BOTTOM): ANDREW YOUNG; LEEK *ET AL.*

<< Battle of the Sexes

Much research on sexual selection has focused either on intrasexual competition between males or on female mating preferences. **Clutton-Brock** (p. 1882) reviews recent studies which show that intrasexual competition between females and male preferences for particular categories of partners are also common and can generate secondary sexual characters that are more highly developed in females. Sexual selection may now need a new conceptual framework that incorporates the effects of intrasexual competition and mating preferences in both sexes.

Aging in Glasses

Glasses age over time, but an understanding of the structural rearrangements that underlie these processes in small-molecule systems is difficult because it is not possible to track the motion of individual molecules, and the overall changes in ordering may be small. **Schall *et al.*** (p. 1895; see the Perspective by **Falk**) tracked the motions of colloidal glasses under small strain motions using confocal microscopy. Localized zones form where the colloidal particles undergo irreversible shear transformations. Further analysis revealed how the sheared colloidal glasses are activated and how they interconnect into networks.

Mechanics of Amyloid Fibrils

Amyloid structures associated with a number of diseases form from a wide range of unrelated polypeptides and show intriguing but poorly understood physical properties. Using atomic force microscopy to image a set of protein fibrils, **Knowles *et al.*** (p. 1900) measured the local mechanical properties and correlated these results with coarse-grained atomistic molecular simulations. By controlling the hydrogen bonding, fibril stability can be altered or reinforced and used to offset specific side-chain interactions.

Heating Mars with SO_2

Evidence that Mars had liquid water on its surface when the planet was young implies that air temperatures were above the freezing point of water, unlike today. If these conditions were mainly the result of greenhouse gas heating by CO_2, then the partial pressure of CO_2 should have been high enough that carbonate minerals would have formed—yet these minerals have not been observed on Mars' surface. **Halevy *et al.*** (p. 1903) propose that volcanically degassed SO_2, emitted under more reducing conditions along with H_2S, would in combination with CO_2 have pushed temperatures over the threshold required by liquid water. Dissolved SO_2 also would have acidified the oceans enough to prevent carbonate minerals from forming. A similar mechanism operating on Earth may explain the absence of carbonate rocks from the Archean.

An Exercise in Quantum Geometry

Quantum computation relies on the ability to coherently manipulate the quantum state of qubits. However, unavoidable coupling to the environment gives the qubit a finite lifetime. It has been proposed that the use of a geometric phase (or Berry's phase, a topological phase that accumulates as an object traverses a path) should be more robust to the effects of decoherence. **Leek *et al.*** (p. 1889, published online 22 November) describe the observation of this geometric phase in a superconducting qubit, which they claim might bring fault-tolerant quantum computation a step closer.

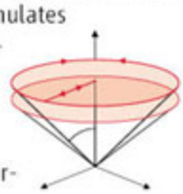

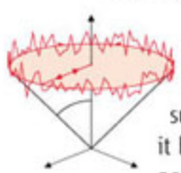

Carbon Nanotube Fiber Fabrication

By twisting together even short segments of string or straw, a strong fiber or rope can be formed as long as the starting material is long enough to properly twist together and is compressed sufficiently to ensure stress transfer between the segments. In theory, carbon nanotubes (CNTs) should be able to form very strong fibers because of their impressive intrinsic properties. **Koziol *et al.*** (p. 1892, published online 15 November) show that they can generate CNT aerogels and directly spin them into strong and stiff fibers. Further densification by treatment with acetone ensured maximal stress transfer between adjoining fibers. The authors compared the strength and stiffness of these fibers to other CNTs and commercial materials such as Kevlar.

Slippery Serpentine Sheets

Serpentinite layers that coat the top of sinking lithospheric slabs have been thought to play a role in subduction zone earthquakes because these layers become heavily deformed. **Hilairet *et al.*** (p. 1910) deformed the serpentine antigorite at high pressures and temperatures and found that it has unusually low viscosity that could account for postseismic deformations after large earthquakes within subduction zones. This property may also enable subduction initiation and may govern convection within subduction zones.

Continued on page 1831

Continued from page 1829

Planet of the Beetles

Beetles represent more than 20% of all described species, although relationships within the order are still speculative. **Hunt *et al.*** (p. 1913) reconstructed the phylogeny of >80% of recognized beetle families and identified previously unknown relationships for many groups. By performing analyses of diversity patterns across the entire order, the authors estimated that diversification of major beetle groups may have occurred in the Jurassic, earlier than previously thought.

Induced Human Pluripotent Stem Cell Lines

Embryonic stem cells can grow for an unlimited time and can turn into essentially every type of cell, which makes them an ideal candidate for regenerative medicine (see the Perspective by **Cibelli**). However, their applications are hindered by potential problems such as immune rejection and ethical concerns about their origin. **Yu *et al.*** (p. 1917, published online 20 November; see the 23 November news story by **Vogel and Holden**) report a method to derive pluripotent stem cells from human fibroblasts. By introducing four genes (*OCT4*, *NANOG*, *SOX2*, and *LIN28*) into human fibroblasts, stem cells sharing essentially all of the features of human embryonic stem cells were obtained. **Hanna *et al.*** (p. 1920) used a method to reprogram mouse cells to a pluripotent state that is similar to that of embryonic stem cells to generate so-called mouse-induced pluripotent stem cells, or iPS cells, from mice with humanized sickle cell anemia. The iPS cells were derived from a skin biopsy of this mouse model, and the genetic defect was eliminated by gene correction. These cells were directed to differentiate into hematopoietic progenitors and then transplanted into donor sickle cell mice, which rescued the disease phenotype.

Orphanages and Fostering in Romania

Studying a time when Romania did not have a foster care system for abandoned children, **Nelson *et al.*** (p. 1937) constructed a foster care system and followed the outcomes of children randomly selected to receive orphanage care or foster care. The results show that children moved to foster care homes had better cognitive outcomes, and that the earlier the child was moved out of the orphanage, the better the outcome. In a Policy Forum, **Millum and Emanuel** discuss the ethical issues posed in such studies and the safeguards needed when parents and guardians are not available to give consent.

Histones Coming and Going

Eukaryotic nuclear DNA is packaged into nucleosomes, which must be removed to allow replication of the genome and then reassembled onto the two newly synthesized daughter strands. Coordination of this removal and deposition process must occur at each replication fork. **Groth *et al.*** (p. 1928) show that this equilibrium is regulated by the histone chaperone antisilencing function 1 (Asf1). Asf1 exists in a nuclear pool associated with the MCM2–7 complex—the putative replication helicase—and histones H3 and H4. Thus, Asf1, through its interaction with the helicase and parental histones, coordinates template unwinding and removal of nucleosomes ahead of the replication fork as well as their deposition behind the fork.

Rapid Reorganization of Neuronal Connectivity

Reorganization of the brain motor cortex output is thought to involve excitability changes within the cortex per se, while the effect of individual output neurons on muscle activity remains constant. However, **Davidson *et al.*** (p. 1934) found that throughput from single motor cortex neurons to muscles can vary so much as to be absent during some behaviors and present during others. In particular, effects not present during a simple movement often appeared when a monkey was rewarded specifically for discharging a neuron and activating a muscle simultaneously. Rapid changes thus occur at subcortical levels, including the monosynaptic connections from motor cortex neurons to spinal motoneurons.

CREDIT: MICHAEL CARROLL

Donald Kennedy is the Editor-in-Chief of *Science*.

Breakthrough of the Year

THE BREAKTHROUGH OF THIS YEAR HAS TO DO WITH HUMANS, GENOMES, AND GENETICS. But it is not about THE human genome (as if there were only one!). Instead, it is about your particular genome, or mine, and what it can tell us about our backgrounds and the quality of our futures.

A number of studies in the past year have led to a new appreciation of human genetic diversity. As soon as genomes are looked at individually, important differences appear: Different single-nucleotide polymorphisms are scattered throughout, and singular combinations of particular genes forming haplotypes emerge. A flood of scans for these variations across the genome has pointed to genes involved in behavioral traits as well as to those that may foretell deferred disease liability. And more extensive structural variations, such as additions, deletions, repeat sequences, and stretches of "backwards" DNA, turn out to be more prevalent than had been recognized. These too are increasingly being associated with disease risks.

High-throughput sequencing techniques are bringing the cost of genomics down. The few "celebrity genomes" (e.g., Watson's and Venter's) will soon be followed by others, we hope in an order not determined by wealth but by scientific need or personal medical circumstance. Our natural interest in personal genealogy, accompanied by worries about our health, will create an incentive structure that even now is creating a sometimes dubious niche market for having one's genome "done."

A strong Breakthrough runner-up arrived at this year's finish line just in time. Two new studies, one published in *Science*, showed how adult human epithelial cells could be reprogrammed, through the virally mediated introduction of just four genes, to behave like pluripotent cells; that is, able to act as embryonic stem cells do, to produce every descendent cell type. This breakthrough has produced some relief, but it also comes with some reservations. James Thompson of the University of Wisconsin, who did the first research with embryonic stem cells, has now taken a major step toward ending the "ethical" controversy over their use. But hold on: That controversy was generated by specific objections from one religion, not some universal ethic. There is every reason to continue research along the old path, with embryo-derived cells: The new methods may carry unknown liabilities, so making the case for changing Bush's 2001 presidential order should continue.

Finally, readers will notice that we usually have a "Breakdown" of the year. That custom produced ambivalence this time around. On the strictly scientific front, progress in climate change research was spectacular. There was new information about the dynamics of the major ice sheets in Greenland and Antarctica, analyses of paleoclimates, new estimates of sea-level rise, and studies of the impacts of global warming on high-latitude ecosystems and sea ice. The Intergovernmental Panel on Climate Change delivered a summary report at year's end emphasizing the seriousness of the risks. But on the breakdown side, continual denial by the Bush Administration added to its long history of failing to mitigate the emission of greenhouse gases.

A specimen case of the Administration's reluctance to acknowledge climate change was added just recently when Julie Gerberding, head of the U.S. Centers for Disease Control and Prevention, was asked to present congressional testimony on the potential impacts of climate change on public health. It is surely no secret that heat spells are a health hazard, or that drought and excess rainfall can influence human susceptibility to pathogen-borne disease—just the kind of thing Congress wanted to know. Gerberding's testimony was reviewed at the White House and soon made to disappear: Virtually all of what she said about climate change—six pages of it—was blacked out of the document filed with the Senate Environment and Public Works Committee (see http://alt.coxnewsweb.com/ajc/pdf/gerberding.pdf). There's an odd behind-the-scenes story here, involving two offices that report to the president. The Office of Science and Technology Policy raised questions about particular statements and made suggestions, but then the Office of Management and Budget, apparently unwilling to work on the suggestions, simply eliminated every section about which questions had been raised. It's worth a look just to understand what these people don't want you to know.

– Donald Kennedy

10.1126/science.1154158

BEHAVIOR

Learning to Sing

Zebra finches.

For full expression, language depends on an interplay between cognitive and motor skills. For example, people with a rare genetic form of developmental verbal dyspraxia have difficulty learning and producing the intricate, coordinated series of muscle movements necessary for speech, a result of a mutation in a brain transcription factor called FOXP2. In songbirds, this same protein is found in a brain region—area X—that is essential for the acquisition of the birds' characteristic song, which they learn under the close tutelage of an adult bird.

Haesler *et al.* tested whether a deficit in FoxP2 would also produce communication deficits in zebra finches. They injected into area X a lentivirus vector carrying RNA interference sequences from *FoxP2*, which reduced *FoxP2* mRNA by 70%. After the 2-month tutoring period, the treated birds' songs—normally a stereotyped series of syllables that remains stable throughout adulthood—were missing syllables and contained inappropriately repeated segments (errors similar to those of humans with dyspraxia). Some of the sounds were also poor copies of their tutor's original. Thus, without sufficient FoxP2, normal developmental motor learning could not take place. The authors speculate that FoxP2 is necessary for structural and functional changes in area X neurons as birds learn their songs. — KK

PLoS Biol. **5**, e321 (2007).

PHYSIOLOGY

Fertile Ground for Cancer Proteins

Leukemia inhibitory factor (LIF) is a secreted glycoprotein first identified, as its name implies, as a regulator of leukemic cell differentiation. More recently, attention has focused on the role of this cytokine in the female reproductive tract. In mice, LIF is one of the few molecules known to be required for implantation of the blastocyst, or early-stage embryo, into the uterus. Thus, it has been hypothesized that drugs targeting LIF activity could (depending on their mode of action) be used either to enhance fertility by promoting implantation or as contraceptives that prevent implantation. Progress on the latter front is reported by White *et al.*, who have developed a potent LIF antagonist that is completely effective in blocking blastocyst implantation when administered systemically to mice. Whether this antagonist—a chemically stabilized mutant version of LIF that binds to its receptor but does not trigger downstream signals—has similar activity in primates remains to be explored. In independent work, Hu *et al.* find that LIF expression in the mouse uterus is positively regulated at the transcriptional level by p53, an intensely studied tumor suppressor protein. Discovery of this link between LIF and p53 raises the possibility that cancer drugs designed to activate p53 might be useful tools for investigating the mechanisms underlying blastocyst implantation or as an alternative means of enhancing fertility. — PAK

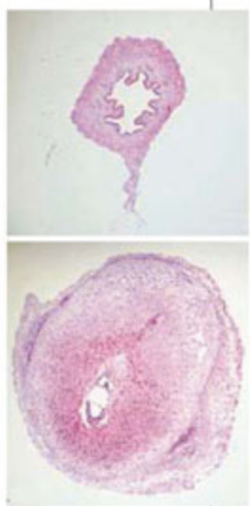

Blocking uterine implantation (bottom) with a LIF antagonist (top).

CREDITS (TOP TO BOTTOM): REINHARD, H./PETER ARNOLD INC.; WHITE *ET AL.*, *PROC. NATL. ACAD. SCI. U.S.A.* **104**, 19357 (2007)

Proc. Natl. Acad. Sci. U.S.A. **104**, 19357 (2007); *Nature* **450**, 721 (2007).

BIOTECHNOLOGY

Still Potent

By introducing defined transcription factors into mouse and human fibroblasts, stem cell researchers have demonstrated that differentiated cells can be reprogrammed to a pluripotent state, in which the resultant iPS (induced pluripotent stem) cells display properties similar to those of embryonic stem cells. This work holds great promise for therapy; however, a number of serious obstacles remain. For example, some reprogramming protocols involve the introduction of the c-Myc transcription factor, which has been shown to increase tumorigenicity in mice. Nakagawa *et al.* describe a modified method for generating mouse and human iPS cells without using c-Myc. This altered protocol shows greater specific induction to iPS cells, albeit at lower efficiency and at a slower rate than when c-Myc is added. — BAP

Nat. Biotechnol. 10.1038/nbt1374 (2007).

MOLECULAR BIOLOGY

A Stringent Policy of Exclusion

With 95 of its 115 exons subject to alternative mRNA splicing, the *Down syndrome cell adhesion molecule* (*Dscam*) gene in *Drosophila* surely deserves a place in the *Guinness Book of Records*, having the potential to form 38,016 protein variants. Remarkably, each Dscam isoform has the same overall structure, as the alternatively spliced exons form clusters, with only one exon from each cluster being included in the translated protein. Olson *et al.* have identified heterogeneous nuclear ribonucleoprotein hrp36 as a factor critical for the mutually exclusive splicing of the exon 6 cluster, which contains 48 distinct exons; in its absence, concatenated exon 6 variants are found in Dscam. Using a RIP-Chip assay, they show that hrp36 binds throughout the exon 6 cluster, where it prevents the binding of another class of splicing

Continued on page 1837

Continued from page 1835

factors, the serine/arginine-rich (SR) proteins, which promote exon inclusion. The authors suggest that hrp36 masks selector sites located just 5′ of each exon variant, thus precluding SR binding, with the result that only one selector site can interact productively with the single docking site upstream of the entire exon 6 cluster. The mutually exclusive nature of the docking site–selector interaction then ensures that only one exon 6 variant is included in each *Dscam* mRNA. Intriguingly, hrp36 has no effect on splicing of the other variable exon clusters, indicating that another mechanism must determine their mutually exclusive splicing. — GR

Nat. Struct. Mol. Biol. **14**, 1134 (2007).

NEUROSCIENCE

Balancing Strength and Number

Homeostasis, the ability to maintain a steady state in the face of stresses, is a fundamental part of life for cells and for organisms. Wilson *et al.* have analyzed homeostatic changes at the level of synaptic connections in hippocampal neurons seeded onto a microfabricated surface. Imprinting the surface with a template of squares of increasing sizes created a series of micrometer-scale islands hosting neurons at identical densities but with an increasing number of potential partners. As the number of neurons on a square increased, the number of synaptic connections increased, but, surprisingly, the functional activity of the neurons as a population (measured in voltage clamp and current clamp experiments) did not. This scaling was mediated by a change in the kinds of connections the neurons made. As network size increased, the proportion of connections between excitatory and inhibitory neurons increased; in other words, neurons made more weaker connections. Changes in neuronal connectivity occur as a consequence of development, aging, and disease (such as Alzheimer's disease and autism), and analyses of this kind may help us to understand the ability of the brain to respond to changes and the pathologies that occur when it cannot. — BJ

J. Neurosci. **27**, 13581 (2007).

APPLIED PHYSICS

Flowing into Focus

Most small-scale fluid systems are dominated by laminar, or nonmixing, flow. Thus, directing particle motion in sorting applications has required either an external applied force, such as that generated by an electrical or magnetic field, or else the use of geometrically complex arrangements of pillars or posts. These methods become less effective as the flow rate of the system increases, and hence the attainable particle throughput is limited. Di Carlo *et al.* show that particle motion can alternatively be controlled by designing channels that induce additional inertial forces. Particles suspended in a flowing fluid are subject to both drag and lift forces, with the lift forces driving the particles away from the center of the fluid channel. Rectangular channels therefore exhibit a four-channel output stream. When the authors incorporated curvature into the channels, the particles were subjected to a rotational flow (termed Dean flow) caused by the fluid's inertia. In symmetric channels, the four output streams were reduced to two; asymmetric curvature confined the particles to a single stream. Faster flow rates increased these additional forces and so induced faster focusing of the particles. In a further twist, asymmetric particles were observed to show positional and rotational ordering. — MSL

Focusing channel.

CREDIT: DI CARLO ET AL., PROC. NATL. ACAD. SCI. U.S.A. 104, 18892 (2007)

Proc. Natl. Acad. Sci. U.S.A. **104**, 18892 (2007).

CHEMISTRY

Setting Serotonin Bait

When small molecules are incorporated into self-assembled monolayers (SAMs) as targets for recognition by larger biomolecules, the tethers used to extend the targets from the surface can often interfere with the recognition process. Moreover, even at low loading, the surface molecules may not disperse but instead phase-separate into clusters, thus creating steric hindrance and increasing the chances of nonspecific binding. Shuster *et al.* present a strategy to overcome these drawbacks in a search to identify yet unknown binding partners for serotonin. First they prepared alkane thiol SAMs on gold that were terminated with oligomers of ethylene glycol. Carboxyl-terminated thiols with twice the number of ethylene glycol repeats were then bound to defect sites in the SAMs and covalently capped with serotonin. Quartz crystal microbalance studies showed that these monolayers preferentially bound serotonin antibodies over those raised against dopamine and were also resistant to binding of bovine serum albumin. — PDS

Adv. Mater. 10.1002/adma.200700082 (2007).

www.sciencemag.org

Science

1200 New York Avenue, NW
Washington, DC 20005
Editorial: 202-326-6550, FAX 202-289-7562
News: 202-326-6581, FAX 202-371-9227

Bateman House, 82-88 Hills Road
Cambridge, UK CB2 1LQ
+44 (0) 1223 326500, FAX +44 (0) 1223 326501

Subscription Services For change of address, missing issues, new orders and renewals, and payment questions: 866-434-AAAS (2227) or 202-326-6417, FAX 202-842-1065. Mailing addresses: AAAS, P.O. Box 96178, Washington, DC 20090-6178 or AAAS Member Services, 1200 New York Avenue, NW, Washington, DC 20005

Institutional Site Licenses please call 202-326-6755 for any questions or information

Reprints: Author Inquiries 800-635-7181
Commercial Inquiries 803-359-4578

Permissions 202-326-7074, FAX 202-682-0816z

Member Benefits AAAS/Barnes&Noble.com bookstore www.aaas.org/bn; AAAS Online Store http://www.apisource.com/aaas/ code MKB6; AAAS Travels: Betchart Expeditions 800-252-4910; Apple Store www.apple/eppstore/aaas; Bank of America MasterCard 1-800-833-6262 priority code FAA3YU; Cold Spring Harbor Laboratory Press Publications www.cshlpress.com/affiliates/aaas.htm; GEICO Auto Insurance www.geico.com/landingpage/go51.htm?logo=17624; Hertz 800-654-2200 CDP#343457; Office Depot https://bsd.officedepot.com/portalLogin.do; Seabury & Smith Life Insurance 800-424-9883; Subaru VIP Program 202-326-6417; VIP Moving Services http://www.vipmayflower.com/domestic/index.html; Other Benefits: AAAS Member Services 202-326-6417 or www.aaasmember.org.

science_editors@aaas.org (for general editorial queries)
science_letters@aaas.org (for queries about letters)
science_reviews@aaas.org (for returning manuscript reviews)
science_bookrevs@aaas.org (for book review queries)

Published by the American Association for the Advancement of Science (AAAS), *Science* serves its readers as a forum for the presentation and discussion of important issues related to the advancement of science, including the presentation of minority or conflicting points of view, rather than by publishing only material on which a consensus has been reached. Accordingly, all articles published in *Science*—including editorials, news and comment, and book reviews—are signed and reflect the individual views of the authors and not official points of view adopted by the AAAS or the institutions with which the authors are affiliated.

AAAS was founded in 1848 and incorporated in 1874. Its mission is to advance science and innovation throughout the world for the benefit of all people. The goals of the association are to: foster communication among scientists, engineers and the public; enhance international cooperation in science and its applications; promote the responsible conduct and use of science and technology; foster education in science and technology for everyone; enhance the science and technology workforce and infrastructure; increase public understanding and appreciation of science and technology; and strengthen support for the science and technology enterprise.

Information for Authors

See pages 120 and 121 of the 5 January 2007 issue or access www.sciencemag.org/feature/contribinfo/home.shtml

EDITOR-IN-CHIEF **Donald Kennedy**
EXECUTIVE EDITOR **Monica M. Bradford**
DEPUTY EDITORS **R. Brooks Hanson, Barbara R. Jasny, Katrina L. Kelner**
NEWS EDITOR **Colin Norman**

Editorial supervisory senior editor Phillip D. Szuromi; **senior editor/perspectives** Lisa D. Chong; **senior editors** Gilbert J. Chin, Pamela J. Hines, Paula A. Kiberstis (Boston), Marc S. Lavine (Toronto), Beverly A. Purnell, L. Bryan Ray, Guy Riddihough, H. Jesse Smith, Valda Vinson, David Voss; **associate editors** Jake S. Yeston, Laura M. Zahn; **online editor** Stewart Wills; **associate online editors** Robert Frederick, Tara S. Marathe; **book review editor** Sherman J. Suter; **associate letters editor** Jennifer Sills; **editorial manager** Cara Tate; **senior copy editors** Jeffrey E. Cook, Cynthia Howe, Harry Jach, Barbara P. Ordway, Trista Wagoner; **copy editors** Lauren Kmec, Peter Mooreside; **editorial coordinators** Carolyn Kyle, Beverly Shields; **publications assistants** Ramatoulaye Diop, Chris Filiatreau, Joi S. Granger, Jeffrey Hearn, Lisa Johnson, Scott Miller, Jerry Richardson, Brian White, Anita Wynn; **editorial assistants** Carlos L. Durham, Emily Guise, Patricia M. Moore, Jennifer A. Seibert; **executive assistant** Sylvia S. Kihara; **administrative support** Maryrose Madrid

News senior correspondent Jean Marx; **deputy news editors** Robert Coontz, Eliot Marshall, Jeffrey Mervis, Leslie Roberts; **contributing editors** Elizabeth Culotta, Polly Shulman; **news writers** Yudhijit Bhattacharjee, Adrian Cho, Jennifer Couzin, David Grimm, Constance Holden, Jocelyn Kaiser, Richard A. Kerr, Eli Kintisch, Andrew Lawler (New England), Greg Miller, Elizabeth Pennisi, Robert F. Service (Pacific NW), Erik Stokstad; **intern** Benjamin Lester; **contributing correspondents** Barry A. Cipra, Jon Cohen (San Diego, CA), Daniel Ferber, Ann Gibbons, Robert Irion, Mitch Leslie, Charles C. Mann, Evelyn Strauss, Gary Taubes; **copy editors** Rachel Curran, Linda B. Felaco, Melvin Gatling; **administrative support** Scherraine Mack, Fannie Groom; **bureaus** New England: 207-549-7755, San Diego, CA: 760-942-3252, FAX 760-942-4979, Pacific Northwest: 503-963-1940

Production director James Landry; **senior manager** Wendy K. Shank; **assistant manager** Rebecca Doshi; **senior specialists** Jay Covert, Chris Redwood; **specialist** Steve Forrester; **Preflight director** David M. Tompkins; **manager** Marcus Spiegler; **specialist** Jessie Mudjitaba

Art director Kelly Buckheit Krause; **associate art director** Aaron Morales; **illustrators** Chris Bickel, Katharine Sutliff; **senior art associates** Holly Bishop, Laura Creveling, Preston Huey, Nayomi Kevitiyagala; **associate** Jessica Newfield; **photo editor** Leslie Blizard

***Science* International**

Europe (science@science-int.co.uk) **editorial: international managing editor** Andrew M. Sugden; **senior editor/perspectives** Julia Fahrenkamp-Uppenbrink; **senior editors** Caroline Ash, Stella M. Hurtley, Ian S. Osborne, Stephen J. Simpson, Peter Stern; **associate editor** Joanne Baker; **editorial support** Deborah Dennison, Rachel Roberts, Alice Whaley; **administrative support** Janet Clements, Jill White; **news: Europe news editor** John Travis; **deputy news editor** Daniel Clery; **contributing correspondents** Michael Balter (Paris), John Bohannon (Vienna), Martin Enserink (Amsterdam and Paris), Gretchen Vogel (Berlin); **intern** Elizabeth Quill

Asia Japan Office: Asca Corporation, Eiko Ishioka, Fusako Tamura, 1-8-13, Hirano-cho, Chuo-ku, Osaka-shi, Osaka, 541-0046 Japan; +81 (0) 6 6202 6272, FAX +81 (0) 6 6202 6271; asca@os.gulf.or.jp; **asia news editor** Richard Stone (Beijing: rstone@aaas.org); **contributing correspondents** Dennis Normile (Japan: +81 (0) 3 3391 0630, FAX 81 (0) 3 5936 3531; dnormile@gol.com); Hao Xin (China: + 86 (0) 10 6307 4439 or 6307 3676, FAX +86 (0) 10 6307 4358; cindyhao@gmail.com); Pallava Bagla (South Asia: +91 (0) 11 2271 2896; pbagla@vsnl.com)

Africa Robert Koenig (contributing correspondent, rob.koenig@gmail.com)

EXECUTIVE PUBLISHER **Alan I. Leshner**
PUBLISHER **Beth Rosner**

Fulfillment Systems and Operations (membership@aaas.org) **director** Waylon Butler; **customer service supervisor** Pat Butler; **specialists** Laurie Baker, Latoya Casteel, LaVonda Crawford, Vicki Linton; **data entry supervisor** Cynthia Johnson; **specialists** Tarrika Hill, Erin Layne, Sheila Thomas

Business Operations and Administration director Deborah Rivera-Wienhold; **assistant director, business operations** Randy Yi; **senior financial analysts** Michael LoBue, Jessica Tierney; **financial analysts** Nicole Nicholson, Farida Yeasmin; **rights and permissions: administrator** Emilie David; **associate** Elizabeth Sandler; **marketing director** John Meyers; **marketing managers** Allison Pritchard, Darryl Walter; **marketing associates** Aimee Aponte, Alison Chandler, Mary Ellen Crowley, Marcia Leach, Julianne Wielga, Wendy Wise; **international marketing manager** Wendy Sturley; **marketing executive** Jennifer Reeves; **marketing/member services executive** Linda Rusk; **Japan sales** Jason Hannaford; **site license sales director** Tom Ryan; **sales manager** Russ Edra; **sales and customer service** Mehan Dossani, Iquo Edim, Kiki Forsythe, Catherine Holland, Phillip Smith, Philip Tsolakidis; **electronic media: manager** Lizabeth Harman; **project manager** Trista Snyder; **assistant manager** Lisa Stanford; **senior production specialist** Walter Jones; **production specialists** Nichele Johnston, Kimberly Oster

Advertising director worldwide ad sales Bill Moran

Product (science_advertising@aaas.org); **consumer & sponsorship sales manager** Tina Morra: 202-326-6542; **midwest** Rick Bongiovanni: 330-405-7080, FAX 330-405-7081; **west coast/w. canada** Teola Young: 650-964-2266; **east coast/e. canada** Christopher Breslin: 443-512-0330, FAX 443-512-0331; **uk/europe/asia** Michelle Field: +44 (0) 1223-326-524, FAX +44 (0) 1223-325-532; **japan** Mashy Yoshikawa: +81 (0) 33235 5961, FAX +81 (0) 33235 5852; **senior traffic associate** Deiandra Simms

Commercial Editor Sean Sanders: 202-326-6430

Classified (advertise@sciencecareers.org); **us: recruitment sales manager** Ian King: 202-326-6528, FAX 202-289-6742; **inside sales manager: midwest/canada** Daryl Anderson: 202-326-6543; **northeast** Alexis Fleming: 202-326-6578; **southeast** Tina Burks: 202-326-6577; **west** Nicholas Hintibidze: 202-326-6533; **sales coordinators** Erika Foard, Rohan Edmonson, Shirley Young; **international: sales manager** Tracy Holmes: +44 (0) 1223 326525, FAX +44 (0) 1223 326532; **sales** Marium Hudda, Alex Palmer, Alessandra Sorgente; **sales assistant** Louise Moore; **Japan** Jason Hannaford: +81 (0) 52 757 5360, FAX +81 (0) 52 757 5361; **advertising production operations manager** Deborah Tompkins; **senior production specialists** Robert Buck, Amy Hardcastle; **senior traffic associate** Christine Hall; **publications assistant** Mary Lagnaoui

AAAS Board of Directors **retiring president, chair** John P. Holdren; **president** David Baltimore; **president-elect** James J. McCarthy; **treasurer** David E. Shaw; **chief executive officer** Alan I. Leshner; **board** John E. Dowling, Lynn W. Enquist, Susan M. Fitzpatrick, Alice Gast, Linda P. B. Katehi, Cherry A. Murray, Thomas D. Pollard, Kathryn D. Sullivan

AAAS
ADVANCING SCIENCE, SERVING SOCIETY

Sea Scum Rebranded

The father of taxonomy would be proud. The first genetic analysis of one of Carl Linnaeus's own specimens has revealed a long-standing botanical error: Scientists have been calling a marine alga by the wrong "Linnaean" name.

The unlucky alga was the sea lettuce *Ulva lactuca*, which Linnaeus collected and christened in the mid-18th century. Sea lettuces are notorious for invading polluted waters and gunking up ships' hulls. Christine Maggs and Frédéric Mineur, both of Queen's University Belfast in the U.K., got samples of the "type specimen" for the species from the Linnean [sic] Society's herbarium in London and finished mapping its genome this month. The results showed that somewhere along the line, naturalists accidentally renamed the alga *U. fasciata* and gave the name *U. lactuca* to a similar species. Now the original *U. lactuca* has its name back, and the misnamed latecomer needs a new one.

Although Linnaeus typically took meticulous notes, for his *Ulva*'s geographic range he wrote only "in oceano." Maggs says this could have contributed to the confusion. But Linnaeus more than made up for his oversight: Whereas his contemporaries left drawings, he preserved DNA. "We can exploit that," Maggs says. "Linnaeus's specimens have undreamed-of value 250 years later."

Left on Campus

Why are academics in the United States so politically liberal? Are conservative students oppressed by a biased professoriate, or are liberals simply smarter?

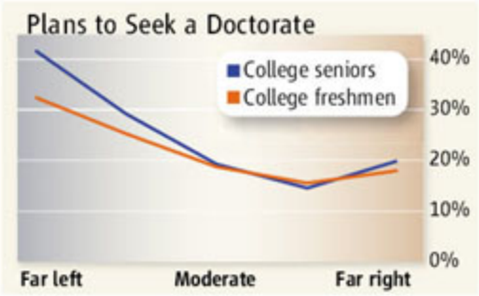

Neither, says public policy expert Matthew Woessner of Pennsylvania State University, Harrisburg, who, with political scientist April Kelly-Woessner of Elizabethtown College in Pennsylvania, has tackled the question using data on more than 15,000 college students collected by the Higher Education Research Institute of the University of California, Los Angeles.

The Woessners found that self-described liberals and conservatives report no difference in grades or in the quality of their education. Yet liberal college students are twice as likely as conservative ones to pursue Ph.D.s. The main reasons, the authors conclude, are differences in values, goals, and preferences. Liberals placed higher values on creativity; conservatives were more oriented toward raising families and making money. As a result, conservatives gravitated more to "professional" majors. But even within the same area, such as social science, almost twice as many liberals wanted advanced degrees. "Our findings hold for the hard sciences as well," says Woessner, who presented a paper on the results last month at a meeting at the American Enterprise Institute in Washington, D.C.

Jeremy Mayer of George Mason University's School of Public Policy in Fairfax, Virginia, says many people pontificating on the subject have "no or bad data, [but] the Woessner paper is simply excellent."

CREDITS (TOP TO BOTTOM): E. ELLIS AND N. RAMANKUTTY; M. WOESSNER; SAINT LOUIS ZOO

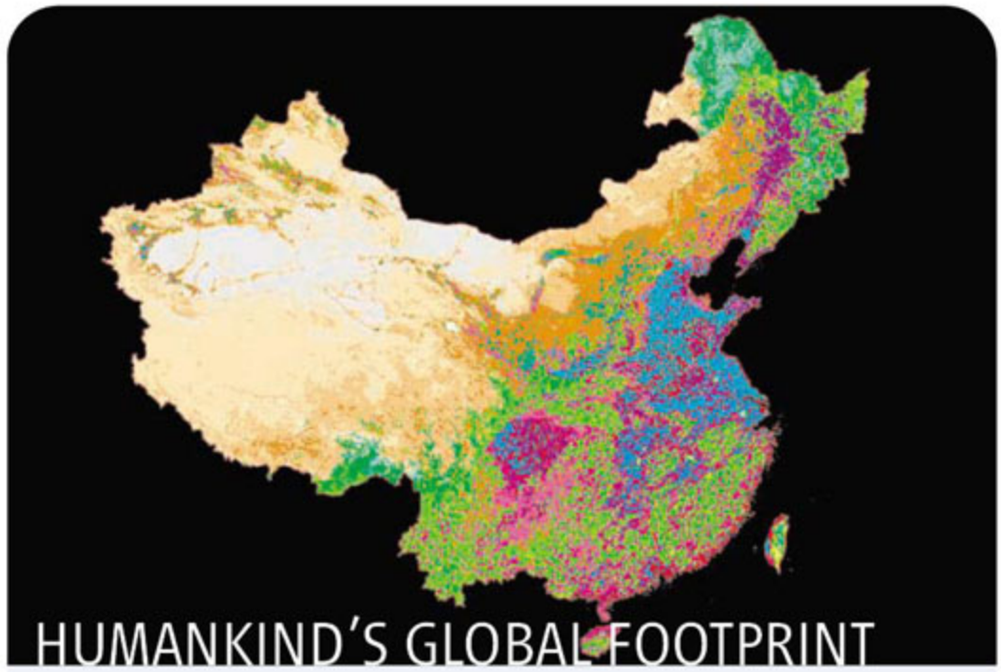

HUMANKIND'S GLOBAL FOOTPRINT

A pair of earth scientists have combined data on population distribution with data on land use and land cover to generate a global map of "anthropogenic biomes." It's "a first go at looking at how humans have restructured the biosphere," says Erle Ellis of the University of Maryland, Baltimore County, who created the map with Navin Ramankutty of McGill University in Montreal, Canada. Existing biome maps have only rudimentary classifications for human-altered areas, Ellis says. This one, presented last week at the meeting of the American Geophysical Union in San Francisco, California, shows 21 categories, including urban (red) and barren (gray), with subdivisions covering various types of villages, croplands, rangelands, forests, and wild lands. The blues in this map of China and Taiwan stand for rice-growing villages and irrigated villages. "I think this [work] is going to have far-reaching effects," says global modeler Jonathan Foley of the University of Wisconsin, Madison. "Now we can better describe the *real* biosphere … in our maps, models, and ecological field studies."

Back to Africa

The scimitar-horned oryx, which once roamed the northern borders of the Sahara, has been extinct in the wild for 25 years. But a team of zoo curators and animal researchers has taken initial steps to bring the species back, using animals raised in captivity. The group has brought nine oryx and 13 addax, another rare desert antelope, from U.S. and European zoos to Tunisia and released them into two government wildlife preserves.

Saint Louis Zoo addax going back to its roots.

Saint Louis Zoo curator William Houston, a leader in the effort, says the project highlights a new push to coordinate U.S. and European programs for captive endangered species, giving managers a larger pool of animals from which to draw. "We want to make sure the animals we give to the Tunisians represent the full range of genetic diversity available in our populations," he says. Researchers hope to eventually release the antelopes into the wild.

EDITED BY YUDHIJIT BHATTACHARJEE

Two Cultures

SAME FREQUENCY. A musical parody of the trials and tribulations of working astronomers has become a hit on YouTube.

Taking a break last year from observation runs at the Mauna Kea Observatory in Hawaii, astronomer and flamenco guitarist Juan Delgado (front, right) began playing "Hotel California"—the Eagles' rock anthem from the 1970s. The moment inspired Kelly Fast (front, left) and her colleagues from NASA's Goddard Space Flight Center in Greenbelt, Maryland, to describe in verse what it's like working at a high-altitude observatory, testing an instrument designed to study the atmospheres of Mars and Venus. "The baseline is drifting / The spectrum looks weird / Are those emission lines? / What's this dip over here?" Fast croons in the video as her frustrated colleagues point at spectrographic data.

"Hotel Mauna Kea" has been viewed more than 10,000 times on YouTube since its posting on 20 November. "It captures in a humorous way the trials and tribulations of observing, especially when one has built an instrument and is struggling to get data," says Alan Tokunaga, an astronomer at the University of Hawaii, Honolulu. Fast says her group has some more songs up its sleeve, so stay tuned.

MOVERS

CHANGE AT CERN. German particle physicist Rolf-Dieter Heuer has been named the next director general of the CERN particle physics lab near Geneva in Switzerland. Heuer will begin his 5-year term in January 2009, half a year after the lab's $3.2 billion Large Hadron Collider (LHC) is scheduled to be up and running.

Heuer worked at CERN from 1984 to 1998 and was spokesperson for the OPAL experiment, representing more than 300 physicists. Since 2004, he has been research director for particle and astroparticle physics at DESY, Germany's particle physics lab near Hamburg, preparing its physicists to work with the LHC and, eventually, the proposed International Linear Collider (ILC).

Heuer is known to be a keen supporter of the ILC. But under Robert Aymar, CERN has backed a rival linear collider technology of its own. Heuer says the worldwide community should pursue both avenues, because in the long run CERN's technique can reach higher energies. "It's a mistake to back just one horse. We need different horses," Heuer says. "Clearly, from the perspective of the ILC, the appointment of the new [director general] is a very, very positive thing," says Barry Barish, leader of the ILC's Global Design Effort. Heuer calls the position "probably the best job in physics research today."

CREDITS (TOP TO BOTTOM): KELLY FAST/NASA/GSFC; COURTESY DIANA ROGERS; CERN

IN BRIEF

Maria Freire has been named head of the New York–based Lasker Foundation, which gives out prizes for clinical and basic life sciences research every year. Freire was most recently chief executive officer of the Global Alliance for TB Drug Development and previously served as head of the Office of Technology Transfer at the National Institutes of Health in Rockville, Maryland. She succeeds Neen Hunt, who has led the foundation since 1995.

Cosmologist George Smoot has donated a portion of money from his share of the 2006 physics Nobel Prize to help establish a new center for cosmology research at the University of California, Berkeley. In addition to the $500,000 endowment from Smoot, the Berkeley Center for Cosmological Physics (bccp.lbl.gov) has received more than $7.5 million in gifts, including a portion of the award Berkeley physicist Saul Perlmutter received this year as a winner of the Gruber Cosmology Prize.

On Campus >>

PERSUADED. Particle physicist Persis Drell has been named director of the 45-year-old Stanford Linear Accelerator Center (SLAC) in Menlo Park, California. Acting director since September after the departure of Jonathan Dorfan, Drell, 51, was leading a search committee when Stanford President John Hennessy and Provost John Etchemendy convinced her that she was the best person for the job. "They prevailed on me," says Drell, who plans to revamp the lab's management to better match SLAC's newly diversified mission.

The daughter of SLAC professor emeritus Sidney Drell, Persis Drell came to the Department of Energy lab in 2002 and has helped broaden its research beyond particle physics. Experimenters will stop smashing particles in September, and in 2009 will begin using an x-ray laser for studies in materials science and biology. The lab is also pursuing astrophysics. "When we had a single mission, ... we had one hill to climb and one flag to capture," Drell says. "It's not so simple anymore."

Drell is a natural leader, says William Madia, executive vice president for laboratory operations at Battelle in Columbus, Ohio. "As lab director, you have to love all your children," he says, "and Persis understands all the parts of SLAC."

BREAKTHROUGH OF THE YEAR

Human Genetic Variation

Equipped with faster, cheaper technologies for sequencing DNA and assessing variation in genomes on scales ranging from one to millions of bases, researchers are finding out how truly different we are from one another

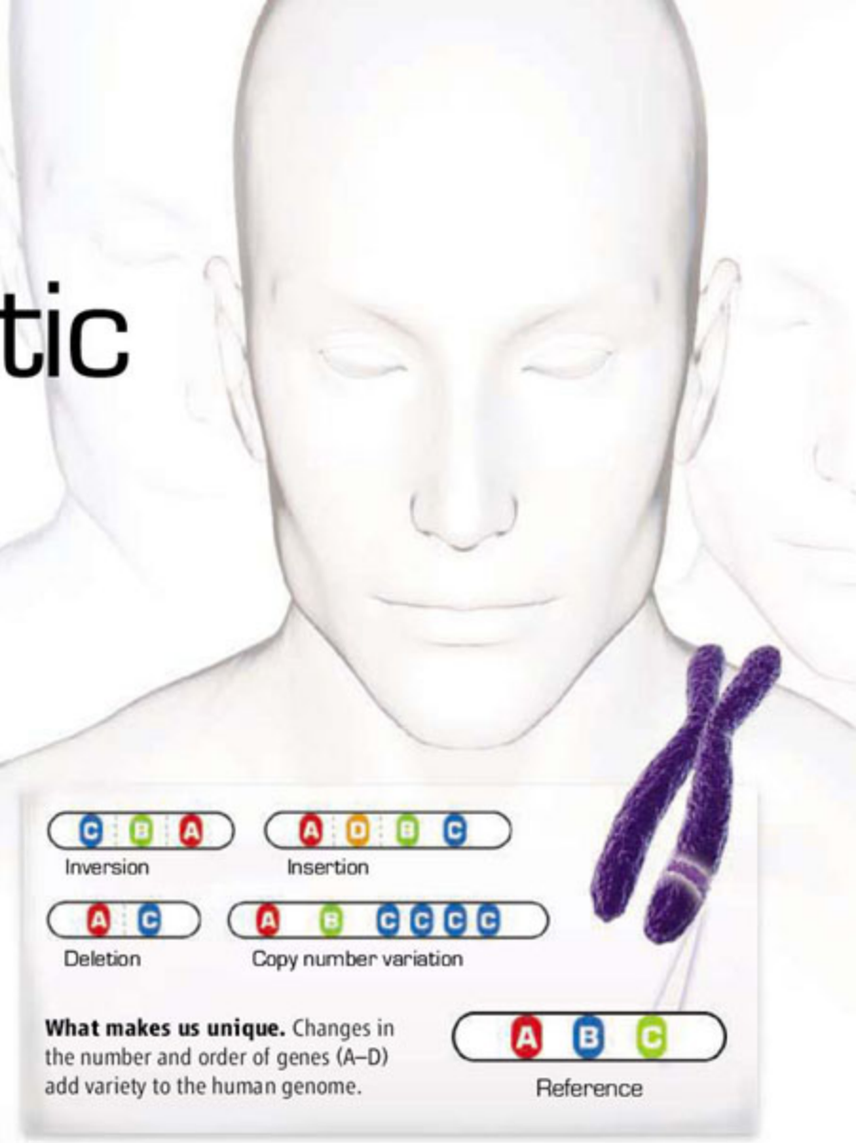

What makes us unique. Changes in the number and order of genes (A–D) add variety to the human genome.

THE UNVEILING OF THE HUMAN GENOME ALMOST 7 YEARS AGO cast the first faint light on our complete genetic makeup. Since then, each new genome sequenced and each new individual studied has illuminated our genomic landscape in ever more detail. In 2007, researchers came to appreciate the extent to which our genomes differ from person to person and the implications of this variation for deciphering the genetics of complex diseases and personal traits.

Less than a year ago, the big news was triangulating variation between us and our primate cousins to get a better handle on genetic changes along the evolutionary tree that led to humans. Now, we have moved from asking what in our DNA makes us human to striving to know what in my DNA makes me me.

BREAKTHROUGH ONLINE

For an expanded version of this section, with references and links, see www.sciencemag.org/sciext/btoy2007

Techniques that scan for hundreds of thousands of genetic differences at once are linking particular variations to particular traits and diseases in ways not possible before. Efforts to catalog and assess the effects of insertions and deletions in our DNA are showing that these changes are more common than expected and play important roles in how our genomes work—or don't work. By looking at variations in genes for hair and skin color and in the "speech" gene, we have also gained a better sense of how we are similar to and different from Neandertals.

Already, the genomes of several individuals have been sequenced, and rapid improvements in sequencing technologies are making the sequencing of "me" a real possibility. The potential to discover what contributes to red hair, freckles, pudginess, or a love of chocolate—let alone quantifying one's genetic risk for cancer, asthma, or diabetes—is both exhilarating and terrifying. It comes not only with great promise for improving health through personalized medicine and understanding our individuality but also with risks for discrimination and loss of privacy (see sidebar, p. 1843).

Turning on the flood lamps

Even with most of the 3 billion DNA bases lined up in the right order, there was still much that researchers couldn't see in the newly sequenced human genome in 2001. Early comparative studies threw conserved regulatory regions, RNA genes, and other features into relief, bringing meaning to much of our genome, including the 98% that lies outside protein-coding regions. These and other studies, including a pilot study called ENCODE, completed this year, drove home how complex the genome is.

There are an estimated 15 million places along our genomes where one base can differ from one person or population to the next. By mid-2007, more than 3 million such locations, known as single-nucleotide polymorphisms (SNPs), had been charted. Called the HapMap, this catalog has made the use of SNPs to track down genes involved in complex diseases—so-called genome-wide association studies—a reality. More than a dozen such studies were published this year.

Traditionally, geneticists have hunted down genes by tracking the inheritance of a genetic disease through large families or by searching for suspected problematic genes among patients. Genome-wide association studies go much further. They compare the distribution of SNPs—using arrays that can examine some 500,000 SNPs at a time—in hundreds or even thousands of people with and without a particular disease. By tallying which SNPs co-occur with symptoms, researchers can determine how much increased risk is associated with each SNP.

In the past, such links have been hard-won, and most have vanished on further study. This year, however, researchers linked variants of more than 50 genes to increased risk for a dozen diseases. Almost all the variants exert relatively small effects, in concert with many other genetic factors and environmental conditions, and in many cases the variant's real role has not yet been pinned down. But the sheer numbers of people studied have made even skeptics hopeful that some of these genetic risk factors will prove real and will help reveal underlying causes.

The Wellcome Trust, the U.K.'s largest biomedical charity, began to put its weight behind genome-wide association studies in 2005 and recruited 200 researchers to analyze the DNA of 17,000 people from

CREDIT: COMPOSITE IMAGE: K. KRAUSE/SCIENCE (HUMAN: 3D4MEDICAL.COM; CHROMOSOME: C. BICKEL/SCIENCE)

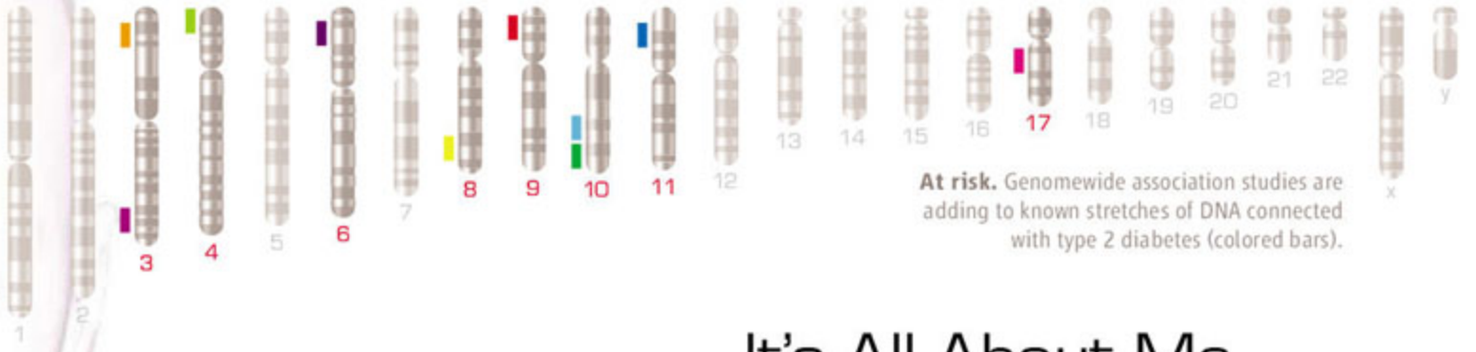

At risk. Genomewide association studies are adding to known stretches of DNA connected with type 2 diabetes (colored bars).

CREDITS (TOP TO BOTTOM): K. KRAUSE/SCIENCE (SOURCE: RICHA SAXENA AND DAVID ALTSHULER, BROAD INSTITUTE OF HARVARD AND MIT); COURTESY OF 23ANDME

across the United Kingdom. The results are part of an avalanche of genetic information becoming available as more and more geneticists agree to share data and as funding agencies require such exchanges. In June, the consortium published a mammoth analysis of seven diseases, including rheumatoid arthritis, bipolar disorder, and coronary artery disease. It also found several gene variants that predispose individuals to type 1 diabetes and three new genes for Crohn's disease.

Several large studies have also pinpointed type 2 diabetes genes. One French study involving nonobese diabetics found that a version of a gene for a protein that transports zinc in the pancreas increased the risk of this disease. Three simultaneous reports involving more than 32,000 participants uncovered four new diabetes-associated gene variants, bringing to 10 the number of known non-Mendelian genetic risk factors for type 2 diabetes. These finds strongly point to pancreatic beta cells as the source of this increasingly common chronic disorder.

New gene associations now exist for heart disease, breast cancer, restless leg syndrome, atrial fibrillation, glaucoma, amyotrophic lateral sclerosis, multiple sclerosis, rheumatoid arthritis, colorectal cancer, ankylosing spondylitis, and autoimmune diseases. One study even identified two genes in which particular variants can slow the onset of AIDS, demonstrating the potential of this approach for understanding why people vary in their susceptibility to infectious diseases.

Genomic hiccups

Genomes can differ in many other ways. Bits of DNA ranging from a few to many thousands, even millions, of bases can get lost, added, or turned around in an individual's genome. Such revisions can change the number of copies of a gene or piece of regulatory DNA or jam two genes together, changing the genes' products or shutting them down. This year marked a tipping point, as researchers became aware that these changes, which can alter a genome in just a few generations, affect more bases than SNPs.

In one study, geneticists discovered 3600 so-called copy number variants among 95 individuals studied. Quite a few overlapped genes, including some implicated in our individuality—blood type, smell, hearing, taste, and metabolism, for example. Individual genomes differed in size by as many as 9 million bases. This fall, another group performed an extensive analysis using a technique, called paired-end mapping, that can quickly uncover even smaller structural variations.

These differences matter. One survey concluded that in some populations almost 20% of differences in gene activity are due to copy-number variants; SNPs account for the rest. People with high-starch diets—such as in Japan—have extra copies of a gene for a starch-digesting protein compared with members of hunting-gathering societies. By scanning the genomes of autistic and healthy children and their parents for copy-number variation, other geneticists have found that newly appeared DNA alterations pose a risk for autism.

New technologies that are slashing the costs of sequencing and genome analyses will make possible the simultaneous genome-wide search for SNPs and other DNA alterations in individuals. Already, the unexpected variation within one individual's published genome has revealed that we have yet to fully comprehend the degree to which our DNA differs from one person to the next. Such structural and genetic variety is truly the spice of our individuality. **–ELIZABETH PENNISI**

It's All About Me

Along with the flood of discoveries in human genetics, 2007 saw the birth of a new industry: personal genomics. Depending on your budget, you can either buy a rough scan of your genome or have the whole thing sequenced. The companies say the information will help customers learn about themselves and improve their health. But researchers worry that these services open up a Pandora's box of ethical issues.

At $300,000 to $1 million per genome, sequencing all 3 billion base pairs is still too costly for all but a few. Although dozens more personal genomes will probably be sequenced in the coming year, most will be done by public and private research organizations—including the institute run by genome maverick J. Craig Venter, whose personal genome was one of three completed in 2007 in the United States and China. In a lower-budget effort, Harvard's George Church this month will deliver initial DNA sequences for the protein-coding sections (1% of the genome) to the first 10 volunteers for his Personal Genome Project. Meanwhile, a new company called Knome is offering full-genome sequencing to 20 customers willing to pay $350,000.

A glimpse of one's genome is already within the reach of ordinary people, thanks to several companies. They include 23andMe, which has financing from Google and may let users link to others with shared traits; Navigenics, which will screen for about 20 medical conditions; and deCODE Genetics in Iceland, a pioneer in disease gene hunting. For $1000 to $2500, these companies will have consumers send in a saliva sample or cheek swab, then use "SNP chips" to scan their DNA for as many as 1 million markers. The companies will then match the results with the latest publications on traits, common diseases, and ancestry.

Although many customers may view this exercise as a way to learn fun facts about themselves—recreational genomics, some call it—bioethicists are wary. Most common disease markers identified so far raise risks only slightly, but they could cause needless worry. At the same time, some people may be terrified to learn they have a relatively high risk for an incurable disease such as Alzheimer's.

Pandora's box? This cheek-swab kit could reveal your intimate secrets.

The rush toward personal genome sequences also sharpens long-held worries about discrimination. A bill to prevent insurers and employers from misusing genetic data is stalled in Congress. Complicating matters, your genetic information exposes your relatives' DNA, too.

The most profound implications of having one's genome analyzed may not be what it reveals now—which isn't much—but what it may show later on. Perhaps to sidestep such questions, some companies will limit which markers to disclose. Others, however, will hand customers their entire genetic identity, along with all the secrets it may hold.

–JOCELYN KAISER

The Runners-Up >>

2 REPROGRAMMING CELLS. The riddle of Dolly the Sheep has puzzled biologists for more than a decade: What is it about the oocyte that rejuvenates the nucleus of a differentiated cell, prompting the genome to return to the embryonic state and form a new individual? This year, scientists came closer to solving that riddle. In a series of papers, researchers showed that by adding just a handful of genes to skin cells, they could reprogram those cells to look and act like embryonic stem (ES) cells. ES cells are famous for their potential to become any kind of cell in the body. But because researchers derive them from early embryos, they are also infamous for the political and ethical debates that they have sparked.

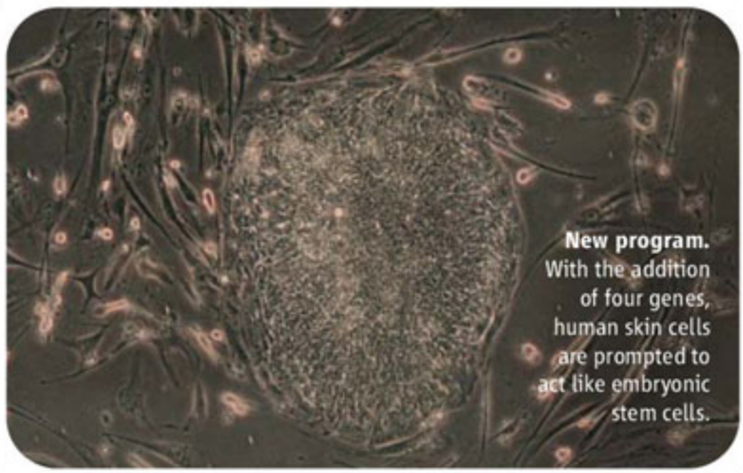

New program. With the addition of four genes, human skin cells are prompted to act like embryonic stem cells.

The new work is both a scientific and a political breakthrough, shedding light on the molecular basis of reprogramming and, perhaps, promising a way out of the political storm that has surrounded the stem cell field.

The work grows out of a breakthrough a decade ago. In 1997, Dolly, the first mammal cloned from an adult cell, demonstrated that unknown factors in the oocyte can turn back the developmental clock in a differentiated cell, allowing the genome to go back to its embryonic state.

Various experiments have shown how readily this talent is evoked. A few years ago, researchers discovered that fusing ES cells with differentiated cells could also reprogram the nucleus, producing ES-like cells but with twice the normal number of chromosomes. Recently, they also showed that a fertilized mouse egg, or zygote, with its nucleus removed could also reprogram a somatic cell.

Meanwhile, the identity of the reprogramming factors continued to puzzle and tantalize biologists. In 2006, Japanese researchers announced that they were close to at least part of the answer. By adding just four genes to mouse tail cells, they produced what they call induced pluripotent stem (iPS) cells: cells that looked and acted like ES cells.

This year, in two announcements that electrified the stem cell field, scientists closed the deal. In a series of papers in June, the same Japanese group, along with two American groups, showed that the iPS cells made from mouse skin could, like ES cells, contribute to chimeric embryos and produce all the body's cells, including eggs and sperm. The work convinced most observers that iPS cells were indeed equivalent to ES cells, at least in mice.

Then in November came a triumph no one had expected this soon: Not one, but two teams repeated the feat in human cells. The Japanese team showed that their mouse recipe could work in human cells, and an American team found that a slightly different recipe would do the job as well.

The advance seems set to transform both the science and the politics of stem cell research. Scientists say the work demonstrates that the riddle of Dolly may be simpler than they had dared to hope: Just four genes can make all the difference. Now they can get down to the business of understanding how to guide the development of these high-potential cells in the laboratory. In December, scientists reported that

CREDITS (TOP TO BOTTOM): UNIVERSITY OF WISCONSIN, MADISON; TERRY SMITH (CRYSTAL BALLS)

HOW'D WE DO?

Rating the predictions we made last year in "Areas to Watch"

World-weary? Hardly. Four spacecraft returned torrents of data from around the solar system. The Venus Express orbiter probed the vicious atmosphere of Earth's near-twin. On its way to Pluto, New Horizons snapped pictures of Jupiter. The Mars Reconnaissance Orbiter revealed unforeseen hazards for future landers. And Europe's Earth-orbiting COROT discovered its first planet orbiting another star, showing that COROT can detect exoplanets as small as Earth.

Skulls and bones. In 2007, paleoanthropologists unveiled the long-awaited postcranial bones of a 1.7-million-year-old *Homo erectus* from Dmanisi, Georgia, bits of a putative gorilla ancestor, and new early *Homo* specimens from Africa. But the world still waits for publication of the skeleton of the enigmatic *Ardipithecus ramidus*, a 4.4-million-year-old Ethiopian hominid that may shed light on the murky roots of the human family tree.

Loads of new primate genes. The published genome sequence of the rhesus macaque did help clarify genetic changes that led to humans, but the analyses of the genomes of the gorilla, orangutan, marmoset, gibbon, galago, tree shrew, and mouse lemur have yet to appear. Eventually, though, these sequence maps will bring a host of evolutionary insights.

A climate of change? High-profile reports, an agenda-setting meeting in Bali, Indonesia, and a

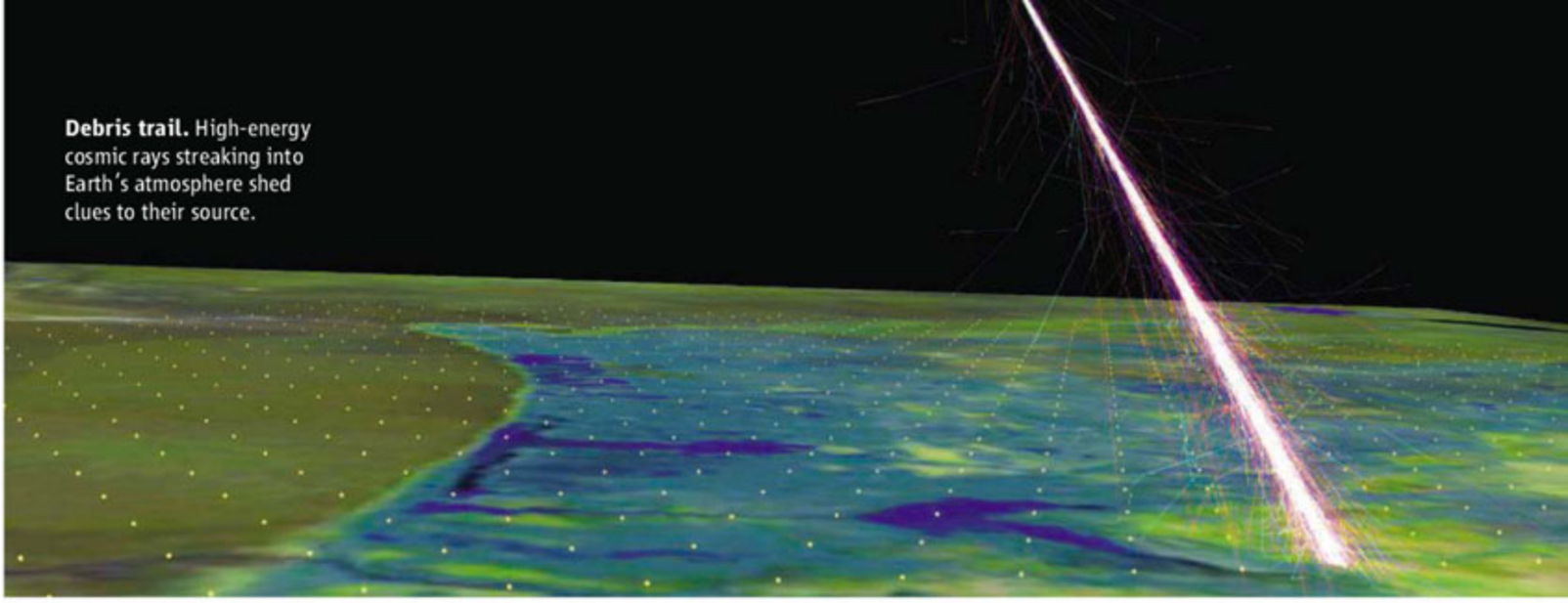

Debris trail. High-energy cosmic rays streaking into Earth's atmosphere shed clues to their source.

CREDIT: M. SUBBARAO, D. SURENDRAN, AND R. LANDSBERG/KICP/ADLER PLANETARIUM AND ASTRONOMY MUSEUM/UNIVERSITY OF CHICAGO

they had already used mouse iPS cells to successfully treat a mouse model of sickle cell anemia. The next big challenge will be finding a way to reprogram human cells without using possible cancer-causing viruses to insert the genes.

Politicians and ethicists on both sides of the debate about embryo research are jubilant. Supporters hope the new technique will enable them to conduct research without political restrictions, and opponents hope it will eventually render embryo research unnecessary. Indeed, several scientists said the new work prompted them to abandon their plans for further research on human cloning.

Officials at the National Institutes of Health said there was no reason work with iPS cells would not be eligible for federal funding, enabling scientists in the United States to sidestep restrictions imposed by the Bush Administration. And President George W. Bush himself greeted the announcement by saying that he welcomed the scientific solution to the ethical problem.

But it's much too early to predict an end to the political controversies about stem cell research. Some researchers say they still need to be able to do research cloning to find out just what proteins the egg uses for its reprogramming magic. And now that science has come a step closer to the long-term goal of stem cell therapy, mouse models won't be adequate for animal studies. Rather, researchers will need to test cell transplantation approaches with primates, a move that will inevitably stir up resistance from animal-rights activists.

Nobel Peace Prize placed global climate squarely in the public eye, but policymakers in the United States, China, and India haven't passed mandatory limits on greenhouse gas emissions that scientists say are needed. (See "Global Warming, Hotter Than Ever," p. 1846.)

Whole-genome association studies. In work that made up part of this year's Breakthrough of the Year (see p. 1842), more than a dozen large-scale comparative studies of human DNA showed the technique's enormous promise for tracking down genes linked to disease.

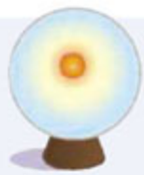

Light crystals. Physicists hope to explore high-temperature superconductivity and other bizarre properties of solids by emulating them in optical lattices, artificial "crystals" based on corrugated patterns of laser light.

The year's hundreds of papers on optical lattices did not include a superconductor stand-in, but a grand entrance can't be far off.

3 TRACING COSMIC BULLETS.

What's smaller than an atom but crashes into Earth with as much energy as a golf ball hitting a fairway? Since the 1960s, that riddle has tantalized physicists studying the highest energy cosmic rays, particles from space that strike the atmosphere with energies 100 million times higher than particle accelerators have reached. This year, the Pierre Auger Observatory in Argentina supplied key clues to determine where in space the interlopers come from.

Many physicists had assumed the extremely rare rays were protons from distant galaxies. That notion took a hit in the 1990s, when researchers with the Akeno Giant Air Shower Array (AGASA) near Tokyo reported 11 rays with energies above 100 exa–electron volts (EeV)—about 10 times more than expected. The abundance was tantalizing. On their long trips, protons ought to interact with radiation lingering from the big bang in a way that saps their energy and leaves few with more than 60 EeV. So the excess suggested that the rays might be born in our galactic neighborhood, perhaps in the decays of supermassive particles forged in the big bang. But researchers with the Hi-Res detector in Dugway, Utah, saw only two 100-EeV rays, about as many as expected from far-off sources.

The Auger team set out to beat AGASA and Hi-Res at their own games. When a cosmic ray strikes the atmosphere, it sets off an avalanche of particles. AGASA used 111 detectors spread over 100 square kilometers to sample the particles and infer the ray's energy and direction; Auger comprises nearly 1500 detectors spread over 3000 square kilometers. The avalanche also causes the air to fluoresce. Hi-Res used two batteries of telescopes to see the light; Auger boasts four. In July, the Auger team reported its first big result: no excess of rays above 60 EeV.

Auger still sees a couple of dozen rays above that level, however. Last month, the team reported that they seem to emanate from active galactic nuclei (AGNs): enormous black holes in the middles of some galaxies. The AGNs lie within 250 million light-years of Earth, close enough that cosmic radiation would not have drained the particles' energy en route. Auger researchers haven't yet proved that AGNs are the sources of the rays, and no one knows how an AGN might accelerate a proton to such stupendous energies.

Expect the controversy to continue. Hi-Res researchers say that they see no correlation with AGNs. With Japanese colleagues, they are completing the 740-square-kilometer Telescope Array in Millard County, Utah, which has 512 detectors and three telescope batteries. But with a much bigger array, the Auger team will surely be first to test its own claims.

4 RECEPTOR VISIONS. Just when some crystallographers were fretting that the task was impossible, researchers nabbed a close-up of adrenaline's target, the β_2-adrenergic receptor. Its structure has long been on the to-do list, but the feat also got pulses racing because of the molecule's family connections. The receptor is one of roughly 1000 membrane-spanning molecules called G protein–coupled receptors (GPCRs). By detecting light, odors, and tastes, the receptors clue us in to our surroundings. GPCRs also help manage our internal conditions by relaying messages from hormones, the neurotransmitter serotonin, and myriad other molecules. From antihistamines to beta blockers, the pharmacopoeia brims with medicines aimed at GPCRs—all of which researchers discovered without the benefit of high-resolution structures. A clear picture of, say, a receptor's binding site might spur development of more potent, safer drugs. But scientists had cracked only one "easy" GPCR structure, for the visual pigment rhodopsin.

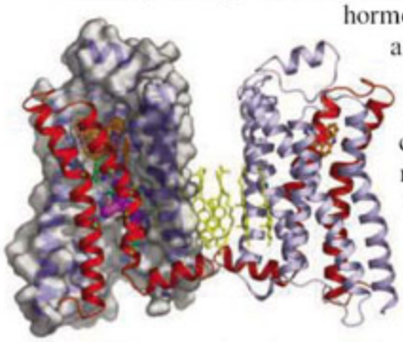

Gotcha! Researchers have worked out the architecture of the adrenaline receptor.

Getting a look at the β_2-adrenergic receptor took the leaders of two overlapping crystallographic teams almost 2 decades. The effort paid off this fall with four papers published in the journals *Science*, *Nature*, and *Nature Methods*. The lab ingenuity that other experts call a technical tour de force shows in the way the teams restrained the molecule's flexible third loop. They either replaced it with the stolid enzyme lysozyme or tacked it down with an antibody.

But this snapshot of the receptor is just the beginning. Before researchers can design compounds to jam the molecule, they need to picture it in its different "on" states. And the other GPCRs awaiting analysis mean that for crystallographers, it's two down and 1000 to go.

5 BEYOND SILICON? Sixty years ago, semiconductors were a scientific curiosity. Then researchers tried putting one type of semiconductor up against another, and suddenly we had diodes, transistors, microprocessors, and the whole electronic age. Startling results this year may herald a similar burst of discoveries at the interfaces of a different class of materials: transition metal oxides.

Transition metal oxides first made headlines in 1986 with the Nobel Prize–winning discovery of high-temperature superconductors. Since then, solid-state physicists keep finding unexpected properties in these materials—including colossal magnetoresistance, in which small changes in applied magnetic fields cause huge changes in electrical resistance. But the fun should really start when one oxide rubs shoulders with another.

If different oxide crystals are grown in layers with sharp interfaces, the effect of one crystal structure on another can shift the positions of atoms at the interface, alter the population of electrons, and even change how electrons' charges are distributed around an atom. Teams have grown together two insulating oxides to produce an interface that conducts like a metal or, in another example, a superconductor. Other combinations have shown magnetic properties more familiar in metals, as well as the quantum Hall effect, in which conductance becomes quantized into discrete values in a magnetic field. Researchers are optimistic that they may be able to make combinations of oxides that outperform semiconductor structures.

Tunable sandwich. In lanthanum aluminate sandwiched between layers of strontium titanate, a thick middle layer (*right*) produces conduction at the lower interface; a thin one does not.

With almost limitless variation in these complex oxides, properties not yet dreamed of may be found where they meet.

6 ELECTRONS TAKE A NEW SPIN. Chalk one up for the theorists. Theoretical physicists in California recently predicted that semiconductor sandwiches with thin layers of mercury telluride (HgTe) in the middle should exhibit an unusual behavior of their electrons called the quantum spin Hall effect (QSHE). This year, they teamed up with experimental physicists in Germany and found just what they were looking for.

GLOBAL WARMING, HOTTER THAN EVER

Climate change, a perennial runner-up for Breakthrough of the Year, broke from the pack this year—both in the pages of this section and in the public arena.

In 2007, the debate about the reality of global warming ended, at least in the political and public realms in the United States. After 6 years of silence, the United Nations' Intergovernmental Panel on Climate Change (IPCC) drew heavy and wholly positive media coverage for a series of wide-ranging reports. The world is warming, IPCC declared; human activity is behind most of it, and if it keeps up we'll pay a price. But the panel also said that much of the climate pain might be avoided if the world agrees to begin sharing the economic pain. Impressed with that performance, the Nobel committee anointed IPCC, as well as climate campaigner Al Gore, with its Peace Prize.

Other reminders also drove home the gravity of the climate change situation. Scientists now worry that the record melt-back of sea ice during the summer might indicate that feedbacks are amplifying the effects of global warming. A steady stream of media reports this year noted record melting of Greenland ice, record-high temperatures in the United States, and surging Antarctic glaciers. And the energy crisis deepened as oil prices increased to $100 a barrel, boosting anxieties about the future of fossil fuels.

Politicians weren't idle, although U.S. climate policymakers still have little to show for their concern. Since gaining control of Congress in January, Democrats have transformed the debate from "if to when for mandatory limits on U.S. emissions," says Paul Bledsoe of the National Commission on Energy Policy in Washington, D.C. But hundreds of hearings and reams of legislative proposals have not translated into legislation.

The status of the most prominent Senate proposal, offered by senators Joseph Lieberman (I–CT) and John Warner (R–VA), illustrates the pitfalls that lie ahead for Democrats. Introduced in October after months of negotiations with corporate lobbyists and environmental groups, the bill would cut U.S. emissions by roughly 15% of 2005 levels by 2020 with innovative proposals for emissions credits to spur new technologies. But the debate at a 5 December markup exposed some of the hurdles that the legislation will face in what experts expect will be a multiyear

CREDITS (TOP TO BOTTOM): CHEREZOV *ET AL.*; J. HUIJBEN/UNIVERSITY OF TWENTE

slog. Democrats from Midwestern and coal states, for example, helped kill a proposed measure that would have given the Environmental Protection Agency the ability to tighten the caps if scientists determined that warming was going to be more than 2°C above the preindustrial average. Meanwhile, the House is even further behind on emissions limits. As *Science* went to press, Congress was poised to pass a landmark automobile fuel law that, if it survives a threatened White House veto, will require 35 miles per gallon (14.9 kilometers per liter, or 6.7 liters per 100 kilometers) efficiency by 2020.

Elsewhere, there have been mixed signs of progress. At press time, in Bali, Indonesia, negotiators from Europe and the developing world were striving to persuade the United States to consider binding cuts for the 2012 follow-on to the Kyoto treaty. China has warmed slightly to carbon limits—if the deadline is far enough away. Meanwhile, growing numbers of prominent climate experts are calling for research into geoengineering, the deliberate tinkering with Earth's climate to reverse warming. Given the slow political progress, says atmospheric scientist David Battisti of the University of Washington, Seattle, "we might need a plan B."

–ELI KINTISCH AND RICHARD A. KERR

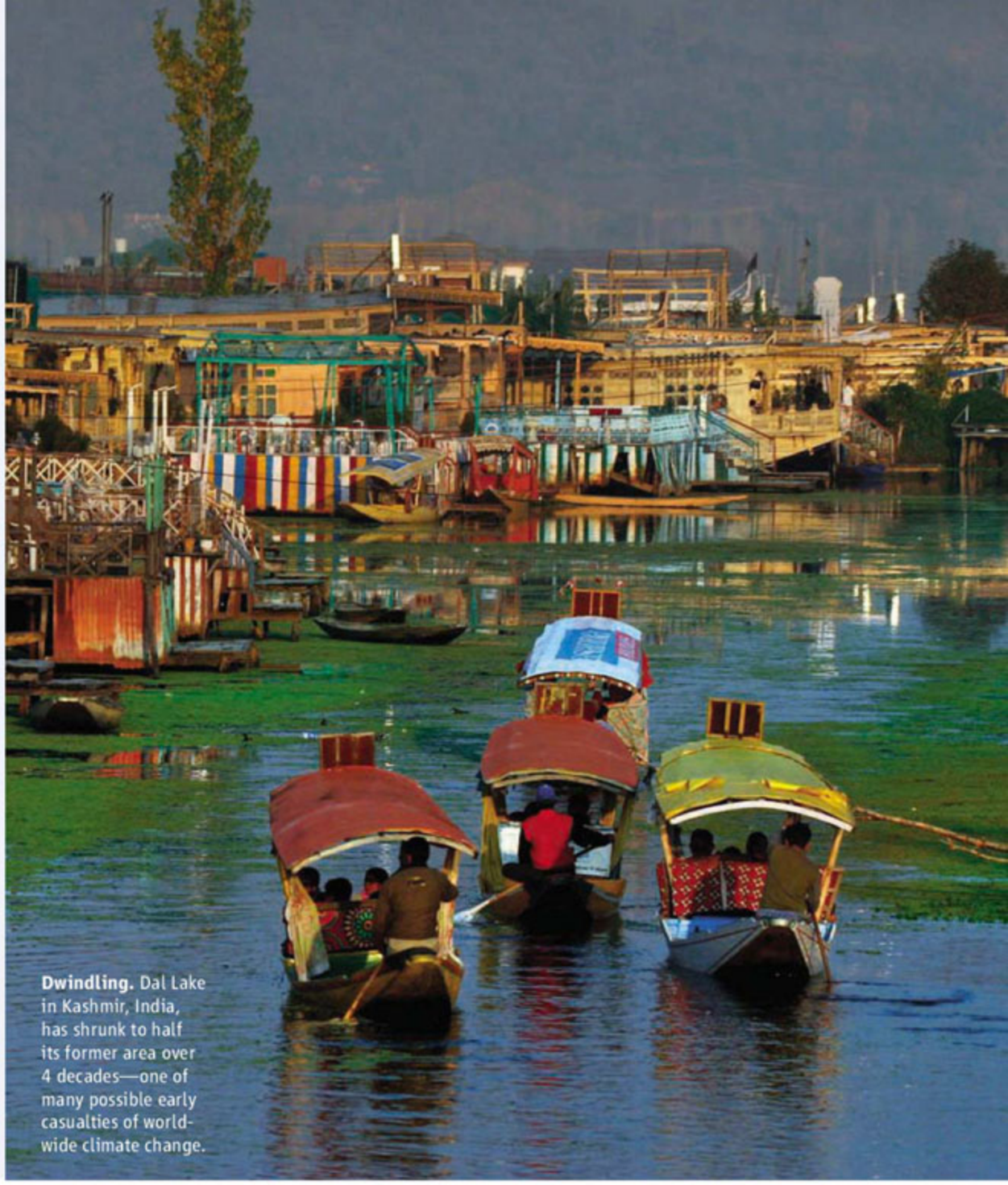

Dwindling. Dal Lake in Kashmir, India, has shrunk to half its former area over 4 decades—one of many possible early casualties of worldwide climate change.

The effect is the latest in a series of oddball ways electrons behave when placed in external electric and magnetic fields. In 1980, researchers in Germany and the U.K. discovered one of these anomalies, called the quantum Hall effect. When they changed the strength of a magnetic field applied perpendicular to charges moving through thin layers of metals or semiconductors, they found that the conductance changed in a stepwise, or quantized, manner. One upshot was that charges flowed in tiny channels along the edges of the materials with essentially no energy loss.

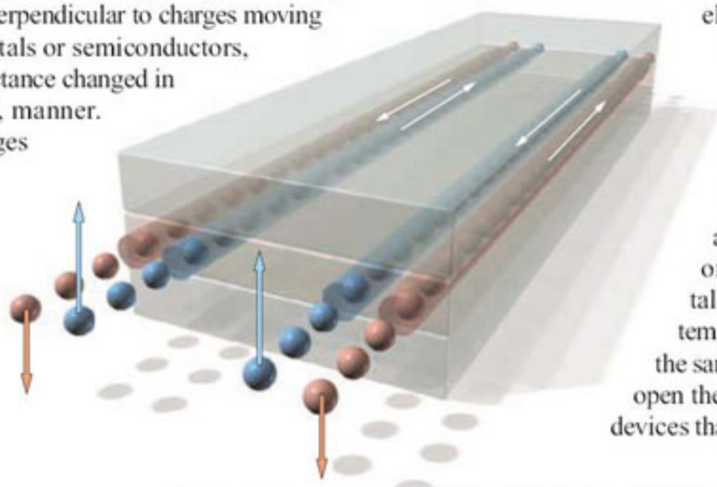

Channeled. Electrons with spins oriented in opposite directions flow along different paths.

The finding triggered hopes of new families of computer chip devices. But because the effect required high magnetic fields and low temperatures, such devices remained pipe dreams.

Luckily for physicists, electrons harbor not only electric charge but also another property known as spin. In recent years, theorists have predicted that materials with the right electronic structure should interact with electric fields to result in the QSHE—and a spin-driven version of near-lossless conduction. Such materials would also do away with the need for high magnetic fields and perhaps even for low temperatures. This year, one of them—the HgTe sandwich—showed telltale (although not ironclad) signs of the effect at temperatures below 10 kelvin. If researchers can do the same trick at room temperature, the discovery could open the door to new low-power "spintronic" computing devices that manipulate electrons by both charge and spin.

CREDITS (TOP TO BOTTOM): ALTAF QADRI/EPA/CORBIS; C. BICKEL/*SCIENCE*

7 DIVIDE TO CONQUER. Fresh evidence illuminating how immune cells specialize for immediate or long-term protection had researchers a little feverish this year. When a pathogen attacks, some CD8 T cells become short-lived soldiers, while others morph into memory cells that loiter for decades in case the same interloper tries again. The new work demonstrates how one cell can spawn both cell types.

A T cell remains passive until it meets a dendritic cell carrying specific pathogen molecules. The liaison between the two lasts for hours. As the cells dally, receptors and other molecules congregate at each end of the T cell. A U.S.–based team tested the proposal that if the T cell then divided, its progeny would inherit different molecules that might steer them onto distinct paths. Such asymmetric divisions are a common method for cell diversification during development.

In March, the team reported experiments showing that different specialization-controlling proteins amassed at each pole of a T cell during its dance with a dendritic cell. When the researchers nabbed newly divided T cells, they found that progeny that had been adjacent to the dendritic cell carried receptors typical of soldiers, whereas their counterparts showed the molecular signature of memory cells.

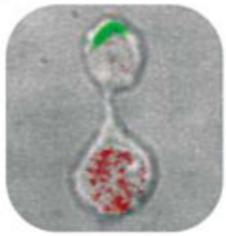

Separate and unequal. As a T cell divides, the upper and lower cells sport distinct molecules.

Unequal divisions could also help generate diversity among CD4 T cells, immune regulators that differentiate into three types. Practical applications of the discovery will have to wait until researchers know more about memory-cell specialization, but eventually they might be able to tweak the process to give vaccines more kick.

8 DOING MORE WITH LESS. Society may finally be embracing energy efficiency and waste reduction, but these attributes have always been prized among synthetic chemists. Extra plaudits and stature go to chemists who carry out desired reactions in the simplest and most elegant ways. One reason: Fewer synthetic steps almost always saves cash. And although such economizing is a perennial goal, this year an impressive array of synthetic successes showed that chemists are gaining a new level of control over the molecules they make and how they make them.

Achieving this control has not been easy. Many desired molecules, such as pharmaceutical and electronic compounds, consist of a backbone of carbon atoms with hydrogen atoms or other more complex functional groups dangling off the sides. When chemists convert a starting compound into one they really want, they typically aim to modify just one of those appendages but not the others. They normally do so either by adorning the starting material with chemical "activators" that prompt the molecule to react only at the tagged site or by slapping "protecting" groups on the sites they want left untouched.

This year, researchers around the globe made major strides in doing away with these accessories. One group in Israel used a ruthenium-based catalyst to convert starting compounds called amines and alcohols directly into another class of widely useful compounds called amides. A related approach enabled researchers in Canada to link pairs of ring-shaped compounds together. Another minimized the use of protecting groups to make large druglike organic compounds. Yet another did much the same in mimicking the way microbes synthesize large ladder-shaped toxins. And those are just a few examples. For chemists, it was an efficient year.

9 BACK TO THE FUTURE. In Greek mythology, the goddess of memory, Mnemosyne, gave birth to the Muses, spirits who inspire imagination. Some modern scientists have seen the kinship as both literal and practical. Remembering the past, they propose, helps us picture—and pre-

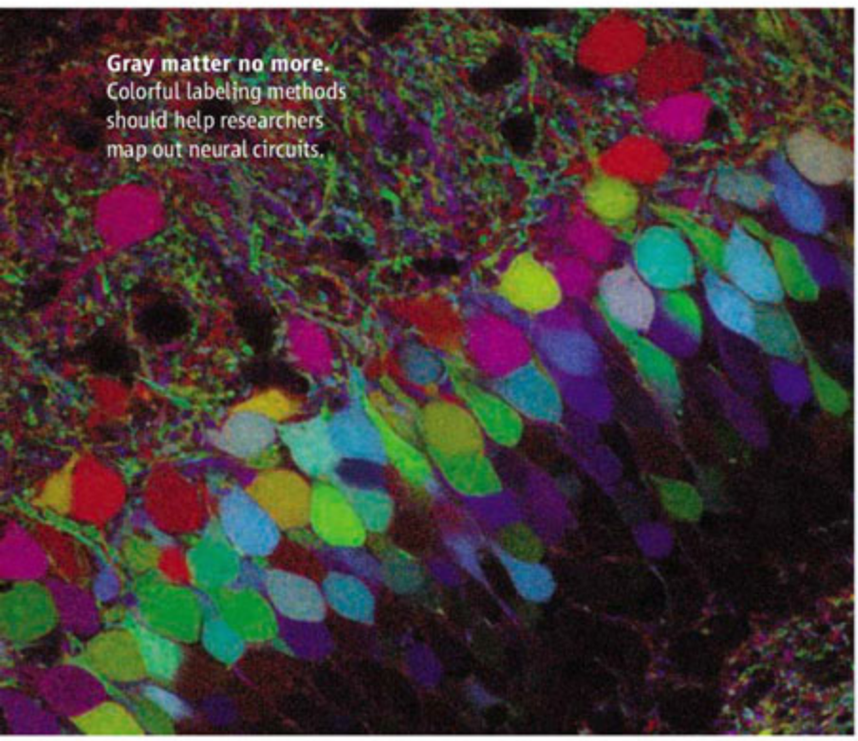

Gray matter no more. Colorful labeling methods should help researchers map out neural circuits.

AREAS TO WATCH

A smashing start? Next summer, physicists will start up the Large Hadron Collider (LHC) at the European particle physics lab, CERN, outside Geneva, Switzerland. Researchers hope this highest-energy collider will reveal plenty of new particles and puzzles, but the immediate question is how fast will it come on? The ultracomplex machine runs at a frigid 1.9 kelvin, and if for some reason researchers have to warm part of it up, it will take months to cool it again. Still, CERN has a record of bringing new machines on line smoothly. Call it a major success if the LHC produces even a little data next year.

Micromanagers. Research on small RNA molecules that control gene expression continues at a rapid clip, and microRNAs are surging to the front of the pack. Roughly 800 papers on the tiny molecules were published in 2007, tying them to a slew of cancers, heart ailments, a healthy immune system, stem cell differentiation, and more. But it's still early days. In 2008, researchers will start using microRNAs to unveil disease mechanisms and will make inroads into solving fundamental puzzles about how they function.

Cell to order. It's hard to separate the hype from the hard science, but

CREDITS (TOP TO BOTTOM): JOHN T. CHANG ; LIVET ET AL., *NATURE* **450**, 7166 (2007)

Something to Muse on. In the brain as in Greek mythology, memory and imagination may be related.

pare for—the future. The notion got a boost this year from several studies hinting at common neural mechanisms for memory and imagination.

In January, researchers in the United Kingdom reported that five people with amnesia caused by damage to the hippocampus, a crucial memory center in the brain, were less adept than healthy volunteers at envisioning hypothetical situations such as a day at the beach or a shopping trip. Whereas healthy subjects described such imagined events vividly, the amnesic patients could muster only a few loosely connected details, suggesting that their hippocampal damage had impaired imagination as well as memory.

In April, a brain-imaging study with healthy young volunteers found that recalling past life experiences and imagining future experiences activated a similar network of brain regions, including the hippocampus. Even studies with rats suggested that the hippocampus may have a role in envisioning the future: One team reported in November that when a rat faces a fork in a familiar maze, neurons in the hippocampus that encode specific locations fire in sequence as if the rat were weighing its options by mentally running down one path and then the other.

On the basis of such findings, some researchers propose that the brain's memory systems may splice together remembered fragments of past events to construct possible futures. The idea is far from proven, but if future experiments bear it out, memory may indeed turn out to be the mother of imagination.

10 GAME OVER.

Computer scientists finally took some of the fun out of the game of checkers. After 18 years of trying, a Canadian team proved that if neither player makes a mistake, a game of checkers will inevitably end in a draw. The proof makes checkers—also known as draughts—the most complicated game ever "solved." It marks another victory for machines over humans: A mistake-prone person will surely lose to the team's computer program.

Proving that flawless checkers will end in a stalemate was hardly child's play. In the United States, the game is played on an eight-by-eight grid of red and black squares. The 12 red and 12 black checkers slide diagonally from black square to black square, and one player can capture the other's checker by hopping over it into an empty space just beyond. All told, there are about 500 billion billion arrangements of the pieces, enough to overwhelm even today's best computers.

So the researchers compiled a database of the mere 39,000 billion arrangements of 10 or fewer pieces and determined which ones led to a win for red, a win for black, or a draw. They then considered a specific opening move and used a search algorithm to show that players with perfect foresight would invariably guide the game to a configuration that yields a draw.

Reported in July, the advance exemplifies an emerging trend in artificial intelligence. Human thinking relies on a modest amount of memory and a larger capacity to process information. In contrast, the checkers program employs relatively less processing and a whole lot of memory—the 39,000-billion-configuration database. The algorithms the team developed could find broad applications, others say, such as deciphering the information encoded in DNA. **–THE NEWS STAFF**

synthetic biologists say humanmade microbes are in reach. By this time next year, one group hopes to put a synthesized genome into DNA-less bacteria; another is incrementally replacing natural DNA with synthetic DNA. The point is to make biofuels—perhaps even microbe-derived gasoline—or pharmaceuticals.

Paleogenomics. Expect a very rough draft of the Neandertal genome by the end of 2008 and more comparisons between the genes of Neandertals and *Homo sapiens* that will continue to flesh out those fossil bones, filling out many features of this extinct human. Thanks to cheaper, faster technologies, there will be more genomes, from more extinct species, rolling out of the sequencing pipelines.

Multiferroics. Relatives of ceramic oxide superconductors, the compounds called multiferroics form a group in which single materials display multiple electronic, magnetic, and structural behaviors. Physicists recently used electric fields to manipulate magnetic domains in a multiferroic. Now, they are racing to better control this switching and shape the materials into novel computer chip devices. Success could pave the way for chips that combine the logic functions normally handled by semiconductors with the memory functions now carried out by magnetic materials.

Megamicrobes. Featured in both the U.S. National Institutes of Health and the European Union plans for 2008, the human microbiome will go under the microscope this year in many labs around the world. Expect the genomes of 200 of the bacteria that call humans home to be sequenced, as well as the first steps toward extensive surveys of gut, skin, mouth, and reproductive-tract microbial communities. Meanwhile, researchers are mapping the distribution of microbes in other environments, including icebergs and hot ash.

New light on neural circuits. Exciting new methods are poised to start revealing how circuits of neurons process information and mediate behavior. Recently, neuroscientists mapped neural connections in mice by genetically tagging neurons with nearly 100 fluorescent hues. Others have been using lasers to control the electrical activity of individual neurons in the brains of rodents, thanks to light-sensitive ion channels introduced by genetic engineering. Meanwhile, a magnetic resonance method called diffusion tensor imaging is providing new detail about connections between regions of the human brain. These techniques should yield important insights into how neural circuits work—and how they break down in brain disorders.

CREDITS (TOP TO BOTTOM): ARTE & IMMAGINI SRL/CORBIS; SOMOS/VEER

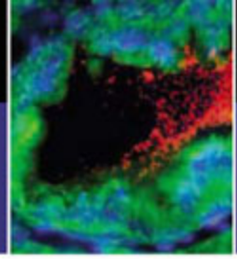

How we tolerate gut microbes
1853

UCSF fires Kessler as dean
1855

CLIMATE CHANGE

Grassroots Effort Pays Dividends On Presidential Campaign Trail

PLAISTOW, NEW HAMPSHIRE—Activists in snowman and polar bear costumes are frolicking at candidate town meetings. Editorials on global warming are appearing in influential newspapers in New Hampshire and Iowa. Most major presidential candidates—from liberal Democratic senator Barack Obama to former Arkansas governor Mike Huckabee, a conservative Republican—have called for caps on the emissions of greenhouse gases.

The run-up to the 2008 U.S. presidential election campaign—which kicks off with the Iowa caucuses on 3 January and the New Hampshire primary 5 days later—has been a coming-out party for climate change. "Climate change is bigger politically than it's ever been," says Navin Nayak of the League of Conservation Voters in Washington, D.C., which tracks the issue.

There are plenty of reasons why. A drumbeat of media stories on climate is an obvious one, and the recent Nobel Peace Prize to Al Gore and the Intergovernmental Panel on Climate Change for the latest in a series of reports has certainly had a big impact. Less well-known, but possibly just as pivotal in this New England state, is a 2-year campaign by a group of scientists, civic leaders, and environmental activists called the Carbon Coalition.

Their rallying cry is a 204-word resolution on climate change that they hammered out in late 2006 and managed to put before 82% of New Hampshire's 221 towns at a round of public meetings held in March across the state. A large majority—164—of those towns adopted the resolution, which calls for a "national program requiring [emissions] reductions," new energy research, and "local steps to save energy." Members of the coalition have used the document to pressure candidates at hundreds of the preprimary events, small and large, in a process that affords citizens repeated, face-to-face access to the contenders.

"I've been thrilled to be a part of it," says climate scientist Cameron Wake of the University of New Hampshire, Durham, a member of the group's governing board. Wake has delivered roughly 30 speeches around the state on the topic and written a report on the impacts of global warming on the state's $400-million-per-year winter tourism industry. "But the volunteers at the Carbon Coalition deserve the majority of the credit," he adds. And the coalition is happy to accept the accolades. "Every time [a skeptical candidate] turns around, there's someone with a Stop Global Warming sticker. It makes them think," says the group's co-chair, Ted Leach, a former Republican state legislator.

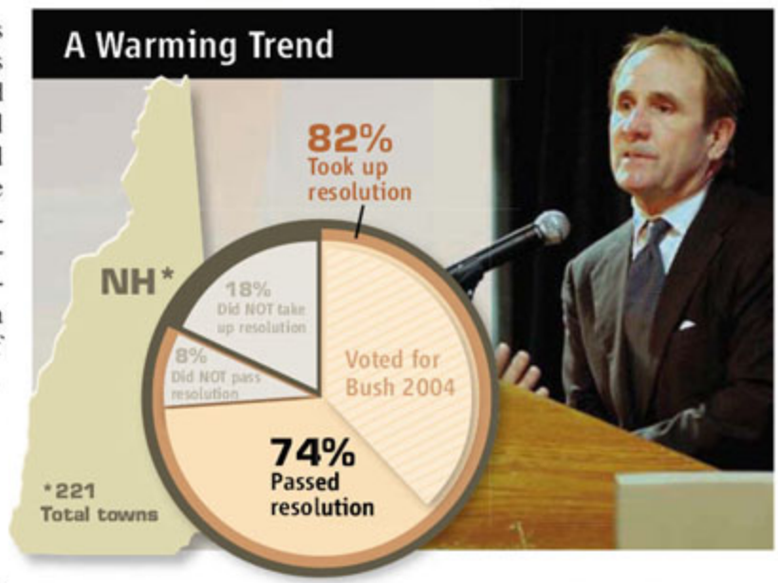

More than hot air. The University of New Hampshire's Berrien Moore speaks at an October conference sponsored by groups that pushed successfully for a climate change resolution passed by many towns across the state.

In Iowa, there's been a smaller effort to publicize the issue by a coalition of green groups called the Iowa Global Warming Campaign. Its small staff works with volunteers to attend the dozens of candidate events that occur each week. "The goal is to get Iowans to talk to candidates about climate change when they get here," says Joe Wilkinson of the Iowa Wildlife Federation in Des Moines.

Both the Iowa and the New Hampshire efforts lay heavy emphasis on how climate change might impact local ecosystems and businesses. "I used to get questions on the [legitimacy of the] science," says Wake of talks he's given around the state during the past 5 years. "Now it's, 'How will climate change affect me?'"

So Wake and a handful of climate scientists have worked hard to document both near-term and long-range effects. In Iowa, the National Wildlife Federation has distributed a report called *The Waterfowler's Guide to Global Warming* that cites federal studies of how warmer temperatures could alter migration routes and disrupt avian ecosystems. "Global warming already has ducks flying in later and leaving earlier," proclaims a radio ad in Iowa paid for by the foundation's political arm, National Wildlife Action. "When the presidential candidates come to town, make sure they spell out their plan to combat global warming."

In New Hampshire, Wake and other scientists have focused on possible effects to the ski and timber industries. In recent years, ski areas have had to make more and more of their snow, and warming threatens the winter landscape that attracts tourists, says Janice Crawford, director of the Mount Washington Valley Chamber of Commerce. The bipartisan success of the March coalition statement led Senator John McCain (R–AZ), a longtime advocate of carbon caps, to remind New Hampshire voters in a radio ad that he has "listened" to their concerns. And at an October candidates' debate sponsored by the Carbon Coalition, Huckabee announced support for a mandatory cap-and-trade system, calling greenhouse gas buildup "our responsibility."

Even candidates who have taken relatively aggressive approaches to slow climate change have faced pressure on the stump. In October, Friends of the Earth (FOE) Action ran advertisements in Iowa asking Senator Hillary Clinton (D–NY) to remove "giveaways to global ▶

SOURCE: THE CARBON COALITION; (PHOTO) CLEAN AIR-COOL PLANET

Animal-rights extremism
1856

Parting words from Britain's science adviser
1862

warming polluters" from a climate bill before a committee on which she sits (*Science*, 14 December, p. 1708). Clinton subsequently offered an amendment that would have toughened the bill, by auctioning more of the emission certificates instead of making them free to industry. Although the amendments failed, "we were pleased," says a spokesperson for FOE Action, which has stopped running the ads.

Activists are also applying pressure to those whose positions are considered fluid. Once Huckabee emerged as a top-tier contender, note activists, he stopped mentioning mandatory caps when asked about climate or energy. That possible "backtracking" worries the Reverend Richard Cizik of the influential National Association of Evangelicals in Washington, D.C., who has teamed with climate researchers to combat warming (*Science*, 24 February 2006, p. 1082). "I call and say to his campaign staff, 'Look, don't listen to his conservatives who are critical of your position; they'll come around,' " says Cizik. "They just have to be educated." **–ELI KINTISCH**

RESEARCH FUNDING

U.K. Cutbacks Rattle Physics, Astronomy

There's little seasonal cheer for British physicists and astronomers this month. A change to the funding arrangements for their disciplines has led to the axing of a number of key projects and a likely cut of 25% in their grants pot for the next 3 years. One unexpected casualty: the International Linear Collider (ILC), now in its design phase.

The sad tidings were revealed last week in the 2008–2011 budget "delivery plan" released by the U.K.'s Science and Technology Facilities Council (STFC). The council was especially blunt about the ILC, concluding: "We do not see a practicable path towards the realization of this facility as currently conceived on a reasonable timescale." That sent shock waves through the physics community. "It's terrible because a domino effect might develop," with other countries pulling out, says Albrecht Wagner, director of Germany's DESY particle physics lab and chair of the International Committee for Future Accelerators.

The United Kingdom currently contributes only 5% of the ILC's development budget but plays a leading role. "The problem is [losing] the intellectual contribution being made by the U.K.," says Barry Barish, head of the ILC's Global Design Effort.

The roots of STFC's woes lie in its origins. It was formed earlier this year by merging two of the U.K.'s seven research-funding councils: Particle physics and astronomy were folded into the council responsible for lab infrastructure. Physicists were reassured that the new STFC would not be saddled with the liabilities of the old facilities council, and things looked good in the fall when the government's Comprehensive Spending Review showed a healthy overall increase for research (*Science*, 19 October, p. 379).

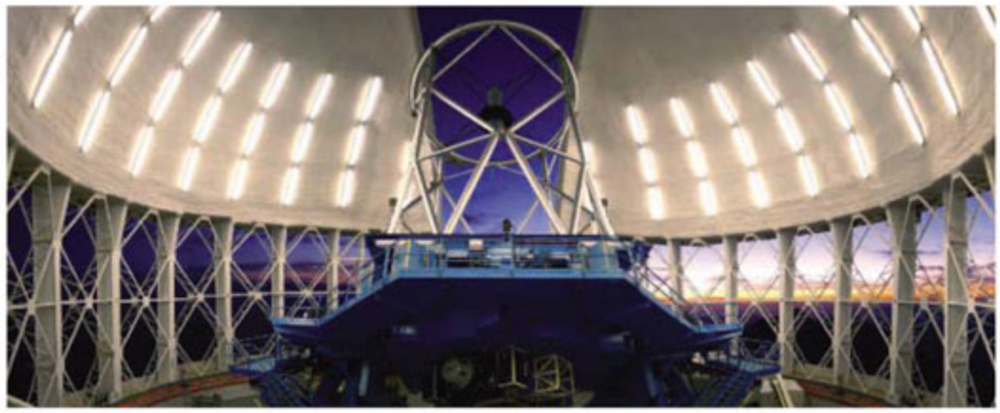

Poor outlook. U.K. astronomers could lose access to Gemini (pictured) and other facilities.

CREDIT: GEMINI OBSERVATORY/AURA

But last month, STFC announced that it was withdrawing support for the Gemini Observatory, an international facility with twin 8-meter telescopes in Hawaii and Chile. The reason is now clear: STFC received one of the smallest funding increases among the research councils, rising from £573 million ($1.2 billion) in 2007–08 to £652 million in 2010–11, an increase of 13.6% over 3 years.

An STFC spokesperson says that increase will pay in part for closing the Synchrotron Radiation Source at the Daresbury Laboratory; it will also fund an increase in the size of grants to university scientists to cover the full economic cost of their research. STFC was denied extra funding for, among other items, expected increases in the running costs of the newly opened Diamond synchrotron and the second target station of the ISIS spallation neutron source, due to open in 2008.

This leaves STFC with an £80 million hole in its budget. STFC has listed a string of cuts to shrink that hole, including the ILC, Gemini, high-energy gamma-ray astronomy, and ground-based solar-terrestrial physics. The council will also review funding for several other astronomy facilities and projects and will likely limit use of Diamond and ISIS. British astronomers were as angry as their physics colleagues. "The government needs to recognize that astrophysics, space science, and solar system science make a direct contribution to the U.K. economy," says Michael Rowan-Robinson, president of the Royal Astronomical Society.

Physicists are particularly concerned about the grant cuts because funding in recent years has been increasingly directed to big, successful physics departments, causing many smaller university departments to close (*Science*, 4 February 2005, p. 668). "The STFC seems landed in a situation where it could inflict seriously damaging cuts on university physics departments," says Martin Rees, Astronomer Royal and president of the Royal Society.

Researchers have been thrown something of a lifeline by the government's announcement last week of a review into the health of key scientific disciplines, starting with physics. Meanwhile, STFC is continuing with its planned cuts. **–DANIEL CLERY**

With reporting by John Travis and Adrian Cho.

AIDS RESEARCH

Trials of NIH's AIDS Vaccine Get a Yellow Light

POTOMAC, MARYLAND—In late September, the U.S. National Institutes of Health (NIH) in Bethesda, Maryland, at the last minute scotched a massive $130 million trial of an AIDS vaccine made by its researchers. The reason: Much to the dismay of the field, a test of a similar vaccine made by Merck & Co. found that it may have actually increased some people's risk of becoming infected with HIV. Last week, NIH's AIDS Vaccine Research Subcommittee met here to discuss the future of the NIH vaccine. Although no final decision has been made, the consensus was to continue testing the vaccine to see whether it works but in a redesigned study that reduces the chance of doing harm. "Everyone seems to think the products are different enough to warrant further testing," said Peggy Johnston, who heads AIDS vaccine research at NIH. "The issue becomes, what's the trial design going to be, and is that design feasible to carry out?"

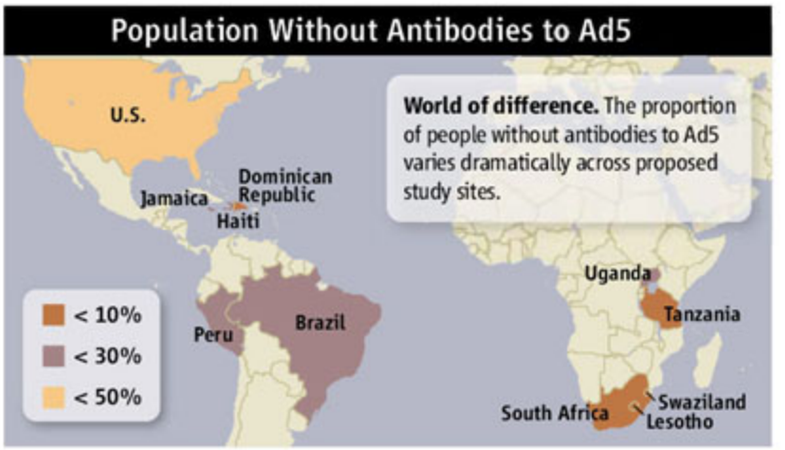

The Merck vaccine and that made by Gary Nabel's team at the NIH Vaccine Research Center (VRC) both deliver HIV genes into the body using a cold virus as a vector. The prevalence of this adenovirus 5 (Ad5)—there are more than 50 subtypes—varies greatly, infecting one-third of the population in some locales and nearly everyone in others. In the Merck study, vaccinated people who had high levels of antibody to Ad5 at the trial's start more readily became infected by HIV. Questions remain about the mechanism and whether the finding is even statistically significant (*Science*, 16 November, p. 1048). But out of caution, the group last week argued to exclude people with Ad5 antibodies from the VRC test.

Originally, Scott Hammer of Columbia University planned to lead a test of the VRC vaccine in 8500 people in the Americas and Africa. Now, as Magdalena Sobieszczyk from his group explained, they think it's prudent to enroll only 2000 to 3300 people in the Americas and Africa who are negative for Ad5 antibodies. Sobieszczyk described study designs that would include both heterosexuals and men who have sex with men.

Yet staging a trial of a vaccine that, even if it works, could not be used by people with Ad5 immunity raises ethical quandaries. "It may not be acceptable in regions where two-thirds of people are seropositive [for Ad5]," Hammer conceded. Another option is to change the vector altogether, but that would delay the trial indefinitely.

Some participants argued that the trial should be focused more narrowly—for instance, on men in the United States who have sex with men. Subcommittee member Jeffrey Lifson of SAIC in Frederick, Maryland, cautioned that the Merck results have been befuddling in part because the vaccine was tested in many different populations and locations. "I am really concerned … to show that we can do clear studies," Lifson said.

David Watkins, a primate researcher at the University of Wisconsin, Madison, argued against doing the trial at all, as monkey studies have suggested the VRC vaccine will fail, regardless of the safety issues. "I just don't get it," Watkins told *Science*. "The science seems to be really ignored." Anthony Fauci, head of the National Institute of Allergy and Infectious Diseases, said he doesn't think the field has the luxury of waiting for convincing efficacy data from monkey studies, which could take more than a decade. But Fauci did not offer his opinion during the meeting, explaining, "I'm going to have to make the final decision, and I don't want to preempt anybody." The Columbia team will present a redesigned study to the same subcommittee in January, then Fauci will announce the fate of the VRC vaccine.

–JON COHEN AND BENJAMIN LESTER

CREDITS (TOP TO BOTTOM): ADAPTED FROM SCOTT HAMMER/COLUMBIA UNIVERSITY; JULIANNE A. RICHTER II

SCIENTIFIC PUBLISHING

Bruce Alberts Named *Science* Editor-in-Chief

Bruce Alberts, professor of biochemistry and biophysics at the University of California, San Francisco (UCSF), and president emeritus of the U.S. National Academy of Sciences, has been named the next editor-in-chief of *Science*. A prominent cell biologist best known for his work on the protein complexes that allow chromosomes to be replicated, Alberts has focused in recent years on public issues, especially the improvement of science education.

Alberts's appointment was announced on 17 December by the board of directors of AAAS, publisher of *Science*. AAAS President David Baltimore, who chaired the search committee that nominated Alberts, says his "experience, skill, and interest in all of science make him the ideal person to continue the tradition of superb editors who have made *Science* the premier journal for the scientific community." Alberts will take over the editorship on 1 March 2008 from Donald Kennedy, who announced earlier this year that he would be retiring. Kennedy has served as editor-in-chief since 2000.

Alberts, 69, earned a doctorate from Harvard University in 1965, spent 10 years on the faculty of Princeton University, and moved to UCSF in 1976. He has published more than 150 research papers and is one of the original authors of a leading textbook, *Molecular Biology of the Cell*. He served two terms as president of the National Academy of Sciences, from 1993 to 2005. Then he returned to UCSF to continue working on issues he emphasized during his tenure at the academies: internationalizing science—especially building links to scientists in the developing world and strengthening scientific infrastructures—and improving science education.

Alberts will retain his UCSF faculty position and expects to devote half of his time to *Science*. "I view *Science* magazine as a critical venue for maintaining the standards of science, as well as for spreading an understanding and appreciation for science around the world," says Alberts. "With the tremendous challenges we face today, both of these important aims need constant attention."

MICROBIOLOGY

Detoxifying Enzyme Helps Animals Stomach Bacteria

Scientists since Louis Pasteur have puzzled over a visceral issue: How can we live in peaceful coexistence with the scads of potentially noxious bacteria in our guts? Last week, a University of Oregon team reported a key insight: When bacteria colonize vertebrate intestines, the tissue produces an enzyme that appears to defuse a dangerous toxin the microbes wield. The work "offers a novel explanation for the ability of humans to coexist with our microflora," says Lora Hooper, an immunologist at the University of Texas Southwestern Medical Center in Dallas. It provides a "satisfying explanation for how we can maintain a friendly relationship with the hundred trillion bacteria in our guts."

In many parts of the body, just a few bacteria may spark a massive inflammatory reaction. One bacterial compound, lipopolysaccharide (LPS), for example, can trigger septic shock, organ failure, and death. But in our intestines, dense populations of bacteria reside without eliciting more than a blink from the immune system. These microbes benefit us in multiple ways. They make essential vitamins, keep menacing germs at bay, help digest food for us, and influence our development and physiology.

To probe how animal intestines tolerate their microbial colonizers, microbiologist Karen Guillemin of the University of Oregon, Eugene, uses zebrafish as a host. These fish are transparent, so investigators can see microbes inside. Moreover, the fish's immune systems and digestive tracts function similarly to those of mammals.

Last year, Guillemin and colleagues reported that cells in the intestinal lining of zebrafish raised under germ-free conditions did not produce intestinal alkaline phosphatase (IAP), an enzyme that clips phosphates from a wide range of molecules but whose function in living organisms is unclear. Adding back typical gut bacteria or LPS restored IAP production, Guillemin found.

Other groups have shown that IAP can remove phosphate groups from LPS, which reduces its toxicity. "So we thought, 'Aha, maybe the normal substrate for IAP is LPS associated with the normal flora,' " says Guillemin. If the enzyme neutralizes LPS, fish with compromised IAP activity should be especially susceptible to LPS, Guillemin reasoned. As predicted, thwarting IAP in zebrafish by chemical or genetic means increased their sensitivity to LPS-induced death, she and her colleagues report in the 13 December issue of *Cell Host & Microbe*.

Next, the researchers found that the intestines of germ-free fish lacked neutrophils, bacteria-killing cells that migrate to infection sites. When bacteria were allowed to colonize the animals' guts, these inflammatory cells showed up as well. And blocking IAP production or activity boosted their numbers. "The hyperinflammation we see in the absence of IAP is in response to something associated with the normal bacteria, most likely LPS," says Guillemin. These findings suggest that IAP dampens the inflammatory response to the normal gut microflora, thus promoting host tolerance to the bacteria.

"It's such a straightforward way to deal with a toxin: Just detoxify it," says microbiologist Victor DiRita of the University of Michigan Medical School in Ann Arbor. "We teach medical students that LPS from normal flora are nontoxic. [Guillemin's] work suggests that it's more complicated. LPS [from some bacteria] are toxic, but the host has a way to deal with that."

Other researchers have established that ▶

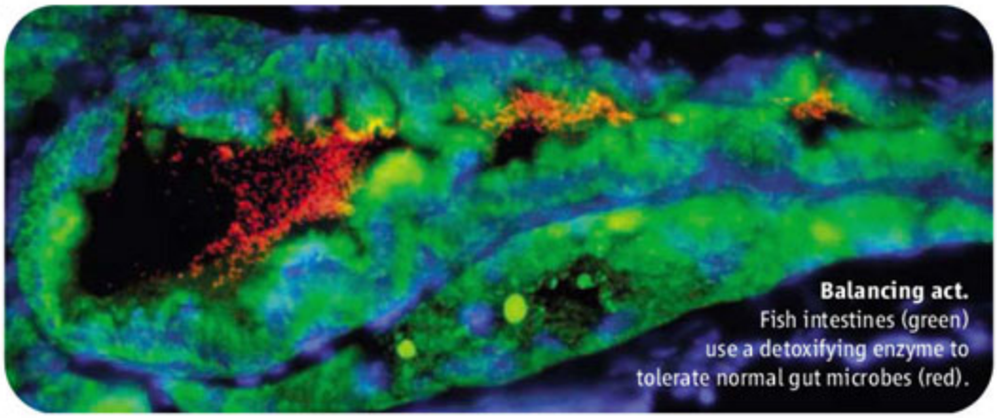

Balancing act. Fish intestines (green) use a detoxifying enzyme to tolerate normal gut microbes (red).

CREDIT: IMAGE COURTESY OF JULIE TOPLIN AND KAREN GUILLEMIN

New Animal-Rights Attacks

Last week, British police arrested well-known animal-rights activist Mel Broughton in connection with arson attacks last year and in the spring against the University of Oxford. The police have not, however, charged him with setting fire to two Oxford professors' cars in early November, actions that also appear related to animal-rights protests. Someone posting on the Animal Liberation Front's Web site has claimed credit on behalf of the group for those previously unreported fires at the homes of "researchers connected to the [university's] notorious Department of Experimental Psychology." A university spokesperson confirmed the car fires but declined to reveal the professors' names.

The car arsons reflect a trend of more-personal attacks by animal-rights extremists (see p. 1856). In contrast, Broughton was arrested in relation to attempted arsons on university facilities. He's charged with two counts of possession of an explosive substance, two counts of having an article with intent to damage, and one count of conspiracy to blackmail. Broughton's lawyer did not respond to a request for comment.

–JOHN TRAVIS

Save the Fish

For the first time, scientists at the U.S. National Marine Fisheries Service in Seattle, Washington, have recommended a cut in Alaska's commercial harvest of pollock (*Theragra chalcogramma*). Although the move will cost this billion-dollar industry tens of millions of dollars, fishing interests have accepted the scientists' reduction. Next year's harvest will be decreased from nearly 1.4 million metric tons to 1 million metric tons—an almost 28% drop and its lowest level since 1999. A further cut may be required in 2009. The reduction stems from annual surveys that track the size and health of different age classes of this groundfish.

For 5 years in a row now, the number of juveniles successfully attaining adulthood has been below average, possibly because of unusually warm bottom waters. Some science advisers to the North Pacific Fishery Management Council, an 11-member panel charged with regulating commercial fishing off the coast of Alaska, think that the harvest should be reduced even further, to 555,000 metric tons, citing concerns from many fishers that the large aggregations of pollock in the Bering Sea that have fueled the fishery for 30 years are difficult to find. "It's time to alter course and further reduce the harvest to save this incredibly lucrative fishery," says Juneau, Alaska, ecologist Michelle Ridgway, a council adviser.

–VIRGINIA MORELL

administering IAP to animals protects them from LPS, and inhibiting the enzyme's activity with chemicals renders rats susceptible to death from injected bacteria. But Guillemin's paper is the first published study to show that animals use IAP to rein in LPS from regular gut bacteria under natural conditions, says developmental biologist José Luis Millán of the Burnham Institute for Medical Research in San Diego, California. His unpublished work on mice that lack IAP bolsters the notion that the enzyme helps hosts maintain a healthy relationship with their gut bacteria.

If these results extend to humans, an individual's degree of IAP activity could shape predisposition to serious ailments, such as sepsis and Crohn's disease. "Perhaps people with less-active IAP would be more resistant to bacterial infections but more prone to chronic inflammation," Guillemin speculates. If so, turning IAP activity up or down either with drugs or by administering the enzyme itself might reset the balance.

–EVELYN STRAUSS

EVOLUTION

Did an Asteroid Shower Kick-Start the Great Diversification?

You've heard of the Cambrian Explosion, the sudden first appearance of all the basic animal forms, about 540 million years ago. And of course, the iconic dinosaurs went out with the bang of a huge impact 65 million years ago. But what about the Great Ordovician Biodiversification Event? That was when some uncharismatic critters living quietly on the sea floor exploded in number and taxonomic variety in life's biggest burst of evolutionary variety, about 465 million years ago. Why some but not all marine life should have taken off like that has puzzled scientists as thoroughly as the death of the dinosaurs ever did.

This week, a team of geologists and paleontologists reports that a collision in the asteroid belt showered Earth with debris just when the Ordovician diversification was getting started. The close coincidence of impacts and diversification suggests—although it does not yet prove—a cause-and-effect connection, researchers say. "It's intriguing," says paleontologist Jan Smit of the Free University of Amsterdam. "The coincidence is very good. The question is, how do you induce an increase in diversity with impacts?"

There hasn't been any doubt about the shower of meteorites in the middle of the Ordovician period. Geologist Birger Schmitz of Lund University in Sweden and colleagues retrieved weathered but recognizable, fist-sized meteorites from mid-Ordovician rock in such abundance that they could calculate a 100-fold surge in meteorite falls over a few million years (*Science*, 5 October 2001, p. 39). At about the same time as the shower on Earth, according to meteorite analyses, a collision had shattered a large asteroid in the asteroid belt, presumably pelting Earth with the sort of debris Schmitz recovered.

In work reported online this week in *Nature Geoscience*, Schmitz and colleagues sharpened their view of the asteroid shower by intensively sampling for smaller markers of asteroidal material at two sites in southern Sweden and one in China. They analyzed the samples for isotopes of the element osmium, because extraterrestrial rock is richer in osmium-187 relative to osmium-188. And they dissolved several score 10- to 30-kilogram-size samples of limestone in acid in search of microscopic grains of the mineral chromite. That is the one extraterrestrial mineral that can survive hundreds of millions of years unaltered. They brought the Ordovician diversification into clearer focus by compiling data from more than 30,000 fossil brachiopods—stalked, clamlike bottom-dwellers—across strata of the same age in southern Sweden.

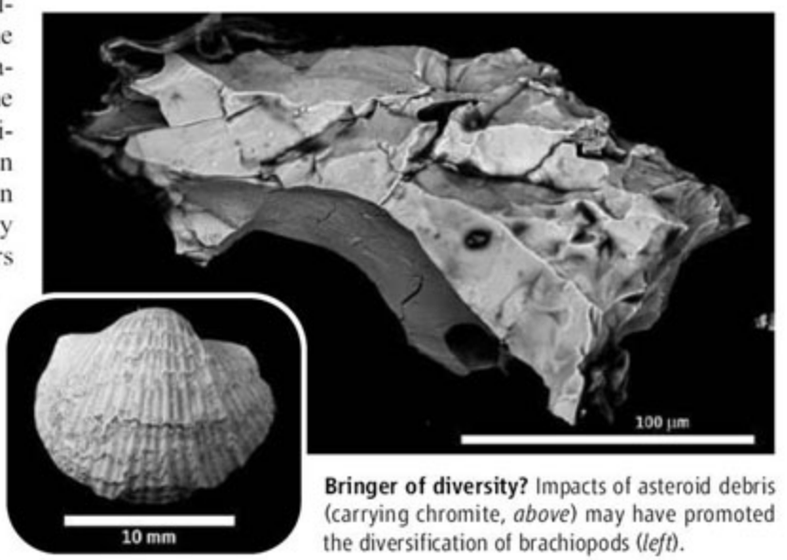

Bringer of diversity? Impacts of asteroid debris (carrying chromite, *above*) may have promoted the diversification of brachiopods (*left*).

The two detailed records from rocks of the same age showed that the onset of the rain of debris on Earth and the main burst of diversification "coincide precisely," writes the group. A sharp spike in new brachiopod species, families, and genera and the beginning of the resulting steep rise in diversity coincide within a few decimeters of rock (a few tens of thousands of years) with a rise in the osmium isotopic ratio. Such an osmium signature marks the arrival of dust from the asteroid disruption, because dust is the first debris to arrive from the asteroid belt. Within less than a meter (roughly half a million years), abundant chromite grains appear at all three sites, borne by larger, later-arriving bits of debris. Later still, the rate of crater-forming impacts increased five- to 10-fold, by Schmitz's estimate, still during the ongoing diversification.

"We have shown the coincidence," says Schmitz, "and the data are reproducible [at three widely separated sites]. There could be some connection between the biggest [asteroid] breakup event and evolution going on in this interval." The group speculates that the pummeling during a few million years might have favored brachiopods and other immobile, filter-feeding organisms over animals such as the trilobites carried over from the Cambrian. Perhaps impacts created a more varied environment with new ecological niches on the sea floor that brachiopods were more adept at filling.

Veterans of the debates about the impact-triggered death of the dinosaurs are impressed by the Ordovician evidence. Claims of other impact-evolution connections have come and gone, but in the Ordovician, "the timing is really perfect," says geologist Philippe Claeys of the Free University of Brussels, Belgium. "That is very convincing." "They have a temporal coincidence," agrees geochemist Christian Köberl of the University of Vienna, Austria, "but they are very vague about a mechanism" linking impacts and diversification. More kinds of fossils from more places are in order, says Claeys, and, adds Köberl, a search for really large impact craters of the right age would help.

–RICHARD A. KERR

CREDITS: A. CRONHOLM; (INSET) D. A. T. HARPER

UNIVERSITIES

Questions Swirl Around Kessler's Abrupt Dismissal From UCSF

David Kessler, the high-profile dean of the University of California, San Francisco (UCSF), School of Medicine, was fired last week, for reasons that have so far not been disclosed by the university. Kessler and the university had been at odds over "financial irregularities" Kessler says he discovered shortly after taking the post in 2003.

In a 17 December statement, the university said that Chancellor J. Michael Bishop asked Kessler, former dean of Yale School of Medicine and former commissioner of the Food and Drug Administration, in June to hand in his resignation by the end of the year. With no resignation forthcoming, Bishop formally dismissed him on 13 December. "The reasons for Dr. Kessler's dismissal … cannot be discussed, as they represent personnel matters that are held confidential in compliance with University policy and state law," the statement read. As *Science* went to press, Bishop was not granting interviews.

Kessler and UCSF had a long-running disagreement involving the amount of discretionary funds available to the dean's office for uses such as research and educational initiatives, faculty recruitment, and renovations. Kessler says there was far less money than he was led to believe when UCSF recruited him away from his Yale post. At that time, Kessler says UCSF gave him documents, which he forwarded to *Science*, showing gross income of $46.4 million for the most recent fiscal year (2001–2002), resulting in a $9.9 million surplus after expenditures. Kessler says this level of funding—which the university projected would continue—was key in his decision to move to UCSF.

But when Kessler asked Jed Shivers, then vice dean for administration, finance, and clinical programs, to conduct a review in late 2004, the numbers didn't match—even for fiscal years that had already come to a close. For 2001–2002, for example, Shivers's analysis showed income of just $28.3 million and a deficit of $7.8 million, which would deplete the dean's account within a few years. Kessler says he was baffled: "For the same closed year, how can you have two different revenue numbers?"

Shivers, now at Albert Einstein College of Medicine in New York City, says his team at UCSF was never able to square the numbers Kessler was originally given. "To this day, we can't figure out how the data he received could be reconciled to the books of the university," he told *Science*. Yet according to UCSF's 17 December statement, the university auditor found no financial irregularities; neither did two additional reviews, one by a group of senior financial officers and another by an outside accountant.

In that statement, UCSF "categorically denies" that Kessler "was dismissed in retaliation for his allegations about financial irregularities in the UCSF School of Medicine." Several senior faculty members say they are confident that Bishop had just cause. "From my experience, Chancellor Bishop would not have made such a decision without considerable reflection and reason," says Peter Carroll, chair of the urology department. "My sense is that this is much more than simply the finances in the dean's office." UCSF biochemist Bruce Alberts (who was named this week as the next editor in chief of *Science*) offers a different hypothesis:

CREDIT: MAJED/UCSF

Ousted. David Kessler was fired from his post as dean of UCSF's School of Medicine.

"David is a very capable person, but he got fixated on this [idea] that he was misled and he was being sabotaged by not having the resources he needed to be an effective dean, and it got in the way of the medical school's relationship with the rest of the university."

Kessler plans to retain his post as professor of pediatrics/epidemiology and biostatistics at UCSF. Samuel Hawgood, chair of the pediatrics department and physician in chief of UCSF Children's Hospital, has been appointed interim dean. **–GREG MILLER**

Researchers: Folly in Bali

Last week's United Nations meeting in Bali, Indonesia, broke little new ground on mandatory emissions targets, say disappointed scientists who attended the conference. The meeting was held to discuss how to follow up the 1997 Kyoto agreement on climate change, which expires in 2012. It was extended for 1 day so that delegates could issue a joint call for negotiations to achieve a "long-term global goal for emission reductions." The conferees also agreed to allow developing countries to protect rainforests now and get credit later.

Kevin Trenberth of the National Center for Atmospheric Research in Boulder, Colorado, called the U.S. role at the meeting "obstructionist." Trenberth joined more than 200 scientists in supporting mandatory caps of at least 50% below 1990 levels by 2050, a position that the Bush Administration opposes.

–ELI KINTISCH

Moon Shot Gets Nod

Astronauts may someday again walk on the moon, but before then, a new mission will look deeply into the lunar interior. NASA last week backed a $375 million effort to measure the moon's gravity field using two orbiting spacecraft. The Gravity Recovery and Interior Laboratory mission, led by geophysicist Maria Zuber of the Massachusetts Institute of Technology in Cambridge, beat out 24 other proposals in NASA's Discovery competition. The spacecraft is slated for a 2011 launch, and NASA science chief S. Alan Stern says the approach could be used on future missions to Mars and other solar system bodies. **–ANDREW LAWLER**

New Euros Flow

The fledgling European Research Council has selected 300 applicants to receive its first set of grants, aimed at those in their first decade of independent research. Chosen from more than 9000 applications, the winners represent 32 nationalities working in 21 countries and will receive total funding of approximately €290 million. The United Kingdom will host the most awardees with more than 50 planning to work there. Martin Bergö of Göteborg University in Sweden, who was awarded €1.7 million to study the proteins involved in cancer and premature aging, says the application process was "absolutely flawless" and devoid of the infamous European Union bureaucracy. The application process for the second round of grants is now under way. **–GRETCHEN VOGEL**

Animal Extremists Get Personal

As animal-rights extremism wanes in the United Kingdom, U.S. researchers have faced increasing threats and harassment

EARLY ONE SUNDAY MORNING LAST JUNE, Arthur Rosenbaum was getting ready to go to a yoga class when his doorbell rang. A neighbor had noticed a suspicious bundle under Rosenbaum's white BMW sedan. The two walked out to the car, which was parked on the street of their leafy neighborhood near the campus of the University of California, Los Angeles (UCLA), where Rosenbaum is chief of pediatric ophthalmology and strabismus at the Jules Stein Eye Institute. Under the right front wheel was a plastic container full of an orangish liquid with a rag sticking out of a nozzle at one end. On the curb was a matchbook with a half-smoked cigarette woven through the matches. Rosenbaum thought it was a prank.

It turned out to be a crude incendiary device. At his neighbor's urging, Rosenbaum called the police, who quickly called in the bomb squad. By midmorning, Rosenbaum's block had been evacuated, and investigators told Rosenbaum that the device could have destroyed his car if it had gone off as intended. They suspected it was the work of animal-rights extremists, who have targeted several UCLA researchers in the past year and a half.

Rosenbaum says that at the time he didn't believe it. After all, he is primarily a surgeon, operating hundreds of times a year to correct the vision of children with eye muscle disorders. He has ties to only one animal-research project, a pilot study to test an electrical stimulator that could bring paralyzed eye muscles back to life.

That one project turned out to be enough to put Rosenbaum on the hit list of a group calling itself the Animal Liberation Brigade, which claimed responsibility for the incident 3 days later in an online communiqué on 27 June. In the subsequent months, Rosenbaum says, anti–animal research activists have staged several protests at his home, sometimes at night, concealing their faces with bandanas and ski masks and using bullhorns to shout insults in "the most obnoxious, vile language." Neighbors within two blocks of Rosenbaum's house have received graphic pamphlets condemning his "imprisonment, torture, and murder of innocent primates," and his wife received a letter stuffed with razor blades and threatening physical harm unless she convinced Rosenbaum to stop his animal research.

Vandalized. This summer, ALF sprayed graffiti on the home of one researcher at Oregon Health and Science University; a colleague received similar treatment earlier this month.

Animal researchers in the United Kingdom have long endured such personal threats and harassment. In the United States, however, research facilities, not individuals, have been the most frequent targets—until recently. U.S. researchers have seen a spate of recent attacks by groups that consider destruction of private property and threats of personal violence to be justifiable tools in their fight to end animal research. And although recent legislation has helped U.K. police crack

CREDITS (TOP TO BOTTOM): OHSU

Warning sign. Following protests at Oregon Health and Science University in April, vandals targeted the homes of two researchers.

down on animal-rights extremists, fewer such measures exist in the United States, leaving universities struggling to come up with ways to safeguard their researchers.

UCLA, which has had more than its share of disturbing incidents, is leading the way. After being criticized for what some considered an anemic response to earlier threats and harassment, the university crafted a plan to protect its researchers that now draws praise from many quarters. "UCLA is showing some genuine leadership," says Norka Ruiz Bravo, deputy director for extramural research at the National Institutes of Health (NIH) in Bethesda, Maryland.

But that's not enough, say some researchers who have been targeted. They and others want to see scientific societies and funding agencies take a more active role. Change is needed on the legal and law enforcement fronts, too. Despite the recent incidents, there's little sense of urgency in the scientific community, says Robert Palazzo, president of the Federation of American Societies for Experimental Biology in Bethesda. "Where's the noise on this?" he asks.

An ugly turn of events

Overall numbers of illegal incidents by U.S. animal-extremist groups are up sharply in recent years, according to figures from the National Association for Biomedical Research (see graphic, p. 1858). Anecdotal evidence suggests that personal threats and home vandalism have risen as well. "It used to be that most of the activities centered around breaking into laboratories, … [but now] the animal activists have decided to go after the homes and families of scientists, which has ratcheted up the anxiety and danger," says Jeffrey Kordower, a neurobiologist at Rush University Medical Center in Chicago, Illinois, and chair of the Society for Neuroscience's Committee on Animals in Research.

The troubles that had been simmering below the surface at UCLA began to boil over the night of 30 June 2006, when an incendiary device was delivered to a home in nearby Bel Air. The device was intended for Lynn Fairbanks, who studies primate genetics and behavior at the UCLA Neuropsychiatric Institute, but instead was left on the doorstep of a 70-year-old neighbor. If it had gone off, investigators concluded, the house and any inhabitants could have been engulfed in flames. On 11 July 2006, the Animal Liberation Front (ALF) claimed responsibility for planting the device.

Shortly after that incident, UCLA neurobiologist Dario Ringach announced that he was giving up his research with nonhuman primates. "Please don't bother my family any more," Ringach wrote in an e-mail to animal activists dated 6 August 2006. The subject line read simply: "You win." Ringach declined to comment for this article, but colleagues say he feared for the safety of his two young children, who had been frightened by masked protesters who came to his home on several occasions, sometimes banging on the children's bedroom window at night. The Fairbanks incident may have been the last straw. Colleagues say Ringach now conducts his research entirely with human volunteers and has not been harassed further.

In the most recent incident, on 20 October, vandals flooded the Beverly Hills home of UCLA neuropharmacologist Edythe London, breaking a first-floor window and inserting a running garden hose. Not at home that night, London and her husband discovered the damage the following day. They expect the repairs to cost about $30,000. In a communiqué dated 25 October, ALF activists wrote that if not for the fear of starting a brushfire, arson would have been their first choice. "It would have been just as easy to burn your house down, Edythe. As you slosh around your flooded house consider yourself fortunate this time."

Unlike many targeted researchers, London spoke out. In a 1 November editorial in the *Los Angeles Times*, she wrote that her research on the biological basis of addiction—which focuses on human brain imaging but also involves some work with primates—was motivated in part by the death of her father, a chronic smoker. "We are also testing potential treatments, and all of our studies comply with federal laws designed to ensure humane care" of animals, she wrote.

The letter elicited a variety of responses, some supportive, some not. One writer compared London, the daughter of Holocaust survivors, to Nazis who experimented on concentration camp prisoners, a common theme on Web sites and blogs of extremist groups. "They honestly and truly believe that animals are equal to Jews in the Holocaust, and they are fighting to liberate them," says one targeted researcher.


SEEKING INFORMATION

IMPROVISED INCENDIARY DEVICE

LOS ANGELES, CALIFORNIA

THE DETAILS SURROUNDING THE CRIME

The FBI, ATF, Los Angeles Police Department, and Los Angeles Fire Department, as part of the Joint Terrorism Task Force, (JTTF), are seeking information regarding an improvised incendiary device placed on the front porch of an elderly resident's home on Rosecrest Road in Los Angeles on June 30, 2006. Although the device failed to ignite as the victim's door, arson investigators believe many innocent lives could have been lost had the device functioned properly.

Investigators has determined that the victim residence was most likely not the intended target of the attack. On July 11, 2006, an animal rights terrorist syndicated that the Animal Liberation Front (ALF) had taken credit for this act, but has yet to admit placing the device at the wrong residence.

REWARD - $60,000

A reward of up to $60,000 is being offered for the identification, arrest, and conviction of the individual or individuals responsible for this crime.

IF YOU HAVE ANY INFORMATION CONCERNING THIS CASE, PLEASE CONTACT YOUR LOCAL FBI OFFICE OR THE NEAREST AMERICAN EMBASSY OR CONSULATE.

ROBERT S. MUELLER, III
DIRECTOR
FEDERAL BUREAU OF INVESTIGATION
UNITED STATES DEPARTMENT OF JUSTICE
WASHINGTON, D.C. 20535
TELEPHONE: (202) 324-3000

CREDIT: FBI

Reward. Despite hefty reward offers, no arrests have been made in two cases involving incendiary devices intended for UCLA researchers.

Learning from the past

In the aftermath of the 2006 attack on Fairbanks and Ringach's decision to give up his animal research, UCLA was sharply criticized for reacting too slowly and without sufficient force. An editorial by *Science* Editor-in-Chief Donald Kennedy noted that then–acting Chancellor of UCLA Norman Abrams waited several weeks before condemning the attacks in a public statement (*Science*, 15 September 2006, p. 1541). Fifteen faculty members in Ringach's department signed a 28 August 2006 letter lamenting the "apathetic" response of the UCLA community.

In mid-September, Abrams appointed a task force to look into what the university should be doing. The task force, chaired by law school professor Jonathan Varat, delivered its report in December 2006. The document argues that the university has an obligation to protect its faculty members not just on campus but at their residences as well. Many of its recommendations have been put into place, says Roberto Peccei, UCLA's vice chancellor for research. For one, the university appointed a high-level point person for all issues related to animal activism who is on call 24/7 to coordinate the response to any incidents. Under new agreements with police in surrounding communities, UCLA campus police now respond to incidents at faculty members' homes and patrol some neighborhoods previously outside their jurisdiction. The university has paid for various security measures at some faculty members' homes. Reaching out to nonviolent student groups that have animal welfare concerns is also part of the plan.

This year, when ALF claimed responsibility for the device left under Rosenbaum's car, Abrams issued a statement immediately condemning the "criminal and deplorable tactics" and reaffirming the university's commitment to protecting its faculty members and their families. UCLA's new chancellor, Gene Block, who took over from Abrams on 1 August, issued a similarly forceful statement after London's home was vandalized. She and Rosenbaum say that they're grateful for the

university's support. "There was a lot of criticism [of the response to the 2006 incidents], and I think the university took that to heart," says Rosenbaum.

Spurred by the attack on Rosenbaum, UCLA also decided not to comply with requests for animal protocols and other research-related materials made via the Freedom of Information Act (FOIA). This and other public-record laws are intended to give private citizens access to information held by public agencies, and animal activists use them to gain access to research records. (The Web site of the Primate Freedom Project, for example, contains a fill-in-the-blanks FOIA request letter for research animal records, along with the addresses of several major primate centers.)

In December 2006, the university received a California Public Records Act request for animal protocols for all primate researchers from Jeremy Beckham of Salt Lake City, Utah, says UCLA campus counsel Patricia Jasper. Researchers at the University of Utah say Beckham has been an active animal-rights campaigner on campus. In response, UCLA provided redacted documents, with some names and details omitted, in April 2007, 2 months before the attack on Rosenbaum. These documents are posted in their entirety on the Animal Liberation Press Office Web site, along with a link to Rosenbaum's research project in NIH's CRISP database. That was the deciding factor, says Peccei. "I presume that this path will eventually lead us to court," Peccei says. "But we have taken the position that at this moment our researchers are in danger, and we are not willing to release these records."

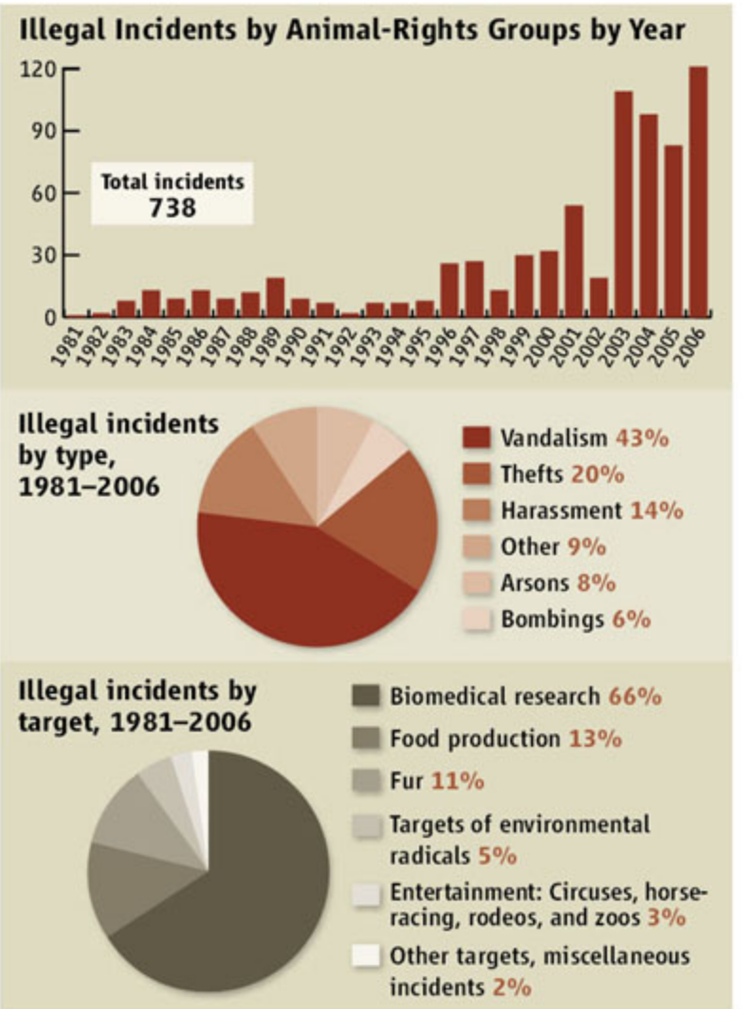

SOURCE: NATIONAL ASSOCIATION FOR BIOMEDICAL RESEARCH

Now what?

Already, the UCLA plan is being used as a model. At the University of Utah in Salt Lake City, where several researchers have been recent targets, faculty members used the UCLA plan as a guide for developing their own, says Jeffrey Botkin, chair of the university's research animals committee. The Society for Neuroscience drew on the UCLA plan for its document, *Best Practices for Protecting Researchers and Research*, scheduled for release early next year, says society president Eve Marder. She hopes that institutions will use the document to prepare before extremists strike "so that they're never blindsided by anything that happens."

Some universities are taking additional proactive steps. The Salt Lake City Council, at the university's urging, passed a law in July that bans protests within 100 feet (30 meters) of private homes. The ordinance was modeled on similar ones in other states that have been used successfully to limit harassment of doctors who perform abortions, Botkin says.

At a workshop on animals in research at the recent Society for Neuroscience annual meeting in San Diego, California, researchers expressed frustration that NIH and other agencies aren't doing more to help protect the scientists they fund. Some, for example, would like to see NIH remove investigators' names and certain key words from the CRISP database to make it harder for animal-rights groups to find them. NIH's Ruiz Bravo balks at that idea: "We have to balance transparency in government with those kinds of genuine concerns." Others at the workshop argued that scientific societies should do more to raise public awareness of the benefits of animal research—for veterinary as well as human medicine—and to counter the assertion that researchers have no concern for animal welfare.

At the end of the day, however, scientists can do only so much, says Simon Festing, director of the Research Defence Society, an advocacy group based in London. "Animal-rights extremism is a criminal matter, and … we have to look to government and police to stop illegal activity." In the United Kingdom, attacks on researchers have declined sharply in recent years, largely as a result of better policing, Festing says. In 2004, for example, the United Kingdom formed a National Extremism Tactical Coordination Unit to advise local police about how to deal with extremists and prevent attacks. The unit helped coordinate a 2-year investigation involving more than 700 police, culminating in May with raids in the United Kingdom, the Netherlands, and Belgium and the arrest of 30 suspected extremists. So far, 19 have been charged with crimes including theft and blackmail.

Legal changes have helped as well, Festing says. The 2005 Serious Organised Crime and Police Act gave police more power to go after extremists who wage an organized campaign of intimidation and violence against a university or some other institution. Amendments to existing laws, such as beefed-up "antisocial behaviour ordinances" that outlaw protests at individual homes that a reasonable person would view as intimidating, have helped close loopholes exploited by animal-rights extremists, Festing says.

Aid for U.S. researchers may eventually come from the federal Animal Enterprise Terrorism Act, signed into law in November 2006. That law expands previous protections for "animal enterprises" such as research centers to include associated individuals and businesses. Under the law, threats and harassment at a researcher's home can now be prosecuted as acts of terrorism. (Peaceful demonstrations and other activities protected by the First Amendment to the Constitution are not affected.) The new law has not yet been used to prosecute anyone because no arrests have been made in appropriate cases, says Janice Fedarcyk, special agent in charge of counterterrorism in the Los Angeles office of the FBI. Fedarcyk says that it's possible the new law could be used to prosecute those behind the UCLA incidents—if and when they are caught.

–GREG MILLER

CLIMATE CHANGE

Global Warming Coming Home to Roost in the American West

Assigning blame for regional climate disasters is hard, but scientists have finally implicated the greenhouse in a looming water crisis

SAN FRANCISCO, CALIFORNIA—The world is warming and humans are to blame, scientists declared with considerable confidence this year, but what about changes that really matter to people? Those often occur on a smaller, regional scale rather than globally, making them harder to pin on human activity with any confidence.

But last week at the fall meeting of the American Geophysical Union here, a group of 11 climate scientists from five institutions announced that they have securely tied the shrinking snowpack of the American West to a human-induced warming there. "Nobody has ever really explained why it's happening," said climatologist Tim P. Barnett of the Scripps Institution of Oceanography in San Diego, California, a leader of the group. "We've got a real serious problem," he said, because the thirsty West depends on a heavy, late-melting snowpack to fill its reservoirs in late spring. Plants and animals are feeling the effects of melting ice and snow as well. If the climate models that simulated the past warming and melting so well are anywhere near the mark, said Barnett, "we're heading for a water crisis in the West."

Barnett and his colleagues tied the water changes in the West to human-triggered greenhouse warming much the way the Intergovernmental Panel on Climate Change linked global warming to humans earlier this year (*Science*, 9 February, p. 754). Changes in the American West during the past few decades had become obvious. It was getting warmer. The amount of snow accumulating during the winter was decreasing. And snow was melting faster in the spring, delivering its water to rivers earlier. That made sense, but was it all just a swing in some natural cycle that would soon switch back to a cooler climate and bigger snowpacks?

To find out, Barnett and colleagues ran specially modified climate models. Starting with two models of the world's climate, they beefed up the level of detail simulated in the models, but only for the West. That provided the needed realism for a climate property as patchy as snowpack without overtaxing the available computer power. They found that the models could produce the observed trends in temperature, snowpack, and river flow of the past few decades only when they included the actual amounts of humanmade greenhouse gases and pollutant hazes. Run without them, the models poked along, warming and cooling without a long-term trend. "There's no way we can make a natural-variability explanation for what we've seen" in the West, said Barnett. "I'd put the odds at between one in 100 and one in 1000 that we were fooled. Quite frankly, it's us."

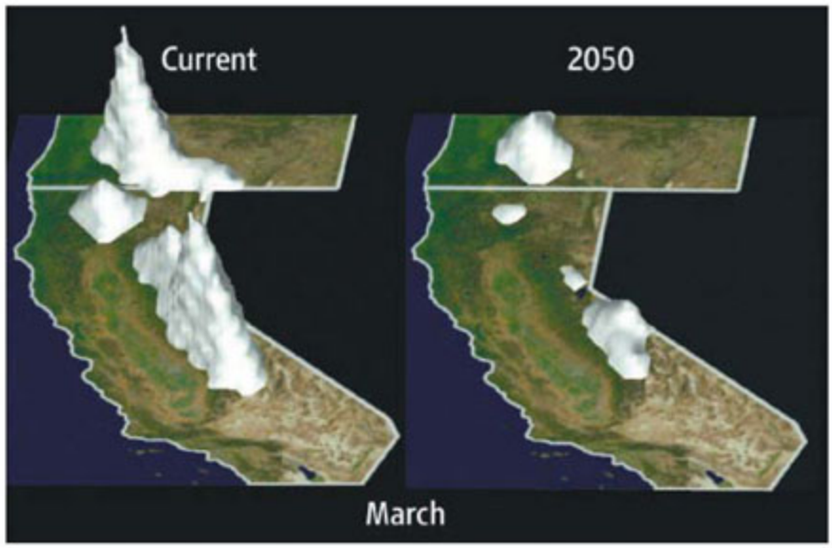

Going, going ... A human-induced warming in the American West has shrunk snowpack, and models project further shrinkage that will leave little early-spring snowpack by mid-century.

CREDIT: DAVE PIERCE/SIO/PNNL

By coincidence, the speaker before Barnett showed how the chain from smokestack to low summertime reservoirs may be longer than commonly supposed. Modeler Martin Hoerling of the National Oceanic and Atmospheric Administration in Boulder, Colorado, and colleagues reported that simulations by 26 different global models suggest that changes in atmospheric circulation, rather than the direct greenhouse effect alone, were responsible for much of the wintertime warming seen across the lower 48 states in the past 50 years. Altered winds blew in more warm air from the subtropics only in models in which mid-latitude oceans warmed as observed; apparently, the warmer oceans altered the circulation. And that ocean warming is widely viewed as being driven by the strengthening greenhouse.

The changes in the American West present a serious challenge to water users, Barnett noted. There's no less precipitation, he said, but thanks to the warming, less is falling as snow and more as rain. Dammed reservoirs in two of the West's three biggest drainage basins—the Columbia River and Sacramento–San Joaquin River basins—are already filled in winter and must pass the added water on, increasing the chance of winter floods downstream. By late spring and early summer, when use of stored water lowers reservoirs so they can receive meltwater from snow, the snowpack is already much depleted and cannot refill the reservoirs. In effect, the warming stretches out the summer dry season.

Humans could shorten the dry season again by building more dams, but the West's water problems won't all be solved by more reservoirs. Geographer Thomas Painter of the University of Utah, Salt Lake City, reported at the meeting that warming-induced melting looks likely not only to eliminate the last glaciers of Glacier National Park within a few decades but also to threaten whole ecosystems there. In the park in far northwest Montana, the iconic denizen of high-mountain streams, the bull trout, likes its late-summer waters icy cold. Without enough melting snow and ice, the bull trout will be in trouble, Painter said. Beyond mountain streams, trees are invading high-elevation meadows uncovered earlier than normal by early melting of the snowpack, reducing habitat for terrestrial alpine wildlife.

Looming water problems are not limited to the American West. Beyond the few well-studied spots, "vast areas don't even know they have a problem," said Barnett. They include large parts of Asia, India, and South America. "I've gotten a look at the future," he said, "and I don't like it."

–RICHARD A. KERR

Not so benign. A chikungunya infection can be extremely painful and even fatal.

INFECTIOUS DISEASES

Chikungunya: No Longer a Third World Disease

An explosive outbreak in a remote corner of France—and fears that it may threaten Europe and the United States—have brought fresh attention to an exotic virus

SAINT-PIERRE, LA RÉUNION—To say that few scientists used to care about the chikungunya virus is putting it mildly. The mosquito-borne disease has caused massive outbreaks for at least half a century, but they all happened in developing countries in Asia and Africa. And although the virus causes severe rashes and joint pains, it never seemed to be fatal; many even called it "benign." Few researchers took an interest.

No longer. Things have changed in large part, researchers say, because chikungunya has finally struck a rich country. In 2005 and 2006, the virus caused a massive outbreak on La Réunion, an island twice the size of New York City 700 kilometers east of Madagascar—and a French *département*. Almost 40% of the population of 785,000 fell ill. In response, the French government mounted a broad research program. A recent meeting* here showed that scientists have learned as much about chikungunya in the past 2 years as in the previous 2 decades.

They have learned that the virus can kill, for instance, that it can be transmitted from mother to child around childbirth, and that a single-point mutation may have caused it to explode here. They set up the largest screening effort ever to look for animal hosts. And already a once-abandoned vaccine is being prepared for new clinical trials, and new drugs are under study.

To date, French researchers and institutes have published the majority of many dozens of new chikungunya papers, as several speakers proudly noted. (One non-French researcher said he smelled a whiff of scientific chauvinism in the air.) But other countries are paying close attention as well, as they, too, may be at risk. The big surprise of the outbreak at La Réunion was that the infamous Asian tiger mosquito, which is spreading fast across Europe and the United States, proved an excellent vector. This summer, Italy had a small chikungunya outbreak, the first ever in Europe. There's no reason why the same couldn't happen elsewhere in Europe or in the United States, says Ann Powers, a chikungunya expert at the U.S. Centers for Disease Control and Prevention (CDC) in Fort Collins, Colorado.

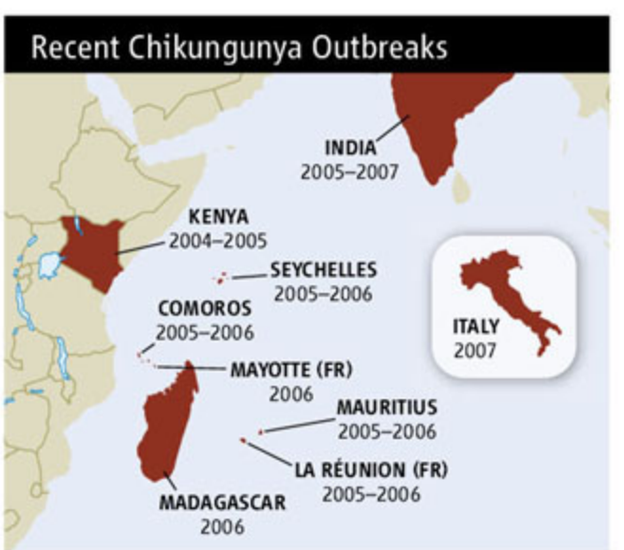

CREDIT: AP; SOURCE: PROMED, WHO

Surprise attack

Chikungunya—or "chik," as some scientists call it—belongs to the alphaviruses, a group that includes the Ross River virus in Australia and the viruses that cause eastern and western equine encephalitis, two serious diseases occurring in the United States. First isolated from a patient in Tanzania in 1953, the chik virus has surfaced occasionally since in countries across Africa, South Asia, and Southeast Asia. It causes high fevers, rash—sometimes with massive blisters—and excruciatingly painful swelling of the joints in fingers, wrists, and ankles.

The outbreak that hit La Réunion appears to have started in Kenya in 2004. It wasn't reported at the time, but in a paper published in 2007, researchers noted that the epidemic started in the coastal towns of Lamu and Mombasa, Kenya. Later, the virus appears to have gone on an island-hopping tour of the Indian Ocean, landing in Madagascar, the Comoro Islands, Mayotte—a much smaller French territory west of Madagascar—Mauritius, and the Seychelles (see map). It reached India, where it hadn't been seen for 32 years, in December 2005, infecting an estimated 1.4 million people so far, Brij Kishore Tyagi of the Centre for Research in Medical Entomology in Madurai reported at the meeting.

La Réunion inhabitants have complained bitterly that mainland France initially appeared to take little interest. Chikungunya first caused a small wave of a few thousand cases between March and July 2005. Then it all but disappeared, only to come roaring back in December. By late January 2006, 47,000 new cases were reported in a single week. Only then was a chikungunya task force set up, led by epidemiologist Antoine Flahault, dean of the French School of Public Health in Rennes and Paris.

La Réunion's location—the flight from Paris takes 11 hours—

* Chikungunya et Autres Arboviroses Emergentes en Milieu Tropical, 3–4 December.

may have contributed to the response lag, says sociologist Michel Setbon of the National Centre for Scientific Research in Aix-en-Provence, but so did the notion that chikungunya isn't such a big deal. However, the outbreak showed that, although the disease burden may get lost in poor countries facing many other scourges, chikungunya is nastier than people assumed. For starters, some patients—mostly older people with other medical conditions—ended up with severe symptoms, such as respiratory failure or brain infections, and more than 250 of them, about 0.1% of all cases, died. But even for those with milder forms of the disease, the word "benign" seemed hardly appropriate. The joint pains are crippling and can last for months, even years. The outbreak also strained the island's health care system and created economic havoc. The collapse of tourism alone—the main source of income here—caused an estimated $160 million in losses.

Currently, doctors can do little more than prescribe painkillers and general anti-inflammatory drugs to chikungunya patients, which is why France made drug discovery a priority. Hoping for a quick lead, a team led by virologist Xavier de Lamballerie of the Hôpital de la Timone in Marseille has screened 150 existing drugs—which could gain approval much faster—for activity against chikungunya in cell cultures. When chloroquine, an old antimalarial drug, seemed promising, a clinical trial was set up to test its effects in La Réunion patients. The study got going when the epidemic was on the wane, however, and only 75 patients were enrolled. Among them, the drug showed no benefit.

A subsequent study using a newly developed animal model suggested that the drug may actually do more harm than good. When Roger le Grand and his colleagues at France's Atomic Energy Commission lab in Fontenay-aux-Roses treated infected macaques with chloroquine, it prolonged infection, for reasons that aren't clear yet. That took chloroquine off the table for good, but in the meantime, two other compounds have been found—one already on the market for another disease, and one very close. They inhibit the virus much more potently, says de Lamballerie, who declined to name them.

Meanwhile, a consortium of French institutes is hoping to start safety trials in 2008 with an old vaccine that the U.S. Army Medical Research Institute of Infectious Diseases (USAMRIID) in Fort Detrick, Maryland, developed in the 1980s but later shelved as priorities shifted. The vaccine is derived from a live, weakened chikungunya strain, and USAMRIID has enough of it in its freezers to produce tens of millions of doses, Flahault says. France has procured two batches, which are now undergoing further testing in the lab; tests in macaques are the next step.

One key question is whether regulatory authorities will allow the use of a vaccine produced decades ago and deep-frozen ever since. If they don't, a pharmaceutical company would need to produce the vaccine from scratch using USAMRIID's old seed virus, which would delay development.

A better vehicle

In Africa, chikungunya is known to be transmitted in a "sylvatic cycle": The virus lurks in primates when it's not infecting humans. In Asia, such animal hosts have never been discovered; there, chikungunya is assumed to be a humans-only disease. In an attempt to find out whether animals might have played a role in the outbreak in La Réunion, a group led by Michel Brémont of the National Institute for Agricultural Research tested almost 4000 animals for signs of infection—from cats, dogs, cows, goats, and sheep to wild birds, rodents, and bats. The tests are still ongoing, but so far, all but a few have come back negative, and there's no indication that any species helped fuel the epidemic.

A more alarming finding is that the Asian tiger mosquito (*Aedes albopictus*) proved to be an efficient vector. Previously, a species called *Ae. aegypti*, which feeds on humans almost exclusively, was always the virus's main vector. *Ae. albopictus*, the predominant species on La Réunion, was considered a poor one, in part because it bites a wide variety of species. But recent studies have suggested why *Ae. albopictus* suddenly became a much better vehicle.

Between the first, small outbreak in early 2005 and the big one that started in December, the virus underwent a point-mutation change that altered a single amino acid in its envelope protein. Papers published last month by Anna-Bella Failloux of the Pasteur Institute in Paris and her colleagues and a team led by Stephen Higgs of the University of Texas Medical Branch in Galveston have shown that the change makes it much easier for the virus to reproduce in the mosquito's midgut. This leads to 100-fold higher virus concentrations in its salivary glands, which in turn increases the virus's chances of being transmitted during the next bite. Those findings strongly suggest that the mutation helped the virus adapt to the mosquito and "enhanced the epidemic," says CDC's Powers.

That's worrisome, because *Ae. albopictus*, originally from eastern Asia, has been spreading across the globe during the past 2 decades. The outbreak this summer in Italy—where *Ae. albopictus* is rampant—got started when a chikungunya patient from India traveled to a small village in the province of Ravenna. Such "imported" cases happen all the time: Mainland France had almost 800 in 2005 and 2006, and the United States 38. It's a matter of time before a patient kicks off a new outbreak in an unexpected place, Higgs says.

If that happens, controlling mosquitoes is the only way to halt the spread of the virus, but *Ae. albopictus* is notoriously difficult to fight. At La Réunion, government agencies sprayed massive amounts of insecticides; the outbreak ended, but opinions differ on how much spraying contributed. The epidemic may just have run its course.

The Italian government is planning to fight *Ae. albopictus* by releasing massive numbers of sterile males, a technique that has been successfully used to drive down populations of agricultural pests (*Science*, 20 July, p. 312). France is interested in the approach as well, says entomologist Didier Fontenille of the Institute of Research for Development in Montpellier, but it would likely start with *Anopheles arabiensis*, a species that can transmit malaria. Several new, less environmentally disruptive insecticides are under study as well.

Chikungunya has disappeared from La Réunion, and with 38% of the population now immune, it may not return for a long time. Scientists say the outbreak was a unique chance to focus attention—and money—on a tropical pathogen that, unfortunately, may well have a bright future in temperate regions.

–MARTIN ENSERINK

An Exploding Field

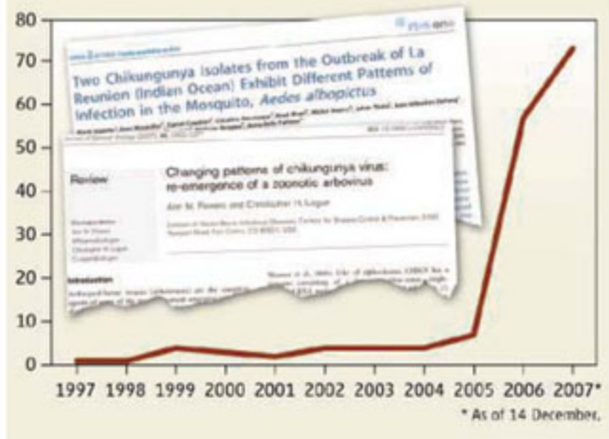

Paper trail. The number of papers with "chikungunya" in the title has risen from fewer than five per year before 2004 to more than 70 in 2007.

SOURCE: PUBMED

INTERVIEW: DAVID KING

U.K. Science Adviser Offers Some Parting Shots

As he ends a roller-coaster 7-year term, the U.K. government's chief science adviser ponders the highs and lows and offers some sage advice

David King is not going quietly. After a stormy 7-year tenure, the University of Cambridge chemist steps down from his role as the United Kingdom's chief scientific adviser at year's end. King has made headlines in Britain the past few weeks with a farewell speech and comments before Parliament in which he endorsed nuclear power, slammed media campaigns against genetically modified (GM) foods and the MMR vaccine, and berated the U.K. health service for its tacit endorsement of homeopathy. King, who next year will begin directing the University of Oxford's new Smith School of Enterprise and the Environment, sat down on 3 December with *Science* to reflect on his tenure and future plans. The following excerpts were edited for brevity and clarity.

–DANIEL CLERY

Q: Soon after your appointment in 2001, you were in the midst of a foot-and-mouth disease outbreak (*Science*, 23 March 2001, p. 2300). What did this teach you about science in government?

D.K.: The first thing was the discovery that despite the fact that government departments have scientists, there is a need for someone who has a big overview of what they're doing, a critical capability. More than that, someone is needed to see that they are using the best of scientific knowledge either inside or outside of government.

We were tackling a situation where we had, on 21 March 2001, 45 new infected farms reported that day. We were working 24/7 with large-scale computers and three different sets of modelers around the country. Then within a few days, we were able to advise the government, on the basis of modeling, that we had come up with a new control procedure. That was the cue for the prime minister to say, "Fine, we're going with this." And it followed through. Within a few days, we'd switched [the virus's] exponential growth into exponential decay, and the cabinet learned in real time that science could model an extremely complex situation and provide very robust advice for action.

Q: Did that advice affect the timing of the general election that year?

D.K.: Oh, yes, I have little doubt. The general election would have been on 3 May, and the models I presented to the prime minister indicated that the epidemic, without the new control measures, would be coming to a maximum about 10 May. With our control

"The cabinet learned in real time that science could model an extremely complex situation and provide very robust advice for action."

—David King

procedures, on a linear graph, it looked as if the epidemic would be over by 7 June. The prime minister queried me about how confident I was that we were on this graph, and when I gave him my assurance, he announced the election date [7 June].

Q: What's been your biggest disappointment or failure?

D.K.: I suppose the single biggest failure in terms of advice was in 2003 when we were producing the white paper on energy. The objective was to reduce our emissions of carbon dioxide by 60% by 2050, and I had argued that we couldn't possibly manage this without nuclear new build, and it looked like the argument was won. Then at a meeting chaired by Deputy Prime Minister John Prescott, a phrase was hammered out that put nuclear energy on hold. I had already gone out in the public domain with my views, and my public position didn't change. That was an important part of establishing myself as an independent voice from within government.

Q: And what was your greatest success?

D.K.: The single biggest success was putting climate change as the top problem to tackle, closely correlated with my success in getting African development to the top of the agenda. I was, most people would agree, very heavily responsible for the prime minister's decision to put climate change at the top of the G8 agenda [at the 2005 Gleneagles summit]. I think the climate change issue was given a very big boost by that process.

If we're going to see sustained development of African economies, the best action we can take is to assist in the entire development of their education systems. Not just primary schools, I mean the whole thing: primary, secondary, tertiary, universities, and even institutes of excellence—to pull the whole thing through.

Q: Tony Blair supported science. How did he become an advocate for research?

D.K.: The prime minister was very impressed by the enormous strength of the science base in Britain. Measured by citations, we're second in volume only to the United States, and measured by citations per pounds invested, we're ahead of the rest of the world by a very long stretch. What followed from that was his understanding that using this enormous strength to create wealth for the U.K. was a key way forward in the competitive globalized economic system.

Interestingly, in my first year with him, he decided to make a major speech on science. It was delivered at the Royal Society, and it was a full 1-hour speech that set out the entire target on science, innovation, and wealth creation in the U.K. It was translated into Chinese, so when Chinese Premier Wen Jiabao came over here, he asked to meet up with me. He wanted to tell me that they had transformed Chinese [science] policy as a result of their understanding of the prime minister's speech.

Q: Do you think Gordon Brown will follow a similar policy?

D.K.: I'm very confident that he will, and the reason I say that is that during Gordon

CREDIT: ALAN WELLER/BLOOMBERG NEWS/LANDOV

Brown's tenure at the Treasury, the science budget going to our research councils went from £1.4 billion in 1998 to £3.6 billion now.

Q: Why are Europeans so hostile to GM food?
D.K.: I think that on the whole, people either felt a visceral reaction to playing around with genes, or they felt that the companies involved were taking them for a ride. When offered a GM potato and a non-GM potato, most citizens thought, "Why should I take the GM?"

After an extensive review, we concluded we should regulate the products. Certainly, we should look to see if they are in any way a health hazard, but don't ban the technology because the technology is precise and potentially a very powerful tool. In my view, British companies and scientists need to be engaged with one of the biggest 21st century challenges—we need a third green revolution to feed a population of 9.5 billion people [by 2050] on this resource-stretched planet of ours.

Q: You argued for a universal ethical code for scientists. Will it do any good if a tiny minority still resort to fraud?
D.K.: The point of the code is that we would first like to get acceptance by the entire active scientific community. Young people being trained in science would just have this drilled into them as part of their training. The importance here is not only that those people practice this but also that the rest of the country, the public at large, knows that there is such a code and that it's being put into practice.

Q: In 2004, you said that climate change was a bigger threat to the world than terrorism. Was that a wake-up call?
D.K.: No question. That appeared in *Science* because I'd been invited to make a plenary lecture at the AAAS meeting in Seattle that year. And because of the publicity it caused, that was certainly the biggest audience I've ever spoken to. Every seat in the house was taken. It was vast. It served the purpose of drawing attention to what I consider to be the world's biggest challenge. So I had no regrets about the language I used in order to do that.

I have now given more than 500 lectures on climate change. Quite simply, I think it is no exaggeration to say that climate change is the biggest problem our civilization has ever had to face up to in its 12,000 years, because it requires a collective response.

Q: Have you always been a supporter of nuclear energy, or has that come out of your concern about climate change?
D.K.: I was not very fond of nuclear power because of my concerns about radioactive waste products. My position on nuclear power is a pragmatic one. We have a technology that enables us to produce the energy we need on the grid cheaply, with low carbon dioxide emissions, and reliably.

Q: What motivated you to accept the position at the new environment institute in Oxford?
D.K.: It offered the opportunity to create a school of enterprise and the environment at the center of the university where the big challenges of the 21st century can be developed and thrashed out at an interdisciplinary level while working with people in their core disciplines. The idea is that all aspects of our teaching and research at Oxford will take on board this massive 21st century challenge. We must mainstream it into disciplines—physics, chemistry, economics, politics—but also mainstream it into enterprise.

Q: Do you think the Bush Administration has been bad for science?
D.K.: It would be very difficult to argue otherwise. If we just take the climate change issue, the Kyoto process was [originally] led by U.S. Vice President Al Gore. [Since then], we have had 10 years of inaction from the United States, certainly 10 years of lack of leadership on this issue. I think it's difficult not to point the finger at the United States. It's the only country in the world that hasn't ratified the very treaty that the United States was a leading proponent of. I look forward to real U.S. leadership on this issue.

Q: What would have been your priorities if, in a parallel universe, you had been President George W. Bush's science adviser?
D.K.: My mantra since I took on this job has been openness, honesty, and transparency, which means that I have delivered my advice to the prime minister and Cabinet, but the prime minister and the Cabinet also know that in order to maintain the trust of the government and the public, I will submit my advice into the public domain. I would not take a job of this nature if I couldn't do that.

Election surprise. Scientific modeling of the 2001 foot-and-mouth outbreak determined the U.K.'s election date.

Counterprotest. David King laments anti-GM attitudes in Europe.

CREDITS (TOP TO BOTTOM): GERRY PENNY/AFP/GETTY IMAGES; SION TOUHIG/GETTY IMAGES

LETTERS

edited by Jennifer Sills

Cancer Filter Déjà Vu

IN A 3 AUGUST NEWS OF THE WEEK STORY ("CANCER TEST DISPUTE PITS RESEARCHER AGAINST a firm she helped create," p. 585), M. Enserink describes a dispute in France about whether a cancer-detection system "first published in 2000" (*1*) should enter the market. This system uses a filter with small holes that allow ordinary blood cells to pass through, but not larger and more rigid cancer cells. The photograph in the News of the Week story shows a plastic sheet irradiated with highly ionizing particles (so as to produce tracks) and then etched to bore holes of the desired size.

The cover photo from the 23 July 1965 issue of *Science* (*2*) includes a virtually identical photo. The caption reads in part, "Filtration of cancer cells by means of a plastic sieve. The holes have been etched to a diameter of 5 microns; holes of this size allow blood cells to pass through, but catch most cancer cells." In short, neither the special filters nor the idea of cancer-cell isolation, identification, and measurement is new.

Three of us at the General Electric Research Laboratory (*3*) produced the earliest plastic filters of controlled hole size. Earlier production of filters from muscovite mica (*4*) suffered from brittleness. After learning of our success with plastic filters, S. H. Seal at the Sloan-Kettering Institute in New York suggested filtering to isolate cancer cells from blood (*5*). The filters were used to show that free-floating cancer cells are present early in the development of a cancer (*6*).

ROBERT L. FLEISCHER

Department of Geology, Union College, Schenectady, NY 12308, USA.

References

1. G. Vona *et al.*, *Am. J. Pathol.* **156**, 57 (2000).
2. R. L. Fleischer, P. B. Price, R. M. Walker, *Science* **149**, 383 (1965).
3. R. L. Fleischer, P. B. Price, E. M. Symes, *Science* **143**, 249 (1964).
4. R. L. Fleischer, P. B. Price, R. M. Walker, *Rev. Sci. Instrum.* **34**, 510 (1963).
5. S. H. Seal, *Cancer* **17**, 637 (1964).
6. J. Song, P. From, W. Morrissey, J. Sams, *Cancer* **28**, 553 (1971).

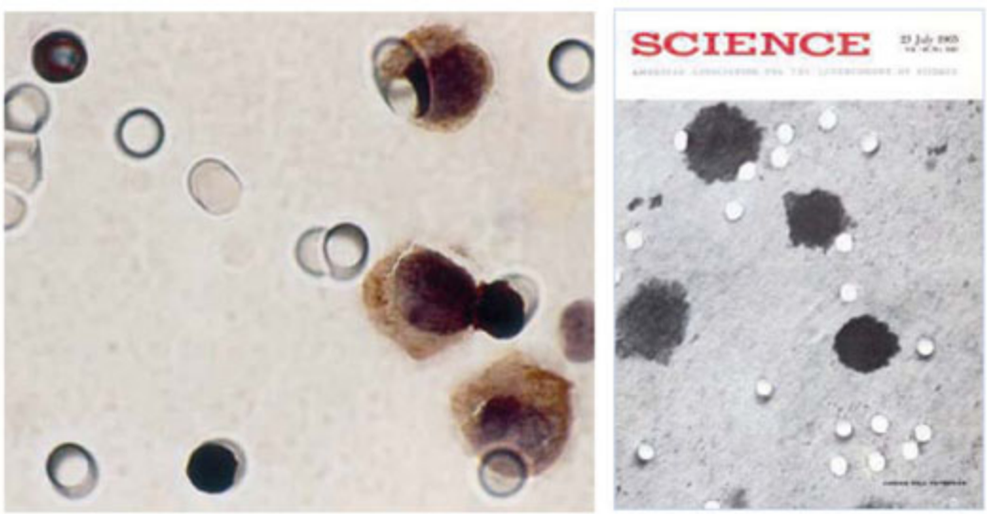

A familiar pattern. The image in a recent News story (**left**) of a filter used for cancer detection is reminiscent of the image that appeared on a *Science* cover in 1965 (**right**).

WE WERE GREATLY AMUSED BY THE NEWS OF the Week story by M. Enserink on identification of cancer cells by filtration of blood (3 August, p. 585). In 1964, the late Sam Seal, then our colleague at Memorial Sloan-Kettering Cancer Center, had the same idea and conceived of a filter for circulating blood that would allow separation of cancer cells by size. Dr. Seal's work led to the invention of the "Nuclepore" filter by the General Electric Corporation. Although Seal's idea to use his filter as a cancer detection system failed (*1*), the filter was useful in studying the circulation of megakaryocytes. At the time of Seal's contribution, the molecular biology of cancer cell identification did not exist, but the fundamental concept of catching large epithelial cancer cells on a filter apparently remains valid. We wish to remember Seal as a pioneer in this area of cancer diagnosis.

LEOPOLD G. KOSS[1] AND MYRON R. MELAMED[2]

[1]Montefiore Medical Center, Department of Pathology, The University Hospital for the Albert Einstein College of Medicine, Bronx, NY 10467–2490, USA. [2]Westchester Medical Center, Valhalla, NY 10595, USA.

Reference

1. S. H. Seal, *Cancer* **17**, 637 (1964).

One Woman's Balancing Act

THE NEWS OF THE WEEK STORY "POSTDOC survey finds gender split on family issues" (Y. Bhattacharjee, 9 November, p. 897) stressed social isolation of female faculty and the lack of high-quality child care. Looking back on a career as a professor and a single parent, I missed out on networking with colleagues and on presenting at conferences because of family obligations. I continued to miss out on these aspects of my career for many years, because, as most parents know, children can be too old to be left alone, as well as too young. (And, in any case, arrangements for overnight conference travel are much more difficult than daytime care.)

When I reached middle age, I saw that there were special programs to encourage women who had delayed professional education until their families were grown, but little "catch-up" help for those of us who had been

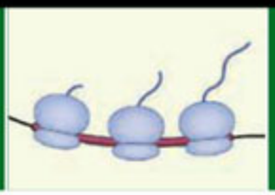

Double duty for microRNAs
1877

Plastic flow in glasses
1880

juggling all along. As an emerita and consultant today, I still feel the effect of the networking deficit. However, the Internet has helped me develop useful collegial connections to work with, now that my family tasks are minimal. Judging from the attitudes reported by the NIH survey, I would say that young professional women today are also more likely to benefit from electronic communication than from changes in social attitudes about family responsibilities.

JEAN MERCER

Department of Psychology, Richard Stockton College, Pomona, NJ 08240, USA.

Stem Cell Breakthrough: Don't Forget Ethics

THERE IS JUSTIFIABLE EXCITEMENT SURrounding the successful induction of pluripotent stem (iPS) cells from human fibroblasts [Yu *et al.*, Reports, 21 December (this issue), p. 1917, and (*1*)]. The removal of dependence on oocytes frees researchers from serious ethical issues that have hindered medical research. This technology could also be of great value in the area of conservation biology. The genes from endangered animals or even an extinct species could be reintroduced to maintain the survival and genetic diversity of the species. However, although one researcher commented that "[p]eople working on ethics will have to find something new to worry about" (*2*), it is crucial that discussions of the ethical use of this technology continue.

Even though the technology is in its early stages, its implications are both enormously important and troublesome. Jaenisch and his colleagues (*3*) have shown in mice that such reprogrammed cells can form viable chimeras and contribute to the germline when injected into blastocysts. When transferred to recipient females, we have confirmed that embryonic stem cells injected into mouse blastocysts or aggregated with 8-cell–stage morulas can contribute to all of the organ systems and to more than 90% of the resulting fetuses and live pups (*4*).

These animals also had the LacZ gene from the embryonic stem cells in their gametes and produced LacZ-positive offspring when crossed with females, confirming that the DNA from the stem cells could be genetically passed on to subsequent generations. The success of this technology in model organisms opens up the possibility that humans might be able to pass on their genes (or genetically modified genes) to future generations from just a few skin cells.

At present, the technique for generating iPS cells requires serious genetic modification, which itself has been associated with an increased incidence of tumors. As with cloning, it would be scientifically and ethically irresponsible—indeed, unscrupulous—to use this technology for reproductive purposes. However, while the technology to clone a human being does not currently exist, the ability to use iPS cells to make a chimeric human (i.e., using iPS cells to contribute to an embryo that would be a chimera) may be much closer to reality.

Considering the immense power of this technology, it is imperative that an effort is made by scientists and governments to understand the ramifications of this new breakthrough and to ensure that it is used in an ethically responsible way for the benefit and progress of humanity.

ROBERT LANZA

Advanced Cell Technology and Institute for Regenerative Medicine, Wake Forest University School of Medicine, Winston-Salem, NC 27157, USA.

References

1. K. Takahashi, *Cell* 10.1016/j.cell.2007.11.019 (2007).
2. G. Vogel, C. Holden, *Science* **318**, 1224 (2007).
3. M. Wernig *et al.*, *Cell Stem Cell* **1**, 55 (2007).
4. Y. Chung *et al.*, *Nature* **439**, 216 (2006).

CO_2 Emissions: Getting Bang for the Buck

IN HIS POLICY FORUM "CRITICAL ASSUMPTIONS in the Stern Review on climate change" (13 July, p. 201), W. Nordhaus's continued argument for high discount rates—i.e., leaving the problems for future generations to deal with—is part of the thinking that got us into trouble in the first place. A fixed and high discount rate has been shown to be inconsistent with human behavior (*1*) and inadequate for long-term environmental decision-making (*2*).

Data from atmospheric and related sciences should guide the scale of society's emissions. Once a safe scale is determined (*3*), an ethical discussion should guide how we divide the remaining emissions, as suggested by N. Stern and C. Taylor in their response to Nordhaus (Policy Forum, 13 July, p. 203). Only after the scale and ethical distribution have been decided should economics step in to help us decide how to use the remaining emissions efficiently.

Nordhaus's argument is "let's get the most bang for our buck," and this is laudable. However, if we look at why we are burning fossil fuels in the first place (i.e., to improve human welfare), then we come to a conclusion very different from Nordhaus's tax-the-future suggestion. In basic economics, we learn that investment should be directed toward factors with the greatest return per unit input. If we rightly assume that CO_2 emissions are a consequence of a growing economy (*4*), and the goal of growing the economy is increasing human welfare, then we need to invest where increased GDP (read CO_2 emissions) returns the most welfare per unit input. Data on proxies for welfare other than GDP, such as life expectancy, quality of health care (*5*), and self-reported levels of happiness (*6*), suggest that our remaining emissions should be allocated to developing and least-developed countries, where the greatest returns are realized.

BRENDAN FISHER

Centre for Social and Economic Research on the Global Environment, University of East Anglia, Norwich NR2 3UF, UK.

References and Notes

1. K. Knetch, *Env. Res. Econ.* **32**, 91 (2005).
2. R. K. Turner, *Env. Res. Econ.* **37**, 253 (2007).
3. W. S. Broecker, *Science* **315**, 1371 (2007).
4. CO_2 emissions data are available from Oak Ridge National Laboratory (2003); http://cdiac.ornl.gov/trends/emis/tre_tp20.htm.
5. WHO, "World Health Report 2006: Working together for health" (WHO Press, Geneva, 2005).
6. C. Kenny, *Soc. Indic. Res.* **73**, 199 (2005).

WILLIAM NORDHAUS (POLICY FORUM, 13 July, p. 201) criticizes the ethical assumptions behind the 0.014 $year^{-1}$ discount rate used in the Stern Review (*1*). Stern's rate, however, is roughly consistent with a well-known theory of policy analysis in which the discount rate is set equal to the sum of two terms: the market rate of return on safe investments plus an appropriate risk premium for uncertainty (*2*, *3*).

Safe financial assets such as money-market funds yield inflation-adjusted returns of ~0.01 $year^{-1}$. Moreover, this theoretical framework implies that the risk premium should not be positive for precautionary actions such as buying insurance. For precautionary actions, the discount rate should thus be no higher than ~0.01 $year^{-1}$.

Climate stabilization is a precautionary investment, similar to buying an insurance policy that secures the livelihoods of future generations (*4*). The Framework Convention on Climate Change calls for preventing "dangerous anthropogenic interference with the climate system" (*5*). By mitigating uncertain—but potentially catastrophic—impacts, climate stabilization reduces the statistical variability of future well-being.

The 20th century began with strong faith in progress and ended with a sense of trepidation about the lives our grandchildren will lead. Returns on past investments in a fossil-fuel economy were high because climate change costs were ignored. Protecting our progeny's environmental rights will result in wholly new prices, including lower discount rates (*6*).

RICHARD B. HOWARTH[1] AND RICHARD B. NORGAARD[2]

[1]Environmental Studies Program, Dartmouth College, Hanover, NH 03755, USA. [2]Energy and Resources Group, University of California, Berkeley, CA 94720, USA. E-mail: RBHowarth@dartmouth.edu (R.B.H.); norgaard@igc.org (R.B.N.)

References

1. N. Stern, *The Economics of Climate Change: The Stern Review* (Cambridge Univ. Press, Cambridge, 2007).
2. A. Sandmo, *Int. Econ. Rev.* **13**, 287 (1972).
3. D. A. Starrett, *Foundations of Public Economics* (Cambridge Univ. Press, New York, 1988).
4. R. B. Howarth, *Land Economics*, **79**, 369 (2003).
5. United Nations, *Framework Convention on Climate Change* (http://unfccc.int/resource/ccsites/senegal/conven.htm), Article 2.
6. R. B. Howarth, R. B. Norgaard, *Am. Econ. Rev.* **82**, 473 (1992).

Response

FISHER SUGGESTS THAT "WE NEED TO INVEST where increased GDP (read CO_2 emissions) returns the most welfare per unit input." I agree with the basic premise that the point of economic activity is to improve the standards of living of present and future generations. However, GDP (gross domestic product) definitely does not equal CO_2 emissions, nor is there an iron law relating the growth of GDP and of CO_2 emissions. Indeed, the cross section of economics and human experience indicates that if the price of carbon emissions is raised above zero—best accomplished by a carbon tax, in my view—then the CO_2 trend line will be flatter, or even turn down. The need for a high global price of carbon is common ground between my work and the Stern Review. The necessary (and probably the sufficient) condition for doing anything substantial in climate policy is for scientists, political leaders, and the public to accept the inconvenient economic truth that the prices of goods and services that contain CO_2 must be raised relative to those of other goods and services.

How sharply or fast should countries individually and collectively bend down the CO_2 trend line? Studies differ on the answer to that question, and the major difference between my work and the Stern Review involves the

CORRECTIONS AND CLARIFICATIONS

Letters: "Virtual worlds, real healing" by A. Gorini *et al.* (7 December, p. 1549). Two author names were omitted. The complete list of authors is Alessandra Gorini,[1,2] Andrea Gaggioli,[1,3] Giuseppe Riva,[1,3] and their affiliations are as follows: [1]Applied Technology for Neuro-Psychology Laboratory, Istituto Auxologico Italiano, 20100 Milan, Italy. [2]Research Institute Brain and Behaviour, Maastricht University, Netherlands. [3]Psychology Department, Catholic University of Milan, Italy. The authors and affiliations have been corrected in the HTML version on the *Science* Web site.

Essays: "GE & *Science* Prize for Young Life Scientists: regional winners" (7 December, p. 1566). The photograph of Bo Huang was placed next to the biography of Takeshi Imai, and the photograph of Takeshi Imai was placed next to the biography of Bo Huang. The photographs were correct in the online version.

News Focus: "Should oceanographers pump iron?" by E. Kintisch (30 November, p. 1368). A table describing the size of the area to be seeded by Planktos in upcoming experiments was incorrect. The company's planned releases would cover a patch of ocean from 2000 to 7750 km², not one as large as 31,000 km².

This Week in *Science*: "Short DNAs stack and order" (23 November, p. 1213). The correct credit is "Giuliano Zanchetta/University of Milano."

Reports: "Transposase-derived transcription factors regulate light signaling in *Arabidopsis*" by R. Lin *et al.* (23 November, p. 1302). In the sixth sentence of the third paragraph on page 1304, an incorrect Web site was referenced. The correct Web site should be The Arabidopsis Information Resource (www.arabidopsis.org). Also, in reference 13 on page 1305, the accession numbers for *Arabidopsis* FAR1, FHY1, and FHL (AAD51282, AAL35819, and CAB82993, respectively) were mistyped as NP_567455, NP_181304, and AAC23638.

Books *et al.*: "Simple maths for a perplexing world" by D. J. Rankin (9 November, p. 919). In the first paragraph, "hoards" should have been "hordes."

Perspectives: "How does radiation damage materials?" by B. D. Wirth (9 November, p. 923). Throughout the Perspective, "Burger's vector" should be "Burgers vector."

This Week in *Science*: "Nearest and dearest" (2 November, p. 713). The correct credit is "Norman Lim/National University of Singapore."

News Focus: "Do wandering albatrosses care about math?" by J. Travis (2 November, p. 742). The bird identified as a wandering albatross (*Diomedea exulans*) in the photograph is a black-browed albatross (*Thalassarche melanophris*).

News Focus: "Malaria treatment: ACT two" by M. Enserink (26 October, p. 560). The UNICEF report referred to is Malaria and Children: Progress in Intervention Coverage, by UNICEF and the Roll Back Malaria Partnership (2007). That report is also the source of the graphics on pp. 560 and 563, as well as the graphics in "Battling over bed nets" on pp. 557 and 559.

Reports: "Permuted tRNA genes expressed via a circular RNA intermediate in *Cyanidioschyzon merolae*" by A. Soma *et al.* (19 October, p. 450). The last sentence on p. 452 referred to an incorrect subunit. The sentence should begin "Permuted noncoding RNA (ncRNA) genes have been reported for *Tetrahymena* mitochondrial large subunit (LSU) ribosomal RNA (rRNA) (*15*)…"

News Focus: "Tooled-up amateurs are joining forces with the professionals" by J. Bohannon (12 October, p. 192). The light curves in the figure should have been credited to Stelios Kleidis in Greece, Paul Van Cauteren in Belgium, and C. W. Robertson in the United States.

Research Articles: "An evolutionarily conserved mechanism delimiting SHR movement defines a single layer of endodermis in plants" by H. Cui *et al.* (20 April, p. 421). In two instances in the fifth paragraph on page 424, one of the rice homologs for *SHR*, *Os03g31880*, was mistyped as *Os03g31750*.

Reports: "Conductance-controlled point functionalization of single-walled carbon nanotubes" by B. R. Goldsmith *et al.* (5 January, p. 77). The horizontal axis in Fig. 1C should have included breaks to indicate that the five redox cycles were not performed continuously. A corrrected version is shown below. The caption should conclude, "The reduction portions of *G* in (C) have been scaled up by 1.32 ± 0.10 to adjust for the electrostatic gating that occurs at the reducing potential." To clarify these corrections, raw data underlying Fig. 1C has been added to the revised Supporting Online Material, accompanied by a complete description of the processing. The caption for Fig. 2C should read, "A composite of AFM topography in grayscale and SGM in red identifies a local region responsible for the gate sensitivity of a device like (A)." The Supporting Online Material has also been corrected to state, "Figs. 3D and S4 depict three different chemical configurations: H_2SO_4 oxidation, Ni deposition, unpassivated Ti electrodes (Fig. 3D); H_2O oxidation, Ni deposition, unpassivated Ti electrodes (Fig. S4A); H_2O oxidation, Pd deposition, unpassivated TiN electrodes (Fig. S4B)" (p. S11). The authors apologize that these errors were incorporated during manuscript revision but note that they do not affect the results or conclusions of the paper.

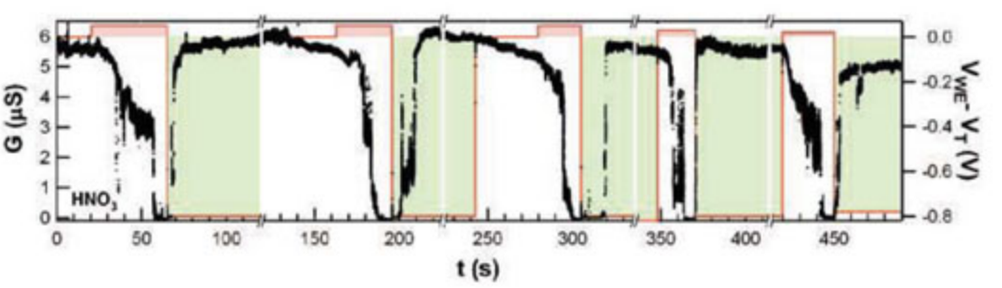

discount rate. The primary point in my Policy Forum (13 July, p. 201) and the background studies (*1*, *2*) is that we need to choose a discount rate for climate investments (such as emission reductions) with a return that is as high as the return on social investments with which climate investments compete. I suggested that it would be difficult to rationalize a rate of return on investment much below 5 to 6% per year in inflation-adjusted terms. Howarth and Norgaard object, arguing that "[s]afe financial assets such as money-market funds yield inflation-adjusted returns of ~0.01 year^{-1}." Their number is too low and only marginally relevant. The closest thing in the world to a safe financial asset is the U.S. Treasury 20-year inflation-protected bond, the yield of which is currently around 2.5% per year. However, this is hardly the relevant cost of capital for the firms borrowing at a real interest rate of 3 to 10% per year, or households paying 18% on credit-card debt, or students around the world who face liquidity constraints and for whom the real returns on educational investments might be 5 or 10 or 20% per year. There are many, many investments with yields far above Howarth and Norgaard's 1% per year.

Both letters make an important point with which I agree: The desired carbon tax or emissions reductions would have a substantial component of risk premium to reduce the chance of triggering poorly understood, low-probability, high-consequence climatic outcomes. Their proposed remedy—to lower the discount rate—is off target, however. The appropriate response is primarily to undertake the scientific studies to better understand the risks, and then to design effective steps to avoid them. Manipulating discount rates does neither.

WILLIAM D. NORDHAUS

Department of Economics, Yale University, New Haven, CT 06511, USA.

References

1. W. D. Nordhaus, *The Challenge of Global Warming: Economic Models and Environmental Policy* (Yale Univ. Press, New Haven, CT, in press); available at http://nordhaus.econ.yale.edu/recent_stuff.html.
2. W. D. Nordhaus, *J. Econ. Lit.*, in press; available at http://nordhaus.econ.yale.edu/recent_stuff.html.

Letters to the Editor

Letters (~300 words) discuss material published in *Science* in the previous 3 months or issues of general interest. They can be submitted through the Web (www.submit2science.org) or by regular mail (1200 New York Ave., NW, Washington, DC 20005, USA). Letters are not acknowledged upon receipt, nor are authors generally consulted before publication. Whether published in full or in part, letters are subject to editing for clarity and space.

FICTION

Virtual Reality, Identity Imposters

Carol W. Berman

After a nearly fatal accident, Mark Schluter, the protagonist of Richard Powers's National Book Award–winning ninth novel, *The Echo Maker*, wakes up from a coma to find he is being cared for by a woman who claims she is his sister Karin. Mark is convinced that she is not but is instead an almost-exact duplicate of her, an imposter. In psychiatry we call this delusion Capgras syndrome, a rare form of misidentification usually seen in schizophrenia, dementia, or brain trauma. Two French psychiatrists, Joseph Capgras and Jean Reboul-Lachaux, first described the disorder in 1923. Their 53-year-old patient believed that her husband, her children, her house, her neighbors, and even she had been replaced by exact doubles and that everyone was plotting to steal her property.

In his paranoid state, Mark begins to believe that there is a government-hatched plot against him. When he finally reaches home after the rehabilitation center, he feels that his property has been replicated. Neurologists call this reduplicative paramnesia, a variant of Capgras syndrome, in which a building or home is replaced. Even his dog seems to be an imposter. According to the theory that he concocts to explain these changes, the government is experimenting by dropping him into a different, but very similar, environment to monitor his reaction.

Mark's attempt to discover who wrote a mysterious note found at his hospital bedside drives the story forward. It read:

I am No One
but Tonight on North Line Road
GOD led me to you
so You could Live
and bring back someone else.

No one seems to know who snuck in and delivered the scrawled note, Mark's only real clue about what happened.

The novelist, a professor of English at the University of Illinois, Urbana-Champaign, explores the recognition of the self and others, segueing into the nature of the self. If Mark's loved ones and his property have changed, who is he? By not acknowledging Karin as his sister, Mark enters a new dimension and alters his own history and memory. At the same time, he induces a change in his sister. She jokes about being a replica and discovers how freeing not having to follow an established identity can be. The changes the principal characters experience provide a dynamic story of substantial transformations. Mark starts out almost brain dead but finds himself and his intellectual capacity again. Karin loses her job and former life to care for Mark. She regresses to a relationship with one old boyfriend, flirts with another, but eventually emerges a renewed individual.

The only changes that strain belief are those that occur in Dr. Gerald Weber, a physician-author in the mold of Oliver Sacks, who is the cognitive neuroscientist brought in on Mark's case. Weber suddenly starts experiencing some of the same neurological and psychological disorders he writes about in his popular books. How simple to portray a psychiatrist as crazy or a cop as a killer. Hollywood movies constantly entertain us with polar opposites like these, but Powers is too talented a writer to have to venture into this clichéd territory. Weber's interactions with his wife—who calls him "Man," while he calls her "Woman"—are unnatural. Nor is the doctor's eventual straying from his marriage psychologically believable. Weber is a neurologist, not a psychiatrist. So why does Mark call him "Shrinky"? I've never heard neurologists or cognitive neuroscientists referred to as a shrink.

The Echo Maker
A Novel
by Richard Powers

Farrar, Straus and Giroux, New York, 2006. 459 pp. $25, C$31. ISBN 9780374146351. Heinemann, London, 2007. £17.99. ISBN 9780434016334. Picador, New York, 2007. Paper, $15. ISBN 9780312426439.

Although the novel shifts its point of view several times from Mark to Karin to Dr. Weber, Powers is a gifted writer who is able to delve into these different perspectives seamlessly. His lyrical style includes hauntingly beautiful descriptions of the sandhill cranes that visit the Nebraska flatlands, symbolizing the unending sequences of nature and the ecosystem. In the opening scene, he writes of one: "The blood-red head bows and the wings sweep together, a cloaked priest giving benediction." In addition, the novelist knows his sciences. His comprehension of neurology, psychiatry, and other branches of medicine is impressive.

Unfortunately, the women characters are relegated into one extreme category or another. They are either weak and hysterical victims, like Karin and Sylvie (Dr. Weber's wife), or they seem unrealistically strong and mysterious, like Barbara (a minor player who looms large late in the story). In contrast, the men are multidimensional and more realistically depicted. Powers's love scenes are unusually well done. His descriptions of birds and nature are awe-inspiring, easing readers into philosophical musings without inducing boredom.

I kept turning the pages trying to solve the mysteries of Mark's accident and the note, but I was slowed down by excessive neurological descriptions—which I, as a psychiatrist, should have enjoyed more. Nonetheless, overall *The Echo Maker* strikes me as a superb melange of science and poetry.

Sandhill cranes (*Grus canadensis*) in the Platte River valley, Nebraska.

CREDIT: SHERMAN SUTER/SCIENCE

The reviewer, the author of *One Hundred Questions and Answers About Panic Disorder*, is in private psychiatric practice in New York City and at the Department of Psychiatry, New York University Medical Center, New York, NY 10016, USA. E-mail: bermac02@popmail.med.nyu.edu

10.1126/science.1150498

GALLERIES: SCIENCE AND THE ARTS

Incubating Inspiration?

Louise Whiteley

The latest organization to promote dialogue between science and the arts recently opened its doors in the heart of Paris. Le Laboratoire is described by its director, David Edwards (a professor of bioengineering at Harvard University), as "the first experiment-driven art and science incubator" (*1*). This is a revealing metaphor, conjuring up an image of Edwards standing over a gargantuan petri dish brimming with scientists and artists, hoping that some will fuse like X and Y chromosomes in flashes of inspiration he refers to as "artscience." Some fertilizations will undoubtedly occur, but it's not at all clear what kind of chimera will emerge.

The idea behind Le Laboratoire is that although science and art diverge in their day-to-day methodology, during periods of scientific innovation there are "surprising kinships" (*2*)—both follow a similar creative method, exploring new connections and pushing the limits of our understanding. Working at MIT in the 1990s, Edwards had what you might call his own personal artscience moment. Struggling with the problem of how to get particles of insulin to fly through the air and stick to the lungs, he suddenly realized that the perforated "whiffle balls" children use for indoor baseball had the perfect structure.

You could complain that this rather Kuhnian picture of science is the exception rather than the rule and that a focus on common creativity obscures important comparisons. But the aims of Le Laboratoire can hopefully transcend these philosophical objections. Like previous projects funded by the profits from Edwards's whiffle-ball idea, the center aims to give scientists space for creative thinking outside the constraints of specialization and grant applications. This is a great idea, although how far it will extend beyond projects with specific practical applications is not entirely clear. Le Laboratoire also supports more traditional collaborations, in which artists respond to science as part of the fabric of our modern lives and scientists gain a novel perspective on their work. Bringing these different approaches together in one cultural venue and displaying the process of collaboration as well as the outcome is a novel and ambitious idea.

Le Laboratoire
4 rue du Bouloi,
75001 Paris.
www.lelaboratoire.org

The opening season comprises two exhibitions (*3*), a pairing that demonstrates the different kinds of experiments the laboratory plans to support. *Bel-Air, News About a Second Atmosphere* is a science-driven design project, led by Edwards and designer Mathieu Lehanneur. Inspired by NASA's use of plants to remove toxic airborne chemicals from inside spacecraft, they are working on a plant-based filter to purify the air inside our chemical-rich homes. The exhibition displays a number of prototypes that would look more at home in an upmarket design store, here sitting forlornly around a treelike pillar. On the other side of the space, a video animation displays a stylized interior with microbelike forms proliferating across the furniture. This collection of objects feels quite disjointed, and the brief accompanying leaflet leaves viewers unsure about what stage of the project they are looking at and how the collaboration developed.

A similarly ascetic approach to information characterizes *Food for Thought*, a collaboration between Paris artist Fabrice Hyber and MIT biomedical engineer Robert Langer. The exhibition explores some of the fascinating and discomforting ideas surrounding stem cell medicine, but it too fails to provide the viewer enough help in understanding what these ideas are. As a neuroscientist, I found echoes of neuronal shapes and wiring diagrams in repeated hourglass and grid motifs. These formed interesting connections with the more obvious connotations of change and reversal, which would have been entirely opaque to someone relying on the short description provided. Moving away from the model of art as simply a method for disseminating scientific knowledge is undoubtedly a good thing, but a little more information would allow people to respond in a richer way to both the art and what it has to say.

Le Laboratoire has many different aims, and the slightly florid exhibition notes almost seem to promise a one-state solution to C. P. Snow's old two-cultures war (*4*). The danger with this kind of approach is that it instead creates a third culture in which the value of each is diluted, producing high-end design products and obscure installation art rather than genuine debate and innovation. The current exhibitions flirt with this danger, but the philosophy behind Le Laboratoire clearly aims to avoid it; future plans include humanitarian design projects and an exploration (supported by the Wellcome Trust) of medicine in the developing world. The magic spark of fertilization can't happen every time, and perhaps, as in science, we need to accept some failed experiments along the way to potentially exciting outcomes and new ways of thinking.

Kekulé is said to have discovered the structure of benzene after dreaming of a ring of snakes, joined tongue to tail. If Le Laboratoire fulfills its potential, Edwards's whiffle ball may well join Kekulé's snakes and Aristotle's bath in the canon of mythological eureka moments.

Artscience experiments. One of the prototype air cleansers from the exhibition *Bel-Air*.

CREDIT: MATHIEU LEHANNEUR AND GAËTEN BOBILLARD/COURTESY LE LABORATOIRE

The reviewer is at the Gatsby Computational Neuroscience Unit, University College, London, Alexandra House, 17 Queen Square, London WC1N 3AR, UK. E-mail: louisew@gatsby.ucl.ac.uk

References and Notes

1. D. Edwards, *Nature* **449**, 789 (2007).
2. "Exhibition notes," Le Laboratoire, October 2007.
3. Both exhibitions continue through 14 January 2008.
4. C. P. Snow, *The Two Cultures and the Scientific Revolution* (Cambridge Univ. Press, Cambridge, 1959).

10.1126/science.1152734

MENTORING

Linking Student Interests to Science Curricula

Explicit networking helps undergraduates get the most out of the diverse curriculum available at a large university.

Lauren A. Denofrio,[1]* Brandy Russell,[1]*† David Lopatto,[2] Yi Lu[1]‡

Attraction and retention of science majors remain difficult in the fields of chemistry and biology (*1*–*6*). The usual sequential and extensive curriculum often does not allow undergraduate students to exercise their curiosity in selecting these subjects, as the starting point of most courses is their technical content rather than students' interests.

To strengthen this weak link between students' interests and science curricula, we began in 2003 a course called "The Chemistry and Biology of Everyday Life" (CBEL) (see figure, right), using students' interests in everyday life as the starting point for instruction. The course content and activities were designed to match each student's background and interests with other courses and research group activities. The course mimics a scientific research group. Students develop skills through literature review (journal club), special topic discussions, and research assignments. Peer mentoring engages students from freshmen to seniors. Visits to laboratories and attendance at scientific meetings broaden students' horizons. Assessment through the Classroom Undergraduate Research Experience (CURE) survey indicates that students who took CBEL believe they have progressed in a number of areas valuable in scientific research. Students following their own interests are more motivated to learn (*3*, *4*, *6*–*11*). CBEL elicits student interests, links those interests to existing science courses, and sustains their interests through independent investigations.

Large-scale changes to traditional curricula often seem costly (*12*) or disruptive (*13*). Rather than changing existing courses, CBEL works within the existing infrastructure and helps students to navigate more than 7500 courses and 2000 research groups at the University of Illinois, assisting them to identify courses and groups that match their interests (see figure, below). In doing so, CBEL allows instructors to experiment with pedagogy without disrupting existing courses. Although the CBEL design addresses concerns that may be particular to large universities, many of the course activities that help students explore their interests could be relevant to other educational institutions.

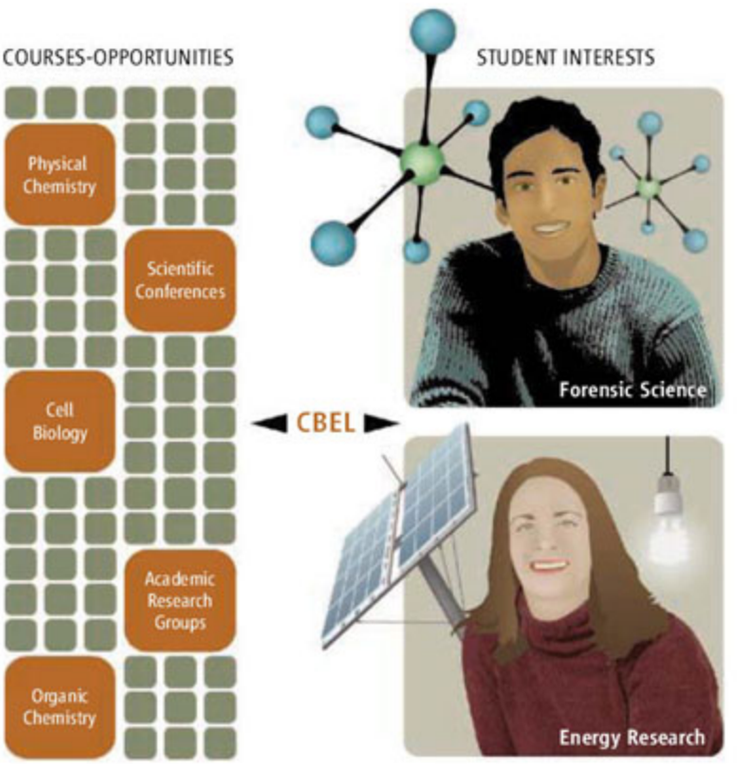

Engaging students in science by harnessing their interests.

Peer Mentoring

Even though the possibility of matching students' interests with science courses exists, carrying out such a match is not trivial. Undergraduate students, particularly freshmen and sophomores, might not have enough experience to identify the courses and laboratories that interest them. Therefore, in our course, mentoring by upperclassmen has an important role. New students join the course in their freshman year and are encouraged to remain in the course until graduation, being mentored at first and becoming mentors later. A pre-enrollment survey (*14*) is conducted each semester to identify students' interests and to build mentoring groups with common interests.

Programs that feature mentorship of novices by experts, whether faculty, graduate students, or undergraduates, have been successful (*15*, *16*). We found that mentoring by students of similar class standing and experience is also effective for two reasons. We have observed that because peers have no control over the mentees' grades, students are more open with one another [see also (*17*)]. Also, undergraduate students have experiences not shared by faculty and graduate students. For example, undergraduate mentors can offer firsthand advice on courses they have taken or laboratories they have worked in. Our students trust and appreciate the advice from undergraduate mentors; each semester, students respond most favorably to guest lectures by former classmates who now have a successful career in the scientific enterprise.

Modeling a Research Group

America is a leader in graduate education; one main reason is that graduate students are placed in research groups. Our course is designed to mimic a scientific research group redesigned for undergraduates, with peer mentoring at its center. In any given semester, the course includes students of different levels of experience and areas of interest or expertise, similar to those of a research group. This class is divided into subgroups of 8 to 10 students, from freshmen to seniors, who have identified similar interests. The group works together all semester to help each other and to complete group projects. All returning students serve as mentors and are trained at the beginning of the semester through meetings with instructors using a textbook (*18*). The mentors and group activities are monitored through subgroup agenda minutes and discussions with instructors (*14*). Being a peer mentor, a senior student is more conscientious about his or her participation in the

[1]Department of Chemistry, University of Illinois at Urbana-Champaign, Urbana, IL 61801; [2]Department of Psychology, Grinnell College, Grinnell, IA 50112, USA.
*These authors contributed equally to this work.
†Current address: Department of Chemistry, Gustavus Adolphus College, St. Peter, MN 56082, USA.
‡ Author for correspondence. E-mail: yi-lu@uiuc.edu.

CREDIT: N. KEVITIYAGALA/SCIENCE

course, providing a review and refreshing his or her understanding of previously learned content.

The subgroup is also the scaffold upon which several skill-building activities rest. In monthly journal club meetings, students present and discuss published articles in subgroups first. Each subgroup then chooses one student to present for the entire class. Another way to encourage critical reading and debate is through discussing a selected broad topic, such as "banning trans fatty acids in food" or "the safety of prescription drugs approved by the U.S. Food and Drug Administration." Each subgroup investigates one area of the topic and makes a presentation as a group to the whole class, which is followed by a lively debate (*14*). Finally, research assignments allow each student to investigate a chosen topic of interest in increasingly complex formats. First-time takers of CBEL complete literature searches and write a report on a topic of their choice. Second-year students give literature seminars, and third-year students submit research proposals outlining how they would investigate their topic within a research laboratory. Fourth-year students, usually graduating seniors, give a thesis defense to the entire class on results of experimental investigations. Each assignment requires students to articulate a question that can be investigated in the literature and the laboratory. With each year, students' topics of interest become more refined and their content knowledge improves as they move toward research within a laboratory (*14*).

Another element in the course is students' exposure to the excitement of discovery by visiting academic and industrial laboratories, such as Abbott Laboratories and the Indiana State Police Laboratory, as well as scientific meetings, such as annual meetings of the American Chemical Society and the American Association for the Advancement of Science. These trips serve as an eye-opening and motivating experience for the students. Because these field trips build community among the students, we now do the scientific meeting field trip toward the beginning of the semester. Course activities after the trip become livelier as the students interact with each other more freely.

Assessment

The effectiveness of the course has been assessed through online CURE surveys conducted before and after the spring semester of 2007 (*9*, *14*). The presurveys found no pattern of differences between our students and the benchmark group on background variables such as science attitude and learning style. However, opinions of their own learning gains at the end of the semester are higher among students who took CBEL than among the reference cohort of students who completed the CURE survey in the spring of 2007 at other colleges and universities (see figure below). The mean learning gains of students in our course are also compared with a national cohort of students who took the Summer Undergraduate Research Experience (SURE) survey in summer 2006. The general trends of the self-reported gains by our students resemble the national trends, even though the gains are higher for CBEL students. For example, the self-reported gain in knowing the "research process" is higher than that of "knowledge construction" for both our students and the national average. There are exceptions, however. Although the national CURE/SURE gains in "lab techniques" are among the highest, our students did not rate themselves as high in this area, because most of our students are freshmen or sophomores who have not had time in the laboratory. Our students did report stronger gains in "oral presentation," bucking the national trend, which may reflect our focus on oral presentations by freshmen.

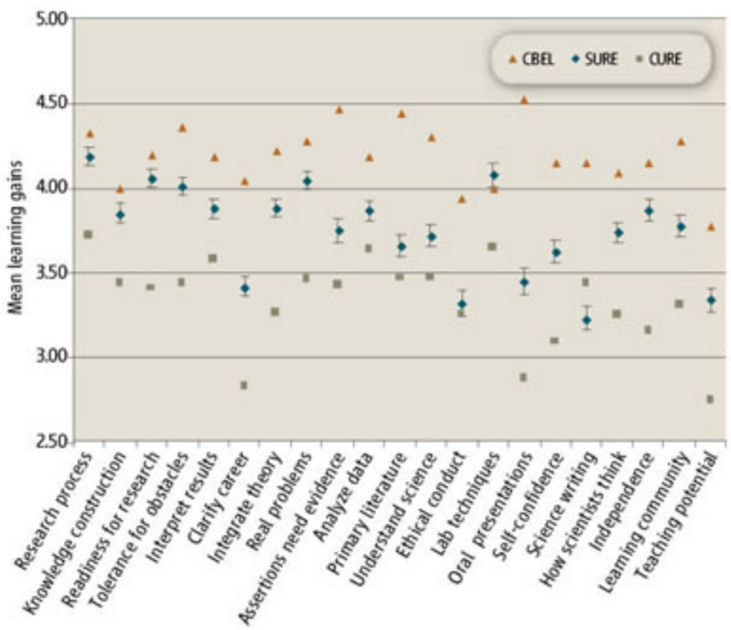

Student rating of learning gains. Students in CBEL from the CURE survey in spring 2007 compared with those of the reference cohort of students who completed the CURE and SURE surveys. Error bars represent 2 SEM.

The next challenge is to make our program adoptable and sustainable (*19*). The primary challenge is the resources it requires, especially time. Analyzing each student's interests and giving individual attention require considerable time from teaching assistants and instructors. Furthermore, many students have difficulty fitting the course, which is not yet required, into their schedule. To address these issues, we are working on adopting small modules from this course into other existing courses, aiming to integrate our most successful ideas into the mainstream curriculum. If peer mentors can provide some of the individualized attention, the course model can be applied to other courses, in other disciplines or in other institutions.

References and Notes

1. National Science Foundation (NSF), *Shaping the Future*, vol. 2, *Perspectives on Undergraduate Education in Science, Mathematics, Engineering, and Technology* (NSF, Arlington, VA, 1998).
2. National Research Council, *Bio2010: Transforming Undergraduate Education for Future Research Biologists* (National Academies Press, Washington, DC, 2003).
3. W. B. Wood, J. M. Gentile, *Science* **302**, 1510 (2003).
4. J. Handelsman *et al.*, *Science* **304**, 521 (2004).
5. B. Alberts, *Cell* **123**, 739 (2005).
6. M. F. Summers, F. A. Hrabowski III, *Science* **311**, 1870 (2006).
7. National Research Council, *How People Learn: Brain, Mind, Experience, and School, Expanded Edition*, J. D. Bransford, A. L. Brown, R. R. Cocking, Eds. (National Academy Press, Washington, DC, 2000).
8. E. Seymour, A.-B. Hunter, S. L. Laursen, T. Deantoni, *Sci. Educ.* **88**, 493 (2004).
9. D. Lopatto, *Cell Biol. Educ.* **3**, 270 (2004).
10. D. I. Hanauer *et al.*, *Science* **314**, 1880 (2006).
11. M. C. Linn, H.-S. Lee, R. Tinker, F. Husic, J. L. Chiu, *Science* **313**, 1049 (2006).
12. B. J. Fishman, T. M. Duffy, *Educ. Tech. Res. Dev.* **40**, 95 (1992).
13. P. S. Zurer, *Chem. Eng. News* **804**, 31 (2002).
14. Supporting materials are available on *Science* Online.
15. C. Pfund, C. M. Pribbenow, J. Branchaw, S. M. Lauffer, J. Handelsman, *Science* **311**, 473 (2006).
16. M. R. Beck, E. A. Morgan, S. S. Strand, T. A. Woolsey, *Science* **314**, 1246 (2006).
17. E. Cohen, *Designing Groupwork Strategies for the Heterogeneous Classroom* (Teachers College Press, New York, 1994).
18. J. Handelsman, C. Pfund, S. M. Lauffer, C. M. Pribbenow, *Entering Mentoring* (University of Wisconsin Press, Madison, 2005).
19. L. Cuban, *How Scholars Trumped Teachers: Change Without Reform in University Curriculum, Teaching, and Research, 1890–1990* (Teachers College Press, New York, 1999).

20. We wish to thank the Howard Hughes Medical Institute Professors Award and the University of Illinois Provost's Initiative for Teaching Advancement for financial supports and teaching assistants, invited speakers, and industrial laboratories, whose names are listed in (*14*), for their help. We thank all of our students for their enthusiastic participation and feedback.

Supporting Online Material
www.sciencemag.org/cgi/content/full/318/5858/1872/DC1

10.1126/science.1150788

ETHICS

The Ethics of International Research with Abandoned Children

Research with abandoned children does not necessarily involve exploitation.

Joseph Millum and Ezekiel J. Emanuel

The aim of human subjects research is to create generalizable knowledge that benefits future patients. Consequently, it risks sacrificing the interests of research participants for the greater good of society. Ethics guidelines exist to minimize this risk. Over the last decade, international biomedical research in the context of substantial health-care inequalities has focused discussion on four ethical issues: (i) standards of care; (ii) informed consent; (iii) ancillary care obligations; and (iv) posttrial benefits (see table, right). It is appropriate to consider these issues relative to the Bucharest Early Intervention Project (BEIP) study (*1*), a randomized trial of the effects of moving institutionalized young children to foster care.

Four International Bioethical Issues

The standard-of-care debate erupted in the 1990s around placebo-controlled trials in developing countries of "short-course AZT" for prevention of maternal-fetal HIV transmission. Short-course AZT was expected to be less effective than the standard AZT treatment available in developed countries. Critics argued that using placebo controls, rather than standard treatment as an active control, constituted a double standard—research forbidden on the wealthy would be carried out on the poor (*2, 3*). Supporters countered that it is permissible to offer research participants in developing countries less-effective interventions than those used in developed countries if doing so (i) is scientifically necessary to answer an important question; (ii) does not deny anyone treatment they would otherwise receive; and (iii) is intended to develop interventions that will benefit the developing country (*4*).

Informed consent is fundamental to ethical research. But some commentators argue that valid informed consent cannot be obtained in developing countries, whose inhabitants are impoverished, poorly educated, deprived of medical services, and unfamiliar with research (*5, 6*). Others reply that this is patronizing and inaccurate. Poverty may constrain choices, but it does not make people coerced or incompetent, and participants in developing countries seem to understand the elements of research as well, or badly, as their wealthier counterparts (*7*).

Ancillary care refers to medical treatments provided by researchers during the trial above and beyond what is required for safety or scientific validity. Although researchers in developing countries often feel obliged to provide other treatments that their subjects desperately need, the nature and extent of these obligations are not well defined. The most complete account justifies ancillary care obligations because research participants entrust aspects of their health to investigators through the procedures they undergo (*8*).

Many believe that researchers have obligations to provide participants posttrial benefits. These benefits are intended to prevent exploitation, which occurs when one party takes unfair advantage of another (*9, 10*). In international research, the fear is that the developed world will get too much of the benefits of medical research and the developing world too much of its burdens. According to the Council for International Organizations of Medical Sciences (CIOMS), research in a community is permissible only if researchers or their sponsors ensure that interventions resulting from the research are made "reasonably available" to the community (*11*). An alternative, the "fair benefits" framework, proposes that posttrial benefits may comprise a myriad of benefits including ancillary care, training of health care personnel, employment, and economic stimulation, as well as the study intervention. The total must be considered fair by the community participating in the research (*10*).

The Ethics of the BEIP Study

The BEIP was a randomized trial comparing institutional and foster care for abandoned children currently in institutions. It took place in Romania, where there are thousands of institutionalized children. Because, at the trial's inception, Romania lacked basic foster care, the researchers developed their own, training foster parents and providing social support. The study found significantly improved cognitive development at 42 and 54 months for children transferred to foster care before 2 years of age compared with institutionalized children.

The initial reaction to the BEIP may be that the extreme vulnerability of abandoned, institutionalized children renders any research on them unethical. Not only are they unable to give informed consent, there is no clear guardian acting in their best interests. This puts them at greater risk of being selected for reasons of convenience rather than scientific necessity. While these are valid concerns, familiar safeguards can protect such children. People who cannot consent can be protected by enrolling them only in minimal-risk research, whose risks do not exceed those of everyday life. None of the study's assessments of functioning were likely to harm the children. Restricting the participation of vulnerable groups, such as prisoners and the institutionalized, to research that

ISSUE	KEY QUESTION	RESPONSE
Standard of care	Must interventions always be tested against the treatment available in developed countries?	Exceptions when scientifically necessary, no harm, and research aims to benefit community
Informed consent	Can poor people in developing countries give valid informed consent to research?	Available data do not show informed consent is invalid
Ancillary care	What treatments should be provided by researchers during the trial beyond those needed for safety or scientific validity?	Depends on the aspects of their health that participants entrust to researchers
Posttrial benefits	What should be provided to research participants and host communities after the research trial?	Two main approaches: reasonable availability of study intervention and fair benefits approved by the community

Four main ethical issues in international research.

Department of Bioethics, The Clinical Center, National Institutes of Health, Bethesda, MD 20892–1156, USA.

*Author for correspondence. E-mail: eemanuel@cc.nih.gov

addresses important questions relevant to their situation protects against unfair subject selection (*12*). The BEIP study aimed to produce results that would primarily benefit abandoned, institutionalized children.

The BEIP has many of the features that have generated special concern about medical research in developing countries. Romania, the host country, is a transition economy with a relatively poor health-care infrastructure and a large number of underserved institutionalized children. The funding and research leadership for the trial came from the United States. Although the results may be relevant to the United States and other developed countries, there have been no American randomized trials comparing foster and institutional care, and no American children would be enrolled in the BEIP. Of greatest concern are the standards of care affected in the trial arms and the distribution of posttrial benefits.

The appropriate standard of care for a clinical trial depends on the research question being answered. Although the importance of equipoise, i.e., uncertainty among experts, is disputed (*13*), ethics requires at least that the research address an important question and be scientifically valid. Trials that do not meet these conditions lack social value. If a research study will not generate socially useful knowledge, it wastes resources and exposes participants to risks and burdens for no good reason.

The BEIP study addresses an important question; the welfare of institutionalized children depends on choosing correctly between further institutional care or switching to foster care. Prior data focused on adoption and did not directly address this comparison, had selection biases, and lacked a definitive randomized trial. Thus, the study appears to fulfill equipoise. Moreover, although both institutional and foster care can sometimes result in maltreatment, study participation was unlikely to cause net harm to the children; no child was put at additional risk to obtain the results, which reduces the ethical reasons for worrying about equipoise.

Guarding Against Exploitation

To judge whether this trial involved exploitation requires assessing whether the study's benefits were distributed fairly among the parties involved. A useful framework is national research. In a developed country, the results of research are expected to eventually be integrated, albeit haphazardly, into that country's health system. Although participants assume risks in research, they, and their fellow citizens, also benefit. If all subject protection requirements are fulfilled (*14*), the research is permissible. But in international research, the people that benefit may not come from the same society as the research participants; no shared national relationship between researchers, subjects, and society exists. Thus, outsourcing research may increase the potential for exploitation.

One way to minimize the chance of exploitation is to emulate national research. According to CIOMS, achieving this in the international context requires that the research be responsive to the health needs of the study population and that the population gains from the research results (*10*, *11*).

The BEIP meets these two conditions. The research responds to the health needs of many abandoned children for whom the state is responsible. Moreover, the instigation of the study by the Romanian Secretary of State for Child Protection and official reaction to its results indicate that the study had a high likelihood of having an impact on these children's lives; state policy was likely to adopt the BEIP conclusions. This impact is not guaranteed: social and economic circumstances or government policies might change, resources may not be made available for foster care, or the conclusions of the research may be disputed. Certainty about implementation cannot be required to ethically proceed with a study. Instead, researchers must judge the likelihood that their work will generate health benefits, and proceed on the basis of its expected benefit. The expected benefits to Romania's abandoned children appear to provide ample justification for the BEIP.

Finally, judging whether exploitation has been avoided by using the responsiveness to needs and reasonable availability criteria can be problematic. These criteria consider benefits to the participants' community. But it is the participants—not the community—who bear the risks of research and are therefore most vulnerable to exploitation. Even when a successful intervention will be available to a population after the trial's completion, supplying it to the research participants themselves may not be possible.

Unfortunately, in many cases harm to participants is inherent in generating valid scientific results. In some trials, data on the effectiveness of an intervention cannot be obtained without some risk to the subjects, perhaps of serious or fatal outcomes. For instance, for a vaccine trial to be successful, some participants must acquire the disease the vaccine is intended to prevent. Otherwise, no intervention can be shown to be superior. But the preventive benefits of the vaccine do no good for participants who became infected during the study. Similar issues arise in many cancer and cardiovascular trials. The BEIP raises the same concern; the children who remained in institutional care cannot now receive the benefit of early foster care, which the trial showed to be superior for some developmental outcomes.

This consideration does not make the BEIP study unethical, just as it does not make vaccine trials unethical. However, it does indicate that researchers need to pay special attention to how results get implemented when the benefits cannot accrue to participants. For instance, trial designs that move participants into the arm that is doing better during the course of the trial can be employed. According to the researchers, limited funds foreclosed this option. Alternatively, as done in the BEIP, researchers can present valid scientific results as soon as possible to those parties who can act on them. These parties have responsibilities to the participants, too; because the children were involved in research for the benefit of Romanian society, the representatives of society should ensure that the children get the care they deserve.

The BEIP researchers did not create and are not responsible for Romania's institutionalization of abandoned children. They conducted research to determine what interventions would benefit these children. This is not exploitation, but shows how research can help benefit participants, as well as the wider population of abandoned institutionalized children.

References and Notes

1. C. A. Nelson III *et al.*, *Science* **318**, 1937 (2007).
2. M. Angell, *N. Engl. J. Med.* **337**, 847 (1997).
3. P. Lurie, S. M. Wolfe, *N. Engl. J. Med.* **337**, 853 (1997).
4. R. K. Lie, E. J. Emanuel, C. Grady, D. Wendler, *J. Med. Ethics* **30**, 190 (2004).
5. G. Annas, M. Grodin, *Am. J. Publ. Health* **88**, 560–563 (1998).
6. N. A. Christakis, *Hastings Cent. Rep.* **18**, 35 (June-July 1988).
7. C. Pace, C. Grady, E. J. Emanuel, *SciDevNet*, 28 August 2003; www.scidev.net.
8. H. S. Richardson, L. Belsky, *Hastings Cent. Rep.* **34**, 25 (January-February 2004).
9. A. Wertheimer, *Exploitation* (Princeton Univ. Press, Princeton, NJ, 1999), p. 10.
10. The participants in the 2001 Conference on Ethical Aspects of Research in Developing Countries, *Hastings Center Rep.* **34**, 17 (May-June 2004).
11. *International Ethical Guidelines for Biomedical Research Involving Human Subjects* (Council for International Organizations of Medical Sciences, Geneva, 2002), Guideline 10.
12. U.S. National Commission for the Protection of Human Subjects of Biomedical and Behavioral Research, *The Belmont Report: Ethical Guidelines for the Protection of Human Subjects of Research* (U.S. Government Printing Office, Washington, DC, 1979).
13. F. Miller, H. Brody, *Hastings Cent. Rep.* **33**, 19 (May-June 2003).
14. E. J. Emanuel, D. Wendler, C. Grady, *JAMA* **283**, 2701 (2000).

15. We thank C. Grady, F. Miller, G. Persad, A. Schulz-Baldes, D. Wendler, and A. Wertheimer. The opinions expressed are the authors' own. They do not reflect any position or policy of the National Institutes of Health, U.S. Public Health Service, or Department of Health and Human Services.

10.1126/science.1153822

HISTORY OF SCIENCE

Hoyle's Equation

Donald D. Clayton

The paper that first explained how the elements form in stars did not receive the acclaim it deserved because it did not display its key equation.

One of the grand theories of science holds that the chemical elements and all of their isotopes were synthesized from hydrogen and helium by nucleosynthesis—nuclear reactions within young massive stars (*1*). The abundances of elements today are thus the product of natural history and evolution. Although this theory is now accepted, the scientific paper that forms its foundation (*1*) has been strangely underappreciated in comparison with later works (*2, 3*). Recently, researchers gathered at an international conference at the California Institute of Technology (*4*) to celebrate the anniversary of two groundbreaking 1957 publications (*2, 3*) that according to its Web site "opened the whole field of nuclear astrophysics into a diverse and thriving scientific and intellectual enterprise." However, I would like to look back at the issue of how this early work of Fred Hoyle (shown in photo) came to be both poorly understood and incongruously undercited.

Stellar pioneer. Fred Hoyle on the Caltech campus in February 1967.

In attending and speaking at the conference (*5*), it became clear to me that even experts are unaware of the contents of Hoyle's 1954 paper. Its undercitation probably resulted from the omission of a written equation that is central to the theory and from which the essence of the origin of the elements can be derived. Subsequent nucleosynthesis theory tended to focus on the specific nuclear processes responsible for specific sets of natural isotopes. Limited controversy did erupt in 1983 after W. A. Fowler, a Caltech coauthor of the paper known as B²FH (for the initials of its authors) (*2*), was awarded the Nobel Prize in physics for his experimental role in clarifying nucleosynthesis rates in stars whereas Hoyle as creator of the theory of nucleosynthesis was omitted.

In what follows, I will offer my own "Hoyle's equation" as determined from my reading of his 1954 paper (*1*). Hoyle's equation addresses the origin from initial hydrogen and helium of the set of very abundant isotopes in stars more than 10 times as massive as the sun—what is now called "primary nucleosynthesis." By contrast, B²FH (*2*) contributed creatively to the "secondary processes" of nucleosynthesis, those that change one preexisting heavy nucleus into another but do not increase the metallicity (that is, the abundance of elements heavier than helium) of the galaxy as it ages. Hoyle's words and quantitative arguments (*1*) are more sweeping than the detail-oriented sequels. Hoyle's discussion is phrased in terms of the mass Δm_{new} of new primary isotopes that are ejected from massive stars, which he saw as their source. His approach to stellar nucleosynthesis takes their galaxy-wide rate of production dm_{new}/dt to be the product of the death rate of stars and the mass Δm_k of isotope k ejected at time t from each star.

Hoyle explained that gravitational contraction causes temperature increases after each central nuclear fuel is consumed, and he described the nuclear burning and associated nucleosynthesis of Δm_k during each sequential advanced core evolution. Because those massive stars all evolve almost instantaneously in comparison with galactic time scale, Hoyle takes $B_{M>}(t)$ to be the birth rate of massive stars at time t. It must on average equal their death rate if the numbers of stars are to change only slowly. The subscript $M>$ characterizes stars too massive to become white dwarfs; for these stars, Hoyle (*1*) predicted that collapse of the final central evolved core is inevitable. So, for the massive stars that his paper focused on, "Hoyle's equation" expresses the rate of ejection of new primary isotopes from carbon to nickel as

$$dm(\text{C-Ni})/dt = B_{M>}(t)\ \mathbf{Ev}^{\text{nucl}}\ \Sigma_k \Delta m_k$$

where $\mathbf{Ev}^{\text{nucl}}$ expresses the nuclear and stellar evolution of a massive star, and $\Sigma_k \Delta m_k$ is the sum over k isotope masses.

Hoyle identified the new primary isotopes created within each successive core burning phase. Each burning core is smaller than the one before, so that the star takes on an onionskin structure containing the residual Δm_k of each burning phase (see the figure). Hoyle also correctly stated that neutrino emission governs the collapse time scale when core temperature exceeds 3×10^9 K. Hoyle's equation expresses a modern view of the nucleosynthesis that increased metallicity during galactic history. Hoyle missed only the full set of reactions involved during silicon burning and the relative numbers of protons and neutrons involved in the nuclear statistical equilibrium. Curiously, B²FH, published 3 years later, with Hoyle as one of its coauthors, did not focus on Hoyle's massive-star picture or on his equation, an oversight that I attribute to his lack of careful proofreading

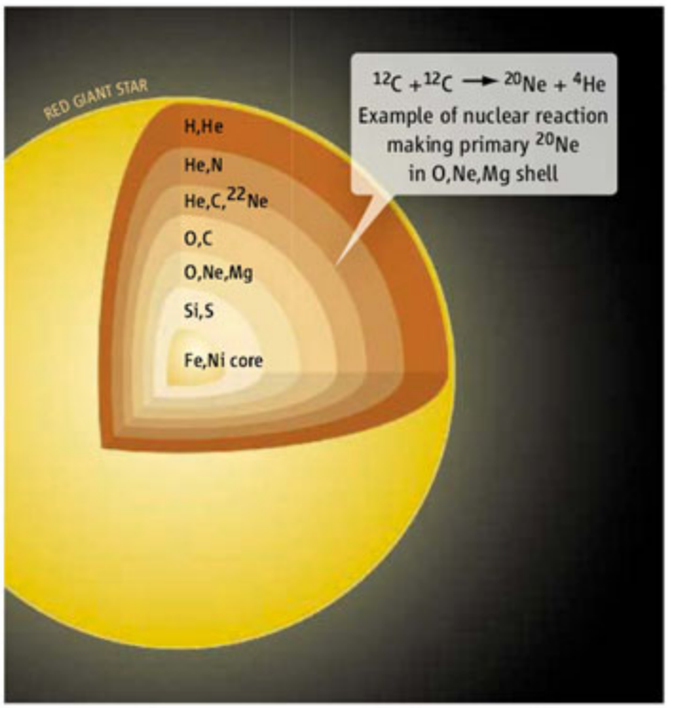

New elements in stars. A massive star develops an onionlike structure with zones in which different elements have been synthesized by nuclear reactions.

The author is in the Department of Physics and Astronomy, Clemson University, Clemson, SC 29634, USA. E-mail: cdonald@clemson.edu

CREDITS: (TOP) DONALD D. CLAYTON/AIP EMILIO SEGRÈ VISUAL ARCHIVES/CLAYTON COLLECTION; (BOTTOM) ADAPTED FROM IMAGE BY NASA

of a manuscript drafted by E. M. and G. R. Burbidge (*6*).

It is unfortunate that he did not put to paper the equation he envisioned and described verbally. Had he done so, unambiguous scientific visibility of his achievement would have followed more easily. In that spirit, I submit Hoyle's equation as implicit in the arguments of his pioneering 1954 paper and suggest that it is one of the landmark papers in the history of science.

References and Notes

1. F. Hoyle, *Astrophys. J. Suppl.* **1**, 121 (1954).
2. E. M. Burbidge, G. R. Burbidge, W. A. Fowler, F. Hoyle, *Rev. Mod. Phys.* **29**, 547 (1957).
3. A. G. W. Cameron, *Chalk River Laboratory Report CRL 41* (Atomic Energy of Canada, Ltd., Chalk River, Ontario, 1957).
4. Nuclear Astrophysics 1957–2007, 23 to 27 July 2007, California Institute of Technology, www.na2007.caltech.edu/.
5. D. D. Clayton, www.na2007.caltech.edu/program2.html.
6. Remarks by G. R. Burbidge at the Caltech conference (*4*).

10.1126/science.1151167

MOLECULAR BIOLOGY

The Two Faces of miRNA

MicroRNAs can enhance or repress messenger RNA translation, depending on whether cells are proliferating or arrested in the cell cycle.

J. Ross Buchan and Roy Parker

MicroRNAs (miRNAs) are 20- to 22-nucleotide RNAs that regulate the function of eukaryotic messenger RNAs (mRNAs) and play important roles in development, cancer, stress responses, and viral infections. miRNAs are well known to inhibit the translation of mRNAs into protein and to promote mRNA degradation. On page 1931 of this issue, Vasudevan *et al.* (*1*) show that miRNAs can also increase translation, broadening the effect of these small RNAs on protein expression.

To function, a miRNA associates with an Argonaute protein, of which there are four in mammalian cells (Ago1 to Ago4). Each miRNA-Ago complex interacts with a specific mRNA, typically through pairing of nucleotide bases between the miRNA sequence and complementary sequences in the mRNA's 3′-untranslated region (3′UTR). Such 3′UTRs are important assembly sites for complexes that affect mRNA localization, translation, and degradation. How Ago-miRNA complexes repress translation and/or promote mRNA degradation is not clear but involves the recruitment of additional protein factors, most notably the GW182 protein (*2*).

Vasudevan *et al.* build on earlier work showing that the 3′UTR of tumor necrosis factor–α (TNF-α) mRNA stimulates translation when mammalian cells are deprived of serum (which contains nutrients and growth factors), arresting the cell division cycle at a particular phase (G_1) (*3*). This stimulation requires Ago2, raising the heretical idea that miRNAs both enhance and repress translation.

Indeed, Vasudevan *et al.* now show that when cultured mammalian cells are serum-starved (G_1 phase arrest), binding of a specific miRNA (miR369-3) to a reporter mRNA (containing the TNF-α 3′UTR) stimulates translation, whereas no stimulation occurs when miR369-3 is absent. In contrast, miR369-3 represses translation during other cell cycle phases. The well-studied "repressive" *let7* miRNA and the artificial miRNA mimic *cxcr* also enhance mRNA translation during starvation-induced G_1 arrest, whereas they repress translation elsewhere in the cell cycle. Thus, multiple miRNAs and associated Ago proteins can enhance or repress translation, depending on the cell cycle state.

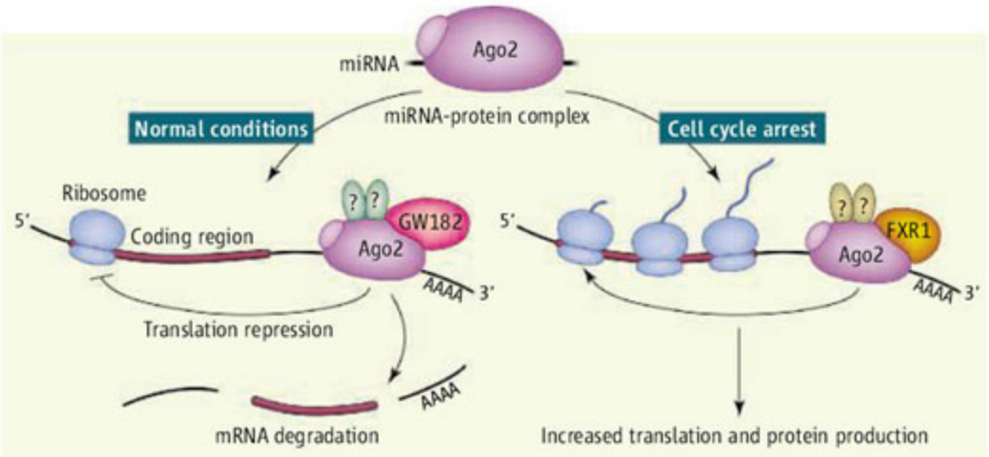

Dual functions of miRNAs. MicroRNAs (miRNAs) can boost or block the translation of target mRNAs. Physiological conditions affect the recruitment of regulatory proteins, which can alter a miRNA's effect.

Stimulation of translation involves a change in the proteins recruited to mRNA by the miRNA-Ago complex (see the figure). During cell cycle arrest, the RNA binding protein FXR1 is recruited to mRNA by the miRNA-Ago complex and stimulates translation (*1*, *3*). Whether other activator proteins are recruited, or repressive proteins (such as GW182) are lost, during this condition is unknown.

The diversity of proteins recruited to mRNAs by miRNAs is further broadened by multiple members of the Ago, GW182, and FXR protein families as well as by the expression levels and posttranslational modifications of Ago-interacting proteins. Moreover, the effect of a miRNA-Ago complex can also be modulated by proteins bound to other sites within the 3′UTR. For example, in response to multiple stresses, increased translation of the *CAT-1* mRNA in hepatic cells depends on specific binding sites for miRNA-122 in *CAT-1* mRNA, and binding of the protein HuR to the 3′UTR (*4*).

The roles of miRNAs in multiple stress responses hint that other environmental changes may convert some miRNAs to activating roles (*5*). Moreover, because many of the Ago-interacting proteins (such as FXR1) also bind RNA, some mRNAs might have sequences that constitutively recruit miRNA-Ago complexes that activate translation.

Differential effects of miRNAs at various cell cycle stages or during cellular stress may explain some confusion in the field, including differences in the extent of repression caused by a given miRNA, and the detection of translationally repressed mRNAs with ribosomes. These differences might be explained if cells are distributed differently across the cell cycle in various experiments.

Small RNAs serving as both activators and

The authors are in the Department of Molecular and Cellular Biology, Howard Hughes Medical Institute, University of Arizona, Tucson, AZ 85721, USA. E-mail: rrparker@email.arizona.edu

repressors of gene expression are perhaps not limited to miRNAs. Specific Piwi-interacting RNAs, thought to repress gene expression, may enhance transcription in the fly *Drosophila melanogaster* (*6*). Moreover, when delivered into mammalian cells, some double-stranded RNAs complementary to promoter sequences increase gene expression (*7*, *8*).

The present work by Vasudevan *et al.* raises many questions. What are the mechanisms by which miRNAs enhance translation? Does miRNA stimulation of translation raise a possible complication, and opportunity, in using miRNAs and small interfering RNAs as therapeutics? Finally, assuming miRNAs generally stimulate translation in cells exiting the cell cycle, what role might miRNAs play in developmental and terminal differentiation processes? In a field replete with activity, this latest twist in function may foreshadow even more faces of these intriguing micromolecules.

References

1. S. Vasudevan, Y. Tong, J. A. Steitz, *Science* **318**, 1931 (2007); published online 29 November 2007 (10.1126/science.1149460).
2. N. Standart, R. J. Jackson, *Genes Dev.* **21**, 1975 (2007).
3. S. Vasudevan, J. Steitz, *Cell* **128**, 1105 (2007).
4. S. N. Bhattacharyya *et al.*, *Cell* **125**, 1111 (2006).
5. A. K. L. Leung, P. A. Sharp, *Cell* **130**, 581 (2007).
6. H. Yin, H. Lin, *Nature* **450**, 304 (2007).
7. L. C. Li *et al.*, *Proc. Natl. Acad. Sci. U.S.A.* **103**, 17337 (2006).
8. B. A. Janowski *et al.*, *Nat. Chem Biol.* **3**, 166 (2007).

10.1126/science.1152623

ATMOSPHERIC SCIENCE

Revisiting Ozone Depletion

New laboratory data imply unknown mechanisms in the formation of the ozone hole, but it is too soon to throw out the old paradigms.

Marc von Hobe

In 1985, Farman *et al.* (*1*) discovered a substantial thinning of the stratospheric ozone layer over Antarctica in spring. This "ozone hole" took the atmospheric research community by surprise because it could not be explained by any catalytic cycles known to remove ozone in the stratosphere. Today, the consensus is that the chemical processes responsible for the formation of this "ozone hole" are reasonably well understood. New laboratory data published recently by Pope *et al.* (*2*) call this consensus into question, but the results must be treated with caution.

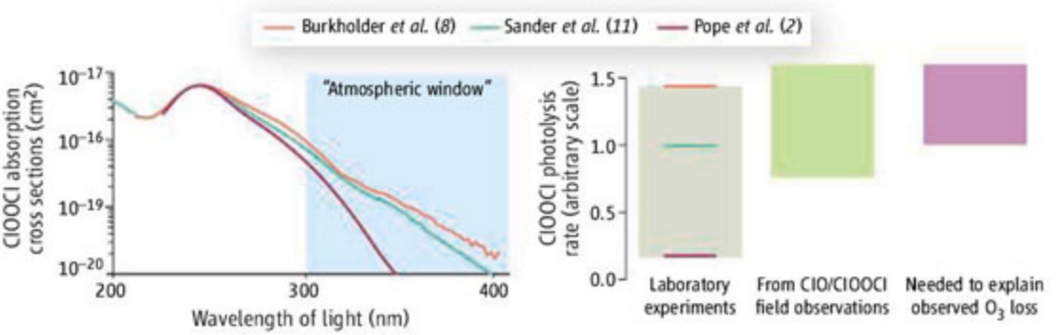

Photolysis of ClOOCl. (Left) ClOOCl absorption cross sections measured by Pope *et al.* (*2*) are lower than those measured previously (*8*, *11*), especially in the "atmospheric window" above 300 nm, where most incoming solar irradiation occurs. **(Right)** The photolysis rate obtained by Pope *et al.* is inconsistent with field observations of chlorine compounds (green bar), whereas rates determined previously (*8*, *11*) agree with field observations. The purple bar shows the range of photolysis rates consistent with observed ozone loss.

Two types of processes are key to understanding the unusually large ozone loss rates in the cold polar stratosphere. First, HCl and $ClONO_2$ are activated on the surfaces of polar stratospheric clouds to form compounds actively involved in catalytic ozone destruction (*3*). Next, these activated species participate in the ClO–dimer (*4*) and ClO–BrO (*5*) catalytic cycles that rapidly destroy ozone at cold temperatures and high solar zenith angles. These two catalytic cycles are believed to be responsible for more than 80% of polar ozone loss during spring (*6*).

The results published by Pope *et al.* (*2*) suggest a much smaller absorption cross section of the ClO dimer ClOOCl (see the left panel of the figure). The absorption cross section is a measure of how efficiently light is absorbed and determines how fast ClOOCl is photolyzed. This photolysis determines the speed of the ClO–dimer cycle and also affects the ClO-BrO cycle. The new result would make both cycles—and hence the overall ozone loss rate—much slower, with possible implications for our ability to predict future polar ozone depletion (*7*).

In their experiment, Pope *et al.* (*2*) have introduced an innovative way to avoid impurities by trapping ClOOCl at –125°C before the absorption measurement. However, they did not present a detailed analysis of how possible systematic errors due to impurities may have affected earlier studies. For example, the difference between cross sections published by Burkholder *et al.* (*8*) and by Pope *et al.* cannot be explained by any linear combination of absorption spectra resulting from known impurities. Moreover, Pope *et al.* failed to add confidence to their results by monitoring infrared and/or microwave absorption as done in earlier studies (*8*). Without these tests, the authors cannot completely rule out heterogeneous chemistry in the cold trap or secondary chemistry in the photolysis cell. This is particularly problematic because the interpretation of their data relies on the assumptions that the ClOOCl absorption spectrum is fully represented by the superposition of two Gaussian functions and that no impurities other than Cl_2 are present.

The challenges posed by the new study may act as an incentive to address the problem on a wider scale. The laboratory studies available today all disagree with each other, and only one—or maybe none—can be correct. To solve this dilemma, we must understand and unambiguously identify the reasons for the discrepancies.

Doubts about the correctness of the Pope *et al.* measurements are supported by the fact that they are at odds with a wealth of atmospheric observations suggesting larger cross sections (*6*, *9*). Most observations of ClO and its dimer—measured in situ and from satellites—are best explained by the cross sections published by Burkholder *et al.* (*8*), which are the largest in the wavelength region relevant for photolysis in the atmosphere (see the right panel of the figure). These cross sections also best

The author is in the Institute for Chemistry and Dynamics of the Geosphere ICG-1: Stratosphere, Forschungszentrum Jülich GmbH, 52425 Juelich, Germany. E-mail: m.von.hobe@fz-juelich.de

reproduce ozone loss in model simulations (*6*, *10*). In contrast, when the cross sections published by Pope *et al.* are used, only about half the observed O_3 loss is reproduced (*9*).

If the Pope *et al.* results do turn out to be correct, then there must be missing reactions that remove the ClO dimer and eventually lead to ozone destruction. Obviously, any such reactions have so far gone undetected in laboratory experiments studying the formation and photolysis of ClOOCl. Therefore, any new or modified atmospheric mechanism would probably involve species additional to those present in these experiments.

Until the issue is completely resolved—either by refuting Pope *et al.* or by establishing modified ozone destruction mechanisms—modelers should probably not use the new photolysis rate for prognostic studies. Even if Pope *et al.* are correct and our current understanding of polar ozone depletion is incomplete, models using rate constants currently recommended by the National Aeronautics and Space Administration/Jet Propulsion Laboratory data evaluation panel (*11*)—the accepted standard for atmospheric modeling—adequately simulate observed past and present ozone loss and are thus likely to correctly predict future ozone loss.

Given the observed close link between ozone loss and stratospheric chlorine (*12*, *13*), it seems very unlikely that chlorine compounds do not play the key role in destroying polar ozone and that the new measurements will compromise the Montreal Protocol on Substances That Deplete the Ozone Layer in any way (*7*). Nevertheless, atmospheric scientists must explain both the substantial discrepancies between different laboratory studies of the ClOOCl cross sections and the discrepancies between atmospheric observations and laboratory data. Whether this will require introducing previously neglected chlorine species and modified ozone destruction mechanisms remains to be seen.

References and Notes

1. J. C. Farman, *et al.*, *Nature* **315**, 207 (1985).
2. F. D. Pope *et al.*, *J. Phys. Chem. A* **111**, 4322 (2007).
3. S. Solomon, R. R. Garcia, F. S. Rowland, D. J. Wuebbles, *Nature* **321**, 755 (1986).
4. L. T. Molina, M. J. Molina, *J. Phys. Chem.* **91**, 433 (1987).
5. M. B. McElroy, R. J. Salawitch, S. C. Wofsy, J. A. Logan, *Nature* **321**, 759 (1986).
6. WMO, *Scientific Assessment of Ozone Depletion* (World Meteorological Organization, Global ozone research and monitoring project, Report no. 50, 2006; http://ozone.unep.org/Assessment_Panels/SAP/Scientific_Assessment_2006).
7. Q. Schiermeier, *Nature* **449**, 382 (2007).
8. J. B. Burkholder, J. J. Orlando, C. J. Howard, *J. Phys. Chem.* **94**, 687 (1990).
9. M. von Hobe *et al.*, *Atmos. Chem. Phys.* **7**, 3055 (2007).
10. K. Frieler *et al.*, *Geophys. Res. Lett.* **33**, 10.1029/2005GL025466 (2006).
11. S. P. Sander *et al.*, *Chemical Kinetics and Photochemical Data for Use in Atmospheric Studies 06-2* (Jet Propulsion Laboratory, 2006).
12. J. G. Anderson *et al.*, *J. Geophys. Res.* **94**, 11465 (1989).
13. P. A. Newman, E. R. Nash, S. R. Kawa, S. A. Montzka, S. M. Schauffler, *Geophys. Res. Lett.* **33**, 10.1029/2005GL025232 (2006).

14. I thank R. Müller and F. Stroh for presubmission review and two anonymous reviewers for comments that helped clarify and strengthen the manuscript.

10.1126/science.1151597

DEVELOPMENT

Is Therapeutic Cloning Dead?

The ability to generate pluripotent stem cells directly from skin fibroblasts may render ethical debates over the use of human oocytes to create stem cells irrelevant.

Jose Cibelli

Ever since it was first suggested by Robert Edwards and Patrick Steptoe in their 1980 book *A Matter of Life* (*1*), it seemed that the path to making immunocompatible cells to potentially treat human diseases would necessitate cloning of a human embryo. This process calls for replacing the DNA of an unfertilized egg (oocyte) with that from the patient's somatic cell, in vitro culture of the reconstructed embryo to the blastocyst stage, and subsequent isolation of pluripotent cells that could potentially differentiate into any cell type. The prediction of Edwards and Steptoe came closer to reality with the arrival of Dolly, the cloned sheep, and derivation of the first human embryonic stem cells by James Thomson's group (*2*, *3*). This procedure of somatic cell nuclear transfer has been referred to as human therapeutic cloning (*4*), and although studies in mice have shown that this approach is possible (*5*, *6*), its proof-of-principle in humans never materialized. Now, two reports in this issue—by Yu *et al.* on page 1917 (*7*) and Hanna *et al.* on page 1920 (*8*)—and a recent report by Takahashi *et al.* (*9*) suggest that human therapeutic cloning may never happen.

Takahashi *et al.* (*9*) report the generation of human induced pluripotent stem cells using four transcription factors: Oct4, Sox2, Klf4, and c-Myc. These are the same transcription factors previously reported by this group and others to produce such stem cells in mice (*10*–*14*). Takahashi *et al.* have now shown that exogenous expression of these genes (delivered by retroviral vectors) can transform newborn and adult human fibroblasts into induced pluripotent stem cells. Two of these factors can be considered predictable in that they appear in most microarray analyses of mouse and human embryonic stem cells and are important in development. But the two other factors, c-Myc and Klf4, were unforeseen, and their presence in the "reprogramming quartet" in mice has been difficult to justify. Nevertheless, the cocktail works in human cells, and now the challenge is to determine each factor's role during the reversion of a mature cell to an earlier, unspecialized form that can then differentiate into multiple cell types.

Yu *et al.* (*7*) also report the production of induced pluripotent stem cells, but use only two factors, Oct4 and Sox2, in combination with

	SCNT-derived cells	ESC from fertilized embryos		iPS cells	
	Mouse	Mouse	Human	Mouse	Human
Stemness markers	Yes	Yes	Yes	Yes	Yes
Unlimited self-renewal (*) when cultured under ESC culture conditions	Yes	Yes	Yes	Yes	Yes
Differentiation into teratomas in immunosuppressed mice	Yes	Yes	Yes	Yes	Yes
Germline transmission	Yes	Yes	n/a	Yes	n/a
Direct differentiation	Yes	Yes	Yes	Yes	Yes
Genetic match with donor	Yes	No	No	Yes	Not yet determined

Features of pluripotent stem cells derived by different procedures. SCNT, somatic cell nuclear transfer; ESC, embryonic stem cells; iPS, induced pluripotent stem cells; asterisk indicates the capacity to proliferate for periods of time longer than those recorded in somatic cells of the same species while maintaining their pluripotent state.

The author is in the Departments of Animal Sciences and Physiology, Cellular Reprogramming Laboratory, Michigan State University, East Lansing, MI 48824, USA, and at the Program for Cell Therapy and Regenerative Medicine of Andalusia, Seville, Spain. E-mail: cibelli@msu.edu

one more predictable transcription factor, NANOG, and a fourth largely unconsidered gene encoding Lin28, a protein thought to be involved in RNA processing (*15*). This combination shares only two of the factors reported by Takahashi *et al.*, raising the question of redundancy among genes that can reprogram cells. Perhaps one master gene upstream of the six now described opens the gate to pluripotency. Yu *et al.* avoid expressing c-*Myc*, which can act as an oncogene and cause cancer, and improve gene delivery by using lentiviral vectors. It is possible that c-Myc promotes the proliferation of induced pluripotent stem cells until the stochastic and progressive process of dedifferentiation has progressed sufficiently to allow self-renewal. c-Myc could be functionally redundant with NANOG, which maintains embryonic stem cell pluripotency. Yu *et al.* further show that from the eight induced pluripotent stem cell lines generated, two expressed Oct4, Sox2, and NANOG alone. It is extraordinary that just three exogenously expressed transcription factors can completely reprogram a cell.

Finally, Hanna *et al.* show that symptoms of sickle cell anemia can be ameliorated with induced pluripotent stem cells in a mouse model of this human disease. Adult somatic cells taken from the tail of a mouse bearing a mutated version of the human β-globin gene were converted into induced pluripotent stem cells. The mutation was then repaired and through expression of the HoxB4 transcription factor, the cells were differentiated into hematopoietic progenitor cells and transferred back into the affected animals. All three animals treated with the induced pluripotent stem cells survived up to 20 weeks, whereas untreated animals died before the seventh week of age. The treated animals also showed increases in red blood cells and hemoglobin. Although it is premature to extrapolate these experiments to humans (we have yet to obtain mature blood cells from human embryonic stem cells), Hanna *et al.* have shown that induced pluripotent stem cells are more than a laboratory amusement: They may not only treat, but potentially cure diseases, at least in an animal model (and for the limited time of the study).

These three reports come on the heels of the announcement by Byrne *et al.* that nonhuman primate embryonic stem cells can be derived from adult fibroblasts using somatic cell nuclear transfer (*16*). The next logical step will be to compare the cells obtained by Byrne *et al.* with those generated using the suite of transcription factors implicated in cell dedifferentiation. Such a comparison is necessary to determine whether the reprogramming process and function of induced pluripotent- or somatic cell nuclear transfer-derived cells are equivalent or not. We may not be able to resolve these questions anytime soon, not only because the mechanism of somatic cell nuclear transfer has yet to be described in detail, but more because we can as yet only follow the transformation of a given somatic cell into an induced pluripotent stem cell when embryonic stem cell–like colonies first emerge, and not any earlier.

The current breakthroughs raise exciting questions. Some are technical, such as whether viral vectors can be replaced with other agents that facilitate transient expression of delivered genes. Others are mechanistic, such as whether the conversion of cells is due to epigenetic modifications of key genetic elements or to a genetic event that has yet to be identified. Another question is whether several events must occur in a given sequence, with a precise amount of each transcription factor at a particular time, for cell dedifferentiation to occur and be sustained. This also raises the issue of whether the converted cell that gives rise to an induced pluripotent cell colony is somehow predisposed to "stemness," given that, in the context of somatic cell nuclear transfer, it is clear that pluripotent cells, such as embryonic stem cells, are easier to reprogram into viable animals than are somatic cells.

Is human therapeutic cloning no longer needed? The short answer is no, but it is likely a matter of time until all the hypothetical advantages of therapeutic cloning will be implemented with induced pluripotent stem cells. More importantly, the controversial issues (ethical and technical) specific to human therapeutic cloning may well be left behind along with the procedure itself, a refreshing change for the field, indeed.

References and Notes

1. R. Edwards, P. Steptoe, *A Matter of Life* (Hutchinson, 1980).
2. I. Wilmut, A. E. Schnieke, J. McWhir, A. J. Kind, K. H. S. Campbell, *Nature* **385**, 810 (1997).
3. J. A. Thomson *et al.*, *Science* **282**, 1145 (1998).
4. R. P. Lanza, J. B. Cibelli, M. D. West, *Nat. Med.* **5**, 975 (1999).
5. T. Wakayama *et al.*, *Science* **292**, 740 (2001).
6. W. M. Rideout 3rd, K. Hochedlinger, M. Kyba, G. Q. Daley, R. Jaenisch, *Cell* **109**, 17 (2002).
7. J. Yu *et al.*, *Science* **318**, 1917 (2007).
8. J. Hanna *et al. Science* **318**, 1920 (2007).
9. K. Takahashi *et al.*, *Cell* **131**, 861 (2007).
10. K. Takahashi, S. Yamanaka, *Cell* **126**, 663 (2006).
11. M. Wernig *et al.*, *Nature* **448**, 318 (2007).
12. K. Okita *et al.*, *Nature* **448**, 313 (2007).
13. A. Meissner *et al.*, *Nat. Biotechnol.* **25**, 1177 (2007).
14. R. Blelloch, M. Venere, J. Yen, M. Ramalo-Santos, *Cell Stem Cell* **1**, 245 (2007).
15. E. Balzer, E. G. Moss, *RNA Biol.* **4**, 16 (2007).
16. J. A. Byrne *et al.*, *Nature* **450**, 497 (2007).

17. Thanks to S. Suhr for helpful comments.

10.1126/science.1153229

MATERIALS SCIENCE

The Flow of Glass

Michael L. Falk

Experiments on colloidal glasses quantify how glass structure accommodates flow.

How does glass bend and flow? This question may seem odd to most people, given that in our common experience glass is something hard and brittle. But for those who have seen a glassblower at work, it is clear that the ability of glass to change shape when heated is crucial to its utility and beauty (see the first figure). The flow of glass is the subject of a revealing set of experiments published by Schall *et al.* on page 1895 of this issue (*1*).

The authors performed their experiments on a system composed of colloids—beads smaller in diameter than a human hair suspended in solution. To appreciate the connection between colloids and glassy materials, it is important to understand that in addition to soda-lime glass (the material composed primarily of silica that constitutes our housewares and windows), glasses can also be made from nearly every other kind of material, including plastics and even metals. So what makes something a glass?

To a large extent, a glass is defined by what it is not: a well-ordered crystal. The vast majority of engineering materials are crystalline, that is, they have an underlying repetitive structure from which they derive their electrical, mechanical, thermal, and optical properties. This structure typically arises when the material is created from a liquid. As the liquid cools, the atoms find an arrangement that optimizes their bonding, giving birth to small crystallites that grow into the final material structure.

Glasses, in clear contrast to their crys-

The author is in the Department of Materials Science and Engineering, University of Michigan, Ann Arbor, MI 48109, USA. E-mail: mfalk@umich.edu

The art of glassblowing. When glasses are heated to very high temperatures, they become highly viscous. Upon cooling, the glass rigidifies. The processes that govern flow in the cooled glass are elucidated by Schall *et al.* in this issue.

talline cousins, are models of disorder. As a glass is cooled, its atoms retain the same disorder that they exhibited as a liquid. The motions of the atoms slow down, resulting in a material just as solid as any crystal but without a crystal's obvious structural order. For this reason, glasses have often been referred to as amorphous (literally "shapeless") solids, but recent investigations have indicated that these materials have their own unique, if subtle, structure (*2*). This structure may explain why a glass, a material with a structure so similar to that of a liquid, does not flow in a liquid-like manner. When simple liquids flow, they tend to do so a little bit at a time everywhere, such that their flow is more-or-less uniform. However, studies like those by Schall *et al*. clearly demonstrate that in glasses, flow is not so simple.

Crystals do not flow naturally, but if you apply enough force to them, you can make them flow. On the atomic scale, this is accomplished by a misalignment in the crystal lattice known as a dislocation (see the second figure, top panel). You can think of it as a bump in a rug. It is possible to get a rug, even a very heavy one, to move a small amount by creating a bump on one end and pushing the bump along the rug. Similarly, once a dislocation is created it can glide through the crystal. As a result, the crystal undergoes an internal slip that changes its shape.

Is there a defect that could act as a dislocation for glasses? Spaepen, one of the authors on the current investigation, theorized in 1977 that "flow defects" were responsible for plastic flow in glasses (*3*). Dislocations can be directly imaged in crystals using transmission electron microscopy (*4*), but such characterization techniques are considerably more difficult to apply to glasses.

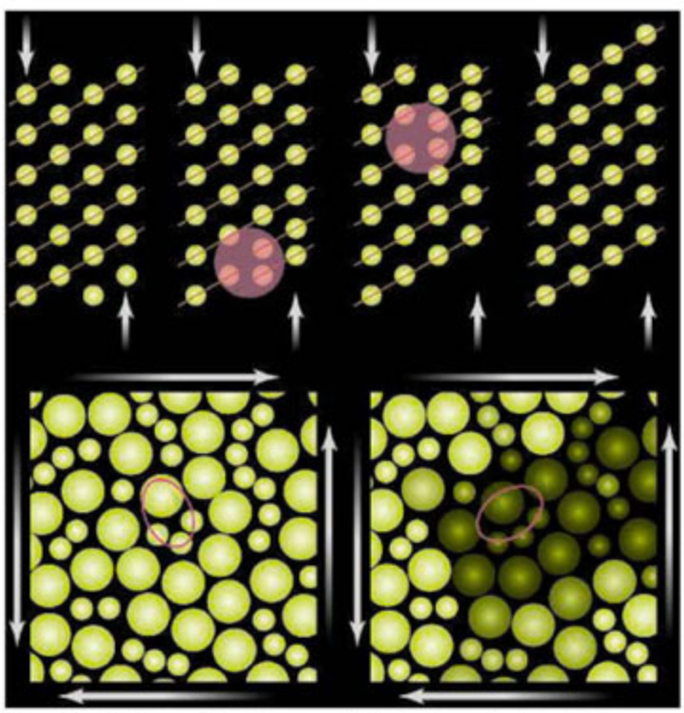

The role of defects. (**Top**) In crystals, flow is determined by dislocations, defects in which the planes of the crystal are shifted relative to each other. These defects change the shape of the material by gliding through the crystal. The arrows denote the applied forces and the red circle shows the location of the dislocation. The diagonal lines emphasize the crystal planes in the atomic arrangement. (**Bottom**) In glasses, a different type of defect—a shear transformation zone—accommodates the flow. When a shear stress is applied in the direction of the arrows, the atoms rearrange from the positions on the left to those on the right. The darker colors denote which atoms on the right have had the most rearrangement in their vicinity. The ovals illustrate the approximate internal rearrangement associated with the shear transformation zone. [Adapted from (*8*)]

PHOTO CREDIT: NIKLAS BERNSTONE/GETTY IMAGES

For this reason, similar but larger-scale systems have long been used to elucidate flow in glasses. Some early investigations were performed in sheared bubble rafts, in which a single layer of millimeter-sized soap bubbles floats on water (*5*, *6*). Based on these experiments, Argon proposed that regions in the glass undergo "shear transformations" (*7*); theories that posit shear transforming flow defects commonly refer to these as shear transformation zones (see the second figure, bottom panel) (*8*). Computer simulations have shown that these zones are associated with regions of enhanced structural disorder (*9*) and are sensitive to pressure (*10*). Schall *et al.* now confirm the existence of shear transformation zones in their colloid system. They also show that they are irreversible and thermally activated, and that their transformation can induce the formation of new shear transformation zones. Furthermore, they quantify the stress needed to cause a shear transformation zone to transform.

There are some important differences between the current work and the model bubble raft systems studied in the 1970s. First, the colloidal system is three-dimensional, providing a more realistic model for a real glass. Second, the authors reveal the detailed dynamics of their system, by means of confocal microscopy and digital data analysis.

These investigations are particularly relevant to understanding the formability, fracture, and failure of an emerging type of material, metallic glasses. While glasses have been made out of metal since the 1960s (*11*), the cooling rates required were so fast that only thin ribbons could be manufactured. It is only in the past two decades that these materials have been produced at moderate quench rates at thicknesses that lend themselves to a broader array of engineering applications (*12*, *13*). Metallic glasses are exceptionally strong and elastic, but when their strength is exceeded they typically fail catastrophically (*14*).

Investigations like those presented by Schall *et al.* provide valuable insights that can provide the underpinnings for predictive theories of glass flow and failure. Such theories are needed to pave the way for new materials that take advantage of the disorder inherent in glasses, which may in the years ahead provide as rich a source of new materials advances as crystals have to date.

References

1. P. Schall *et al.*, *Science* **318**, 1895 (2007).
2. H. W. Sheng, *Nat. Mater.* **6**, 192 (2007).
3. F. Spaepen, *Acta Mater. Acta Metall.* **25**, 407 (1977).
4. S. M. Ohr, J. Narayan, *Philos. Mag. A* **41**, 81 (1980).
5. A. W. Simpson, P. H. Hodkinson, *Nature* **237**, 320 (1972).
6. A. S. Argon, H. Y. Kuo, *Mater. Sci. Eng.* **39**, 101 (1979).
7. A. S. Argon, *Acta Metall.* **27**, 47 (1979).
8. M. L. Falk, J. S. Langer, *Phys. Rev. E* **57**, 7192 (1998).
9. D. Deng *et al.*, *Philos. Trans. R. Soc. London Ser. A* **329**, 549 (1989).
10. C. A. Schuh, A. C. Lund, *Nat. Mater.* **2**, 449 (2003).
11. W. Klement *et al.*, *Nature* **187**, 869 (1960).
12. A. Inoue *et al.*, *Mater. Trans.* **31**, 177 (1990).
13. A. Peker, W. L. Johnson, *Appl. Phys. Lett.* **63**, 2342 (1993).
14. C. A. Schuh *et al.*, *Acta Mater.* **55**, 4067 (2007).

10.1126/science.1150919

Sexual Selection in Males and Females

Tim Clutton-Brock

Research on sexual selection shows that the evolution of secondary sexual characters in males and the distribution of sex differences are more complex than was initially suggested but does not undermine our understanding of the evolutionary mechanisms involved. However, the operation of sexual selection in females has still received relatively little attention. Recent studies show that both intrasexual competition between females and male choice of mating partners are common, leading to strong sexual selection in females and, in extreme cases, to reversals in the usual pattern of sex differences in behavior and morphology.

In the *Descent of Man* (1871), Darwin provided the first coherent explanation of the elaborate weapons and ornaments found in males and, less commonly, in females in many animals. These "secondary" sexual characters did not appear likely to increase survival, and he argued that they were a result of intrasexual competition either for breeding opportunities or to attract the opposite sex. He termed this evolutionary process "sexual selection," describing it as selection that "depends on the advantage which certain individuals have over others of the same sex and species solely in respect of reproduction" (*1*, p. 209).

Our current understanding of Darwin's theory, based on seminal papers by Bateman (*2*) and Trivers (*3*), is that reduced investment in gametes and parental care by males increases their potential rate of reproduction (PRR) (*4*, *5*), biasing the relative numbers of sexually active males to receptive females at any one time (the operational sex ratio, or OSR) (*6*). Biased OSRs, in turn, lead to increased intensity of intrasexual competition, greater variance in breeding success, and stronger selection for traits affecting competitive ability in males than in females (*3*, *6*, *7*). In addition, they are likely to favor the evolution of greater selectivity in choice of mating partners by females, generating selection pressures in males for traits that display their quality as breeding partners (*3*, *8*). Where secondary sexual characters confer important reproductive benefits, they may develop to a point where their benefits are offset by substantial costs to survival, either among juveniles or among adults (*3*, *9*).

Although the assumptions and predictions of the theory of sexual selection have withstood repeated testing (*10*), recent reviews have pointed to inconsistencies in relationships between parental investment, reproductive competition, and sex differences in behavior and morphology, as well as to the scarcity of detailed studies of the operation of sexual selection in females (*11*–*15*). Roughgarden *et al.* (*16*) recently argued, in this journal, that "sexual selection theory is always mistaken, even when gender roles superficially match the Darwinian templates" and went on to advocate its replacement by a novel theory of social selection. That 40 evolutionary biologists cooperated to write 10 letters rejecting these criticisms shows that Roughgarden's views are unusual (*17*), but it is clear that the mechanisms underlying sex differences in reproductive competition and the traits associated with them are both more diverse and more complex than was initially realized. In the wake of Roughgarden *et al.*'s review, both the exceptions to the basic structure of sexual selection theory and the operation of sexual selection in females deserve further attention.

Department of Zoology, University of Cambridge, Downing Street, Cambridge CB2 3EJ, UK. E-mail: thcb@cam.ac.uk

Sexual Selection in Males

It is now clear that relationships between relative gamete size, the evolution of parental care, OSRs, the relative intensity of competition, and the extent of selectivity in the two sexes are not as straightforward as was originally supposed. Sex differences in parental care are not an inevitable consequence of sex differences in gamete size because patterns of parental care are likely to coevolve and feedbacks may be complex (*18*, *19*). Sex differences in parental investment are not the only factors affecting the OSR (*5*, *15*): Biases in the sex ratio at birth or hatching, sex differences in juvenile or adult survival or in the proportion of individuals acquiring the resources necessary to breed, and variation in the costs of competing may all affect the relative numbers of males and females competing for mates in the two sexes (*5*, *20*–*22*). Finally, the OSR is not the only factor affecting the relative intensity of intrasexual competition and mate selection in the two sexes, and the sex that competes most intensely for breeding partners is not always less selective in its choice of mates. For example, the usual tendency for females to be more selective than males can be reversed where variance in female quality is large and males can increase their fitness by selecting superior partners (*13*, *23*, *24*).

Relationships between intrasexual competition and reproductive variance are also more complex than early papers suggested. Although variance in fitness is a prerequisite for selection, a substantial proportion of reproductive variance in

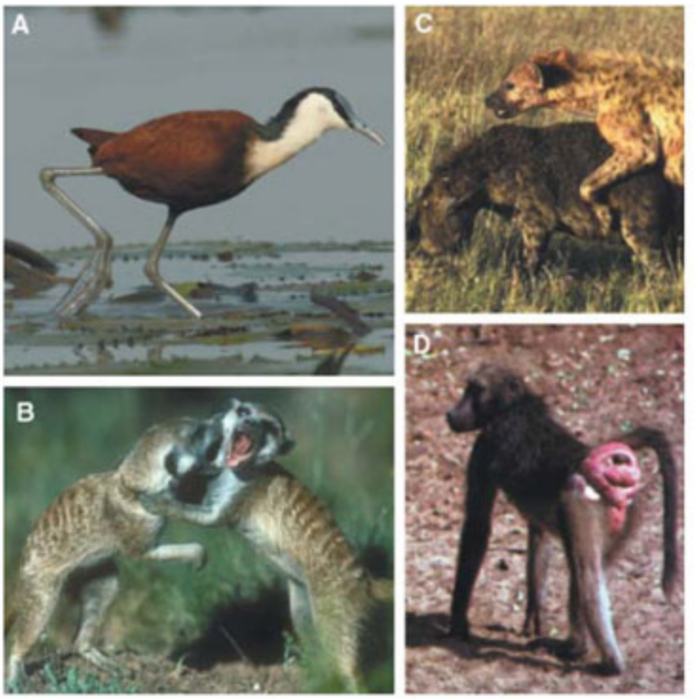

Fig. 1. In many animals, competition between females for breeding opportunities is intense, and females show pronounced secondary characters. In polyandrous birds, where males invest heavily in parental care, females compete intensely more frequently for breeding opportunities than males and are commonly larger than males as in (**A**) female African jacana (*Actophilornis africanus*). Female competition for breeding opportunities is also intense in a number of social mammals where female rank and breeding success are closely correlated, including (**B**) Kalahari meerkats (*Suricata suricatta*) and (**C**) spotted hyenas (*Crocuta crocuta*). Females have developed pronounced secondary sexual ornaments that attract males in some polygynous or promiscuous species, including (**D**) savannah baboons (*Papio cynocephalus*). In a number of birds, both sexes have similar ornaments probably as a result of mutual mate-choice, while in a few species, males and females display in different sites and have developed contrasting coloration. [Credits: (A and B) A. Young; (C) M. L. East and H. Hofer; (D) T. Clutton-Brock]

both sexes is often caused by age, by random processes that do not contribute to selection, or by phenotypic differences that have no heritable basis (*7*, *13*, *14*, *25*–*27*), and these effects may often differ between the sexes. For example, the higher PRR of males may generate increased random variance in breeding success in males compared to females (*25*). In addition, because breeding success is often more strongly influenced by age in males than in females, calculation of relative variance in breeding success across individuals of unknown age often overestimates variance in male reproductive success and underestimates variance in female success (*7*).

Finally, relationships between relative reproductive variance in the two sexes and the evolution of sex differences are complex and inconsistent. Qualitative differences in the selection pressures operating in males and females are common, leading to the evolution of contrasting secondary sexual characters in males in different species (*7*). For example, in some polygynous shore birds, males fight on the ground, selection favors large body size, and males are larger than females, whereas in species where males compete in aerial displays, selection for agility favors small size in males and males are smaller than females (*28*). Similarly, in ungulates, where males fight in pushing contests, there is strong selection for male size and sexual dimorphism is pronounced, whereas in species where males fight by biting, body size does not increase the competitive ability of males and sex differences in body size are small (*7*). In other cases, sex differences in ornamentation are associated with qualitative differences in the selection pressures operating in males and females rather than with sex differences in reproductive variance. For example, in some birds, males and females compete at different sites and have developed contrasts in plumage color related to the sites where they display (*29*). Recent examples of sexual antagonism also provide further evidence of the importance of qualitative differences in the selection pressures operating on the two sexes (*27*, *30*, *31*). It is consequently unfortunate that more attention continues to focus on sex differences in reproductive variance than on differences in the selection pressures operating in males and females.

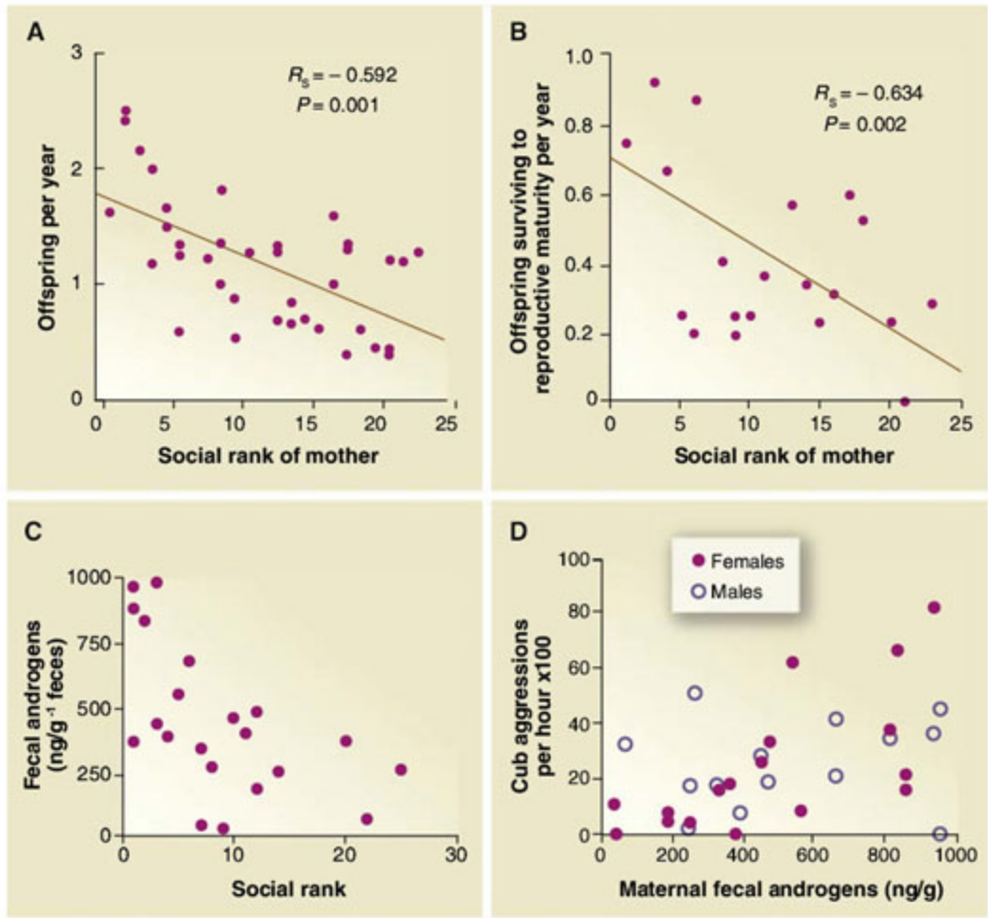

Fig. 2. Correlates of female rank in spotted hyenas. (**A**) Total number of offspring produced per year by the mother shown as a function of the social rank of the mother. (**B**) Number of offspring surviving to reproductive maturity produced per year as a function of the social rank of the mother. (**C**) The relationship between fecal androgens and social rank in female spotted hyenas during the second half of gestation. (**D**) The relationship between maternal androgens measured during the second half of gestation and rates of aggression in hyena cubs aged 2 to 6 months. [(A) and (B) reproduced from (*39*) by permission of the Society for Reproduction and Fertility (2007); (C) and (D) reproduced from (*43*) by permission]

Sexual Selection in Females

Although secondary sexual characters are widespread in females (Fig. 1), Darwin paid little attention to them, noting in passing that "in almost every great class a few anomalous cases occur, where there has been an almost complete transposition of the characters proper to the two sexes; the females assuming characters which properly belong to the males" (*1*). Subsequent research on birds showed that a small number of shore birds have polyandrous mating systems, which generate female-biased OSRs, more intense reproductive competition among females than males, and greater development of secondary sexual characters in females (*3*, *6*). However, with the exception of polyandrous species, relatively little attention has been paid to the operation of sexual selection or the evolution of secondary sexual characters in females.

Intense reproductive competition among females is not confined to species where males invest more heavily than females in their offspring and OSRs are biased toward males and is widespread in species where males are the principal competitors. Sexual selection operating in females may reduce the degree of sexual dimorphism, in some cases leading to monomorphism. For example, in a number of birds where females and males have similar ornaments, both sexes are commonly involved in aggressive displays with rivals, indicating that intrasexual competition may be involved (*32*, *33*). In a small number of animals, the resources necessary for successful breeding in females are so heavily concentrated that reproductive competition between females is more frequent or more intense than between males, despite greater investment in parental care by females (*34*). Examples include several cooperative breeders where a single female monopolizes reproduction in each group and her offspring are reared by other group members (*32*, *35*, *36*) as in Kalahari meerkats (*Suricata suricatta*), where females invest more heavily in parental care than males but depend on access to groups of nonbreeding subordinates to rear their young (*37*). Fewer females than males breed as dominants, and variance in breeding success is higher in females than in males (*34*). In naked mole-rats (*Heterocephalus glaber*), breeding females suppress reproduction in other females, evicting or killing challengers, and are larger and more frequently aggressive than other group members and dominant to males (*38*). More intense intrasexual competition among females than males also occurs in some mammals where multiple females breed in each group. For example, in spotted hyenas (*Crocuta crocuta*), females compete intensely for social rank, which is closely related to their breeding success (Fig. 2) (*39*).

In many species where females compete intensely for breeding opportunities, they show unusual behavioral, physiological, or anatom-

ical characteristics. Female meerkats are more frequently aggressive to each other than are males, and their body weight has a stronger influence on their chances of acquiring and maintaining dominant status (*34*). Both in meerkats and in naked mole-rats, females that attain dominant status show elevated levels of testosterone at particular stages of the reproductive cycle, as well as a secondary period of growth (*40*, *41*). Heightened testosterone levels in breeding females also occur in spotted hyenas (*42*, *43*) and in some lemurs (*44*, *45*), as well as in some breeds of domestic cattle where females have been selected for competitive ability (*46*). In a number of these species, the genitalia of females show evidence of masculinization (*44*, *45*, *47*, *48*) while, in the cooperative cichlid fish (*Neolamprologus pulcher*), not only are testosterone levels consistently higher in dominant females than in subordinates, but the brain gene expression profiles of dominant females resemble those of males (*36*).

Male mate choice is also widespread in species where OSRs are male-biased and is often associated with female courtship of males as well as with the evolution of conspicuous sexual ornaments in females. In some cases, female ornaments reflect individual differences in fecundity and males prefer highly ornamented partners (*21*, *49*, *50*). For example, in some empidid dance flies where males provide nuptial gifts for females, females have developed enlarged pinnate leg scales that honestly reflect their fecundity and males choose females with large leg scales (*51*). Fat-padded breasts, thighs, and buttocks in human females may have evolved for similar reasons (*52*). In other cases, female ornaments appear to reflect temporal changes in reproductive status. In some primates that live in groups where females have an opportunity to mate with more than one male, females show pronounced swellings of the perineal region that are largest and brightest around the time of ovulation and attract the attention of males (*53*, *54*). The relative size of sexual swellings differs between females, so these differences may also signal individual variation in reproductive performance (*55*). Mutual mate choice by males and females also occurs in a number of monogamous birds and, like intrasexual competition, may lead to the evolution of similar ornaments in males and females (*24*, *49*, *56*).

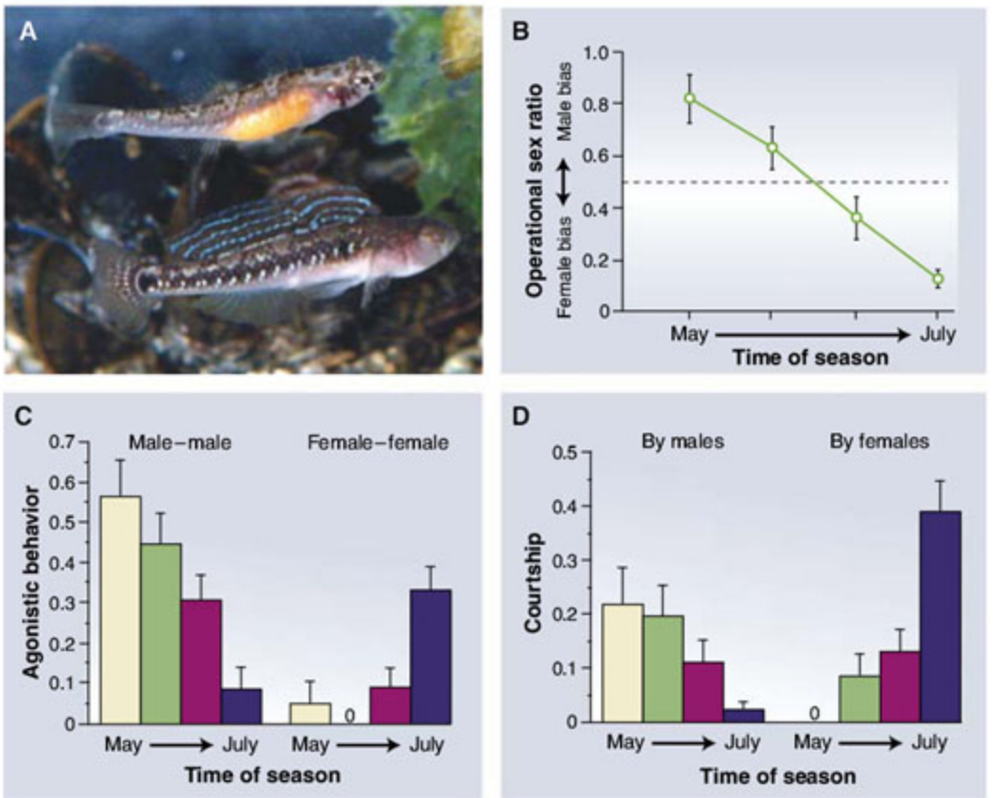

Fig. 3. Seasonal changes in the relative frequency of competition and display in two-spotted gobies (*Gobiusculus flavescens*) [reproduced from (*66*) by permission]. (**A**) Female and male two-spotted gobies. (**B**) Seasonal changes in the operational sex ratio. (**C**) Change in male and female propensity to behave agonistically when encountering same-sex individuals. (**D**) Change in male and female propensity to perform courtship.

Where both sexes invest heavily in their progeny, the OSR and the relative intensity of breeding competition in the two sexes sometimes vary throughout the reproductive cycle. In some fish, intense male:male competition and frequent male displays at the beginning of the season are replaced by active competition between females for males and female displays as the season progresses (Fig. 3). Similarly, in some polygynous ungulates where males initially compete intensely for females, females that have entered estrus and need to mate rapidly compete for the attentions of defending males (*57*, *58*). Several studies of species where both sexes make large investments in their offspring have shown that the relative intensity of reproductive competition in the two sexes can be changed by manipulating resource availability and reversing sex differences in PRR (*59*, *60*).

Contrasts in the Operation of Sexual Selection in Males and Females

Although intrasexual competition for breeding opportunities and consistent mating preferences in the opposite sex appear to have played an important role in the evolution of secondary sexual characters in both sexes, there are fundamental differences in the operation of sexual selection in males and females. Because of their greater energetic investment in gametes and parental care, females more commonly compete with each other for access to resources necessary for successful reproduction (including breeding sites, parental care, and social rank) than for access to gametes produced by the opposite sex (*33*, *34*). As a result, the relative intensity of intrasexual competition and the development of traits that increase competitive success in females may be more strongly influenced by differences in resource distribution than by variation in mating systems. Intrasexual competition between females for resources may generate large individual differences in fecundity (*61*) that strengthen selection on males to identify and prefer superior partners and selection on females to signal temporal and individual differences in fecundity. Strong selection on females to maximize the growth and survival of their offspring may also generate selection pressures for mating with genetically compatible partners which, in some cases, may favor mating with multiple males (*62*).

There may also be qualitative differences in the costs of reproductive competition and secondary sexual characters to the two sexes. Although male competition and the evolution of increased body size in males is commonly associated with higher juvenile mortality and reduced longevity in males compared to females (*9*), there is little evidence that sex differences in survival are reversed in species where reproductive competition is more intense and secondary sexual characters are more highly developed in females. One possibility is that the costs of female expenditure on competition or ornamentation depress fecundity or parental investment and that these effects constrain the development of secondary sexual characters below the level at which they have measurable costs to female survival (*33*). For example, where increased competitive success in females is associated with elevated testosterone levels, these may have adverse effects on the fecundity of females (*63*) or on the development of their offspring (*64*), which constrain the evolution of further increases.

Contrasts in the operation of sexual selection in the two sexes raise the question of whether adaptations to intrasexual competition in females should be regarded as products of sexual selection. In the *Descent of Man*, Darwin commonly describes sexual selection as a process operating through intrasexual competition to breed, though where he discusses its operation in males, he describes it as operating through competition for mates. Sexual selection is now commonly defined as a process operating through intrasexual competition for mates or mating opportunities, with the result that selection pressures arising from intrasexual competition between females to conceive or rear young are generally excluded and sexual selection is, by definition, a process that is largely confined to males. An unfortunate consequence of this is that characteristics that increase the competitive ability of individuals are likely to be attributed to sexual selection if they occur in males—but not if they occur in females. As a result, it may be helpful to return to a broader definition of sexual selection as a process operating through intrasexual competition for reproductive opportunities, providing a conceptual framework that is capable of incorporating the processes leading to the evolution of secondary sexual characters in both sexes (*65*).

Conclusions

Three main conclusions should be drawn from this review. First, the theory of sexual selection still provides a robust framework that explains much of the variation in the development of secondary sexual characters in males, although the mechanisms controlling the relative intensity of reproductive competition and the relative development of secondary sexual characters in the two sexes are more complex than was originally supposed. The recognition of these complexities helps to refine the assumptions and predictions of the theory of sexual selection but does not undermine its basic structure.

Second, sexual selection operating both through intrasexual competition for breeding opportunities and through male mating preferences is common in females and can lead to the evolution of pronounced secondary sexual characters in females, as well as in males, though there are important differences in the form and costs of intrasexual competition between the two sexes. Consequently, satisfactory explanations of the evolution of sex differences requires an understanding of the operation of sexual selection in females as well as in males.

Finally, many important questions about the operation of sexual selection in females and the evolution of sex differences have yet to be answered. Where females compete directly with each other, it is often unclear precisely what they are competing for. Where females have developed obvious secondary sexual characters, it is often uncertain whether these are used principally to attract males or in intrasexual competition for resources, and how their development is limited is unknown (*33*, *49*). And, where males show consistent mating preferences for particular categories of females, we do not yet know whether they are usually selecting for heritable differences in female quality or for nonheritable variation in fecundity or for both. There is still much to be done.

References and Notes

1. C. Darwin, *The Descent of Man and Selection in Relation to Sex* (Modern Library, New York, 1871/1958).
2. A. J. Bateman, *Heredity* **2**, 349 (1948).
3. R. L. Trivers, in *Sexual Selection and the Descent of Man, 1871-1971*, B. Campbell, Ed. (Aldine-Atherton, Chicago, 1972), pp. 136–179.
4. T. H. Clutton-Brock, G. A. Parker, *Q. Rev. Biol.* **67**, 437 (1992).
5. I. Ahnesjo, C. Kvarnemo, S. Merilaita, *Behav. Ecol.* **12**, 397 (2001).
6. S. T. Emlen, L. W. Oring, *Science* **197**, 215 (1977).
7. T. H. Clutton-Brock, in *Evolution from Molecules to Men*, B. J. Bendall, Ed. (Cambridge Univ. Press, Cambridge, 1983), pp. 457–481.
8. R. A. Fisher, *The Genetical Theory of Natural Selection* (Clarendon, Oxford, ed. 1, 1930).
9. T. H. Clutton-Brock, S. D. Albon, F. E. Guinness, *Nature* **313**, 131 (1985).
10. M. Andersson, *Sexual Selection*, J. R. Krebs, T. H. Clutton-Brock, Eds., *Monographs in Behavior and Ecology* (Princeton Univ. Press, Princeton, 1994).
11. P. A. Gowaty, in *Feminism and Evolutionary Biology*, P. A. Gowaty, Ed. (Chapman & Hall, New York, 1997), pp. 351–384.
12. P. A. Gowaty, in *Sexual Selection in Primates*, P. Kappeler, Ed. (Cambridge Univ. Press, Cambridge, 2004), pp. 37–54.
13. Z. Tang-Martinez, T. B. Ryder, *Integr. Comp. Biol.* **45**, 821 (2005).
14. P. A. Gowaty, S. P. Hubbell, *Integr. Comp. Biol.* **45**, 931 (2005).
15. H. Kokko, M. D. Jennions, R. Brooks, *Annu. Rev. Ecol. Evol. Syst.* **37**, 43 (2006).
16. J. Roughgarden, M. Oishi, E. Akcay, *Science* **311**, 965 (2006).
17. T. Pizzari *et al.*, *Science* **312**, 690 (2006).
18. D. C. Queller, *Proc. R. Soc. London B. Biol. Sci.* **264**, 1555 (1997).
19. A. I. Houston, J. M. McNamara, *Biol. Philos.* **20**, 933 (2005).
20. L. W. Simmons, C. Kvarnemo, *Proc. R. Soc. London B. Biol. Sci.* **273**, 465 (2006).
21. C. Kvarnemo, G. I. Moore, A. G. Jones, *Proc. R. Soc. B* **274**, 521 (2007).
22. J. Isaac, *Mamm. Rev.* **35**, 101 (2005).
23. M. R. Evans, B. J. Hatchwell, *Behav. Ecol. Sociobiol.* **29**, 413 (1992).
24. R. A. Johnstone, J. D. Reynolds, J. C. Deutsch, *Evolution* **50**, 1382 (1996).
25. W. J. Sutherland, *Oxford Surv. Evol. Biol.* **1**, 90 (1985a).
26. S. P. Hubbell, S. K. Johnson, *Am. Nat.* **130**, 91 (1987).
27. A. Pischedda, A. K. Chippindale, *PLoS Biol.* **4**, e356 (2006).
28. T. Szekely, R. P. Freckleton, J. D. Reynolds, *Proc. Natl. Acad. Sci. U.S.A.* **101**, 12224 (2004).
29. R. Heinsohn, S. Legge, J. A. Endler, *Science* **309**, 617 (2005).
30. W. R. Rice, *Science* **256**, 1436 (1992).
31. K. Foerster *et al.*, *Nature* **447**, 1107 (2007).
32. M. J. West-Eberhard, *Q. Rev. Biol.* **55**, 155 (1983).
33. N. R. LeBas, *Trends Ecol. Evol.* **21**, 170 (2006).
34. T. H. Clutton-Brock *et al.*, *Nature* **444**, 1065 (2006).
35. M. E. Hauber, E. A. Lacey, *Integr. Comp. Biol.* **45**, 903 (2005).
36. N. Aubin-Horth *et al.*, *Mol. Ecol.* **16**, 1349 (2007).
37. T. H. Clutton-Brock, *Science* **296**, 69 (2002).
38. H. K. Reeve, P. W. Sherman, in *The Biology of the Naked Mole-Rat*, P. W. Sherman, J. U. M. Jarvis, R. D. Alexander, Eds. (Princeton Univ. Press, Princeton, NJ, 1991), pp. 337–357.
39. K. E. Holekamp, L. Smale, M. Szykman, *J. Reprod. Fertil.* **108**, 229 (1996).
40. M. J. O'Riain, S. Braude, in *Dispersal*, J. Clobert, E. Danchin, A. A. Dhondt, J. D. Nichols, Eds. (Oxford Univ. Press, Oxford, 2001), pp. 143–154.
41. A. F. Russell, A. A. Carlson, G. M. McIlrath, N. R. Jordan, T. H. Clutton-Brock, *Evol. Int. J. Org. Evol.* **58**, 1600 (2004).
42. T. M. Yalcinkaya *et al.*, *Science* **260**, 1929 (1993).
43. S. M. Dloniak, J. A. French, K. E. Holekamp, *Nature* **440**, 1190 (2006).
44. J. Ostner, M. Heislermann, P. M. Kappeler, *Naturwissenschaften* **90**, 141 (2003).
45. C. M. Drea, *Horm. Behav.* **51**, 555 (2007).
46. P. Plusquellec, M. F. Boussou, *Appl. Anim. Behav. Sci.* **72**, 1 (2001).
47. P. M. Kappeler, in *Perspectives in Ethology*, P. P. G. Bateson, P. H. Klopfer, W. S. Thompson, Eds. (Plenum, New York, 1993), pp. 143–158.
48. N. J. Place, S. E. Glickman, *Adv. Exp. Med. Biol.* **545**, 243 (2004).
49. T. Amundsen, *Trends Ecol. Evol.* **15**, 149 (2000).
50. T. Amundsen, E. Forsgren, *Proc. Natl. Acad. Sci. U.S.A.* **98**, 13155 (2001).
51. N. R. LeBas, L. R. Hockham, M. G. Ritchie, *Proc. R. Soc. London B. Biol. Sci.* **270**, 2159 (2003).
52. L. Mealey, *Sex Differences: Developmental and Evolutionary Strategies* (Academic Press, New York, 2000).
53. T. H. Clutton-Brock, P. H. Harvey, in *Growing Points in Ethology*, P. P. G. Bateson, R. A. Hinde, Eds. (Cambridge Univ. Press, Cambridge, 1976), pp. 195–237.
54. D. Zinner, C. Nunn, C. P. van Schaik, P. M. Kappeler, in *Sexual Selection in Primates*, P. M. Kappeler, C. P. van Schaik, Eds. (Cambridge Univ. Press, Cambridge, 2004), pp. 71–89.
55. L. G. Domb, M. Pagel, *Nature* **410**, 204 (2001).
56. K. Kraaijeveld, F. J. L. Kraaijeveld-Smit, J. Komdeur, *Anim. Behav.* **74**, 657 (2007).
57. J. Bro-Jorgensen, *Proc. Natl. Acad. Sci. U.S.A.* **99**, 9290 (2002).
58. N. Bebie, A. G. McElligott, *Mamm. Biol.* **71**, 347 (2006).
59. D. T. Gwynne, L. W. Simmons, *Nature* **346**, 172 (1990).
60. L. W. Simmons, *Nature* **358**, 61 (1992).
61. T. H. Clutton-Brock, in *Reproductive Success*, T. H. Clutton-Brock, Ed. (Univ. of Chicago Press, Chicago, 1988), pp. 472–486.
62. M. D. Jennions, M. Petrie, *Biol. Rev.* **75**, 21 (2000).
63. C. M. Drea *et al.*, *Proc. R. Soc. London B. Biol. Sci.* **269**, 1981 (2002).
64. R. C. Knickmeyer, S. Baron-Cohen, *J. Child Neurol.* **21**, 825 (2006).
65. T. H. Clutton-Brock, in *Sexual Selection in Primates: New and Comparative Perspectives*, P. M. Kappeler, C. P. van Schaik, Eds. (Cambridge Univ. Press, Cambridge, 2004), pp. 24–36.
66. E. Forsgren, T. Amundsen, A. A. Borg, J. Bjelvenmark, *Nature* **429**, 551 (2004).

67. Many thanks to P. Gowaty, R. Trivers, W. Sutherland, P. Lawrence, C. Kvarnemo, S. Hubbard, G. Parker, L. Simmons, S. Hodge, A. Young, M. Andersson, and J. Silk for discussion and comments on the manuscript.

10.1126/science.1133311

SCIENCE & SECURITY

In a Time of Tension, Scientists Build Hopeful U.S.-Iran Links

The diplomatic conflict between Iran and the West was growing more intense by the day, and global headlines focused on Russian President Vladimir Putin's trip to Tehran. At the same time, but with far less fanfare, a delegation of U.S. science and engineering leaders was arriving in the Iranian capital on a mission of science diplomacy.

Among the U.S. visitors was Norman P. Neureiter, director of the AAAS Center for Science, Technology, and Security Policy. He recalls a reception that few would have predicted: When Nobel laureate Joseph H. Taylor of Princeton spoke at Sharif University of Technology, students jammed the hall and treated him like a celebrity. Former President Mohammad Khatami had a cordial visit with the Americans. President Mahmoud Ahmadinejad wanted to arrange a meeting, but Putin's visit made that impossible. And the Iranian news media covered the tour extensively.

"It was phenomenally favorable, from the first day," Neureiter said in an interview. "It's amazing how popular Americans are in Iran. Intuitively, you would think it would be just the opposite."

The October visit offered clear proof that the science communities of the two countries share a reservoir of common interest and good will that could support a more constructive overall relationship, he said. This month's U.S. intelligence conclusion that Iran suspended its nuclear weapons program in 2003 is a "remarkable development," he added, "but there are still many issues of contention between the U.S. and Iran. What we are proposing is greater engagement at the people level despite the political problems."

An optimistic view came from engineering Professor Abolhassan Vafai, who helped organize the visit as editor-in-chief of the international scientific journal *Scientia Iranica* and a member of National Academy of Sciences of Iran. "I am pretty sure that in the future this misunderstanding between the governments will be resolved, and two great nations—the U.S. and Iran—should get together to work for the benefit of humanity," Vafai said. Citing climate change, hunger, and water shortages, he added: "There are so many common challenges for our people….It is up to us scientists to provide avenues for that work."

Sharif University, in cooperation with the Iranian Academy of Sciences, hosted the visit from 13 to 22 October. The U.S. delegation was organized by the National Academies and led by Wm. A. Wulf, recently retired president of the National Academy of Engineering.

(Left to right) Biologist Michael Clegg, National Academy of Sciences foreign secretary; Norman P. Neureiter, director of the AAAS Center for Science, Technology, and Security Policy; computer scientist Wm. A. Wulf, president emeritus of the National Academy of Engineering; unidentified man; Ayatollah Mostafa Mohaghegh Damad, Iranian Institute of Philosophy; and Grand Ayatollah Mousavi Ardebili. The group met in Qom, Iran.

Despite the tension of recent years, Neureiter's center has maintained contacts with Iran's science community. He visited three cities in Iran in 2004, lecturing at several universities and technology parks. Reza Mansouri, an Iranian physicist and science policy expert, spoke at AAAS's Washington, D.C., headquarters last year. In late November, Neureiter and his wife, Georgine, hosted a dinner for 20 Iranian medical scientists in the U.S. for a visit focused on food-borne diseases under the State Department's International Visitors Program.

Neureiter trained as a research chemist; in the 1960s, during tense years of the Cold War, he became the first U.S. science attaché in Eastern Europe. Later he served in President Richard Nixon's Office of Science and Technology, helping craft scientific elements of historic agreements with the Soviet Union and China. He served as science adviser to the U.S. Secretary of State from 2000 to 2003.

Neureiter's experience left him committed to the use of scientific and technological cooperation to build better global relationships. "I would hope that such a course might be fruitful with Iran," he said.

Though funding is limited, Iran today is pursuing an S&T renaissance. University enrollment is growing. International research publications and joint projects are up. New research centers and technology incubators are opening across the country. The Iranian blueprint for growth emphasizes sustainable, knowledge-based development, and environmental protection. Many scientists and engineers leading the effort were educated in the United States and Europe, and they are eager to restore strong ties to Western colleagues.

Neureiter sees little risk that engagement would allow Iran to obtain sensitive data; the U.S. Treasury Department's Office of Foreign Assets Control regulates programs with Iran, and U.S. scientists would not be cooperating with Iran in sensitive areas. Both he and Vafai stressed the potential benefits for both nations. That sentiment was repeated throughout the visit—not just by members of the U.S. delegation, but by Khatami, Grand Ayatollah Mousavi Ardebili, and other Iranian leaders. Iran's vice president for science and technology, Sadegh Vaezzadeh, challenged researchers from both countries to cooperate in preventing the misuse of science.

Neureiter cited several areas of strength for Iranian science: engineering, theoretical physics, chemistry, medicine, and cognitive science. He suggested that collaboration also could focus on earthquake and addiction research.

AAAS officials, including Chief International Officer Vaughan Turekian, are exploring other ways to engage with Iran. "The benefits of joint visits are real, but they're also fleeting," Neureiter said. "So we should work with our Iranian colleagues to find ways to make these relationships sustainable and enduring."

COMMUNICATION

AAAS Names Science Journalism Winners

An inquiry into mysterious elk deaths in Wyoming, a profile of a largely unknown black chemist who was a pioneer in the synthesis of medicinal drugs from plants, and a skeptical look at the effects of telling children they are smart are among the winners of the 2007 AAAS Science Journalism Awards.

- **Large Newspaper—(Circulation >100,000):** Kenneth Weiss and Usha Lee McFarling, *Los Angeles Times*, for "Altered Oceans," 30 July to 3 August 2006.
- **Small Newspaper—(Circulation <100,000):** Jennifer Frazer, *Wyoming Tribune-Eagle*,

CREDIT: GLENN SCHWEITZER

for "Getting to the Bottom of Mysterious Elk Deaths," 26 November and 3 December 2006.

- **Magazine:** Po Bronson and Ashley Merryman, *New York*, for "How Not to Talk to Your Kids," 19 February 2007.
- **Television:** Llewellyn Smith and Stephen Lyons, WGBH/NOVA, for "Forgotten Genius," 6 February 2007.
- **Radio:** Keith Seinfeld, KPLU-FM, Seattle/Tacoma, for "The Electric Brain," 8 to 11 January 2007.
- **Online:** Katie Alvord, KeweenawNow.com, for "Lake Superior Basin Climate Change" series, 3 May; 3 June; and 30 June 2007.
- **Children's Science News:** Mona Chiang, Scholastic *Science World*, for "A Whale of a Mystery," 15 January 2007.

The judging panel also awarded a special Certificate of Merit for Sina Loeschke, the runner-up in the Children's Science News category, for her 7 February 2007 article on sea slugs in the German science magazine *GEOlino*.

The awards, established in 1945, are sponsored by Johnson & Johnson Pharmaceutical Research & Development, L.L.C. Each category carries a $3000 award. The winners will pick up their plaques at the AAAS Annual Meeting in Boston in February 2008.

—*Earl Lane*

Results of the 2007 Election of AAAS Officers

Following are the results of the 2007 election. Terms begin on 19 February 2008.

General Offices
President-Elect: Peter C. Agre
Board of Directors: Nancy Knowlton, Thomas A. Woolsey
Committee on Nominations: Diana Hicks, Karen A. Holbrook, Peter H. Raven, Lydia Villa-Komaroff

Section on Agriculture, Food, and Renewable Resources
Chair-Elect: Daniel Bush
Member-at-Large: Sally Mackenzie
Electorate Nominating Committee: Pamela J. Green, Charles W. Rice

Section on Anthropology
Chair-Elect: Michael A. Little
Member-at-Large: Dennis H. O'Rourke
Electorate Nominating Committee: William R. Leonard, Karen R. Rosenberg

Section on Astronomy
Chair-Elect: Steven V. W. Beckwith
Member-at-Large: Nancy D. Morrison
Electorate Nominating Committee: Lynn R. Cominsky, William S. Smith Jr.

Section on Atmospheric and Hydrospheric Sciences
Chair-Elect: Margaret Leinen
Member-at-Large: Eugenia Kalnay
Electorate Nominating Committee: Syukuro Manabe, Terry Whitledge
Council Delegate: Claire L. Parkinson

Section on Biological Sciences
Chair-Elect: Barbara L. Illman
Member-at-Large: Diana G. Myles
Electorate Nominating Committee: Michael W. Nachman, Baldomero "Toto" Olivera

Section on Chemistry
Chair-Elect: Geraldine Richmond
Member-at-Large: Peter B. Armentrout
Electorate Nominating Committee: Alison Butler, Mark A. Ratner

Section on Dentistry and Oral Health Sciences
Chair-Elect: Huw F. Thomas
Member-at-Large: Susan W. Herring
Electorate Nominating Committee: Mark W. Lingen, Janet Moradian-Oldak
Council Delegate: Jacques E. Nör

Section on Education
Chair-Elect: Judith A. Dilts
Member-at-Large: Robert Tinker
Electorate Nominating Committee: Judy Diamond, Susan H. Hixson
Council Delegate: Rodger W. Bybee

Section on Engineering
Chair-Elect: Robert M. Nerem
Member-at-Large: Cristina H. Amon
Electorate Nominating Committee: Kristi S. Anseth, Cindy Atman

Section on General Interest in Science and Engineering
Chair-Elect: Charles N. Haas
Member-at-Large: Erika C. Shugart
Electorate Nominating Committee: Joann Ellison Rodgers, John L. Safko Sr.
Council Delegate: Julie Ann Miller

Section on Geology and Geography
Chair-Elect: Susan Trumbore
Member-at-Large: Jill S. Baron
Electorate Nominating Committee: Kam-biu Liu, Ellen Mosley-Thompson

Section on History and Philosophy of Science
Chair-Elect: Alan J. Rocke
Member-at-Large: Paul Lawrence Farber
Electorate Nominating Committee: Rachelle D. Hollander, Phillip R. Sloan

Section on Industrial Science and Technology
Chair-Elect: S. Tom Picraux
Member-at-Large: Ray H. Baughman
Electorate Nominating Committee: Tingye Li, Robert W. Sprague

Section on Information, Computing, and Communication
Chair-Elect: Edward D. Lazowska
Member-at-Large: Benjamin Kuipers
Electorate Nominating Committee: James D. Foley, Clifford A. Lynch
Council Delegate: Lewis M. Branscomb

Section on Linguistics and Language Science
Chair-Elect: Annie Zaenen
Member-at-Large: Mark Aronoff
Electorate Nominating Committee: Joan Maling, Sally McConnell-Ginet
Council Delegate: Keren Rice

Section on Mathematics
Chair-Elect: Keith Devlin
Member-at-Large: Warren Page
Electorate Nominating Committee: Harold P. Boas, Deborah F. Lockhart

Section on Medical Sciences
Chair-Elect: Christine A. Biron
Member-at-Large: R. Arlene H. Sharpe
Electorate Nominating Committee: Harry B. Greenberg, Margaret K. Hostetter

Section on Neuroscience
Chair-Elect: Mahlon R. DeLong
Member-at-Large: Hollis T. Cline
Electorate Nominating Committee: Rosemarie Booze, Charles D. Gilbert

Section on Pharmaceutical Sciences
Chair-Elect: William E. Evans
Member-at-Large: C. Anthony Hunt
Electorate Nominating Committee: F. Douglas Boudinot, Günter Hochhaus
Council Delegate: Patrick J. Sinko

Section on Physics
Chair-Elect: Bill R. Appleton
Member-at-Large: Gene D. Sprouse
Electorate Nominating Committee: Robert P. Redwine, Antoinette (Toni) Taylor

Section on Psychology
Chair-Elect: Edward Taub
Member-at-Large: Susan Goldin-Meadow
Electorate Nominating Committee: Jeffrey R. Alberts, Jeri S. Janowsky

Section on Social, Economic, and Political Sciences
Chair-Elect: Karen S. Cook
Member-at-Large: Judith M. Tanur
Electorate Nominating Committee: Henry E. Brady, Nancy M. Gordon

Section on Societal Impacts of Science and Engineering
Chair-Elect: Dan Kammen
Member-at-Large: Kerri-Ann Jones
Electorate Nominating Committee: Thomas Dietz, Michele Garfinkel
Council Delegate: Robert Cook-Deegan

Section on Statistics
Chair-Elect: W. Michael O'Fallon
Member-at-Large: Randall K. Spoeri
Electorate Nominating Committee: Joseph L. Gastwirth, Fritz Scheuren
Council Delegate: David L. DeMets

Combinatorial Synthesis of Peptide Arrays onto a Microchip

Mario Beyer,[1*] Alexander Nesterov,[1*] Ines Block,[1] Kai König,[1] Thomas Felgenhauer,[1] Simon Fernandez,[1] Klaus Leibe,[1] Gloria Torralba,[2] Michael Hausmann,[2] Ulrich Trunk,[2] Volker Lindenstruth,[2]† F. Ralf Bischoff,[1]†‡ Volker Stadler,[1]†‡ Frank Breitling[1]†‡

High-complexity oligonucleotide arrays are combinatorially synthesized by lithographic methods (*1*), localized electrolysis (*2*), or electrophoretic transport of the four different nucleotides (*3*). In all these methods, each of the monomers is coupled layer by layer consecutively to the solid support. Therefore, they all depend on an excessive number of coupling cycles to generate a peptide array from the 20 different amino acid monomers, which explains why peptide arrays lag behind nucleotide arrays in terms of complexity (*4*).

In order to upgrade peptide array density over currently available 22 peptides per cm^2 (*5*) and to avoid an excessive number of coupling cycles, we manufactured 20 different kinds of chargeable amino acid particles that are guided step by step onto a microchip surface by electric field patterns from individual pixel electrodes (Fig. 1, A and E). Because the solid particle matrix effectively "freezes" the activated amino acid derivatives, coupling reaction ensues only when finally a completed layer of all 20 different kinds of amino acid particles is melted at once (Fig. 1, C and F). This releases activated amino acids to diffuse to free amino groups incorporated into the chip's coating (*6*). Thereby, only nine repeated coupling cycles resulted into an array of nonameric peptides, with the density only restrained by the sizes of particles and pixel electrodes (Fig. 1, D and G).

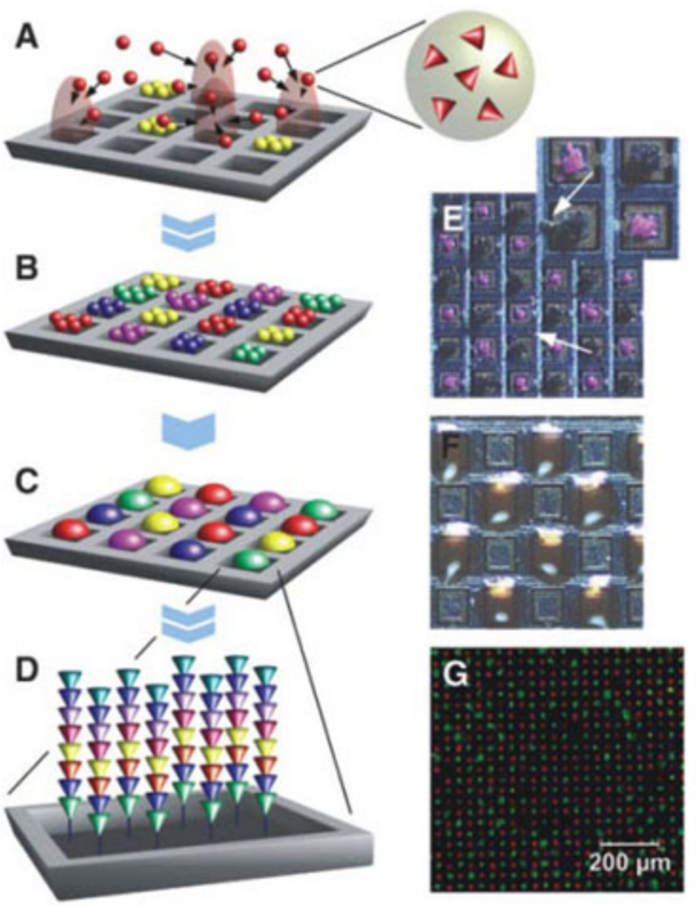

Fig. 1. Particle-based synthesis of peptide arrays. Activated amino acids are embedded within particles that are addressed onto a chip by electrical fields generated by individual pixel electrodes (**A**). A whole layer of consecutively addressed amino acid particles (**B**) is melted at once to induce coupling (**C**). Repetitive cycles generate a peptide array (**D**). Consecutively deposited, unmelted particles stick to the surface because of strong adhesion forces. Arrows point to wrongly deposited particles (**E**). Melted particles delimit individual coupling areas. For better visualization, pixel areas are overloaded (**F**). Particle-based in situ synthesis of chessboard-arranged FLAG (green) and HA epitopes (red) with a density of 40,000 cm^{-2}. Peptides were stained with rabbit antibodies against FLAG and monoclonal mouse antibodies against HA (**G**).

When we consecutively addressed different kinds of commercial color toner particles to microchips manufactured by a standard lithographic process, few wrongly deposited particles were observed (Fig. 1E, arrows), which was also true for our amino acid particles. Strong adhesion forces keep unmelted microparticles sticking to defined addresses even when the pattern of pixels switched on voltage is changed. The amino acid particles mainly comprise OPfp (pentafluorophenyl) esters of Fmoc (9-fluorenylmethoxycarbonyl)-protected amino acids and a higher homolog of standard solvents, for example, the solid diphenyl formamide, which adds the trait of an oily solvent that forms spatially confined reaction cavities when melted (Fig. 1F).

When we compared our particle-based method to standard Merrifield synthesis, we found similar yields of synthesized peptides, no conversion of L to D form amino acids during synthesis, and a rather surprising stability of Fmoc–amino acid–OPfp esters immobilized inside particles (fig. S1). We observed a negligible decay rate of <1% Fmoc–amino acid–OPfp ester per month at room temperature with 19 amino acid particles analyzed, except for Fmoc-Arg-OPfp, with a corresponding decay rate of 5%.

Next, we synthesized an array of peptides Tyr-Pro-Tyr-Asp-Val-Pro-Asp-Tyr-Ala [hemaglutinin (HA)] and Asp-Tyr-Lys-Asp-Asp-Asp-Asp-Lys (FLAG) onto the microchip's surface. Peptides were differently labeled with FLAG-and HA-specific antibodies, which revealed an epitope-specific staining pattern with a density of 40,000 peptide spots per cm^2 (Fig. 1G).

In contrast to other methods, the particle-based approach renders the delivery of monomers to individual pixels completely independent from the coupling reaction; that is, we reduced the number of coupling cycles to one per layer. In addition, the independence of particle production, storage, deposition, and coupling reaction allows for rigorous quality control of individual steps. Our method should be especially helpful in the field of proteomics because it allows for the translation of whole proteomes into arrays of overlapping peptides. Such high complexity peptide arrays could be used in diagnosis and biomedical research, for example, to scan the humoral immune response toward a pathogen's proteome.

References and Notes

1. S. P. Fodor *et al.*, *Science* **251**, 767 (1991).
2. R. D. Egeland, E. M. Southern, *Nucleic Acids Res.* **33**, e125 (2005).
3. M. J. Heller, A. H. Forster, E. Tu, *Electrophoresis* **21**, 157 (2000).
4. J. P. Pellois *et al.*, *Nat. Biotechnol.* **20**, 922 (2002).
5. R. Frank, *Tetrahedron* **48**, 9217 (1992).
6. M. Beyer *et al.*, *Biomaterials* **27**, 3505 (2006).
7. We thank D. Freidank, T. Kühlwein, and J. Kretschmer for technical assistance; M. Schnölzer (German Cancer Research Center) for mass spectrometry; and M. Grunze and R. Dahint (University of Heidelberg) for help in surface analysis. This work was supported by grants from the Federal Ministry of Education and Research (03N8710 to V.S. and NGFN-0313375 to F.R.B. and V.L.), the Hemholtz Association (VH-VI-108 to F.B. and V.L.), and the Human Frontier Science Program Organization (RGP5/2006 to F.B.).

Supporting Online Material

www.sciencemag.org/cgi/content/full/318/5858/1888/DC1
Materials and Methods
Figs. S1 and S2
References

27 August 2007; accepted 18 October 2007
10.1126/science.1149751

[1]German Cancer Research Center, INF 580, 69120 Heidelberg, Germany. [2]Kirchhoff Institute for Physics, University of Heidelberg, INF 227, 69120 Heidelberg, Germany.

*These authors contributed equally to this work.
†To whom correspondence should be addressed. E-mail: f.breitling@dkfz.de (F.B.); r.bischoff@dkfz.de (F.R.B.); v.stadler@dkfz.de (V.S.); voli@kip.uni-heidelberg.de (V.L.)
‡These authors contributed equally to this work.

Observation of Berry's Phase in a Solid-State Qubit

P. J. Leek,[1]* J. M. Fink,[1] A. Blais,[2] R. Bianchetti,[1] M. Göppl,[1] J. M. Gambetta,[3,4] D. I. Schuster,[4] L. Frunzio,[4] R. J. Schoelkopf,[4] A. Wallraff[1]*

In quantum information science, the phase of a wave function plays an important role in encoding information. Although most experiments in this field rely on dynamic effects to manipulate this information, an alternative approach is to use geometric phase, which has been argued to have potential fault tolerance. We demonstrated the controlled accumulation of a geometric phase, Berry's phase, in a superconducting qubit; we manipulated the qubit geometrically by means of microwave radiation and observed the accumulated phase in an interference experiment. We found excellent agreement with Berry's predictions and also observed a geometry-dependent contribution to dephasing.

When a quantum mechanical system evolves cyclically in time such that it returns to its initial physical state, its wave function can acquire a geometric phase factor in addition to the familiar dynamic phase (*1*, *2*). If the cyclic change of the system is adiabatic, this additional factor is known as Berry's phase (*3*), which, in contrast to the dynamic phase, is independent of energy and time.

In quantum information science (*4*), a prime goal is to use coherent control of quantum systems to process information, accessing a regime of computation unavailable in classical systems. Quantum logic gates based on geometric phases have been demonstrated in both nuclear magnetic resonance (*5*) and ion trap–based quantum information architectures (*6*). Superconducting circuits (*7*, *8*) are a promising solid-state platform for quantum information processing (*9*–*14*), in particular because of their potential scalability. Proposals for the observation of geometric phase in superconducting circuits (*15*–*19*) have existed since shortly after the first coherent quantum effects were demonstrated in these systems (*20*).

Geometric phases are closely linked to the classical concept of parallel transport of a vector on a curved surface. Consider, for example, a tangent vector $\mathbf{v}$ on the surface of a sphere being transported from the sphere's north pole around the path P shown in Fig. 1A, with $\mathbf{v}$ pointing south at all times. The final state of the vector $\mathbf{v}_f$ is rotated with respect to its initial state $\mathbf{v}_i$ by an angle ϕ equal to the solid angle subtended by the path P at the origin. Thus, this angle is dependent on the geometry of the path P and is independent of the rate at which it is traversed. As a result, departures from the original path that leave the solid angle unchanged will not modify ϕ. This robustness has been interpreted as a potential fault tolerance when applied to quantum information processing (*5*).

The analogy of the quantum geometric phase with the above classical picture is particularly clear in the case of a two-level system (a qubit) in the presence of a bias field that changes in time. A familiar example is a spin-½ particle in a changing magnetic field. The general Hamiltonian for such a system is $H = h\mathbf{R} \cdot \boldsymbol{\sigma}/2$, where $\boldsymbol{\sigma} = (\sigma_x, \sigma_y, \sigma_z)$ are the Pauli operators, h is Planck's constant divided by 2π, and $\mathbf{R}$ is the bias field vector, expressed in units of angular frequency. The qubit dynamics is best visualized in the Bloch sphere picture, in which the qubit state $\mathbf{s}$ continually precesses about the vector $\mathbf{R}$, acquiring dynamic phase $\delta(t)$ at a rate $R = |\mathbf{R}|$ (Fig. 1B). When the direction of $\mathbf{R}$ is now changed adiabatically in time (i.e., at a rate slower than R), the qubit additionally acquires Berry's phase while remaining in the same superposition of eigenstates with respect to the quantization axis $\mathbf{R}$. The path followed by $\mathbf{R}$ in the three-dimensional parameter space of the Hamiltonian (Fig. 1C) is the analog of a path in real space in the classical case. When $\mathbf{R}$ completes the closed circular path C, the geometric phase acquired by an eigenstate is $\pm\Theta_C/2$ (*3*), where Θ_C is the solid angle of the cone subtended by C at the origin. The $\pm$ sign refers to the opposite phases acquired by the ground or excited state of the qubit, respectively. For the circular path shown in Fig. 1C, the solid angle is given by $\Theta_C = 2\pi(1 - \cos\theta)$, depending only on the cone angle θ.

We describe an experiment carried out on an individual two-level system realized in a superconducting electronic circuit. The qubit is a Cooper-pair box (*21*, *22*) with an energy level separation of $h\omega_a \approx h \times 3.7$ GHz when biased at charge degeneracy, where it is optimally protected from charge noise (*23*). The qubit is embedded in a one-dimensional microwave transmission line res-

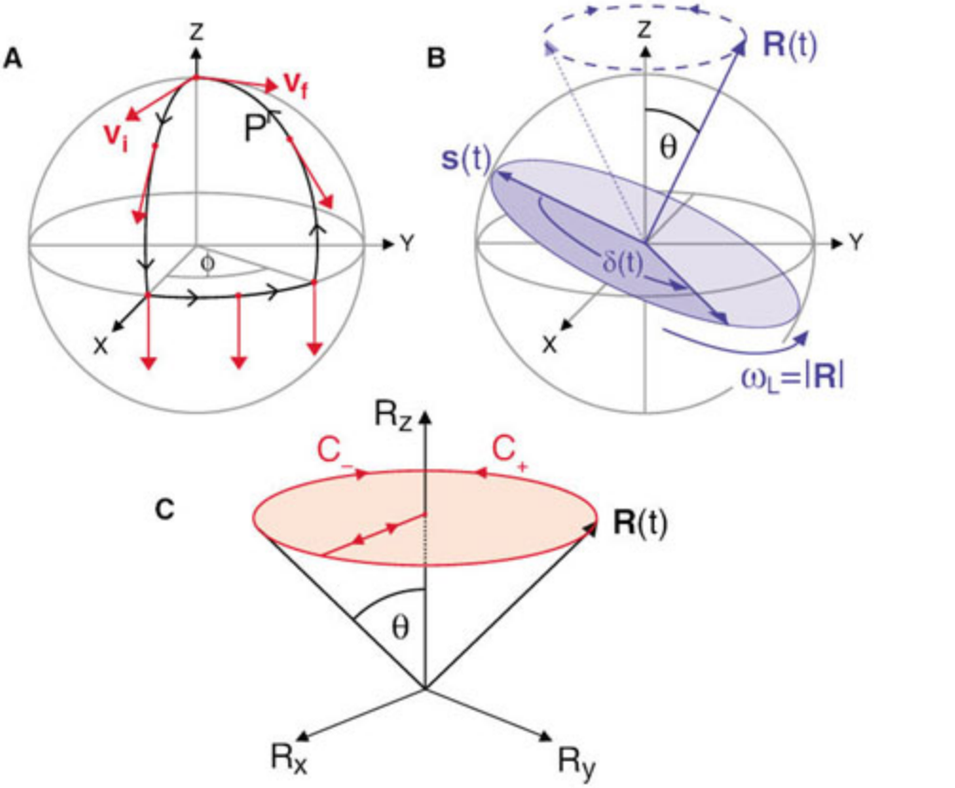

Fig. 1. (**A**) Parallel transport of the vector $\mathbf{v}_i$ on a spherical surface around the closed path P results in it rotating by a geometric angle ϕ to $\mathbf{v}_f$ when it returns to its initial position. (**B**) Dynamics of the Bloch vector $\mathbf{s}$ of a qubit in the presence of a bias field $\mathbf{R}$ tilted by an angle θ from the z axis. The vector $\mathbf{s}$ precesses about $\mathbf{R}$ at the Larmor rate $\omega_L = |\mathbf{R}|$. (**C**) Parameter space of the Hamiltonian for the same case.

[1]Department of Physics, Eidgenössische Technische Hochschule (ETH) Zürich, Schafmattstrasse 16, 8093 Zürich, Switzerland. [2]Département de Physique, Université de Sherbrooke, Sherbrooke, Québec J1K 2R1, Canada. [3]Institute for Quantum Computing and Department of Physics and Astronomy, University of Waterloo, Waterloo, Ontario N2L 3G1, Canada. [4]Departments of Applied Physics and Physics, Yale University, New Haven, CT 06520, USA.

*To whom correspondence should be addressed. E-mail: leek@phys.ethz.ch (P.J.L.); andreas.wallraff@phys.ethz.ch (A.W.)

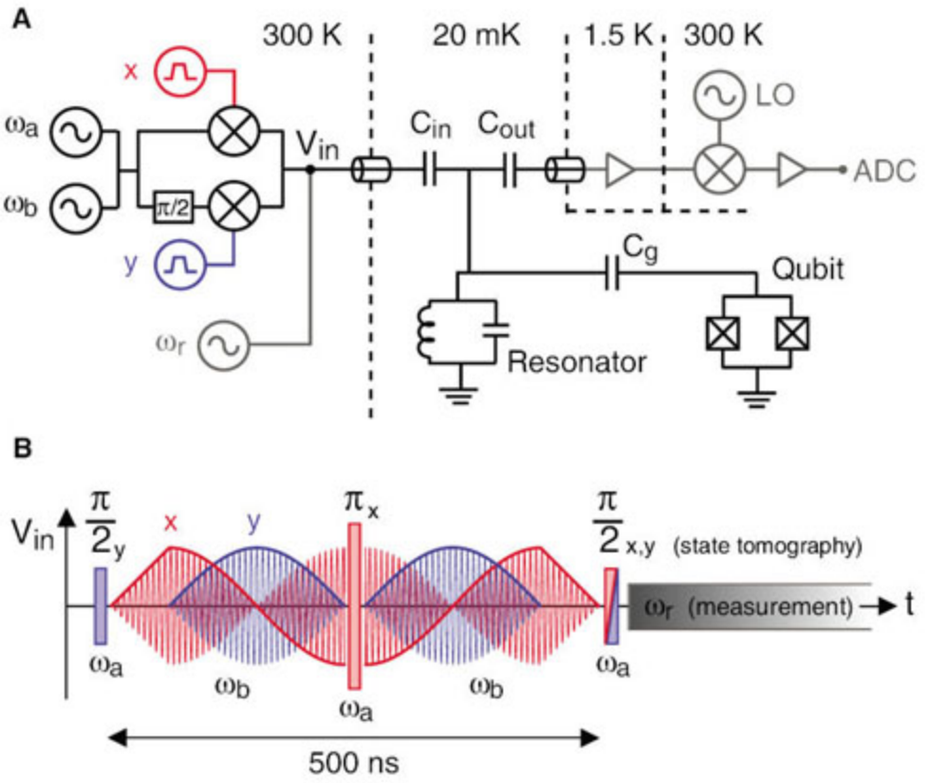

Fig. 2. (**A**) Simplified circuit diagram of the experimental setup. In the center at 20 mK is the resonator-qubit system, with the resonator represented by a parallel inductance and capacitance, and the qubit, a split Cooper-pair box, capacitively coupled to the resonator through C_g. The resonator is coupled to input and output transmission lines via the capacitors C_{in} and C_{out}. Three different pulse-modulated microwave frequency signals are applied to the resonator input. The two signals required for qubit manipulation, one at the qubit transition frequency $\omega_a/2\pi$ and a detuned signal $\omega_b/2\pi$, are modulated using mixers to the pattern shown in (B). The signal at the resonator frequency $\omega_r/2\pi$, used to measure the qubit state, is turned on after the pulse sequence is applied. (**B**) Schematic pulse sequence for the case $n = 0.5$. Resonant pulses, shown as shaded rectangles, are 12 ns in length. The two quadrature bias microwave fields (x, red; y, blue) are represented as sinusoids with modulation amplitude shown by solid lines. The linear ramps at the start and end of these sections correspond to moving adiabatically from $\Omega_R = 0$ to the circle of constant Ω_R depicted in Fig. 1C.

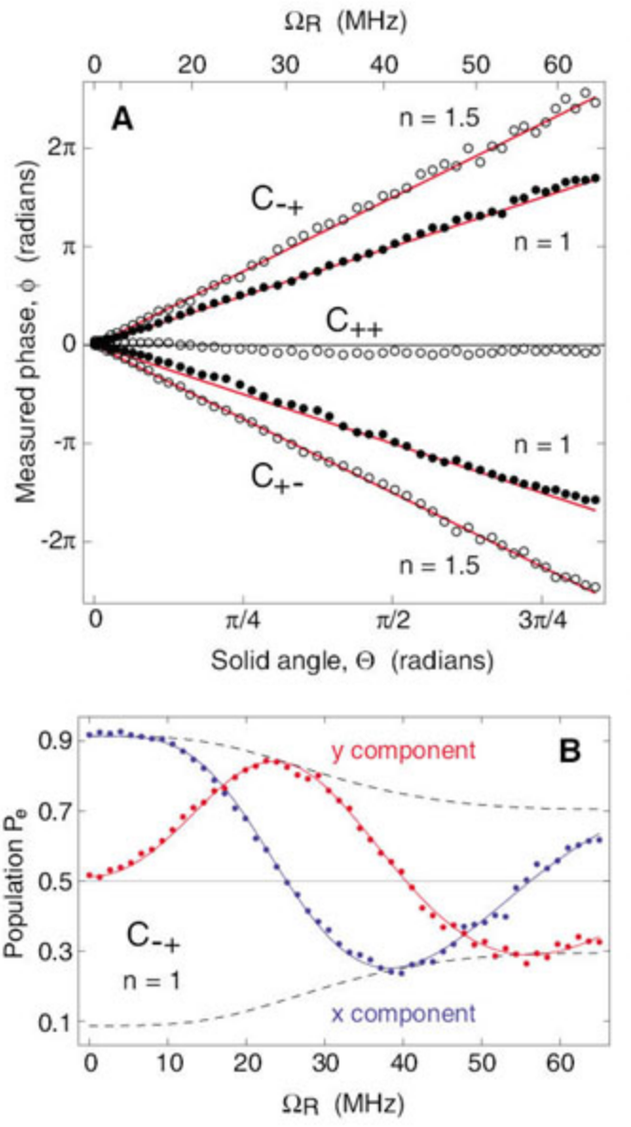

Fig. 3. (**A**) Measured phase ϕ versus solid angle Θ of a single conical path (lower axis). The applied microwave field amplitude is indicated on the upper axis (in units of the induced Rabi frequency Ω_R for resonant driving). Solid circles correspond to experiments in which $n = 1$ circular paths are traversed during each half of the spin-echo sequence, and open circles to the case $n = 1.5$. Subscripts $\pm$ of labels $C_{\pm\pm}$ correspond to the path direction before and after the spin-echo π pulse. Red solid lines are of slope $n = \pm 1, \pm 1.5$. The C_{++} experiment was carried out with $n = 1.5$. (**B**) State tomography data for the C_{-+} experiment with $n = 1$. Plotted is the qubit excited-state population after tomography pulses to extract $\langle\sigma_x\rangle$ [blue, $p_e = (\langle\sigma_x\rangle + 1)/2$] and $\langle\sigma_y\rangle$ [red, $p_e = (\langle\sigma_y\rangle + 1)/2$]. Lines are fits to Berry's phase, with a geometric dephasing envelope function (dashed lines, described in the text and Fig. 4). In all cases, the total pulse sequence time is $T = 500$ ns and the detuning is $\Delta/2\pi \approx 50$ MHz. Sequences are repeated 2×10^5 times to accumulate measurement statistics.

onator with resonance frequency $\omega_r/2\pi \approx 5.4$ GHz (Fig. 2A). In this architecture, known as circuit quantum electrodynamics (QED) (*24*, *25*), the qubit is isolated effectively from its electromagnetic environment, leading to a long energy relaxation time of $T_1 \approx 10$ μs and a spin-echo phase coherence time of $T_2^{echo} \approx 2$ μs. In addition, the architecture allows for a high-visibility dispersive readout of the qubit state (*26*).

Fast and accurate control of the bias field **R** for this superconducting qubit is achieved through phase and amplitude modulation of microwave radiation coupled to the qubit through the input port of the resonator (Fig. 2A). The qubit Hamiltonian in the presence of such radiation is

$$H = \frac{h}{2}\omega_a\sigma_z + h\Omega_R\cos(\omega_b t + \varphi_R)\sigma_x \quad (1)$$

where $h\Omega_R$ is the dipole interaction strength between the qubit and a microwave field of frequency ω_b and phase φ_R, and t is time. Thus, $\Omega_R/2\pi$ is the Rabi frequency that results from resonant driving. The above Hamiltonian may be transformed to a frame rotating at the frequency ω_b by means of the unitary transformation

$$H' = UHU^{-1} - ihU\dot{U}^{-1} \quad (2)$$

where $U = \exp(i\omega_b t\sigma_z/2)$, and $\dot{U}$ denotes its time derivative. Ignoring terms oscillating at $2\omega_b$ (the rotating wave approximation), the transformed Hamiltonian takes the form

$$H' \approx \frac{h}{2}(\Delta\sigma_z + \Omega_x\sigma_x + \Omega_y\sigma_y) \quad (3)$$

where $\Omega_x = \Omega_R\cos\varphi_R$ and $\Omega_y = \Omega_R\sin\varphi_R$. This is equivalent to the generic situation depicted in

Fig. 1, B and C, where $\mathbf{R} = (\Omega_x, \Omega_y, \Delta)$ and $\Delta = \omega_a - \omega_b$ is the detuning between the qubit transition frequency and the applied microwave frequency. In our experiment, we keep Δ fixed and control the bias field to trace circular paths of different radii Ω_R.

We measure Berry's phase in a Ramsey fringe interference experiment by initially preparing an equal superposition of the qubit ground and excited states, which acquires a relative geometric phase $\gamma_C = 2\pi(1 - \cos\theta)$, equal to the total solid angle enclosed by the cone depicted in Fig. 1C, with $\cos\theta = \Delta/(\Omega_R^2 + \Delta^2)^{1/2}$. As the bias field adiabatically follows the closed path $C_\pm$, the qubit state acquires both a dynamic phase $\delta(t)$ and a geometric phase γ_C, corresponding to a total accumulated phase $\phi = \delta(t) \pm \gamma_C$ (the $\pm$ sign denoting path direction), which we extract by performing full quantum-state tomography (*4*). To directly observe only the geometric contribution, we use a spin-echo (*27*) pulse sequence that cancels the dynamic phase, as explained below.

The complete sequence (Fig. 2B) starts by preparing the initial σ_z superposition state with a resonant $\pi/2$ pulse. Then the path C_- is traversed, causing the qubit to acquire a phase $\phi_- = \delta(t) - \gamma_C$. Applying a resonant spin-echo π pulse to the qubit about an orthogonal axis now inverts the qubit state, effectively inverting the phase ϕ_- ; traversing the control field path again, but in the opposite direction C_+, adds an additional phase $\phi_+ = \delta(t) + \gamma_C$. This results in total in a purely geometric phase $\phi = \phi_+ - \phi_- = 2\gamma_C$ being acquired during the complete sequence, which we denote as C_{-+}. Note that unlike the geometric phase, the dynamic phase is insensitive to the path direction and hence is completely canceled.

At the end of the sequence, we extract the phase of the qubit state by means of quantum-state tomography. In our measurement technique (*26*), the z component of the qubit Bloch vector $\langle\sigma_z\rangle$ is determined by measuring the excited-state population $p_e = (\langle\sigma_z\rangle + 1)/2$. To extract the x and y components, we apply a resonant $\pi/2$ pulse rotating the qubit about either the x or y axis and then perform the measurement, revealing $\langle\sigma_y\rangle$ and $\langle\sigma_x\rangle$, respectively. The phase of the quantum state after application of the control sequence is then extracted as $\phi = \tan^{-1}(\langle\sigma_y\rangle/\langle\sigma_x\rangle)$.

In Fig. 3A we show the measured phase ϕ and its dependence on the solid angle of the path for a number of different experiments, all carried out at $\Delta/2\pi \approx 50$ MHz, and total pulse sequence time $T = 500$ ns. Three parameters are varied: the path radius Ω_R (upper x axis), the number n of circular loops traversed in each half of the spin-echo sequence, and the direction of traversal of the paths (C_{-+} and C_{+-}). The measured phase is in all cases seen to be linear in solid angle as Ω_R is swept, with a root-mean-square deviation across all data sets of 0.14 rad from the expected lines of slope $2n$. Thus, all results are in close agreement with the predicted Berry's phase, and it is clear that we are able to accurately control the amount of phase accumulated geometrically. Note also that the dynamic phase is indeed effectively eliminated by the spin echo. Reversing the overall direction of the paths is observed to invert the sign of the phase (Fig. 3A). Traversing the circular paths on either side of the spin-echo pulse in the same direction (C_{++}) as a control experiment results in zero measured phase (Fig. 3A).

Observation of a pure Berry's phase requires adiabatic qubit dynamics, which in turn requires the rate of rotation of the bias field direction to be much less than the Larmor rate R of the qubit in the rotating frame. For the case of constant cone angle θ, this translates to the requirement that the adiabaticity parameter $A = \dot{\varphi}_R \sin\theta/2R \ll 1$. If the Hamiltonian is changed nonadiabatically, the qubit state can no longer exactly follow the effective field $\mathbf{R}$, and the geometric phase acquired deviates from Berry's phase (*28*). For the experiments here, $A \leq 0.04$, and deviation of the measured phase from Berry's phase is not discernible. We have also verified experimentally that in this adiabatic limit, the observed phase is independent of the total sequence time T.

Figure 3B shows a measurement of the x and y components of the qubit state from which the Berry's phase is extracted. Interestingly, the visibility of the observed interference pattern is seen to have a dependence on Ω_R. Because the data were taken at a fixed total sequence time, this is not due to conventional T_2 dephasing, which is also independently observable as a function of time, but can be explained as due to geometric dephasing, an effect dependent on the geometry of the path (*29*).

In our experiment, dephasing is dominated by low-frequency fluctuations in the qubit transition frequency ω_a (and thus Δ) induced by charge noise coupling to the qubit (*30*). The spin-echo pulse sequence effectively cancels the dynamic dephasing due to the low-frequency noise. However, the geometric phase is sensitive to slow fluctuations, which cause the solid angle subtended by the path at the origin to change from one measurement to the next (Fig. 4A). The effect on the geometric phase of such fluctuations in the classical control parameters of the system has been studied theoretically (*29*). In the limit of the fluctuations being slower than the time scale of the spin-echo sequence, the variance of the geometric phase σ_γ^2 has itself a purely geometric dependence, $\sigma_\gamma^2 = \sigma_\omega^2(2n\pi\sin^2\theta/R)^2$, where σ_ω^2 is the variance of the fluctuations in ω_a (*29*). In Fig. 4B, we show the observed dependence of the coherence on geometry explicitly by plotting $(\langle\sigma_x\rangle^2 + \langle\sigma_y\rangle^2)^{1/2}$ versus Ω_R, which fits well to the expected dependence $\exp(-\sigma_\gamma^2/2)$. This is also in agreement with the raw data in Fig. 3B.

We have observed an important geometric contribution to dephasing that occurs when geometric operations are carried out in the presence of low-frequency fluctuations. In contrast, higher-frequency noise in ω_a is expected to have little influence on Berry's phase (provided adiabaticity is maintained), because its effect on the solid angle is averaged out (Fig. 4C). This characteristic robustness of geometric phases to high-frequency noise may be exploitable in the realization of logic gates for quantum computation, although the effect of geometric dephasing due to low-frequency noise must be taken into account.

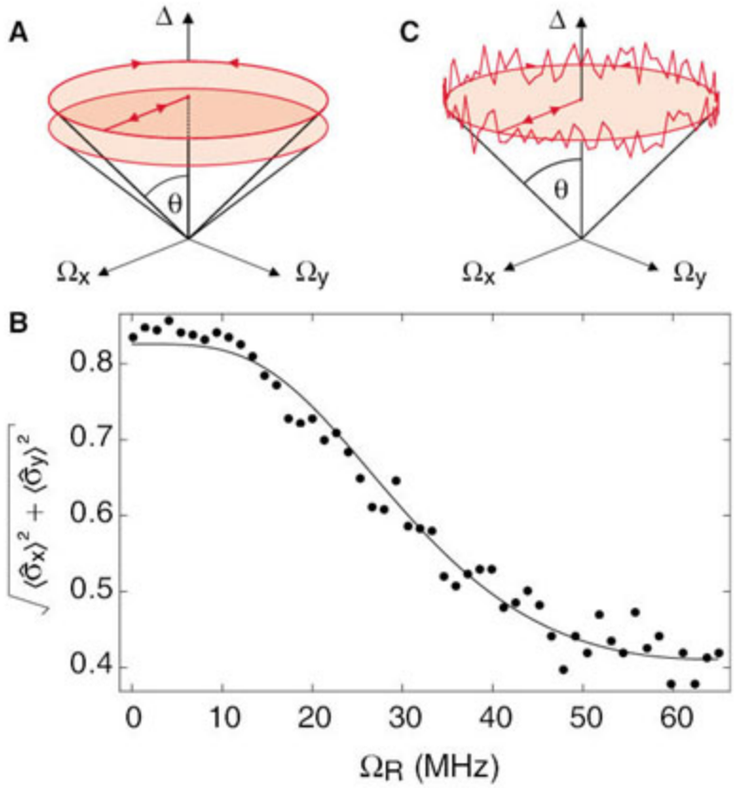

Fig. 4. (**A**) Low-frequency fluctuations in Δ change the solid angle enclosed by the path from one measurement to the next, and cause geometric dephasing with a characteristic dependence on the cone angle and bias field amplitude. (**B**) Magnitude of the equatorial component of the Bloch vector $(\langle\sigma_x\rangle^2 + \langle\sigma_y\rangle^2)^{1/2}$ for the data shown in Fig. 3B, plotted as a function of drive amplitude Ω_R. The fit is to a geometric dephasing factor $\exp(-\sigma_\gamma^2/2)$, where σ_γ^2 is the variance of the geometric phase. (**C**) The conical parameter space path in the presence of high-frequency ($f >> T^{-1}$) noise in Δ, having no effect on the total solid angle.

References and Notes

1. A. Shapere, F. Wilczek, *Geometric Phases in Physics* (World Scientific, Singapore, 1989).

2. J. Anandan, *Nature* **360**, 307 (1992).
3. M. V. Berry, *Proc. R. Soc. London Ser. A* **392**, 45 (1984).
4. M. A. Nielsen, I. L. Chuang, *Quantum Computing and Quantum Information* (Cambridge Univ. Press, Cambridge, 2000).
5. J. A. Jones, V. Vedral, A. Ekert, G. Castagnoli, *Nature* **403**, 869 (2000).
6. D. Leibfried *et al.*, *Nature* **422**, 412 (2003).
7. G. Wendin, V. Shumeiko, *Handbook of Theoretical and Computational Nanotechnology*, M. Rieth, W. Schommers, Eds. (American Scientific, Los Angeles, 2006), vol. 3 (www.arxiv.org/abs/cond-mat/0508729v1).
8. M. H. Devoret, A. Wallraff, J. M. Martinis, www.arxiv.org/abs/cond-mat/0411174v1 (2004).
9. T. Yamamoto, Y. A. Pashkin, O. Astafiev, Y. Nakamura, J. S. Tsai, *Nature* **425**, 941 (2003).
10. M. Steffen *et al.*, *Science* **313**, 1423 (2006).
11. A. O. Niskanen *et al.*, *Science* **316**, 723 (2007).
12. J. H. Plantenberg, P. C. de Groot, C. J. P. M. Harmans, J. E. Mooij, *Nature* **447**, 836 (2007).
13. J. Majer *et al.*, *Nature* **449**, 443 (2007).
14. M. A. Sillanpää, J. I. Park, R. W. Simmonds, *Nature* **449**, 438 (2007).
15. G. Falci, R. Fazio, G. M. Palma, J. Siewert, V. Vedral, *Nature* **407**, 355 (2000).
16. X. B. Wang, M. Keiji, *Phys. Rev. B* **65**, 172508 (2002).
17. A. Blais, A. M. S. Tremblay, *Phys. Rev. A* **67**, 012308 (2003).
18. Z. H. Peng, M. J. Zhang, D. N. Zheng, *Phys. Rev. B* **73**, 020502 (2006).
19. M. Mottonen, J. P. Pekola, J. J. Vartiainen, V. Brosco, F. W. J. Hekking, *Phys. Rev. B* **73**, 214523 (2006).
20. Y. Nakamura, Y. A. Pashkin, J. S. Tsai, *Nature* **398**, 786 (1999).
21. A. Shnirman, G. Schön, Z. Hermon, *Phys. Rev. Lett.* **79**, 2371 (1997).
22. V. Bouchiat, D. Vion, P. Joyez, D. Esteve, M. H. Devoret, *Phys. Scr.* **T76**, 165 (1998).
23. D. Vion *et al.*, *Science* **296**, 886 (2002).
24. A. Blais, R. S. Huang, A. Wallraff, S. M. Girvin, R. J. Schoelkopf, *Phys. Rev. A* **69**, 062320 (2004).
25. A. Wallraff *et al.*, *Nature* **431**, 162 (2004).
26. A. Wallraff *et al.*, *Phys. Rev. Lett.* **95**, 060501 (2005).
27. A. Abragam, *Principles of Nuclear Magnetism* (Oxford Univ. Press, Oxford, 1961).
28. Y. Aharonov, J. Anandan, *Phys. Rev. Lett.* **58**, 1593 (1987).
29. G. De Chiara, G. M. Palma, *Phys. Rev. Lett.* **91**, 090404 (2003).
30. G. Ithier *et al.*, *Phys. Rev. B* **72**, 134519 (2005).

31. We thank P. Maurer and L. Steffen for their contributions to the project, and A. Shnirman, J. Blatter, G. De Chiara, and G. M. Palma for valuable discussions. Supported by the EC via an Intra-European Marie Curie Fellowship (P.J.L.), the Natural Sciences and Engineering Research Council of Canada, Canadian Institute for Advanced Research, and Fonds Québécois de la Recherche sur la Nature et les Technologies (A.B.), the National Security Agency under the Army Research Office, NSF, and Yale University (D.I.S., L.F., and R.J.S.), Consiglio Nazionale delle Ricerche–Istituto di Cibernetica, Pozzuoli, Italy (L.F.), the Ontario Research Development Challenge Fund and Mathematics of Information Technology and Complex Systems (J.M.G.), the Swiss National Science Foundation, and ETH Zürich.

29 August 2007; accepted 1 November 2007
Published online 22 November 2007;
10.1126/science.1149858
Include this information when citing this paper.

High-Performance Carbon Nanotube Fiber

Krzysztof Koziol,[1] Juan Vilatela,[1] Anna Moisala,[1] Marcelo Motta,[1] Philip Cunniff,[2] Michael Sennett,[2] Alan Windle[1]*

With their impressive individual properties, carbon nanotubes should form high-performance fibers. We explored the roles of nanotube length and structure, fiber density, and nanotube orientation in achieving optimum mechanical properties. We found that carbon nanotube fiber, spun directly and continuously from gas phase as an aerogel, combines high strength and high stiffness (axial elastic modulus), with an energy to breakage (toughness) considerably greater than that of any commercial high-strength fiber. Different levels of carbon nanotube orientation, fiber density, and mechanical properties can be achieved by drawing the aerogel at various winding rates. The mechanical data obtained demonstrate the considerable potential of carbon nanotube assemblies in the quest for maximal mechanical performance. The statistical aspects of the mechanical data reveal the deleterious effect of defects and indicate strategies for future work.

High-performance synthetic fibers, based on polymer molecules or graphene sheets, have been under development for the past half century, motivated by the high strength and stiffness of the covalent carbon-carbon bond and by the ability to achieve alignment of these bonds with the fiber axis. The key to producing such fibers is to maximize the number of covalently bonded carbon atoms per unit volume or mass, and thus to reduce the proportion of other types of atoms or groups attached to polymer chains. The advantage of pure carbon fibers is that the mechanical properties are derived from the in-plane stiffness and strength of graphene sheets, without the adulterating effect of additional atoms to satisfy available carbon bonds. However, the route to carbon fibers involves the alignment of precursor structures, which are then covalently bonded to each other to create the final structure. This second phase of chemistry not only complicates the processing operation, but also creates a structure in which the basic mechanism that generates toughness in linear polymer systems (i.e., chain pullout) is not available. Carbon fibers are thus comparatively brittle, especially when they are heat-treated to maximize stiffness.

The very high axial strength and stiffness of individual carbon nanotubes, demonstrated both by experiment (*1*–*3*) and modeling (*4*–*6*), opens up the possibility of processing them directly into fibers without the need for a subsequent cross-linking step. Thus, the benefits of high-performance polymeric fibers—especially directness of processing and fiber toughness (measured as energy absorbed up to fracture)—can be combined with the advantages of a fiber consisting only of carbon atoms. If one views carbon nanotubes as extremely strong and stiff polymer molecules, it is not surprising that the processing routes developed so far borrow concepts from polymer fiber–processing technologies. The leading approaches for production of nanotube fibers are (i) spinning from a lyotropic liquid crystalline suspension of nanotubes, in a process similar to that used for polymeric fibers such as aramids (*7*); (ii) spinning from multiwall nanotubes previously grown on a substrate as semi-aligned carpets (*8*, *9*); and (iii) spinning directly from an aerogel of single- and double-walled carbon nanotubes as they are formed in a chemical vapor deposition reactor (*10*). This last process is the one we used (*11*). In terms of mechanical properties, the various techniques have met with different degrees of success. Fibers produced by the liquid crystalline route (*7*) showed an encouraging stiffness of 120 GPa but only modest strengths on the order of 0.1 GPa. Fibers spun from carbon nanotube carpets and subsequently twisted (*9*) have now been made (*12*) with strengths up to 1.9 GPa and stiffnesses up to 330 GPa. An individual strength value of 3.3 GPa was also mentioned (*13*). Until now, the highest strength reported for direct-spun carbon nanotube fiber was 2.2 GPa, and the highest stiffness reported was 160 GPa (*14*).

The mechanical properties of a material are limited by defects within an otherwise perfect structure. In the case of high-performance polymer fibers, these defects consist of chain ends and

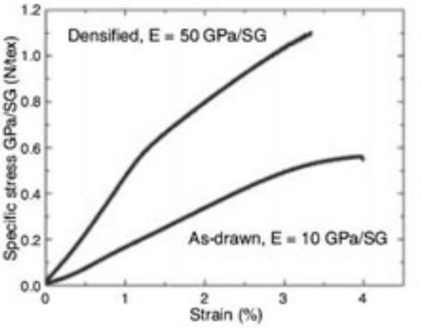

Fig. 1. Specific stress-strain curves for an as-drawn fiber and an acetone-densified fiber. These curves are as-recorded, and the gauge length in each case was 20 mm.

[1]Department of Materials Science, University of Cambridge, Pembroke Street, Cambridge CB2 3QZ, UK. [2]U.S. Army, Natick Soldier Research Development and Engineering Center, 15 Kansas Street, Natick, MA 01760, USA.

*To whom correspondence should be addressed. E-mail: ahw1@hermes.cam.ac.uk

topological defects such as chain entanglements (which prevent perfect alignment and optimum chain packing). Other factors that limit strength are inclusions or voids within the fiber and surface defects, although these are normally eliminated during process development. The first requirement in making high-strength fibers from carbon nanotubes is the availability of nanotubes that are as long and as structurally perfect as possible. Single- or double-walled tubes can be made comparatively free of grown-in defects that lead to kinks, and they also show a tendency to assemble in parallel into bundles. The second step is to align all nanotubes as perfectly as possible with the fiber axis, so as to maximize the translation of their axial properties to those of the fiber. The bonding between adjacent nanotubes is weak in shear (graphite is a lubricant); hence, as great a contact length as possible is necessary to transfer the load into any given nanotube. Another advantage of thin-walled nanotubes (single or double) is that they tend to facet or flatten so as to maximize their contact area. Alignment is typically achieved through mechanical forces, whether applied to a partly linked array of fibers or through fluid-flow forces on a lyotropic suspension. The nanotubes we created are mainly double-walled and of unusually large diameter (4 to 10 nm) and collapse against each other, further enhancing the contact area. They are also on the order of 1 mm long and thus have an axial ratio on the order of 10^5 (*11*).

We describe the results of applying the principles of polymer processing to the direct-spinning method, and we show that exceptional fiber properties can be realized without recourse to fiber twisting (which may detract from ultimate stiffness) or to incorporation of polymers or other agents by subsequent back-diffusion (which will have the same effect). These latter two strategies [suggested by (*9*, *15*)] are, of course, available as post-treatments to the fibers described here. In our process, the act of pulling the aerogel out of the reaction zone axially orients the nanotubes and condenses them into a fiber of low specific gravity (SG), typically 10^{-2} (SG is the density of the material divided by the density of water and is thus a dimensionless parameter). The densification is completed by running the fiber through an acetone vapor stream, which evaporates before the fiber is eventually spooled. A similar, surface tension–based densification phenomenon has been reported on carbon nanotube ribbons (*15*).

The on-line densification process is shown in movie S1 and fig. S1. It is a key processing step, although it does not itself improve carbon nanotube orientation; however, it optimizes the stress transfer between the nanotubes, thus ensuring that the largest proportion of them is fully load-bearing. Figure 1 shows typical stress-strain curves for two fibers: an as-spun fiber in which partial densification has been achieved to give an SG of ~10^{-2}, and a fiber made under exactly the same conditions with an out-of-the-furnace winding rate of 20 m/min but after on-line acetone vapor densification to give an SG of ~1. The strength unit used is specific stress, expressed as GPa/SG, which has exactly the same numerical value as N/tex (tex, a unit widely used in the fiber industry, is the linear density in g/km) (*16*).

Figure 2A shows the effect of fiber winding rate on the orientation of the nanotubes, as measured both by polarized Raman scattering and by small-angle x-ray scattering (SAXS). A basic precept of polymer science is that a higher winding rate results in superior orientation and properties (*17*), and more recently this principle has been shown to apply to carbon nanotubes (*18*). Maximal orientation is particularly desirable in the case of an assembly of carbon nanotubes, as it is crucial to controlling the contact efficiency between the relatively rigid neighboring nanotubes and thus the efficiency of load transfer. The enhancement of densification with improved orientation is shown in Fig. 2B as the effect of winding rate on the SG of the fiber. The plot also shows the decrease in linear density as the fiber is drawn down more at the higher winding rates. The SG values were calculated from measurements of mean fiber diameter and tex, the former ranging from 20 μm at 5.6 m/min to 7 μm at 20 m/min. Figure 2C shows the variation in strength and stiffness of the fibers with changing winding rate, using samples of 2-mm gauge length. The improvement is seen as being principally the result of improved fiber orientation. Although the trends are upward with increasing winding rate and the orientation achieved (orientation parameter = 0.85 from SAXS) should be capable of further improvement, attempts to wind at rates beyond 20 m/min led to increased process difficulty and breakage of the aerogel.

Fibers that were wound at 20 m/min, the optimized condition, were subjected to more extensive mechanical analysis. Figure 3A shows the distribution of specific fiber strengths seen for a range of gauge lengths of fiber with linear density of 0.04 tex. The plot is based on 75 tensile tests. Although the strength distribution for 20-mm gauge lengths peaks close to 1 GPa/SG, at 2-mm and 1-mm gauge lengths the strength distribution becomes bimodal with a second peak at 6.5 GPa/SG, with values in its high tail extending beyond 9 GPa/SG. Such behavior is indicative of "weak points" along the fiber at (random) intervals, at spacings on the same order as the gauge length and much greater than the fiber diameter. The lower-strength peak corresponds to chance occurrence of a defect within the gauge length, and the upper peak to the absence of any such defect. This type of behavior is often recognized at an early stage in the development of any commercial fiber, where the higher-strength peak is sometimes referred to as the "intrinsic strength" (*19*–*23*); in such cases, the challenge of the final elimination of processing defects often is not overcome until the process is scaled up to industrial proportions.

To eliminate variations (on a millimeter scale along the fiber) in the amount of carbon in any cross section of the fiber as an explanation for the apparent high specific strength at short gauge lengths, we used scanning electron microscopy and energy-dispersive x-ray spectroscopy (EDS) to measure the carbon content along lengths of fiber. A typical longitudinal scan for total carbon is shown in fig. S2. It shows a variation of carbon

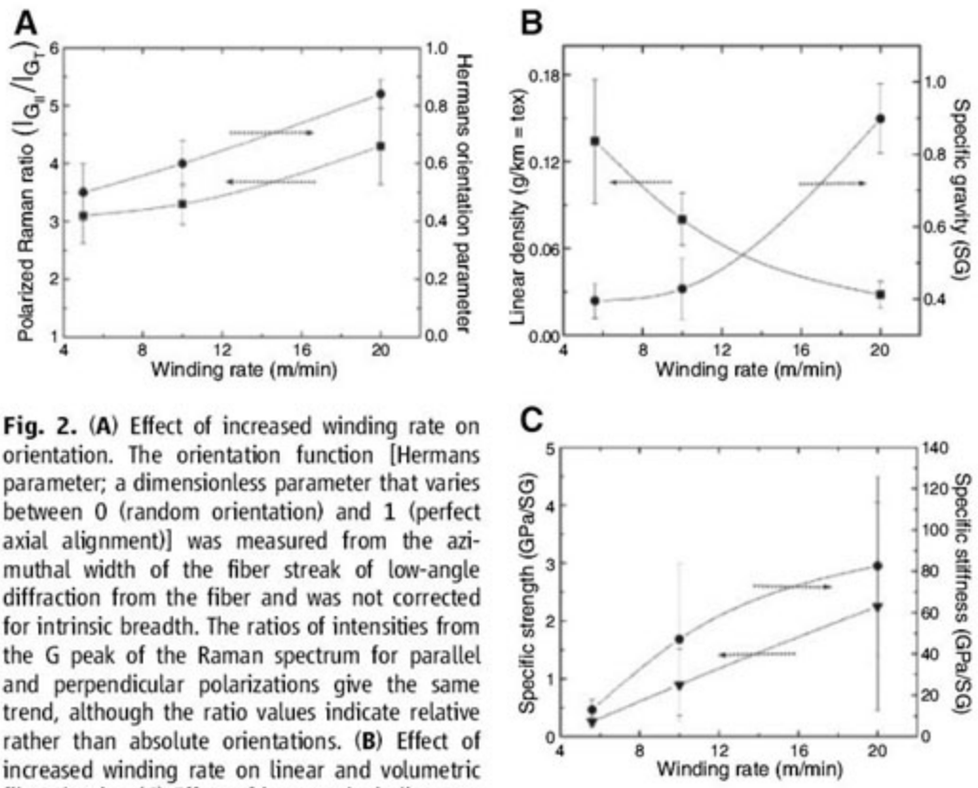

Fig. 2. (**A**) Effect of increased winding rate on orientation. The orientation function [Hermans parameter; a dimensionless parameter that varies between 0 (random orientation) and 1 (perfect axial alignment)] was measured from the azimuthal width of the fiber streak of low-angle diffraction from the fiber and was not corrected for intrinsic breadth. The ratios of intensities from the G peak of the Raman spectrum for parallel and perpendicular polarizations give the same trend, although the ratio values indicate relative rather than absolute orientations. (**B**) Effect of increased winding rate on linear and volumetric fiber density. (**C**) Effect of increased winding rate on average specific strength and average specific stiffness for specimens of 2-mm gauge length.

content along the fiber of between 5 and 7% of the mean. The standard deviation of the diameter was 15.7% of the mean, although we had no guarantee of the fiber roundness, so the cross-sectional area is likely to vary by less than the diameter squared. None of these variations could account for the range of strengths seen in the samples of shorter gauge length. Use of a micro balance to measure the linear density of the samples is quite demanding, as the mass of a sample is on the order of 1 μg and the sensitivity of the balance is on the order of 0.1 μg. The random error associated with these measurements needs to be taken into account; to avoid any risk of exaggerating the strengths reported, we used the highest measurement of linear density (0.04 tex) as the basis for all the strength measurements reported in Figs. 3 and 4.

Figure 3B shows stress-strain curves recorded for three specimens of 1-mm gauge length: one from the lower-strength peak of the distribution, one from the high-strength "intrinsic" peak, and the strongest specimen seen at the upper limit of the distribution. They are compared with a curve for Kevlar 49 measured in our laboratory, which is typical of literature values. An interesting aspect of these curves is that the weaker specimens also show a lower initial modulus. There is also some suggestion of a yield stress, above which the load increases less rapidly with strain, and after which there is not full recovery on unloading before fracture. Figure 3C is a plot of strength versus stiffness, corrected for strain in the grips (a correction that becomes larger for the shortest gauge length, although it was not applied to the nanotube fiber stress-strain curves of Fig. 3B,

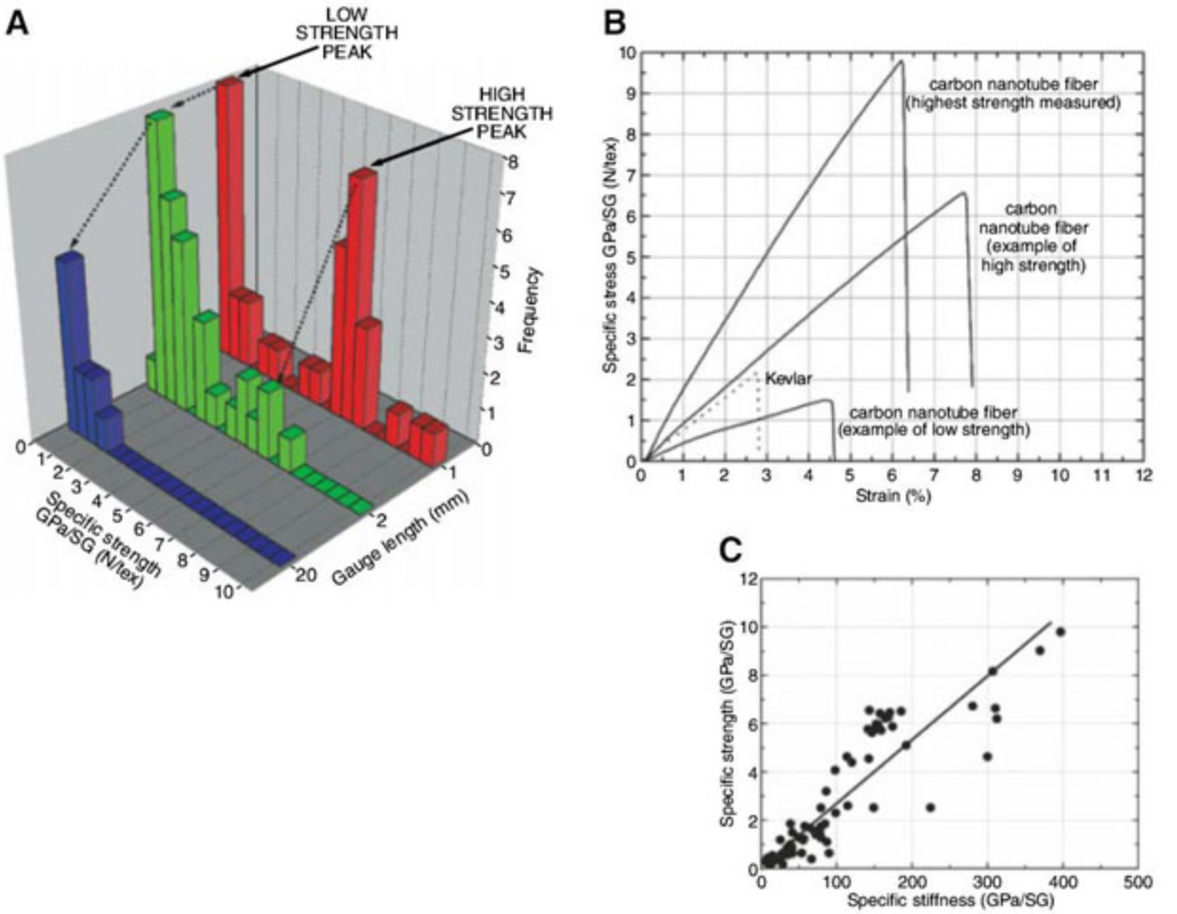

Fig. 3. (**A**) Specific strength distribution of carbon nanotube fibers for different gauge lengths. (**B**) Stress-strain curves for 1-mm specimens for the two strongest carbon nanotube fibers and for fibers typical of the high-strength and low-strength peaks in the distribution. A curve for Kevlar 49 is included as a benchmark. (**C**) Correlation between fiber specific strength and specific stiffness, covering all three gauge lengths. The stiffnesses here are calculated for the low-strain part of the curves with correction for grip strain.

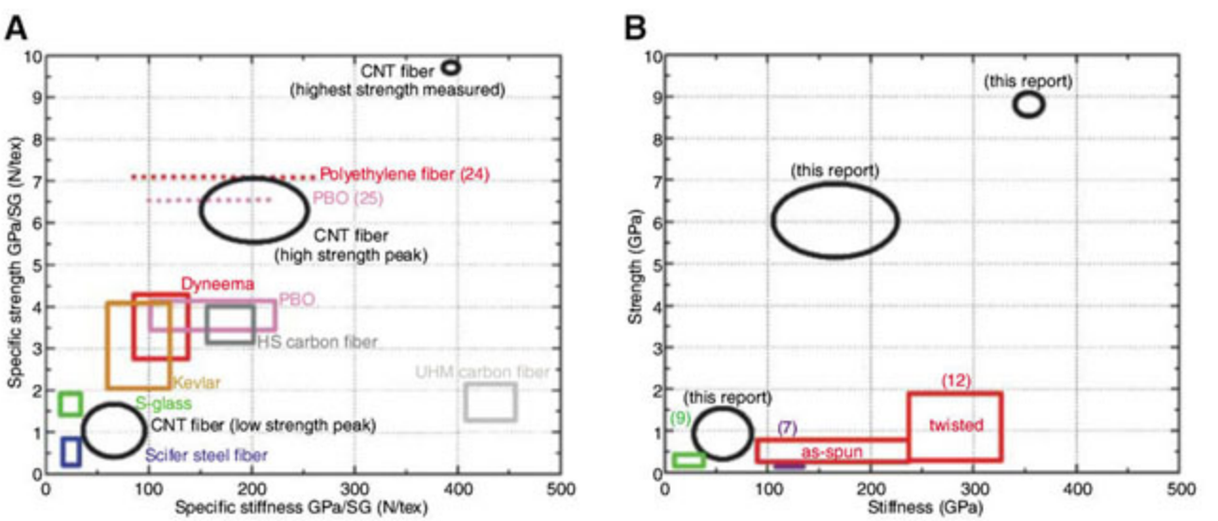

Fig. 4. (**A**) Comparison of the strength and stiffness of our strongest sample and of fibers typical of the high-strength and low-strength peaks in the 1-mm gauge length distribution versus the properties of other commercially available high-performance fibers; two laboratory observations of higher strengths in commercialized systems are also included (reference numbers are shown). (**B**) Similar to (A), but with the strength ranges of our carbon nanotube fibers compared with literature data for other carbon nanotube fibers made by different processes. In this case, the comparison is in terms of GPa instead of GPa/SG. Only data where strength and stiffness values are available from the same samples are included here.

which are as-recorded); this plot reveals a positive correlation between strength and stiffness.

The implication of the correlation between strengths and stiffnesses is that although the fiber samples we created have defects at random intervals on the millimeter scale along the gauge length, these flaws do not have the nature of a stress raiser in a brittle fiber, which would be expected to reduce strength but to have little or no effect on stiffness. It is much more likely that these defects are associated with local deficiencies in densification, which would preclude successful stress transfer by shear between some of the bundles of nanotubes. Consequently, in some sections of the fiber, not all of the nanotube bundles carry an equal share of the load, resulting in both lower fracture strength and decreased stiffness. We believe that these defects are associated with included carbonaceous particles (fig. S3), which induce failure in interbundle stress transfer over much greater distances along the fiber than that occupied by the particle alone. Such particles are seen microscopically with a frequency that is consistent with their distribution at millimeter-scale spacings along the fiber. The strengths reported here represent a measure of success in reducing the level of such included particles, and we expect further levels of process refinement to enable the realization of such high strengths over much longer fibers.

Figure 4A (and table S1) set the strength and stiffnesses of our fibers in the context of a range of mechanical data from commercially available high-performance fibers, as well as reports of properties of other carbon nanotube fibers in the recent literature. The strains shown, and thus the stiffness and energy absorbed up to fracture (table S1), have been corrected for grip strain. Under laboratory conditions, higher strengths than those guaranteed in a commercial product are sometimes seen. Two reported strengths from laboratory fiber work, one for high-strength polyethylene (*24*) and one for poly(*p*-phenylene-2,6-benzobisoxazole) (PBO) (*25*), are plotted as horizontal lines in Fig. 4A. Table S1 also sets the measurements of energy absorbed at fracture (toughness) in the context of other fibers. In Fig. 4B, the performance of our fiber is compared with values reported in the literature for carbon nanotube fibers made by different methods. As some laboratories have not recorded the density of their fibers, we have made this comparison in terms of strength and stiffness rather than specific strength and specific stiffness. One consequence of using these (nonspecific or direct) units is that the estimated error of our measurements is slightly increased.

References and Notes

1. M. F. Yu, B. S. Files, S. Arepalli, R. S. Ruoff, *Phys. Rev. Lett.* **84**, 5552 (2000).
2. M. M. J. Treacy, T. W. Ebbesen, J. M. Gibson, *Nature* **381**, 678 (1996).
3. B. G. Demczyk *et al.*, *Mat. Sci. Eng. A* **334**, 173 (2002).
4. T. Dumitrica, M. Hua, B. I. Yakobson, *Proc. Natl. Acad. Sci. U.S.A.* **103**, 6105 (2006).
5. T. Belytschko, S. P. Xiao, G. C. Schatz, R. S. Ruoff, *Phys. Rev. B* **65**, 235430 (2002).
6. T. Natsuki, K. Tantrakarn, M. Endo, *Carbon* **42**, 39 (2004).
7. L. M. Ericson *et al.*, *Science* **305**, 1447 (2004).
8. K. L. Jiang, Q. Q. Li, S. S. Fan, *Nature* **419**, 801 (2002).
9. M. Zhang, K. R. Atkinson, R. H. Baughman, *Science* **306**, 1358 (2004).
10. Y.-L. Li, I. A. Kinloch, A. H. Windle, *Science* **304**, 276 (2004); published online 11 March 2004 (10.1126/science.1094982).
11. See supporting material on *Science* Online.
12. X. Zhang *et al.*, *Small* **3**, 244 (2007).
13. Q. W. Li *et al.*, *Adv. Mater.* **18**, 3160 (2006).
14. M. Motta, A. Moisala, I. A. Kinloch, A. H. Windle, *Adv. Mater.* **19**, 3721 (2007).
15. B. Vigolo *et al.*, *Science* **290**, 1331 (2000).
16. We express stress as GPa divided by SG, a unit known as specific stress in materials science that is exactly numerically equivalent to newtons per tex.
17. I. M. Ward, Ed., *Structure and Properties of Oriented Polymers* (Halsted/Wiley, New York, 1975).
18. T. Liu, S. Kumar, *Nano Lett.* **3**, 647 (2003).
19. T. Amornsakchai, D. L. M. Cansfield, S. A. Jawad, G. Pollard, I. M. Ward, *J. Mater. Sci.* **28**, 1689 (1993).
20. I. M. Ward, in *Solid Phase Processing of Polymers*, I. M. Ward, P. D. Coates, M. M. Dumoulin, Eds. (Hanser Gardner, Munich, 2000), p. 133.
21. N. Lissart, J. Lamon, *J. Mater. Sci.* **32**, 6107 (1997).
22. R. D. Maurer, Ed., *Strength of Inorganic Glass* (Plenum, New York, 1985).
23. J. D. H. Hughes, H. Morley, E. E. Jackson, *J. Phys. D* **13**, 921 (1980).
24. H. van der Werff, A. J. Pennings, *Colloid Polym. Sci.* **269**, 747 (1991).
25. W. A. Adams, personal communication.

26. Supported by Consejo Nacional de Ciencia y Tecnología (Mexico), the Engineering and Physical Sciences Research Council (UK), and the U.S. Army International Technology Center–Atlantic. We thank S. Fraser for valuable comments and M. Pick for his considerable technical contribution to this research.

Supporting Online Material

www.sciencemag.org/cgi/content/full/1147635/DC1
Materials and Methods
Figs. S1 to S3
Table S1
Movie S1
References

11 July 2007; accepted 2 November 2007
Published online 15 November 2007;
10.1126/science.1147635
Include this information when citing this paper.

Structural Rearrangements That Govern Flow in Colloidal Glasses

Peter Schall,[1,2]* David A. Weitz,[2,3] Frans Spaepen[2]

Structural rearrangements are an essential property of atomic and molecular glasses; they are critical in controlling resistance to flow and are central to the evolution of many properties of glasses, such as their heat capacity and dielectric constant. Despite their importance, these rearrangements cannot directly be visualized in atomic glasses. We used a colloidal glass to obtain direct three-dimensional images of thermally induced structural rearrangements in the presence of an applied shear. We identified localized irreversible shear transformation zones and determined their formation energy and topology. A transformation favored successive ones in its vicinity. Using continuum models, we elucidated the interplay between applied strain and thermal fluctuations that governs the formation of these zones in both colloidal and molecular glasses.

The hallmark of any glass is a very low atomic or molecular mobility within a disordered solid, many orders of magnitude smaller than that of a fluid. This mobility is a result of thermally induced structural rearrangements, which typically occur at a very low rate. Structural rearrangements must also occur as a response of the glass to an externally applied shear; this causes a directional bias in the structural rearrangements that produces the macroscopic strain (*1*). Because the glass structure is so highly constrained, these structural rearrangements must entail reorganization of the constituent molecular units over some larger length scale (*2*). Nevertheless, in molecular glasses, these length scales are still too small and the time scales are too short for direct observation. The only direct evidence for the existence of local shear transformation zones that produce macroscopic strain comes from bubble raft experiments (*3*) and computer simulations of two-dimensional (*4*–*6*) and three-dimensional (3D) glasses (*7*–*10*). Direct real-space visualization of structural rearrangements can be made in suspensions of colloidal particles as they can be quenched into a glassy state by rapid densification of the particles from a fluid state (*11*, *12*). These systems lose ergodicity due to crowding at high particle volume fraction, ϕ, leading to a transition to a glassy state at $\phi_g \approx 0.58$ (*13*). Experiments and simulations suggest that when ϕ_g is approached from the fluid phase, particle rearrangements occur cooperatively on increasing length scales (*2*, *14*, *15*). For $\phi > \phi_g$, such rearrangements are

[1]Van der Waals-Zeeman Institute, University of Amsterdam, Valckenierstraat 65, 1018 XE Amsterdam, Netherlands. [2]Harvard School of Engineering and Applied Sciences, Cambridge, MA 02138, USA. [3]Department of Physics, Harvard University, Cambridge, MA 02138, USA.

*To whom correspondence should be addressed. E-mail: pschall@science.uva.nl

highly constrained (*15*). Nevertheless, thermally induced aging, often called "structural relaxation," occurs (*13*, *16*) and must entail some form of cooperative motion.

We visualize structural rearrangements in colloidal glasses in three dimensions and in real time by following the microscopic strain distribution under shear. We identify the shear transformation zones and show that they have a spatial extent of a few particle diameters and involve a highly localized structural rearrangement that results in a strain of ~0.1 immediately in the vicinity of the central particle. We determine their activation energy, $E^* \sim 16\ k_BT$, where k_BT is the thermal energy; thus, they can be induced by thermal fluctuations. They also can be induced through application of very small shears. Moreover, the elasticity of the glass results in coupling between the transformation zones, which, upon increasing strain, leads to a network of transformation zones that extends across the sample.

We prepared a 42-μm-thick colloidal glass by quenching silica spheres with a diameter of 1.5 μm and a polydispersity of 3.5% (*17*) from a dilute suspension onto a coverslip by centrifugation to a volume fraction of roughly 0.61, well into the colloidal glassy state. Because the density of the silica spheres is greater than that of the solvent, ϕ increases with sample depth. The sample is sufficiently deep into the glassy state that crystallization is not observed. Boundary-induced crystallization is suppressed by a layer of polydisperse spheres sintered onto the coverslip. The silica particles are suspended in a mixture of water and dimethylsulfoxide, which matches their refractive index. We added a small amount of fluorescein to the solvent so that under fluorescent imaging, particles appear as dark spots on a bright background. We carefully introduced a fine metal grid (*18*) from above to fix the top of the sediment, and we used a piezoelectric translation stage to move the coverslip to apply shear at very small rates of $\sim 10^{-5}\ s^{-1}$. We used confocal microscopy to image individual particles in a 47 μm by 50 μm by 23 μm volume and determined their positions in 3D with an accuracy of 0.03 μm in the horizontal and 0.05 μm in the vertical direction (*15*). We tracked the motion of individual particles for the 60-min duration of each experiment by acquiring 3D image stacks every 150 s; each image stack took 60 s to acquire.

Structural rearrangements can be thermally activated even in the absence of shear. We follow particle trajectories in an unsheared glass for 20 min and identify the nearest neighbors of each particle as those separated by less than r_0, the first minimum of the pair correlation function. To calculate the time-dependent strain, we determine the symmetric part of the best affine deformation tensor that transforms the change of the nearest-neighbor vectors over the time interval (*6*), and we smooth the results by averaging over nearest neighbors (*19*, *20*). The *x*, *y*, and *z* directions are chosen along the edges of the imaged volume (Fig. 1A). We focus on the shear component ε_{yz} of the strain tensor and illustrate its value for two subsequent 2.5-min intervals in 3-μm-thick sections at $z = 13.5$ μm in Fig. 1, B and C. Red and blue spheres indicate regions with positive and negative shear strain, respectively. Regions of strain extending over many particles are evident (arrows). Furthermore, by comparing red and blue regions, we find that localized regions of large strain reverse their sign in subsequent images as highlighted by the arrows in Fig. 1, B and C. We interpret these strain oscillations as thermal fluctuations. To check this hypothesis, we calculate the elastic energies associated with the shear strain distribution and determine the relative frequency of the energies. We divide the volume into cubes of size $a = 3$ μm, so that each cell contains about nine particles, roughly equal to the number of nearest neighbors. The magnitude of ε_{yz} calculated for cells centered at $z = 13.5$ μm and for the second time interval (Fig. 1C) is plotted in Fig. 1D (*21*). We calculate the elastic energy in each cell, $E/\mu = (1/2)(2\varepsilon_{yz}^2)a^3$, where we have normalized by the shear modulus, μ. The probability distribution of the normalized energies is well described by an exponential as expected for a thermally equilibrated system, as shown in Fig. 1E. Because $\ln f(E) = -\mu(E/\mu k_BT)$, we obtain the shear modulus, $\mu = 0.056$ Pa, from the fit, indicated by the straight line in Fig. 1E. This value is consistent with $\mu = 0.1$ Pa,

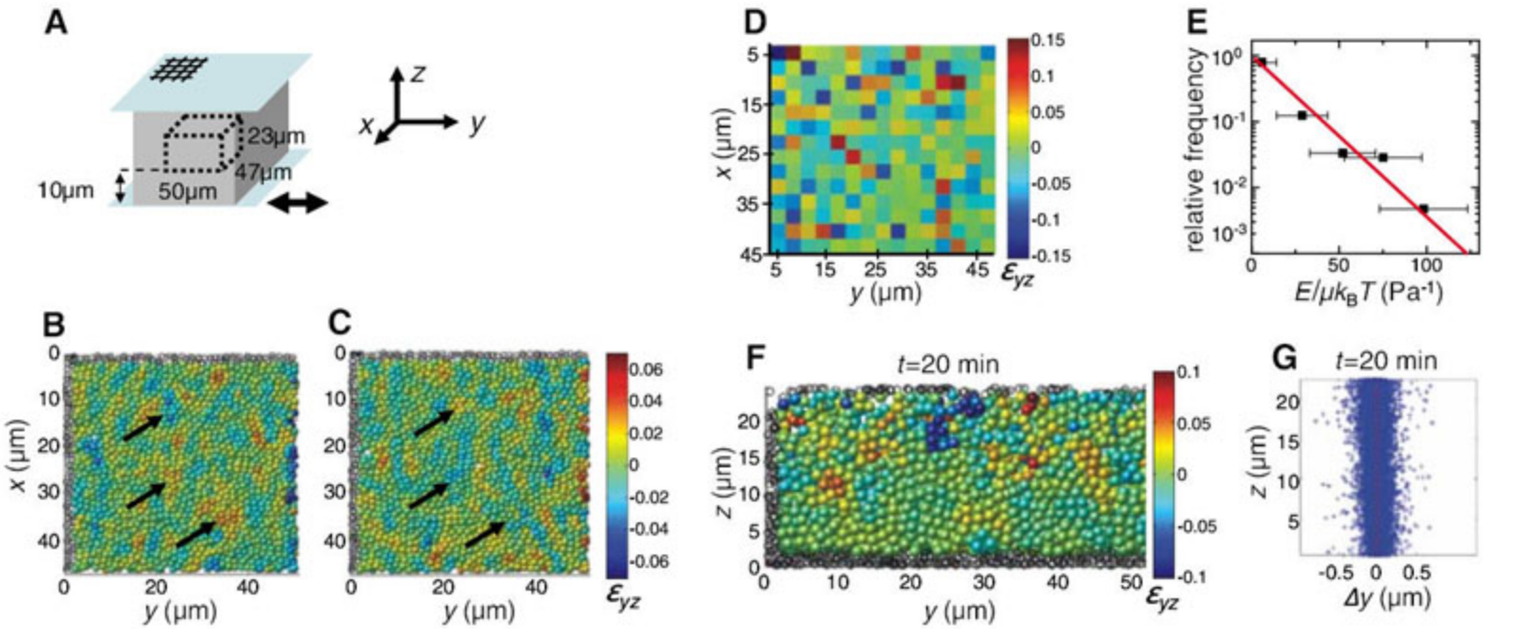

Fig. 1. Thermally induced strain fluctuations (**A**) Schematic showing the colloidal glass (gray), and the bottom coverslip and top grid (blue) with respect to the 47 μm by 50 μm by 23 μm section depicted in (B) to (D) and (F). (**B** to **F**) Strain fluctuations in the unsheared glass. Color in (B) to (D) and (F) indicates the value of the local shear strain, ε_{yz} (see color scale). (B and C) *x*-*y* sections (3 μm thick) at $z = 13.5$ μm, showing the distribution of the incremental shear strain during two consecutive 2.5-min intervals. Arrows mark regions in which the strain changes sign from (B) to (C). (D) Array of 3 μm by 3 μm squares, showing values of the incremental shear strain in 3 μm by 3 μm by 3 μm cells at $z = 13.5$ μm for the section shown in (C). Each cell contains roughly nine particles. (E) Distribution of normalized strain energies, $E/\mu k_BT$, calculated from the strain values depicted in (D). Squares at $E/\mu k_BT = 23n$ Pa^{-1} with $n = 0,1,2,\ldots$ indicate the relative frequency of energy values in intervals $[23n,\ 23(n+1)]$ Pa^{-1}. Horizontal bars indicate the uncertainty in energy associated with the uncertainty in strain due to the limited accuracy in particle positioning. We assume that the measured particle coordinates have a Gaussian distribution of width 0.03 μm in the *x* and *y* direction, and 0.05 μm in the *z* direction, around the real positions. The red line has a slope of −0.056 Pa. (F) *y*-*z* section (8 μm thick) centered at $x = 14$ μm showing the cumulative shear strain at $t = 20$ min. Red and blue regions persist at even later times. (**G**) Cumulative displacements, Δy, from $t = 0$ to $t = 20$ min of particles (+) at height between $z = 0$ and $z = 23$ μm.

measured for crystals of similar thickness and made of the same particles (*22*). Similar oscillations exist for all components of strain, both shear and uniaxial. This supports our hypothesis that the strain oscillations are indeed caused by thermal fluctuations.

Thermal fluctuations can also induce irreversible rearrangements. To probe these, we determine the cumulative strain that occurs during the entire 20-min interval. We plot a reconstruction of an 8-μm-thick section in the *yz* plane centered at $x = 14$ μm in Fig. 1F. Localized regions with strain amplitudes even larger than those of the strain fluctuations have developed, and we confirm that these regions persist at longer times. These structural rearrangements do not, however, lead to macroscopic strain as confirmed by the plot of the z coordinates of the individual particles as a function of their cumulative displacements in the y direction; no shear gradient is observed, as shown in Fig. 1G.

To investigate these structural rearrangements more closely, we study their behavior upon application of shear. We apply positive shear strain by displacing the bottom coverslip in the negative y direction while keeping the top plate at a fixed position. We find that the mean Δy increases almost linearly with z corresponding to a nearly uniform shear strain, as shown by the plot of the z coordinates of all particles as a function of their y displacements in Fig. 2A. The slight curvature of the data indicates a somewhat reduced shear strain at small z. We attribute this to the higher density at the bottom of the sediment. We determine the macroscopic shear strain, γ, from the difference of the mean of the Δy distributions across the full sample height $\Delta z = 23$ μm (slope of the red line). We obtain $\gamma = 0.03$ for the 50-min time interval, which corresponds to an average strain rate of 10^{-5} s^{-1}.

We can again identify localized regions of structural rearrangements, but now induced by the applied strain. We show the cumulative strain ε_{yz} in a 7-μm-thick section at $x = 10$ μm in Fig. 2B. Red spheres indicate local shear strain in the direction of the applied shear, whereas blue spheres indicate shear strain opposite to the applied strain. The shear strain is not distributed homogeneously, but is instead localized as shown by the zones of concentrated red spheres. These regions are typically a few particle diameters wide. We focus on an individual region (arrow) and investigate the strain distribution when it is first formed. A large portion of the strain occurs in one time step, which allows us to identify its formation. Reconstructions centered on this region with adjacent frames measured just before and just after its formation are shown in Fig. 2, C and D. The red spheres in Fig. 2D (arrow) indicate high local shear strain associated with the formation of the shear transformation zone. We find that before the zone is formed, opposite strain concentrates in the same region (blue spheres in Fig. 2C). This suggests that the formation of the zone is caused by a thermally induced strain fluctuation. During the time step in which the shear transformation zone is formed, four zones of negative shear strain (−) surround the center region shown by red in Fig. 2D. This fourfold symmetric strain distribution is characteristic of the distortion of an elastic matrix around a volume that undergoes a shear transformation (*23*). We determine the magnitude of ε_{yz} as a function of distance, r, from the shear transformation zone center, by plotting the strain values of all particles in the lower left sector of a cylinder centered at $y = 25$ μm and $z = 15$ μm as a function of their distance from the cylinder axis (Fig. 2E). Black dots show the averaged strain values depicted in Fig. 2D, whereas the red triangles represent values of ε_{yz} that have not been averaged over nearest neighbors. The averaged values are significantly smaller, which we attribute to the truncation of the strain magnitude that results from the averaging; we use the nonaveraged strain values for further calculations. The shear strain is constant at small r, and decays as r^{-3} at larger r (dashed lines in Fig. 2E), as expected for the strain field around a volume that undergoes a shear transformation (*23*). The crossover defines the radius of the core of the shear transformation zone, $r_c = 2.3$ μm, which is roughly equal to three particle radii. To explore the strain distribution in the third direction, we show a 5-μm-thick section along the *xz* plane that contains the same shear transformation zone in Fig. 2F. The core of the zone is elongated along the x direction, bounded by regions of slightly negative strain. To determine its extent in x, we consider particles within 1.5 μm of the dotted line, which goes through the center of the zone, and plot their ε_{yz} as a function of x in Fig. 2G. We observe a maximum of $\varepsilon_0 \approx 0.08$ centered between $x = 10$ μm and $x = 15$ μm with a crossover to negative strain values on either side. Thus, we take the width of the core of the shear transformation zone to be $\Delta x_c = 5$ μm.

We calculate the energy cost, E_f, and activation volume, $V^* = k_B T d\ln \dot{\gamma}/d\tau$, where $\dot{\gamma}$ is the macroscopic shear rate and τ the applied stress, associated with the formation of the shear transformation zone using a continuum-elastic model. We first determine the strain field of an elastic matrix around a spherical inclusion of radius r_c that undergoes a uniform shear transformation of ε_0 (*24*). We calculate the total elastic strain energy inside and outside the inclusion by integrating the total energy density $w = (1/2)(2\mu\varepsilon_{ij}^2 + \lambda\varepsilon_{kk}^2)$ (*25*) over the volume. We

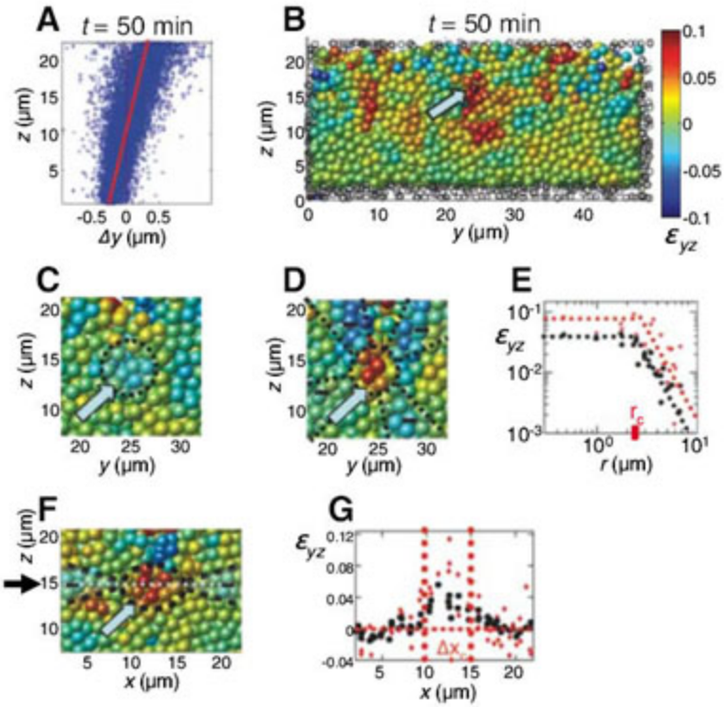

Fig. 2. Response of a glass to shear strain (**A**) Shear-induced displacements, Δy, of particles (+) at height between $z = 0$ and $z = 23$ μm after 50 min of shear. (**B** to **G**) Strain distribution and shear transformation zones in the sheared glass. Particle color indicates the value of the local shear strain ε_{yz} (see color scale). (B) *y*-*z* section (7 μm thick) centered at $x = 10$ μm, showing the distribution of the cumulative shear strain after 50 min of shear. Arrow indicates a shear transformation zone, the incremental strain distribution around which is shown for two subsequent time intervals in (C) and (D). (C and D) *y*-*z* sections (15 μm by 15 μm by 7 μm) centered around the zone marked in (B). (C) Incremental shear strain between $t = 25$ min and $t = 27.5$ min. Dashed circle indicates a region of negative shear strain. (D) Incremental shear strain between $t = 27.5$ min and $t = 30$ min. Dashed circle indicates a zone of high positive shear strain. Dashed straight lines delineate four regions of negative shear strain that surround the high–shear strain zone in the center. (E) Shear strain values versus r, the radial distance of particles from the shear transformation zone axis along x through $y = 25$ μm and $z = 15$ μm. Black dots and red triangles show averaged and nonaveraged strain values, respectively. Dashed lines with the slopes $m = 0$ and $m = -3$ are guides to the eye. (F) *x*-*z* section (5 μm thick) at $y = 25$ μm, showing the incremental shear strain between $t = 27.5$ min and $t = 30$ min. The dashed ellipse indicates the intersection of the boundary of the high–shear strain zone with the plane shown. Black dashed lines on both sides of the ellipse delineate regions of slightly negative strain adjacent to the shear transformation zone. (G) Shear strain values versus x for particles within 1.5 μm of the blue dashed line at $z = 15$ μm (arrow) in (F). Dashed vertical lines indicate the extension of the shear transformation zone along x.

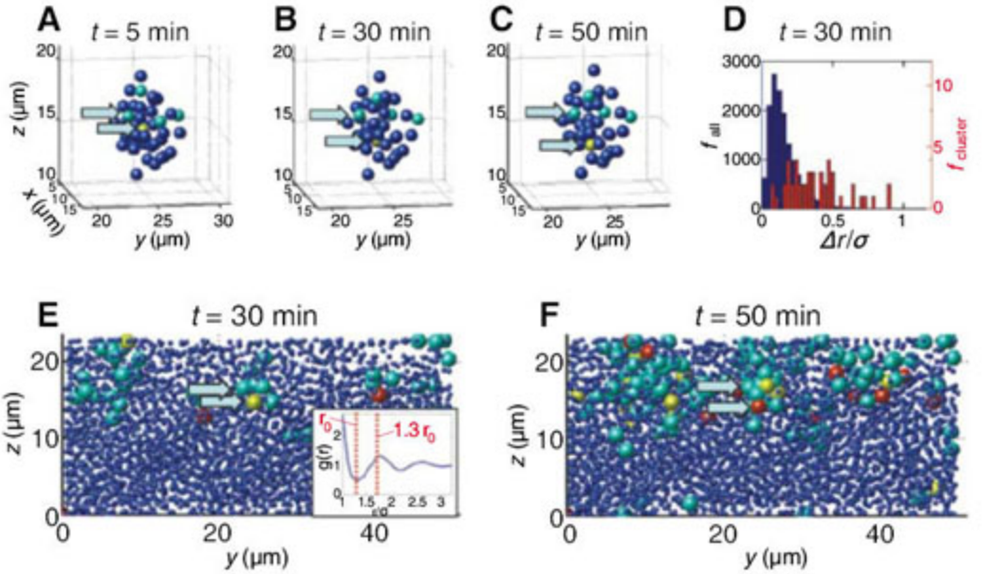

Fig. 3. Structural rearrangements at the particle scale. (**A** to **C**) Reconstructed images showing particle arrangements within the shear transformation zone of Fig. 2, B to G, at t = 5, 30, and 50 min. Arrows mark one yellow and four green particles, which are nearest neighbors at t = 5 min and become separated at later times. (**D**) Histograms showing the normalized particle displacements, $\Delta r/\sigma$, where σ is the particle radius, at t = 30 min, for shear transformation zone particles (red bars, right scale) and for all particles outside the shear transformation zone (blue bars, left scale). Particles within the shear transformation zone exhibit many more large displacements. (**E** and **F**) Reconstruction of a 10-μm-thick glass section centered at x = 7 μm shows nearest-neighbor changes in the sheared glass at t = 30 min and t = 50 min. Large green, yellow, and red spheres indicate particles that lose one, two, and three nearest neighbors, respectively. All other particles are drawn as smaller spheres for clarity. Nearest-neighbor changes occur in high–shear strain regions (compare to Fig. 2B). Arrows indicate the same particles as marked in (A) to (C). The inset in (E) shows the radial distribution function, $g(r)$, of the glass used for identifying nearest neighbors at t = 0. Particles with distances smaller than r_0 (left dashed line) are nearest neighbors; all particles that move farther away than 1.3 r_0 from their nearest neighbor (right dashed line) are defined as having lost their neighbor.

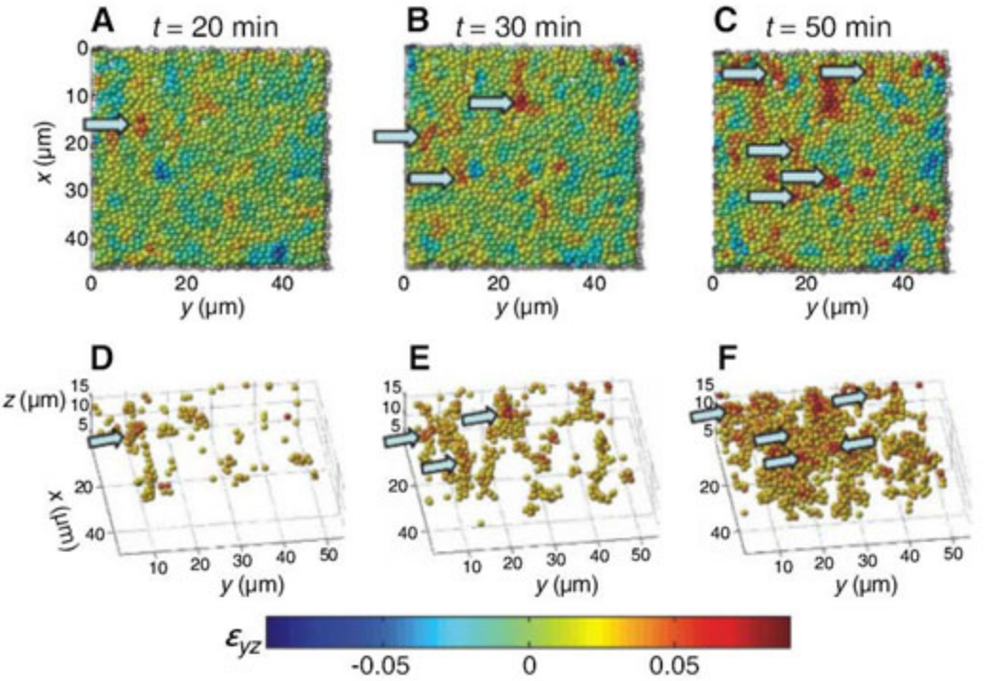

Fig. 4. Strain evolution during shear. Distribution of the cumulative shear strain after 20, 30, and 50 min of shear. For each frame, arrows indicate shear transformation zones that have been formed in the time interval before the frame shown. Shear transformation zones appear to form a connected network at t = 50 min. (**A** to **C**) x-y sections (5 μm thick) centered at z = 13.5 μm. (**D** to **F**) Perspective view of 16-μm-thick sections showing particles with shear strain values larger than 0.025 only.

approximate the Lamé constant λ by $2\nu\mu/(1-2\nu)$ using the Poisson ratio ν = 1/3 and obtain E_f' = 18.9 k_BT. We calculate the activation volume by integrating the distribution of the technical shear strain $\gamma = 2\varepsilon_{yz}$ over the volume and obtain $V^{*\prime}$ = 6.9 μm^3. We correct E_f' and $V^{*\prime}$ for the ellipsoidal shape of the shear transformation zone by multiplying by $\Delta x_c/2r_c$ and obtain E_f = 20.5 k_BT and V^* = 7.5 μm^3. We determine the volume of a particle, V_0 = 1.88 μm^3, from the peak of the pair correlation function at 1.53 μm; thus, the activation volume is roughly four particle volumes. Interestingly, this value is of the same order as those for metallic glasses determined from measurements of the stress dependence of the strain rate; for example, for a PdNiCuP alloy, V^* is about eight atomic volumes (*26*).

Because the rearrangements in the shear transformation zones contribute to plastic flow, they must be irreversible and persist after they have been created. To check this, we reversed the shear direction and confirmed that the shear transformation zones that we investigated here do not reverse but remain locked in their sheared configurations (*27*). To elucidate this irreversibility, we investigated the structural rearrangements on the single-particle level in the core of the shear transformation zone. We show reconstructions of the arrangement of particles in the shear transformation zone core at t = 5, 30, and 50 min in Fig. 3, A to C. We highlight a particle in the zone center (yellow sphere), which exhibits a large displacement downward and thereby loses some of its nearest neighbors (green spheres). To quantify the particle displacements in this zone, we determined the displacement of the particles relative to the average displacement of particles at the same height, $\Delta r = [(\Delta x - \langle\Delta x\rangle)^2 + (\Delta y - \langle\Delta y\rangle)^2 + (\Delta z - \langle\Delta z\rangle)^2]^{0.5}$. We plot the distribution of Δr at t = 30 min in Fig. 3D. The magnitudes of the displacements of particles in the shear transformation zone (red bars) are significantly larger than those of the particles outside the zone

Table 1. Activation parameters of individual shear transformation zones. Activation volume V^*, energy of formation E_f, and activation energy $E^* = E_f - \tau V^*$ of shear transformations were determined from the individual incremental strain distributions associated with the formation of the transformations. The shear stress τ was taken to be $\tau = \gamma_0\mu$ with γ_0 = 0.012, the macroscopic shear strain at formation of the first shear transformation, and the shear modulus μ = 0.056 Pa (Fig. 1E). The particle volume V_0 is 1.88 μm^3.

V^*/V_0	E_f (k_BT)	E^* (k_BT)
4.0	20.5	19.2
4.6	19.3	17.8
3.6	13.9	12.7
3.7	16.5	15.3
3.4	16.5	15.4
3.8	19.6	18.4

(blue bars). Two particles in the shear transformation zone move almost as much as their radius; one of these is the yellow sphere in Fig. 3, A to C. Such large displacements of isolated particles cause notable changes in their nearest-neighbor configuration, as illustrated by the motion of the yellow sphere. This causes the irreversibility of the shear transformation. To characterize this irreversibility, we identify all particles that lose one or more nearest neighbors, where we define loss of a nearest neighbor to occur when that particle moves farther away than βr_0, where we arbitrarily choose $\beta = 1.3$, as shown in the inset of Fig. 3E. We show these particles in a 10-μm-thick slice in the *yz* plane at two different times in Fig. 3, E and F; large green, yellow, and red spheres illustrate particles that have lost one, two, and three nearest neighbors, respectively. These spheres concentrate in regions, which grow with time and coincide with the zones that exhibit high shear strain (Fig. 2B). This supports our interpretation that shear transformations are irreversible: The nearest-neighbor changes lead to new particle configurations, stabilizing the transformed zone.

The existence of these shear transformation zones indicates that locally, the strain is highly concentrated. The long-range strain field of a shear transformation may facilitate the nucleation of another shear transformation zone in its vicinity: The formation of new zones may be spatially and temporally correlated. To explore this possibility, we follow the evolution of the ε_{yz} distribution over the entire duration of the experiment. To smooth the thermally induced strain fluctuations, we average the particle positions over two adjacent frames and calculate the time-averaged shear strain, ε_{yz}*. We show the evolution of the ε_{yz}* distribution in Fig. 4. A 5-μm-thick section in the *xy* plane centered at $z = 13.5$ μm is shown in Fig. 4, A to C. Three-dimensional reconstructions of a thicker slice, 16 μm in height, depicting only particles with $\varepsilon_{yz}^* > 0.025$, are shown in Fig. 4, D to F. The number of shear transformation zones increases with strain; new zones appear, while existing ones persist. The images show that a shear transformation zone induces new ones in its vicinity. For example, the zone formed at the earliest time (arrows in Fig. 4, A and D) induces the formation of three adjacent zones (arrows in Fig. 4, B and E), each of which again induces additional adjacent zones (Fig. 4, C and F). That this coupling results from the long-range strain fields is corroborated by the observation that branches of positive strain develop between the individual shear transformation zones, as shown by the more yellow-colored particles between the zones. These branches connect the individual shear transformation zones into a network, which ultimately permeates the entire field of view at 50 min (Fig. 4F).

Even though the applied strain helps induce these shear transformation zones, they are nevertheless still predominantly thermally activated. We can understand this by comparing the energy induced by the applied shear with the energy of formation of the shear transformation zone. The external work due to the applied shear stress τ is τV^*. We estimate the shear stress to be constant once the sample has exceeded the macroscopic yield strain, where the first shear transformation occurs, $\gamma_0 = 0.012$; thus, we take $\tau = \gamma_0 \mu$. We calculate the activation volumes, V^*_i, from the individual strain distributions of several shear transformation zones and list them in Table 1. Because the average activation volume is $V^*_{av} = 3.8\ V_0$, the typical work due to shear is ~1 k_BT. By comparison, we calculate the formation energy of the same shear transformation zones (Table 1). Although there is some variation, their typical value is $E_f = 18\ k_BT$, significantly larger than the work done by the applied shear. Thus, the shear transformation zones are thermally activated with an activation energy of $E_i^* = E_{f,i} - \tau V^*_i$, and we also list these values in Table 1.

The average activation energy is $E^*_{av} = 16.5\ k_BT$; this should be compared with the measured value of E^* determined from the rate, J, at which shear transformation zones are induced. We use $J = f_0 m \exp(-E^*/k_BT)$, where $m = 3400$ is the total number of particles, and $f_0 = 100\ s^{-1}$ is a characteristic frequency of the particles determined by their diffusion time between nearest-neighbor particles (*20*). We determine $J = 3 \times 10^{-3}\ s^{-1}$ from the total number of shear transformation zones observed during the 50-min interval in the 5-μm-thick section; thus, $E^* = 18.5\ k_BT$, in very good agreement with E^*_{av} determined from the strain distributions.

These results highlight the role of the shear transformation zone in the flow of glasses. The structural rearrangements are thermally activated and are highly localized. Although these results are obtained on colloidal glasses, similar behavior should occur in metallic and molecular glasses. Application of the measured strain distribution on the atomic scale to a metallic glass with $\mu \sim 30$ GPa (*28*) yields a shear-zone energy close to that found for our colloidal glass. Although activation energies determined from isoconfigurational viscosity measurements on metallic glasses at 600 K are roughly four times as large as this value (*29*), the ratio of the activation energy to the thermal energy is only a factor of 2 larger than in our colloidal system. This reflects the 10 orders of magnitude higher attempt frequency in metallic glasses at equal nucleation rates. The ratio of the external work τV^* to the thermal energy is of the same order as in typical deformation tests on metallic glasses at the same strain rate (*26*), which indicates that the effects of thermal fluctuations in our experiment are similar to those in deformation of metallic glasses. Our results also highlight the coupling between shear transformation zones: The long-range elastic stress field of each zone induces new zones in its vicinity, and upon sufficient external strain, these zones extend throughout the volume. A similar coupling between shear transformation zones is expected in atomic and molecular glasses.

References and Notes

1. F. Spaepen, *Acta Metall.* **25**, 407 (1977).
2. G. Adam, J. H. Gibbs, *J. Chem. Phys.* **43**, 139 (1965).
3. A. S. Argon, Y. Kuo, *Mater. Sci. Eng.* **39**, 101 (1979).
4. K. Maeda, S. Takeuchi, *Phys. Status Solidi A* **49**, 685 (1978).
5. C. Maloney, A. Lemaitre, *Phys. Rev. Lett.* **93**, 195501 (2004).
6. M. L. Falk, J. S. Langer, *Phys. Rev. E* **57**, 7192 (1998).
7. S. Kobayashi, K. Maeda, S. Takeuchi, *Acta Metall.* **28**, 1641 (1980).
8. K. Maeda, S. Takeuchi, *Philos. Mag. A* **44**, 643 (1981).
9. D. Srolovitz, V. Vitek, T. Egami, *Acta Metall.* **31**, 335 (1983).
10. A. C. Lund, C. A. Schuh, *Acta Mater.* **51**, 5399 (2003).
11. P. N. Pusey, W. van Megen, *Nature* **320**, 340 (1986).
12. A. van Blaaderen, P. Wiltzius, *Science* **270**, 1177 (1995).
13. W. van Megen, T. C. Mortensen, S. R. Williams, J. Müller, *Phys. Rev. E* **58**, 6073 (1998).
14. C. Donati, S. C. Glotzer, P. H. Poole, *Phys. Rev. Lett.* **82**, 5064 (1999).
15. E. R. Weeks, J. C. Crocker, A. C. Levitt, A. Schofield, D. A. Weitz, *Science* **287**, 627 (2000).
16. N. B. Simeonova, W. K. Kegel, *Phys. Rev. Lett.* **93**, 035701 (2004).
17. Micromod, Sicastar, 1.5 μm.
18. SPI supplies, G1000HS, Ni grid, mesh size 25 μm.
19. For each particle with center at $\mathbf{r}(t)$, we determine the vectors $\mathbf{d}_j(t) = \mathbf{r}(t) - \mathbf{r}_j(t)$ to all nearest neighbors j at time t. We then compare these vectors with the nearest-neighbor vectors at time t-Δt, $\mathbf{d}_j(t\text{-}\Delta t)$. The best affine deformation tensor, α, that transforms the nearest-neighbor vectors at the earlier time, $t - \Delta t$, to the vectors at time t is determined by minimizing the mean square difference, $\sum_j [\mathbf{d}_j(t - \Delta t) - \alpha \mathbf{d}_j(t)]^2$ (*6*). The symmetric part of α corresponds to the strain tensor of the particle under consideration. To smooth the resulting strain distribution, we average the strain tensor of each particle with those of its nearest neighbors and assign the resultant average strain tensor to the particle under consideration.
20. P. Schall, I. Cohen, D. A. Weitz, F. Spaepen, *Nature* **440**, 319 (2006).
21. We first find the particle whose center is closest to the center of the cell. For this particle with center at $\mathbf{r}(t)$ at time t, we determine the vectors $\mathbf{d}_j(t) = \mathbf{r}(t) - \mathbf{r}_j(t)$ to all other particles j in the cell. We compare these vectors with the interparticle vectors at time $t - \Delta t$, $\mathbf{d}_j(t - \Delta t)$. We use the difference between $\mathbf{d}_j(t)$ and $\mathbf{d}_j(t - \Delta t)$ to calculate the strain tensor by the procedure described in (*19*).
22. P. Schall, I. Cohen, D. A. Weitz, F. Spaepen, *Science* **305**, 1944 (2004).
23. G. Picard, A. Ajdari, F. Lequeux, L. Bocquet, *Eur. Phys. J. E* **15**, 371 (2004).
24. J. D. Eshelby, *Proc. R. Soc. A* **252**, 561 (1959).
25. L. D. Landau, E. M. Lifshitz, *Theory of Elasticity*, Course of Theoretical Physics, vol. 7 (Elsevier Butterworth-Heinemann, Oxford, ed. 3, 1986).
26. M. Heggen, F. Spaepen, M. Feuerbacher, *J. Appl. Phys.* **97**, 033506 (2005).
27. When shearing back to zero strain, we observe that some shear transformation zones reverse. These may be considered as anelastic. The ones of interest here, however, do not go back.
28. T. Soshiroda, M. Koiwa, T. Masumoto, *J. Non-Cryst. Solids* **22**, 173 (1976).
29. A. I. Taub, F. Spaepen, *Acta Metall.* **28**, 1781 (1980).

30. We thank J. Hutchinson for assistance in the calculation of the shear energy around an inclusion and I. Cohen for the use of the shear cell. This work was supported by the Innovational Research Incentives Scheme ("VIDI" grant) of the Netherlands Organization for Scientific Research (NWO) (P.S.) and by the NSF (DMR-0602684) and the Harvard Materials Research and Engineering Center (DMR-0213805).

16 August 2007; accepted 30 October 2007
10.1126/science.1149308

Role of Intermolecular Forces in Defining Material Properties of Protein Nanofibrils

Tuomas P. Knowles,[1,2*] Anthony W. Fitzpatrick,[2*] Sarah Meehan,[3] Helen R. Mott,[4] Michele Vendruscolo,[3] Christopher M. Dobson,[3]† Mark E. Welland[1]†

Protein molecules have the ability to form a rich variety of natural and artificial structures and materials. We show that amyloid fibrils, ordered supramolecular nanostructures that are self-assembled from a wide range of polypeptide molecules, have rigidities varying over four orders of magnitude, and constitute a class of high-performance biomaterials. We elucidate the molecular origin of fibril material properties and show that the major contribution to their rigidity stems from a generic interbackbone hydrogen-bonding network that is modulated by variable side-chain interactions.

Amyloid fibrils are highly organized protein aggregates. They were originally discovered as products of uncontrolled protein misfolding, through their involvement in chronic disorders such as Alzheimer's disease, but are now recognized as a common form of protein structure, in some cases having functional biological roles (*1*–*3*) as bacterial coatings (*1*) or scaffolds for catalytic reactions (*4*). In addition, approaches have recently emerged that exploit the stability and accurate self-assembly (*5*, *6*) of artificial amyloid-like structures for technological applications (*7*, *8*). Amyloid fibrils, in images obtained by electron microscopy or atomic force microscopy (AFM), typically appear as unbranched filaments that are a few nanometers in diameter and up to a micrometer or more in length, and x-ray fiber diffraction studies indicate that they have a common core structure (*9*). This evidence, along with the finding that they can be formed from a range of very different polypeptide sequences, has led to the suggestion that the amyloid configuration is a generic, widely accessible, stable structure of peptides and proteins (*2*, *10*). This situation contrasts with that of the native states of proteins, where structure is strongly dependent on the specific amino acid sequence, and complex environments or careful regulation is frequently required for correct self-assembly into folded structures. This observation therefore raises the question of the nature of the interactions that stabilize the amyloid forms of proteins: a question that lies at the heart of a detailed understanding of both the normal and aberrant roles of proteins in living systems, as well as the use of proteins both in biotechnology and as nanoscale materials.

[1]Nanoscience Centre, University of Cambridge, J. J. Thomson Avenue, Cambridge CB3 0FF, UK. [2]Cavendish Laboratory, University of Cambridge, Madingley Road, Cambridge CB3 0HE, UK. [3]Department of Chemistry, University of Cambridge, Lensfield Road, Cambridge CB2 1EW, UK. [4]Department of Biochemistry, University of Cambridge, Tennis Court Road, Cambridge CB2 1GA, UK.

*These authors contributed equally to this work.
†To whom correspondence should be addressed. E-mail: cmd44@cam.ac.uk (C.M.D.); mew10@cam.ac.uk (M.E.W.)

For this study, we selected representative polypeptide chains with low sequence similarity, different lengths, and diverse native structures, but these chains can all be converted readily into amyloid fibrils (*11*). After deposition onto a mica surface, AFM topographic data were acquired (Fig. 1) for at least 50 individual fibrils of each system, a total of more than 900 fibrils in all, to enable analysis of the decay of tangent correlations along the fibril. Shape fluctuations of filaments, which lead to such a decay as described by theories of semiflexible polymers, accurately reflect the mechanical properties of the structures (*12*–*14*). We use such an analysis (*11*) of the AFM data to measure the bending rigidity (C_B) for all the types of fibrils studied here (Fig. 1).

Analysis of the resulting data reveals that the bending rigidities of the different structures vary over nearly four orders of magnitude. Some fibrils, such as those of α-lactalbumin (Fig. 1, top row; $C_B = 1.4 \times 10^{-28}$ N·m^2), appear to be very flexible, whereas others, such as those formed by the short peptide TTR(105–115) from transthyretin (Fig. 1, bottom row; $C_B = 1.3 \times 10^{-24}$ N·m^2), are extremely stiff. We calculated (*11*) the cross-sectional moments of inertia (I) for each type of fibril from their average heights in the AFM measurements, and a plot (Fig. 2) of I versus C_B reveals the existence of a strong correlation (correlation coefficient = 0.91) between the

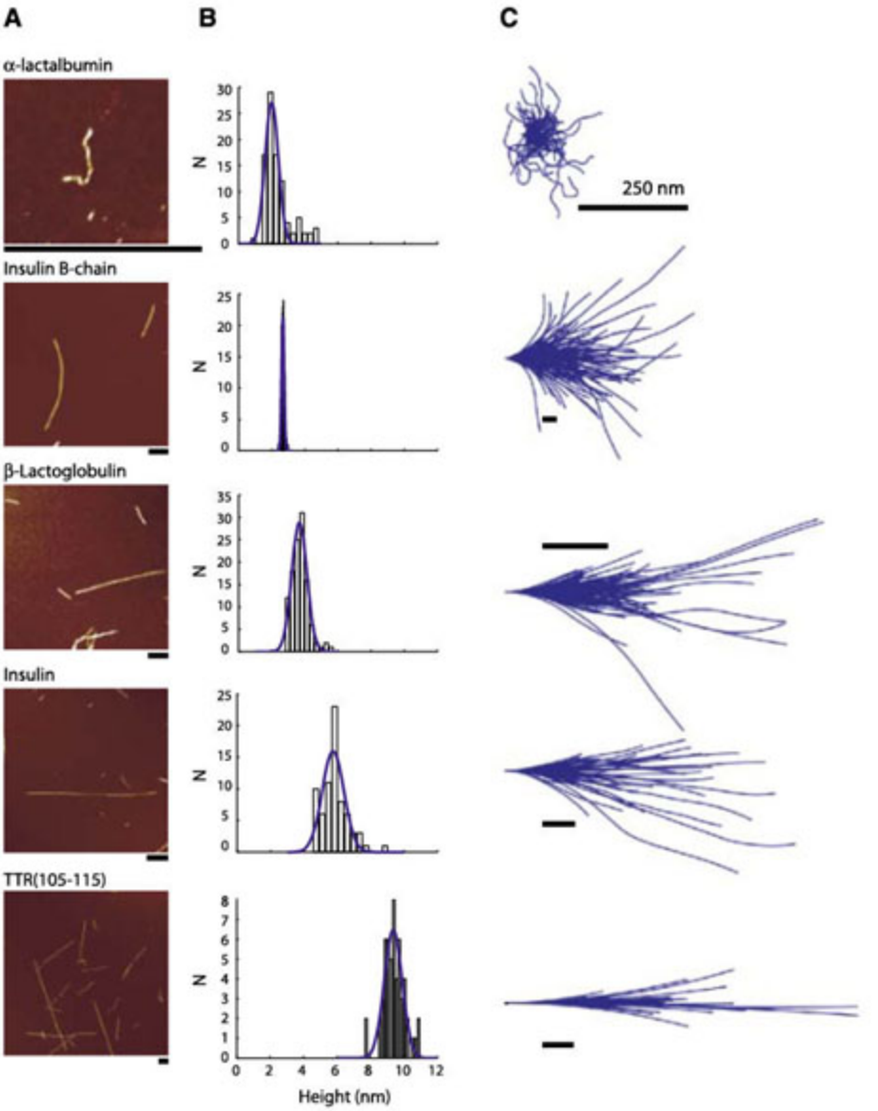

Fig. 1. Variability in the rigidity of amyloid fibrils. Using the AFM topographic data (**A**), we measured the heights (**B**) and the shapes (**C**) of the fibrils (*11*). The initial tangents of the traced fibrils were aligned horizontally in (C) to facilitate visualization.

rigidity and the moment of inertia for eight of the 10 systems that were analyzed (blue squares, Fig. 2). In the AFM images (Fig. 1A and fig. S2), these eight systems have the appearance of highly regular fibrils. The strong correlation reflects an isometric scaling law that, from a material science point of view, implies that the mechanical properties can be described by an elastic modulus $Y = C_B/I$, which is similar (from 2 to 14 GPa) for all these fibrils. By contrast, two systems (i.e., the structures formed by α-lactalbumin and αB-crystallin) appear from AFM images to (i) have an irregular morphology typical of the species, often described as protofibrils, observed before the assembly of mature amyloid fibrils (*15*), and (ii) indeed have substantially lower elastic moduli of 0.14 and 0.4 GPa, respectively (green squares, Fig. 2). These results suggest that the underlying intermolecular interactions stabilizing the eight relatively rigid fibrils are similar to each other but differ substantially from those stabilizing the two protofibrillar structures. In addition, trends emerge within the group of fully formed amyloid fibrils (blue squares, Fig. 2): The short peptide, comprising the B chain of insulin, assembles into fibrils with a higher modulus than that observed for both morphological forms of the full insulin protein or the other larger proteins examined in this work, implying that the additional constraints that are associated with the packaging of longer and sometimes cross-linked polypeptide chains into the cross-β amyloid core might destabilize the resulting structure. Similar trends toward higher moduli are found for the other short peptides examined in this study, namely, the peptide fragments of Sup35 and TTR, as well as the Aβ peptide. In addition, for many longer polypeptide chains, not all of the sequence is incorporated into the amyloid structure; however, the parts outside the fibril core, which in some cases can even retain biological activity (*16*), contribute to the cross-sectional moment of inertia, thereby leading to a lower elastic modulus.

We set out to theoretically predict the stiffness of fully formed amyloid fibrils by examining the structures of a variety of models. These models include a structure for the Aβ(17–42) fragment (*17*) and the WW domain (*18*) from nuclear magnetic resonance measurements and eight structures for short amyloid-forming peptides (*19*–*21*) from microcrystal x-ray diffraction studies. All the structural models examined share a common cross-β core structure composed of a stack of β strands, with each strand oriented perpendicular to the fibril axis (Fig. 3), which is consistent with general x-ray fiber diffraction characteristics of amyloid fibrils (*9*).

The elastic modulus for each of these structures was computed (*22*) by examining the dependence of the total interaction energy $U(\delta_\beta+\varepsilon)$ on the interstrand displacement $\delta_\beta+\varepsilon$ about the equilibrium position δ_β. The modulus of elasticity Y is then given by $Y = l_0 k_{tot}/A$ with a spring constant $k_{tot} = [d^2U/d\varepsilon^2]_{\varepsilon=0}$, where l_0 is the equilibrium length of the structure along the fibril axis, and A is the cross-sectional area. The calculations result in elastic moduli between 13 and 42 GPa for the different structures [Fig. 3, blue square in the main graph (first column from left)], values that are notably consistent with the experimental data for the eight well-defined fibrillar structures [Fig. 3, blue lines in the main graph (second column from left) and inset]. This finding suggests that the measured rigidities for these fibrils are close to the maximal values expected for defect-free structures, which is consistent with the near-crystalline level of structural order previously characterized by AFM (*13*). Such a situation could arise not just through the direct assembly of the fibril but because of the action of a self-healing mechanism, where the presence of structural defects would result in the preferential fracture of the fibril at the defect location, thereby enabling the ordered growth to resume.

The experimentally established correlation (Fig. 2) between the cross-sectional moment of inertia and the bending rigidity of fibrils indicates that the interactions stabilizing different types of fibril are closely similar, a finding that is consistent with the idea that the key elements of all amyloid fibrils are generic (*10*). We further explore the nature of the interactions within amyloid fibrils by decomposing the elastic modulus $Y = Y_{BB}+Y_{SC}$ into contributions from the common polypeptide backbone (Y_{BB}) and the side chains (Y_{SC}). To this effect, we repeated the calculations of the elastic moduli but, during this iteration, omitted the contributions to the total energy of all of the atoms located in the side chains (N_{SC}), leaving the number of atoms located in the backbone (N_{BB}), which varies from one residue to the next. These calculations show that the main-chain interactions contribute about half of the total modulus ($\langle Y_{BB}/Y\rangle = 51\%$) (Fig. 3). The number of atoms in the common backbone is, however, on average much smaller than that in the side chains, and normalizing the moduli Y_{BB} and Y_{SC} with the respective N_{BB} and N_{SC} values reveals that the backbone interactions are on average more than twice ($\langle Y_{BB}/N_{BB}\rangle/\langle Y_{SC}/N_{SC}\rangle = 2.2$) as important as the side-chain interactions in determining the modulus of the fibril, highlighting the importance of the sequence-independent polypeptide backbone for amyloid structures.

The molecular basis for the material properties of the fibrils was then further explored by examining the role of the characteristic arrays of hydrogen bonds connecting the common backbone atoms in the amyloid cross-β structure (Fig. 3). We considered a coarse-grained model in which a fibril is represented as a simple network of hydrogen bonds linking rigid monomers along the long axis of the fibril (Fig. 3, rightmost structure in the bottom row). This type of Gaussian network model (GNM) (*23*) predicts the elastic modulus of the material to be $Y_{GNM} = \delta_\beta\zeta k_H = 17.2 \pm 1.5$ GPa, where the universal intersheet spacing of amyloid fibrils is $\delta_\beta = 4.8$ Å (*9*) and where the hydrogen-bond density in the cross section parallel to the fibril axis is taken to be $\zeta = 1/(10\text{ Å} \times 3.5\text{ Å})$, which originates from an interresidue spacing of 3.5 Å and an intersheet spacing of 10 Å. The single adjustable parameter

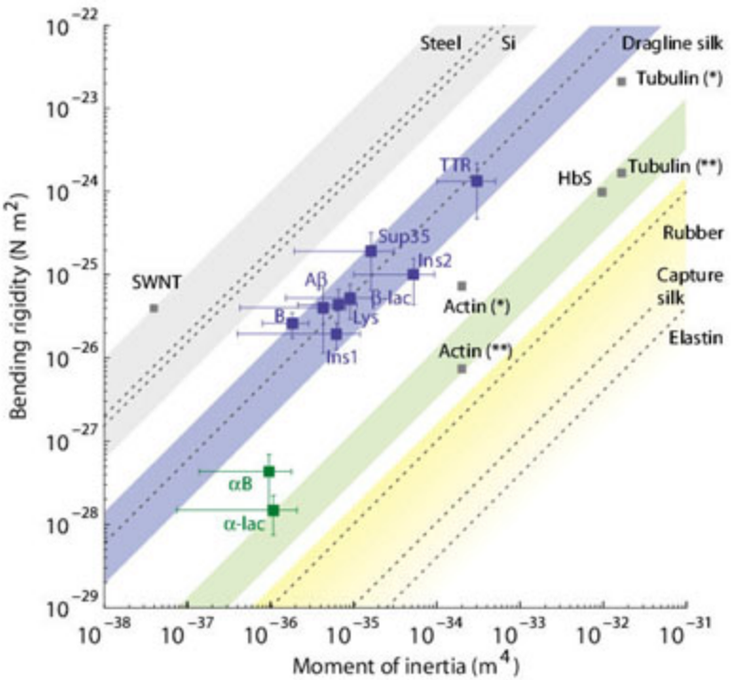

Fig. 2. Comparison among different classes of materials. The gray band shows the range of elastic moduli for covalent and metallic materials (*28*), the blue band shows that of hydrogen-bonded protein nanostructures, the green band encompasses materials held together by amphiphilic interactions (*11*), and the yellow band shows the range resulting from predominantly entropic elasticity. Blue squares show the ranges determined for the bending rigidities of amyloid fibrils as a function of their cross-sectional moments of inertia. From top to bottom: TTR(105–115), TTR; GNNQQNY (*30*) fragment of the yeast prion Sup35, Sup35; insulin 2 filament, Ins 2 [data from (*14*)]; β-lactoglobulin, β-lac; lysozyme, Lys; Aβ(1–42) peptide, Aβ; insulin B chain, B; and insulin single filament, Ins 1 [data from (*13*)]. The blue band encompasses the range of moduli. Green squares show less-organized protofibrillar structures: α-lactalbumin (α-lac) and αB-crystallin (αB). For comparison, values for single-walled carbon nanotubes (SWNT), steel, silicon, dragline silk (*27*), tubulin [tubulin (*) from (*25*) and tubulin (**) from (*26*)], HbS (*12*), actin [actin (*) from (*26*) and actin (**) from (*29*)], rubber, capture silk (*27*), and elastin are shown.

of the model, the hydrogen-bond spring constant k_H, is fixed to 12 to 13 N/m from existing spectroscopic data (*11*). A comparison in Fig. 3 between this coarse-grained value of the elastic modulus and the results (Y_{BB}) from the structural models, calculated for the contribution of just the backbone atoms, reveals that the values are in excellent agreement (on average, within 30% of the constant coarse-grained modulus). This demonstrates that the dominant common backbone interactions stem predominantly from the hydrogen-bonding network that is characteristic of the cross-β structure.

In addition to the fundamental importance of backbone interactions in amyloid materials as demonstrated by our data, the sequence-specific side chains can considerably affect the propensity to form fibrils and the regions of a given polypeptide chain that are more prone to be incorporated into the cross-β core structure. Furthermore, energetically favorable side-chain interactions can additionally stabilize the basic cross-β core structure: These can take the form of hydrophobic interactions (*5*) or inter–side-chain hydrogen bonds (*19*, *20*). Indeed, this type of effect also emerges from our results: All of the structures with computed moduli above 22 GPa belong to systems where large numbers of additional side-chain hydrogen bonds are present. On the other hand, in the case of Aβ (where less than 10% of the side chains are involved in hydrogen bonding), the elastic modulus is found to be lower (17.2 GPa), and the relative importance of backbone hydrogen bonding is greater ($\langle Y_{BB}/Y \rangle$ = 74%). In this light, the role of side-chain interactions within different sequences results in variations on a common theme (*2*, *10*) and is illustrated elegantly in the variety of structures now emerging from x-ray diffraction studies of three-dimensional amyloid-like microcrystals (*19*, *20*).

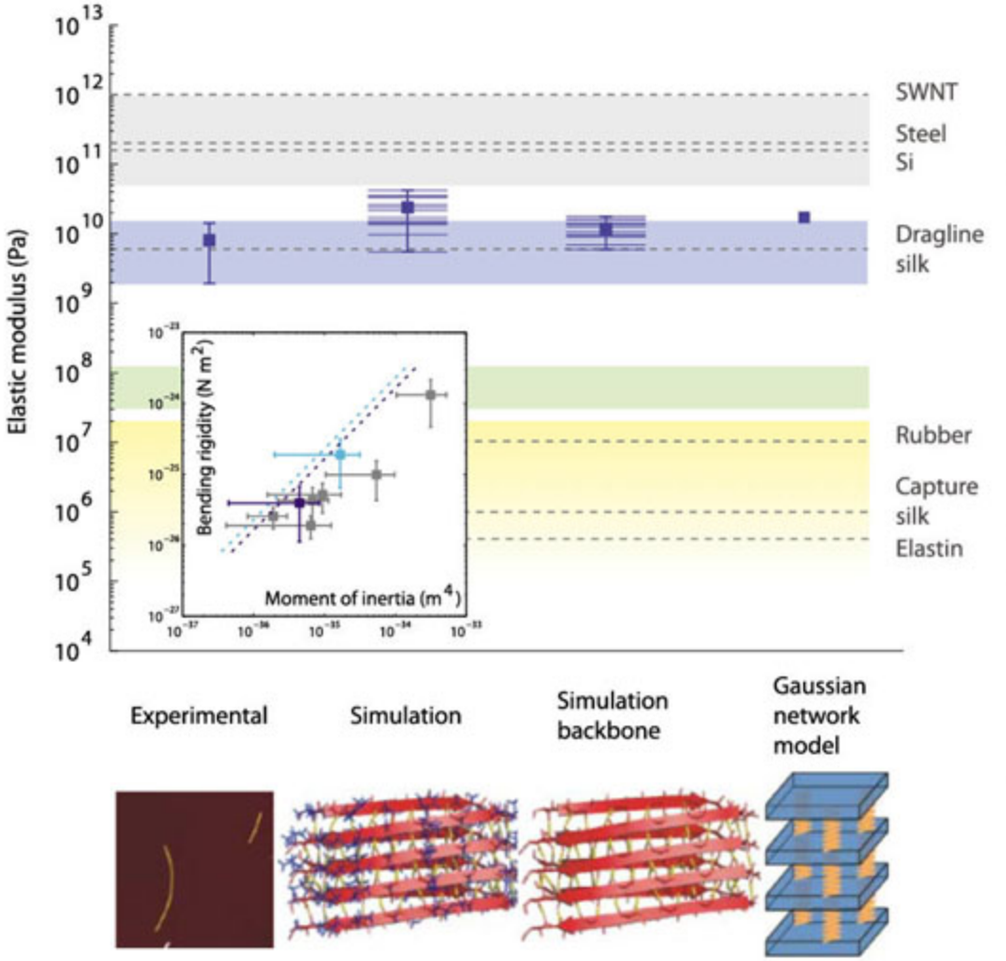

Fig. 3. Comparison of the elastic modulus *Y* of fibrils from (left to right) AFM measurements ("experimental"), full-atom simulations, contribution of backbone alone, and the result from the GNM as described in the text. Full-atom ("simulation") and backbone-only ("simulation backbone") Aβ structures (*17*) are shown with the hydrogen-bonding network in yellow and side chains in blue in the middle panels of the bottom row. The blue lines in the main graph (second column from left) depict atomistic computations of the elastic moduli of structural models (*11*) [from top to bottom: GNNQQNY (Sup35) form 2, GNNQQNY (Sup35) form 1, SNQNNF (prion protein), NNQQNY (Sup35), NNQQ (Sup35) form 2, GNNQQNY filament, NNQQ (Sup35) form 1, Aβ (Amyloid β), VQIVYK (τ protein), SSTSAA (ribonuclease), WW domain, RAD16II (*24*) maximum, and RAD16II minimum]. The blue lines in the main graph (third column from left) depict backbone moduli [from top to bottom: GNNQQNY form 2, SNQNNF, GNNQQNY form 1, VQIVYK, NNQQNY, Aβ, GNNQQNY filament, NNQQ form 2, SSTSAA, WW domain, and NNQQ form 1]. Inset compares measured moduli (squares) with calculations for GNNQQNY filament (light blue dashed line) and Aβ (dark blue dashed line). Other fibril measurements, for which there are no available structures, are shown in gray.

The contributions to the material properties of protein assemblies from intermolecular interactions that are mediated by the variable side chains in the absence of a rigid framework provided by intermolecular hydrogen bonding can be estimated from a coarse-grained model based on the surface tension γ resulting from hydrophilic and hydrophobic side chains in the fibril. This model has previously been discussed in the context of lipid layers and protein filaments (*24*) and predicts, for the case of amyloid fibrils (*11*), a modulus of $Y_{amph} = 2\ \gamma/h$ (*24*), where h = 8 to 12 Å is taken to be the intersheet spacing. The expected range for γ spans from 20×10^{-3} to 50×10^{-3} J/m^2, resulting in a modulus in the range Y_{amph} = 0.03 to 0.13 GPa. This range is shown as a green band in Figs. 2 and 3 and is between one and two orders of magnitude below the experimental and calculated values for amyloid fibrils, highlighting the importance of the intermolecular nature of the hydrogen-bonding interactions in stabilizing these structures. Therefore, the fundamental forces present in proteins allow structures, which have characteristics of soft materials [with monomers linked together mainly by amphiphilic intermolecular interactions (green band, Figs. 2 and 3)] or hard materials [consisting of regular hydrogen-bonding networks that connect the individual molecules together (blue band, Figs. 2 and 3)], to be built up.

The present measurements enable comparisons to be made between the material properties of amyloid fibrils and those of other structures of biological origin or indeed of synthetic polymers or inorganic materials including metals and covalent materials (Fig. 2), showing that amyloid fibrils are stiffer than most functional intracellular biological filaments. The polymerization of species such as tubulin and actin, however, is readily reversible and can be highly regulated, which are essential aspects of their role in defining the motility of cells; it is therefore likely that some long-range mechanical rigidity has been sacrificed in return for other characteristics essential for their biological role.

The two examples of studied fibrils (α-lactalbumin and αB-crystallin) with less regular structures than those discussed above have elastic moduli similar to those of natural assemblies found within cells, such as tubulin and actin (*25*, *26*), or fibrillar aggregates of native-like structures, such as sickle-cell hemoglobin (HbS) fibrils (*12*). This finding suggests that these structures are held together by relatively weak intermolecular forces, and indeed their modulus is consistent with the coarse-grained model discussed above for amphiphilic interactions (green band, Figs. 2 and 3). The fact that the intermolecular interactions stabilizing beadlike protofibrillar aggregates are relatively weak as compared with those in mature fibrils

could be an important factor in their association with some neurodegenerative diseases (*15*) and might allow their dissociation into oligomers, which can interact with cellular components. The differences between the moduli of mature amyloid fibrils and HbS fibrils further highlight the different balance of inter- versus intramolecular interactions. Thus, in both cases, a sizable fraction of residues participates in hydrogen bonds: within α helices for HbS and within β sheets for amyloid fibrils. However, for HbS fibrils, these bonds are all within one individual molecule, and the intermolecular interactions are mediated by weaker surface interactions; on the other hand, for amyloid fibrils, some or all of the hydrogen bonds are intermolecular when they can contribute to the long-range stability of the fibril and the high elastic modulus. These conclusions are exemplified by the orb-weaving spider's use of two forms of silk. Dragline silk, which contains a high fraction of densely hydrogen-bonded domains, is used to provide the structural scaffold for the web (*27*) and has an elastic modulus that is comparable to hydrogen-bonded cross-β protein nanofibrils (Fig. 2). On the other hand, web capture silk, which serves for arresting prey, is a viscid biofilament containing cross-linked polymer networks and has an elastic modulus that is comparable to that of elastomers such as rubber and elastin (*27*).

The finding that the rigidity of amyloid fibrils is described by a common elastic modulus, defined predominantly by intermolecular interactions involving the common polypeptide main chain, provides quantitative evidence for the idea (*2*) that these structures form a generic class of material. In addition, our results provide insight into the changes in the distribution of inter- versus intramolecular bonding interactions associated with the transition of proteins from their native globular structures into polymeric supramolecular assemblies. Finally, comparisons between artificial self-assembling protein fibrils and natural cellular structures exemplify the design criteria used in nature to select materials for structural applications and provide inspiration for the design of novel nanoscale biomaterials.

References and Notes

1. D. M. Fowler, A. V. Koulov, W. E. Balch, J. W. Kelly, *Trends Biochem. Sci.* **32**, 217 (2007).
2. F. Chiti, C. M. Dobson, *Annu. Rev. Biochem.* **75**, 333 (2006).
3. M. Tanaka, S. R. Collins, B. H. Toyama, J. S. Weissman, *Nature* **442**, 585 (2006).
4. D. M. Fowler *et al.*, *PLoS Biol.* **4**, e6 (2005).
5. S. Zhang, *Nat. Biotechnol.* **21**, 1171 (2003).
6. S. Zhang, T. Holmes, C. Lockshin, A. Rich, *Proc. Natl. Acad. Sci. U.S.A.* **90**, 3334 (1993).
7. F. Gelain, D. Bottai, A. Vescovi, S. Zhang, *PLoS ONE* **1**, e119 (2006).
8. T. Scheibel *et al.*, *Proc. Natl. Acad. Sci. U.S.A.* **100**, 4527 (2003).
9. M. Sunde *et al.*, *J. Mol. Biol.* **273**, 729 (1997).
10. C. M. Dobson, *Trends Biochem. Sci.* **24**, 329 (1999).
11. Materials and methods are available as supporting material on *Science* Online.
12. J. C. Wang *et al.*, *J. Mol. Biol.* **315**, 601 (2002).
13. T. P. J. Knowles, J. F. Smith, A. Craig, C. M. Dobson, M. E. Welland, *Phys. Rev. Lett.* **96**, 238301 (2006).
14. J. F. Smith, T. P. J. Knowles, C. M. Dobson, C. E. Macphee, M. E. Welland, *Proc. Natl. Acad. Sci. U.S.A.* **103**, 15806 (2006).
15. P. T. Lansbury, H. A. Lashuel, *Nature* **443**, 774 (2006).
16. S. Sambashivan, Y. Liu, M. R. Sawaya, M. Gingery, D. Eisenberg, *Nature* **437**, 266 (2005).
17. T. Lührs *et al.*, *Proc. Natl. Acad. Sci. U.S.A.* **102**, 17342 (2005).
18. N. Ferguson *et al.*, *Proc. Natl. Acad. Sci. U.S.A.* **103**, 16248 (2006).
19. M. R. Sawaya *et al.*, *Nature* **447**, 453 (2007).
20. R. Nelson *et al.*, *Nature* **435**, 773 (2005).
21. L. Esposito, C. Pedone, L. Vitagliano, *Proc. Natl. Acad. Sci. U.S.A.* **103**, 11533 (2006).
22. R. J. Hawkins, T. C. B. McLeish, *Phys. Rev. Lett.* **93**, 098104 (2004).
23. T. Halilioglu, I. Bahar, B. Erman, *Phys. Rev. Lett.* **79**, 3090 (1997).
24. J. Park, B. Kahng, R. D. Kamm, W. Hwang, *Biophys. J.* **90**, 2510 (2006).
25. A. Kis *et al.*, *Phys. Rev. Lett.* **89**, 248101 (2002).
26. F. Gittes, B. Mickey, J. Nettleton, J. Howard, *J. Cell Biol.* **120**, 923 (1993).
27. F. Vollrath, D. Porter, *Soft Matter* **2**, 377 (2006).
28. M. F. Ashby, D. R. H. Jones, *Engineering Materials: An Introduction to Their Properties and Applications* (Pergamon, Oxford, ed. 1, 1980).
29. J. Käs, H. Strey, E. Sackmann, *Nature* **368**, 226 (1994).
30. Single-letter abbreviations for the amino acid residues are as follows: A, Ala; C, Cys; D, Asp; E, Glu; F, Phe; G, Gly; H, His; I, Ile; K, Lys; L, Leu; M, Met; N, Asn; P, Pro; Q, Gln; R, Arg; S, Ser; T, Thr; V, Val; W, Trp; and Y, Tyr.

31. We acknowledge helpful discussions with E. Terentjev, R. Hawkins, S. Rogers, and J. Smith, as well as financial support from the Engineering and Physical Sciences Research Council and the Interdisciplinary Research Collaboration in Nanotechnology. We thank S. Shammas, A. Brorsson, and G. Devlin for preparing the Aβ and TTR fibrils, and A. Tickler for synthesizing the TTR peptide. The work of C.M.D is supported, in part, by Programme Grants from the Wellcome Trust and the Leverhulme Trust.

Supporting Online Material

www.sciencemag.org/cgi/content/full/318/5858/1900/DC1
Materials and Methods
Figs. S1 and S2
References

4 September 2007; accepted 9 November 2007
10.1126/science.1150057

A Sulfur Dioxide Climate Feedback on Early Mars

Itay Halevy,[1]* Maria T. Zuber,[2] Daniel P. Schrag[1]

Ancient Mars had liquid water on its surface and a CO_2-rich atmosphere. Despite the implication that massive carbonate deposits should have formed, these have not been detected. On the basis of fundamental chemical and physical principles, we propose that climatic conditions enabling the existence of liquid water were maintained by appreciable atmospheric concentrations of volcanically degassed SO_2 and H_2S. The geochemistry resulting from equilibration of this atmosphere with the hydrological cycle is shown to inhibit the formation of carbonates. We propose an early martian climate feedback involving SO_2, much like that maintained by CO_2 on Earth.

Martian geomorphology indicates the existence of liquid surface water, perhaps even an ocean (*1*), during the late Noachian epoch [~3.8×10^9 years ago (*2*)], when surface temperatures were marginally above freezing (*3*) but still considerably warmer than at present. The element conditions are most likely explained by an optically thicker atmospheric greenhouse (*4*) that may also have had to compensate for a dimmer sun (*5*). A CO_2-rich atmosphere could have been supplied by vigorous volcanism associated with the emplacement of the Tharsis igneous province (*6*) as well as with earlier episodes of crustal formation. Although attempts at explaining the existence of liquid water with an atmosphere of pure CO_2 are complicated by CO_2 condensation (*7*), the possible existence of infrared-reflective CO_2 ice clouds (*8*) or atmospheric heating due to absorption of solar radiation by trace amounts of SO_2 (*9*) has been suggested to resolve this difficulty.

If early volcanic activity on Mars did sustain a thick CO_2 atmosphere, one might expect the existence of a carbon cycle similar to Earth's, where the release of CO_2 from volcanoes is balanced by burial of calcium carbonate through silicate weathering reactions that remove protons and release alkalinity to seawater (*10*). The dependence of silicate weathering on temperature and precipitation creates a negative feedback on the atmospheric abundance of CO_2, stabilizing the climate to maintain surface conditions with adequate liquid water for weathering as long as the volcanic release of CO_2 continues. Existence of such a carbon cycle on Mars would have left carbonate sediments at the surface as well as abundant clays left over from the weathering process. For example, a carbon outgassing flux of 7×10^{12} mol C $year^{-1}$, about the same as the modern volcanic outgassing rate on Earth (*11*), maintained for 10^8 years would result in a global carbonate layer ~180 m thick. The same mass of carbonate precipitated in an ocean covering 30% of Mars (*1*) would form a layer ~600 m thick.

[1]Department of Earth and Planetary Sciences, Harvard University, Cambridge, MA 02138, USA. [2]Department of Earth, Atmospheric, and Planetary Sciences, Massachusetts Institute of Technology, Cambridge, MA 02139, USA.

*To whom correspondence should be addressed. E-mail: ihalevy@fas.harvard.edu

The virtual absence of carbonate minerals above the detection limit of a few weight percent (*12*), coincident with evidence for an early climate warm enough for liquid water, is therefore puzzling.

A possible resolution of this contradiction may involve the abundance of sulfur on the surface of Mars. Martian soil and rock analyses show significant enrichment in sulfur relative to terrestrial soils (*13*); recent analysis of data obtained by the rovers identified soils with sulfur contents as high as 7.5 weight % SO_3 (*14*). Like carbon, sulfur in some forms can play an important role in radiative forcing and in silicate weathering. In this paper, we explore the implications of an active sulfur cycle, linked to the carbon cycle, on the climate and surface chemistry of early Mars.

In an early martian sulfur cycle, volcanic outgassing of sulfur to the atmosphere and surface environment, primarily as SO_2 and H_2S, would be balanced by photochemical sinks and precipitation of sulfur-bearing minerals. The modern martian atmosphere is relatively oxidized after billions of years of hydrogen escape (*15*), although earlier in martian history oxygen escape (*16*) as well as emission of reduced gases from hydrothermal alteration of basaltic crust (*17*) likely resulted in a more reducing atmosphere. During the emplacement of Tharsis as with any period of high, sustained volcanism, the additional emission of reduced gases, including H_2S and SO_2, would drive the oxidation state even lower. The lifetime of sulfur species that today are rapidly oxidized in Earth's atmosphere is longer under such conditions. In the absence of biological catalysis, kinetic barriers to changes in the valence state of sulfur would enable the coexistence of atmospheric and aquatic sulfide (S^{2-}), sulfite (S^{4+}), and sulfate (S^{6+}) in proportions depending on the relative magnitudes of their sources and sinks.

In an atmosphere with significant quantities of reduced sulfur gases, SO_2 would play a particularly important role, not only climatically as a powerful greenhouse gas but also in the chemistry of the surface environment. SO_2 is highly soluble in water, so its early martian geochemical cycle would have been dominated by aquatic reservoirs, such as a northern hemisphere ocean (*1*) or regions of sustained groundwater upwelling (*18*). The presence of even a small amount of SO_2 in a CO_2-rich atmosphere lowers the pH of surface waters, suppressing carbonate precipitation in favor of sulfite minerals. The resulting geochemical cycle is analogous to the terrestrial carbon cycle (*10*), with a silicate weathering feedback on climate involving SO_2 instead of CO_2 and the pH of water bodies buffered by the solubility of sulfite minerals and the partial pressure of SO_2 instead of the solubility of calcite and the partial pressure of CO_2.

Details of this geochemical cycle depend on relative rates of sulfur outgassing, photochemical transformations, silicate weathering, and mineral precipitation. Sulfur outgassing from Tharsis is limited by the solubility of sulfur in basaltic melts. The sulfur content of martian melts has recently been estimated at 1400 parts per million (ppm) (*19*), one to three times the concentration in Hawaiian lavas (*20*). Degassing of the entire volume of Tharsis magma [3×10^8 km^3 (*6*)] implies a maximum flux of ~4×10^{11} mole S $year^{-1}$ if the emplacement of Tharsis took 10^8 years. This is about twice the present sulfur outgassing flux on Earth [~13×10^6 metric tons SO_2 $year^{-1}$ (*21*)], although its impact on the surface of Mars would have been much greater given the smaller volume of the atmosphere. Because the speciation of sulfur coming from volcanic outgassing depends on the oxygen fugacity of the magma, the oxidation state of martian basalts (*22*) implies that at least 50% of the sulfur, or ~2×10^{11} mole S $year^{-1}$, was emitted as H_2S (*23*).

Removal of SO_2 from the atmosphere normally occurs by gas-phase oxidation, by reaction pathways after photolysis, and by a variety of physical sinks leading to deposition and subsequent oxidation. The reducing power from volcanic fluxes of H_2S and SO_2 described above, combined with hydrothermal emission of hydrogen and methane, would compensate for even the most optimistic estimates of hydrogen escape [summarized in (*16*)], implying decreased gas-phase oxidation of SO_2 (*24*). Furthermore, deposition of SO_2, typically followed by rapid heterogeneous oxidation, would instead lead to saturation of the martian surface and return fluxes to the atmosphere at steady state (*25*). Aqueous disproportionation of sulfite could potentially prevent saturation of the aquatic reservoir with species of S^{4+} (*26*). However, the rates of these reactions in the absence of biological catalysis have only been examined above 100°C (*27*) and are likely slow at low temperature [Supporting Online Material (SOM) text].

It has been suggested that reaction of the products of SO_2 photolysis with atmospheric oxidants recycles SO_2, resulting in little net loss (*28*). However, a low abundance of oxidants limits these reactions as well, introducing another potentially important sink: SO_2 photolysis followed by disproportionation to sulfate and elemental sulfur (*29*). This sink was likely also of low magnitude under early martian conditions, because a higher ultraviolet flux attributed to the young Sun (*30*) would have occurred in wavelengths where absorption and Rayleigh scattering by a thick CO_2 atmosphere afforded significant shielding (*31*). Moreover, absorption by the abundance of sulfur volatiles, including S_8 possibly generated by SO_2 photochemistry (*25*), would have further attenuated the energy available for SO_2 photodissociation (fig. S1). Wong *et al.* (2003) (*32*) simulated the local atmospheric chemical impact of a volcanic event on the present oxidizing martian atmosphere, calculating a mixing ratio of more than 100 ppm SO_2 in the lower 60 km of the atmosphere and a very low photolysis rate constant of 6.1×10^{-18} s^{-1} at an altitude of 10 km. During the emplacement of Tharsis, a volcanic flux several orders of magnitude higher, sustained over hundreds of millions of years, means that the photolysis sink was unlikely to be of primary importance.

Accumulation of 10^{-6} to 10^{-4} bars of SO_2 in a CO_2-rich atmosphere, made possible by its small total photochemical sink and by saturation of the surface, would have had a substantial radiative effect (*33*), perhaps enough to have maintained liquid water on the surface of early Mars. Under such conditions, temperature and precipitation are much more sensitive to changes in the partial pressure of SO_2 (pSO_2) than to changes in the

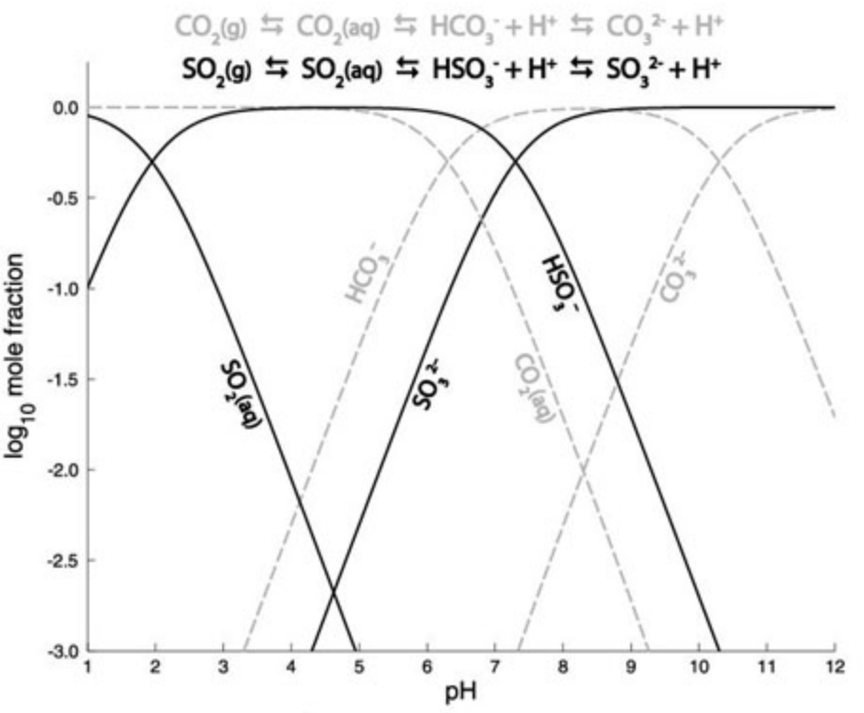

Fig. 1. pH dependence of aqueous S^{4+} (black) and C (gray) speciation, expressed by the chemical equilibrium reactions in the figure. At pH between 2 and 6, most of the S^{4+} is present as HSO_3^- (bisulfite), whereas carbon is predominantly in the form of CO_2 (aq).

partial pressure of CO_2 (pCO_2), mainly because of the large difference between the atmospheric abundances of SO_2 and CO_2 but also because of saturation of the infrared absorption lines of CO_2. Additionally, because of the high solubility of SO_2, most of the S^{4+} would have been present in the aquatic reservoir and would have had a dominant role in the surface environment. Because hydration of SO_2 forms sulfurous acid (H_2CO_3) (H_2SO_3), which is much stronger than carbonic acid (*34*), the pH of water in equilibrium with CO_2 and SO_2 is essentially independent of pCO_2 when $pSO_2 > \sim 1 \times 10^{-5}$ bars (fig. S2). With climate and the pH of rainwater controlled predominantly by the atmospheric abundance of SO_2, the rate of silicate weathering in the system we describe would have also responded mainly to changes in pSO_2.

Cations released by silicate weathering reactions, electrochemically balanced by bisulfite (HSO_3^-) and bicarbonate (HCO_3^-) anions, are delivered by streams to larger water bodies, eventually resulting in precipitation of salts. Like carbon, the aqueous speciation of S^{4+} depends on pH (Fig. 1). Because H_2SO_3 is a stronger acid, at low pH the concentration of the sulfite (SO_3^{2-}) anion can be orders of magnitude higher than that of carbonate (CO_3^{2-}), depending on the ratio of pSO_2 to pCO_2. Thermodynamic equilibrium predicts that, for $pSO_2/pCO_2 \geq \sim 5.0 \times 10^{-8}$, hannebachite ($CaSO_3 \cdot \frac{1}{2}H_2O$) reaches saturation at a lower concentration of Ca^{2+} than calcite ($CaCO_3$). Precipitation of hannebachite then limits the availability of Ca^{2+}, suppressing calcite precipitation (Fig. 2) (*35*). A similar limitation of Mg^{2+} availability by $MgSO_3 \cdot 6H_2O$ precipitation occurs at $pSO_2/pCO_2 \geq \sim 1.2 \times 10^{-4}$, preventing the precipitation of magnesite ($MgCO_3$). The actual precipitate may be a mixed Ca-Mg sulfite analogous to dolomite, suppressing magnesite precipitation at an even lower ratio of SO_2 to CO_2. No geologically feasible conditions lead to precipitation of ferrous sulfite instead of highly insoluble siderite ($FeCO_3$). However, formation of iron-bearing clays as products of basalt alteration (*36*) as well as precipitation of pyrite (FeS_2) could limit the availability of Fe^{2+}, making siderite a minor phase and perhaps preventing its precipitation altogether. We propose that, in an atmosphere rich in SO_2, carbonates of iron, magnesium, and calcium rarely form; it is then unnecessary to explain their absence by burial (*37*), photodisintegration (*38*), dissolution (*39*), or destruction via reaction with atmospheric SO_2 (*13*). Unlike some of the mechanisms proposed to explain the absence of carbonates (*40*), suppression of carbonate precipitation by this mechanism occurs even at mildly acidic pH (~6), allowing the formation of clays and consistent with their detection on the ancient martian surface (*41*).

Without biologically mediated oxidation and reduction of sulfur, cycles of S^{6+} and S^{2-} would exist alongside the geochemical cycle of S^{4+}. Even in a reducing atmosphere, some sulfate would be produced by SO_2 disproportionation during photochemical reactions. Like acid rain on Earth, this flux of H_2SO_4 could slightly depress rainwater pH. However, the pH of water bodies, including a martian ocean, would be buffered by pSO_2 and sulfite mineral solubility, just as the pH of the surface ocean on Earth is controlled by pCO_2 and calcite solubility. The main impact of H_2S on the aqueous chemistry of a mildly acidic water reservoir containing iron is the possible contribution of pyrite to the mineral assemblage.

The dependence of weathering rates on atmospheric SO_2 and the precipitation of sulfite minerals as a sink for SO_2 create a climate feedback analogous to that involving CO_2 on Earth; if the volcanic supply of SO_2 increases, causing atmospheric pSO_2 to rise, then temperature increases, causing an acceleration of weathering reactions and removal of SO_2 by precipitation of sulfite minerals, until these balance the increased volcanic supply. Furthermore, the vast reservoir of dissolved S^{4+} in the surface aquatic system serves as a buffer to the atmospheric abundance of SO_2 and would thus stabilize surface temperatures. Relative to the carbonic acid weathering of granitic crust on Earth, the sulfurous acid–driven feedback on the basaltic crust of Mars would be more sensitive to changes in temperature. As a result, the temperature required to

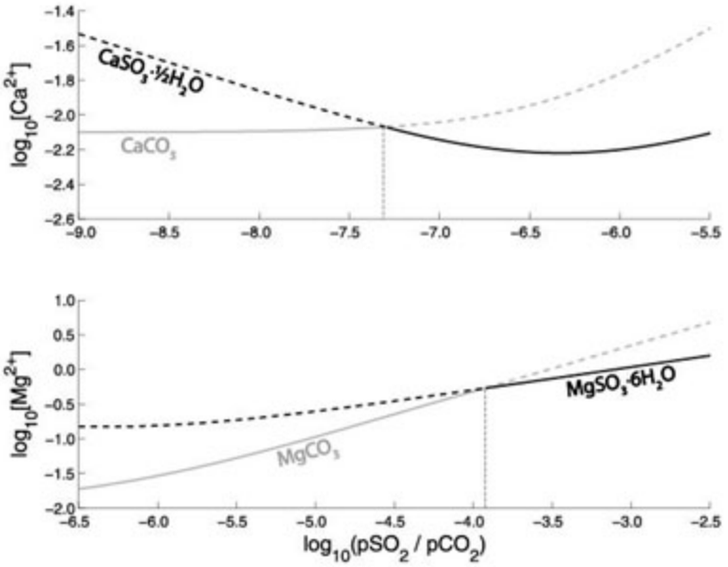

Fig. 2. Cation concentration limits imposed by sulfite (black) or carbonate (gray) mineral saturation as a function of pSO_2/pCO_2. (**Top**) Ca mineral saturation and (**bottom**) Mg mineral saturation. The curves are solid in the range of pSO_2/pCO_2 in which precipitation of the represented mineral is the limiting factor on cation concentrations. Thin dashed lines mark the critical value of pSO_2/pCO_2 above which concentrations are limited by saturation of sulfite rather than carbonate minerals.

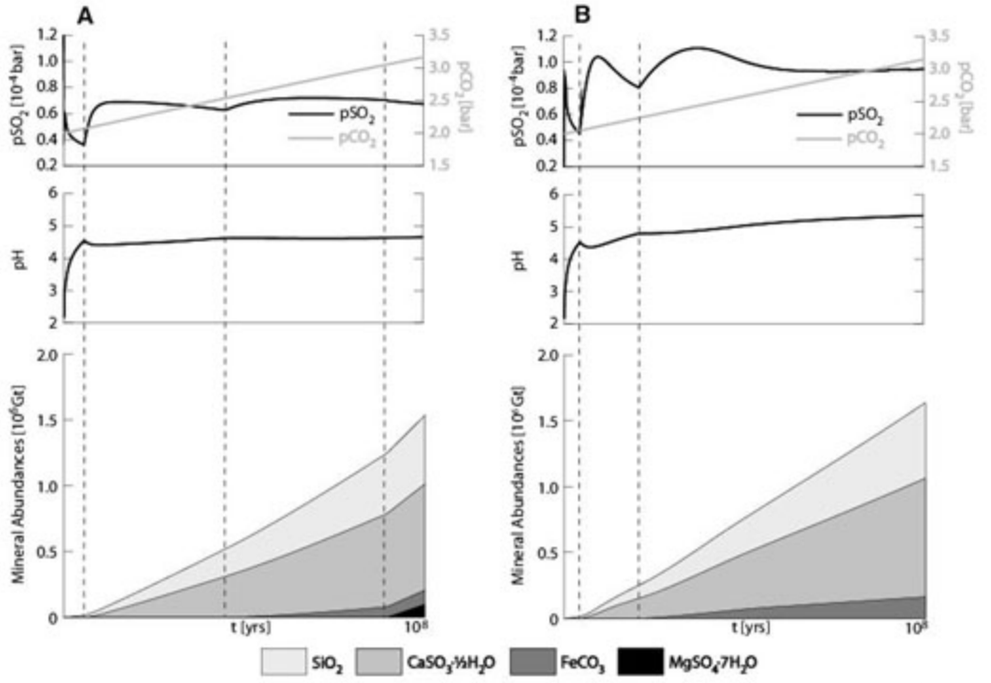

Fig. 3. Time (t) evolution of pSO_2, pCO_2 (top), surface water pH (middle), and the precipitated mineral assemblage (bottom), for (**A**) 70% and (**B**) 20% photochemical destruction of all SO_2 outgassed or produced. The volcanic outgassing rate during this simulation was 2×10^{11} mole year^{-1} SO_2 and H_2S, each. Note that the onset of calcium sulfite and ferrous carbonate precipitation (vertical dashed lines) is accompanied by a decrease in pH because of removal of alkalinity and an increase in pSO_2 because of water body acidification.

balance SO_2 outgassing would be relatively low, perhaps just above the temperature necessary to sustain liquid water. This result is consistent with geochemical evidence that Mars in the late Noachian was likely never very warm (*3*).

To explore this feedback cycle, we constructed a model of the sulfur and carbon cycles of early Mars, including an ocean covering ~30% of the planet, an area about equivalent to the area covered by the Vastitas Borealis Formation, inferred to be of aqueous sedimentary origin (*1*). The model tracks the evolution of the surface (*42*) reservoirs of carbon, the sulfur in its different valence states, and the dissolved reservoirs of weathering-derived cations and SiO_2. Carbon is supplied by volcanic emission of CO_2 and removed by carbonate mineral precipitation. SO_2 (S^{4+}) and H_2S (S^{2-}) are also volcanically outgassed and are removed from the surface reservoir by either mineral precipitation or photochemical transformations, leading to formation and deposition of elemental sulfur (S^0) or sulfate (S^{6+}). Cations are supplied to the ocean by silicate weathering, a function of pCO_2, pSO_2, and the photochemical production of H_2SO_4. Minerals may precipitate if concentrations of their dissolved components exceed experimentally determined degrees of supersaturation. Aqueous disproportionation of sulfite was not considered in the model because of its sluggish kinetics at low temperature. Further model details are in the SOM text.

Simulated pSO_2, pH, and precipitated mineral assemblage depend on the relative importances of the sinks of SO_2, as summarized in Fig. 3. Figure 3A shows the time evolution of the system with the photochemical sink removing 70% of all SO_2 outgassed or produced by H_2S oxidation, whereas Fig. 3B is for 20% photochemical removal of SO_2. Atmospheric pSO_2, shown in the top graphs, is lower when the photochemical sink is important. This is due to the smaller overall size of the S^{4+} reservoir and despite water body acidification, which has the effect of increasing the vapor pressure of SO_2 for a given reservoir size. Water body pH, shown in the middle graphs, is lower when photochemical production of H_2SO_4 is sufficiently rapid, despite the decrease in pSO_2. Lastly, at higher relative photochemical destruction (sulfate production) rates, the mineral assemblage contains less siderite and a greater mole fraction of sulfate minerals, at the expense of sulfites, as shown in the bottom graphs. In all of our simulations, pCO_2 rises because of the negligible precipitation of siderite. If precipitation of pyrite occurs, siderite may be altogether absent from the mineral assemblage (fig. S3). Sulfate minerals and Mg^{2+}-bearing minerals (whether sulfates or sulfites) are last to precipitate, leaving the aquatic reservoir relatively rich in Mg^{2+} and SO_4^{2-}. This has implications for the mineral assemblage that forms when such water bodies freeze or evaporate and is consistent with the observation that hydrated magnesium sulfate is an important phase on the surface of Mars (*43*). Our computations show that the pH and the concentrations of major rock-forming cations in large water bodies can be controlled by equilibrium with SO_2 and saturation of sulfite minerals, resulting in suppression of carbonate mineral precipitation.

Application of our hypothesis to martian history yields the following sequence of events: Volcanic outgassing of CO_2, SO_2, and H_2S during the Noachian exhausted the oxidant supply, allowing SO_2 to reach concentrations of a few ppm to several hundred ppm near the planet's surface. The partial pressure of CO_2 increased gradually until it reached a critical level, perhaps during the period of most-rapid emplacement of Tharsis, when the combined radiative effect of CO_2 and SO_2 enabled the existence of liquid surface water. The SO_2 climate feedback described above stabilized surface temperature, with precipitation of sulfite minerals from mildly acidic surface solutions preventing massive carbonate precipitation while allowing the formation of clays.

When volcanism subsided, SO_2 was rapidly removed from the atmosphere by continued photolysis and by reaction with oxidants, now supplied at a faster rate than reduced gases. Without the radiative contribution of SO_2, the surface temperature dropped below the freezing point of water, surface water bodies froze, becoming more concentrated and precipitating the remaining ions in a progression of increasingly soluble salts. Water frozen at the surface was gradually redistributed by sublimation and refreezing because of seasonal cycling and changes in obliquity (*44*).

Under a now-oxidizing atmosphere, sulfite minerals at the surface would be episodically exposed to small amounts of surface or ground water and altered to sulfate, releasing acidity that would be stored in the soil. This oxidation of sulfites, in combination with oxidation of siderite and pyrite, is one possible way of creating the acidic environments proposed for later periods in martian history (*45*, *46*) as well as the observed surface mineralogy. If the high volcanic flux persisted for 10^8 years accompanied by precipitation of sulfite minerals, elemental sulfur, and perhaps sulfides, then the supply of oxidants associated with hydrogen escape (*16*) would require about a billion years to transform all of the precipitates to sulfate. A shorter duration of clement conditions would imply a shorter oxidation time scale.

Despite subfreezing surface temperatures, the early geothermal gradient of Mars was high enough to maintain hydrothermal circulation in the crust (*47*). Subsurface silicate weathering coupled with carbonate mineral precipitation in crustal pores and fractures would have slowly removed the remaining atmospheric CO_2, consistent with the carbonate minerals found in veins in some martian meteorites (*48*). Estimates of martian crustal porosity (*49*) easily accommodate several bars of CO_2, sequestered in carbonate minerals. Three billion years of this process, in combination with atmospheric loss associated with large impacts and more efficient molecular escape after termination of the magnetic field of Mars, resulted in the present thin CO_2 atmosphere.

Our hypothesis for a SO_2 climate feedback successfully accounts for salient features observed on the surface of Mars and in the martian meteorites (*13*, *14*, *41*, *48*, *50*). Validation of our hypothesis would come from detection of sulfites on the martian surface, although the exclusion of sulfites from spectral libraries used for mineral detection on Mars, along with their tendency to oxidize, might make such detection difficult. Our hypothesis should apply to any planet with a reducing atmosphere and volcanically outgassed SO_2 and may also explain the apparent scarcity of carbonate sediments in the Archean Earth (*51*).

References and Notes

1. M. H. Carr, J. W. Head, *J. Geophys. Res.* **108**, 5042 (2003).
2. G. Neukum, B. A. Ivanov, W. K. Hartmann, *Space Sci. Rev.* **96**, 55 (2001).
3. D. L. Shuster, B. P. Weiss, *Science* **309**, 594 (2005).
4. J. B. Pollack, *Icarus* **91**, 173 (1991).
5. M. J. Newman, R. T. Rood, *Science* **198**, 1035 (1977).
6. R. J. Phillips *et al.*, *Science* **291**, 2587 (2001); published online 15 March 2001 (10.1126/science.1058701).
7. J. F. Kasting, *Icarus* **94**, 1 (1991).
8. F. Forget, R. T. Pierrehumbert, *Science* **278**, 1273 (1997).
9. Y. L. Yung, H. Nair, M. F. Gerstell, *Icarus* **130**, 222 (1997).
10. J. C. G. Walker, P. B. Hays, J. F. Kasting, *J. Geophys. Res.* **86**, 9776 (1981).
11. N. A. Morner, G. Etiope, *Global Planet. Change* **33**, 185 (2002).
12. P. R. Christensen *et al.*, *J. Geophys. Res.* **106**, 23823 (2001).
13. B. C. Clark *et al.*, *Science* **194**, 1283 (1976).
14. A. S. Yen *et al.*, *Nature* **436**, 881 (2005).
15. E. V. Ballou, P. C. Wood, T. Wydeven, M. E. Lehwalt, R. E. Mack, *Nature* **271**, 644 (1978).
16. H. Lammer *et al.*, *Icarus* **165**, 9 (2003).
17. J. Horita, M. E. Berndt, *Science* **285**, 1055 (1999).
18. J. C. Andrews-Hanna, R. J. Phillips, M. T. Zuber, *Nature* **446**, 163 (2007).
19. S. S. Johnson, M. T. Zuber, T. L. Grove, M. A. Mischna, in *Workshop on Martian Sulfates as Recorders of Atmospheric-Fluid-Rock Interactions*, Lunar and Planetary Institute, Houston, TX, 22 to 24 October 2006, abstr. no. 7038.
20. M. L. Coombs, T. W. Sisson, P. W. Lipman, *J. Volcanol. Geothermal Res.* **151**, 19 (2006).
21. G. J. S. Bluth, C. C. Schnetzler, A. J. Krueger, L. S. Walter, *Nature* **366**, 327 (1993).
22. C. D. K. Herd, L. E. Borg, J. H. Jones, J. J. Papike, *Geochim. Cosmochim. Acta* **66**, 2025 (2002).
23. P. J. Wallace, I. S. E. Carmichael, *Am. Mineral.* **79**, 161 (1994).
24. F. P. Fanale, S. E. Postawko, *Lunar Planet. Sci. Conf.* **XXVI**, 391 (1995).
25. J. F. Kasting, K. J. Zahnle, J. P. Pinto, A. T. Young, *Origins Life Evol. Biosphere* **19**, 95 (1989).
26. L. V. Haff, in *Chemical Analysis*, J. H. Karchmer, Ed. (Wiley, New York, 1970), vol. 29, pp. 183–283.
27. A. F. Ryabinina, V. A. Oshman, *Tr. Ural. Lesotekh. Inst.* **28**, 182 (1972).
28. V. A. Krasnopolsky, *Icarus* **178**, 487 (2005).
29. K. Zahnle, R. M. Haberle, in *Workshop on Martian Sulfates as Recorders of Atmospheric-Fluid-Rock Interactions*, Lunar and Planetary Institute, Houston, TX, 22 to 24 October 2006, abstr. no. 7046.
30. K. J. Zahnle, J. C. G. Walker, *Rev. Geophys.* **20**, 280 (1982).
31. G. J. Molina-Cuberos, W. Stumptner, H. Lammer, N. I. Komle, *Icarus* **154**, 216 (2001).
32. A. S. Wong, S. K. Atreya, T. Encrenaz, *J. Geophys. Res.* **108**, 5026 (2003).
33. S. E. Postawko, W. R. Kuhn, *J. Geophys. Res.* **91**, D431 (1986).

34. The first and second acid dissociation constants of sulfurous acid are $10^{-7.2}$ and $10^{-1.85}$, respectively, whereas those of carbonic acid are $10^{-10.3}$ and $10^{-6.3}$.
35. Pre-industrial atmospheric pSO_2/pCO_2 is ~3×10^{-7}. However, sulfite minerals do not precipitate because Earth's ocean is not in equilibrium with these atmospheric concentrations. As soon as it dissolves, sulfite is either rapidly oxidized in the aqueous phase to sulfate or reduced by bacteria to sulfide.
36. R. G. Burns, *Geochim. Cosmochim. Acta* **57**, 4555 (1993).
37. A. Banin, F. X. Han, I. Kan, A. Cicelsky, *J. Geophys. Res.* **102**, 13341 (1997).
38. L. M. Mukhin, A. P. Koscheev, Y. P. Dikov, J. Huth, H. Wanke, *Nature* **379**, 141 (1996).
39. N. J. Tosca, S. M. McLennan, *Earth Planet. Sci. Lett.* **241**, 21 (2006).
40. A. G. Fairen, D. Fernandez-Remolar, J. M. Dohm, V. R. Baker, R. Amils, *Nature* **431**, 423 (2004).
41. F. Poulet *et al.*, *Nature* **438**, 623 (2005).
42. Surface reservoirs include the combined aquatic and atmospheric reservoirs.
43. A. Gendrin *et al.*, *Science* **307**, 1587 (2005); published online 17 February 2005 (10.1126/science.1109087).
44. B. M. Jakosky, R. M. Haberle, in *Mars*, H. H. Kieffer, Ed. (Univ. Arizona Press, Tucson, AZ, 1992), pp. 969–1016.
45. S. W. Squyres, A. H. Knoll, *Earth Planet. Sci. Lett.* **240**, 1 (2005).
46. A. H. Knoll *et al.*, *Earth Planet. Sci. Lett.* **240**, 179 (2005).
47. D. P. Schrag, M. T. Zuber, in *Sixth International Conference on Mars*, Pasadena, CA, 20 to 25 July 2003, abstr. no. 3113.
48. J. C. Bridges *et al.*, *Space Sci. Rev.* **96**, 365 (2001).
49. J. C. Hanna, R. J. Phillips, *J. Geophys. Res.* **110**, E01004 (2005).
50. J. P. Bibring *et al.*, *Science* **312**, 400 (2006).
51. A. B. Ronov, A. Yaroshev, *Geochem. Int.* **4**, 1041 (1967).

52. Discussions with J. Dufek, J. Dykema, W. Fischer, J. Higgins, P. Hoffman, M. Jellinek, S. Johnson, C. Langmuir, and S. Leroy contributed to this work. Support was provided by the NASA Planetary Geology and Geophysics Program and a Radcliffe Fellowship to M.T.Z., by the George Merck Fund of the New York Community Trust to D.P.S. and by a Harvard Origins of Life Initiative Graduate Fellowship to I.H.

26 June 2007; accepted 8 November 2007
10.1126/science.1147039

Coupled ^{142}Nd-^{143}Nd Isotopic Evidence for Hadean Mantle Dynamics

Vickie C. Bennett,[1,2]* Alan D. Brandon,[3] Allen P. Nutman[4]

The oldest rocks—3.85 billion years old—from southwest Greenland have coupled neodymium-142 excesses (from decay of now-extinct samarium-146; half-life, 103 million years) and neodymium-143 excesses (from decay of samarium-147; half-life, 106 billion years), relative to chondritic meteorites, that directly date the formation of chemically distinct silicate reservoirs in the first 30 million to 75 million years of Earth history. The differences in ^{142}Nd signatures of coeval rocks from the two most extensive crustal relicts more than 3.6 billion years old, in Western Australia and southwest Greenland, reveal early-formed large-scale chemical heterogeneities in Earth's mantle that persisted for at least the first billion years of Earth history. Temporal variations in ^{142}Nd signatures track the subsequent incomplete remixing of very-early-formed mantle chemical domains.

Isotope data for short-lived decay schemes such as the ^{146}Sm-^{142}Nd system [half-life ($T_{1/2}$), 103 million years (My)] obtained from samples of the Moon, Mars, and meteorites are revealing the complexities of early planetary differentiation that occurred soon after accretion [e.g., (*1*–*4*)]. Attempts to demonstrate ^{142}Nd variations in Earth were initiated in the 1990s (*5*), with recent measurements of some ancient rocks [dating from >3.6 billion years ago (Ga)] (*6*–*10*) now firmly establishing variable ^{142}Nd/^{144}Nd ratios in Earth relative to modern terrestrial compositions. This is important because detectable ^{142}Nd isotopic variations can only be generated from Sm/Nd fractionation during the largely unknown first ~300 My of Earth history, while ^{146}Sm is still actively decaying. Previous studies focused largely on the ~3.7- to 3.8-billion-year (Gy)–old regions of the Isua supracrustal belt of West Greenland, representing largely one, albeit important, spatial and temporal point in Earth evolution. Interpreting the large range of reported ^{142}Nd/^{144}Nd ratios [0 to +17 parts per million (ppm) higher than modern terrestrial compositions] in terms of early planetary processes is complicated because many of the analyzed rocks were either metasedimentary mixtures of eroded terranes (*7*–*9*) or metabasalts (*6*, *9*, *10*) from areas that experienced widespread secondary chemical alteration [e.g., (*11*, *12*)].

Tantalizing hints of Hadean Era (>4.0 Ga) Earth dynamics come from the recent recognition that all crust and upper mantle rocks today have a ^{142}Nd/^{144}Nd excess of ~20 ppm compared with primitive chondritic meteorites (*2*, *13*, *14*), which were the building blocks of Earth. This requires not only that chemically distinct domains with high and low Sm/Nd, evolving to high and low ^{142}Nd, respectively, formed during or soon after accretion but also that these domains must have persisted to the present in order to account for the continued isotopic offset between chondrites and modern terrestrial rocks. Additionally, the more extreme ^{142}Nd excesses measured in some Archean rocks (*6*, *7*, *9*, *10*) require the early existence of an older, or more severely depleted (higher Sm/Nd) mantle, whose extent and longevity is unknown. To track the origin, distribution, and interaction of these global chemical domains requires precise ^{142}Nd data for ancient rocks with a range of ages and from a variety of localities.

Here, we present high-precision ^{142}Nd data (Table 1) (*15*) combined with ^{143}Nd data from samples of the two most aerially extensive >3.6-Gy-old terranes: the 3000 km^2 Itsaq Complex (*16*) of southern West Greenland, of which the Isua supracrustal belt is one component, and the Narryer Gneiss Complex of the Yilgarn craton, Western Australia. In contrast to previous studies, the emphasis is on analysis of the oldest tonalites, a juvenile granitic rock type typically representing the earliest formed continental crust in a region and from which direct age information in the form of U-Pb zircon ages can be obtained. Archean tonalites are melts of young oceanic crust [e.g., *17*)], derived from the upper mantle. The intermediate basalt stage is likely short compared with the time scale of ^{147}Sm decay and with Sm/Nd similar to that of the mantle source.

The Itsaq samples span a 210-My age range (3.64 to 3.85 Gy old) and include crystalline rocks from newly recognized localities of homogeneous 3.85-Gy-old tonalites (*18*) and >3.85-Gy-old mafic rocks (*15*). These samples are some of the oldest terrestrial rocks yet discovered. The two 3.73-Gy-old Narryer Gneiss Complex tonalitic gneisses are the oldest rocks from the Australian continent (*19*). All rocks are from our field collections and represent the most geologically pristine materials, with well-defined crystallization ages having minimal secondary chemical alteration (table S1) (*15*).

Homogenized powdered samples weighing from 0.1 to 0.3 g were dissolved and processed to isolate >500 ng Nd. The ^{142}Nd/^{144}Nd isotopic compositions were measured as Nd^+ on a Triton thermal ionization mass spectrometer using a multidynamic data collection scheme (*9*). Measurements of a standard Nd solution run interspersed with the samples yielded an external reproducibility (2 SD) of ±3.5 ppm (fig. S1) (in-run precisions were from 1.0 to 2.5 ppm, 2 SE). Replicate analyses of 14 modern rocks yielded the same external precision as the standard data (fig. S2), which demonstrates the validity of this precision for chemically processed samples. The ^{147}Sm-^{143}Nd data were obtained on separate powder samples using standard isotope-dilution methods (*15*).

Fifteen samples from the Itsaq Complex all have well-resolved ^{142}Nd excesses of 9 to 20 ppm relative to the modern terrestrial reference composition (Table 1). The six basalts with ages

[1]Research School of Earth Sciences, The Australian National University, Canberra ACT, 0200 Australia. [2]Lunar and Planetary Institute, Houston, TX 77058, USA. [3]NASA Johnson Space Center, Mail Code KR, Houston, TX 77058, USA. [4]Institute of Geology, Chinese Academy of Geological Sciences, 26 Baiwanzhuang Road, Beijing, 100037, China.

*To whom correspondence should be addressed. E-mail: vickie.bennett@anu.edu.au

of 3.8 Gy and >3.85 Gy have slightly higher, and more variable, ^{142}Nd than the similar age tonalites. In contrast, the four oldest (~3.85 Gy) tonalites collected from four separate localities have a narrow range of compositions, with mean ^{142}Nd excess of +15.3 ± 1.2 ppm (2 SD), and the three youngest (3.64 Gy) samples have a ^{142}Nd excess = +12.0 ± 0.9 ppm (2 SD).

High ^{142}Nd relative to modern rocks now appears to be a pervasive feature in the vast Archean terranes of southwest Greenland. The regional extent of this signature was likely much greater in the early Archean, as the analyzed rocks from the northern and southern parts of the Itsaq Complex, now >150 km distant, represent at least two different terranes, each with a distinct Eoarchean geologic history, that were later juxtaposed (*20*). In contrast to all of the Greenland samples, the two granitic samples from the Yilgarn craton have identical ^{142}Nd ≈ +5 ppm. The lack of ^{142}Nd excesses in a few previously analyzed Itsaq rocks (*8*, *10*) raises the question of how much confidence to place in these two samples representing the Yilgarn craton. We emphasize first that all granitic rocks (not metabasalts or metasediments) from the diverse Archean terranes of West Greenland give consistent results, with 100% of the analyzed >3.6-Gy-old granitic rocks (13 samples total) (Table 1) (*9*) having well-resolved ^{142}Nd excesses. Second, the two Western Australian samples were selected specifically to be equivalent to the Greenland samples in having similar juvenile tonalitic compositions, reflecting the earliest known granitic rocks in each terrane, with a similar degree of good preservation, such that they can be expected to yield reliable isotopic records.

Although this demonstration of global heterogeneity is powerful evidence for early differentiation on Earth, ^{142}Nd variations alone cannot be modeled uniquely in terms of time or extent of mantle depletion. However, concordant data from the two Sm-Nd decay schemes measured from the same sample can be combined to yield both the formation age of the mantle reservoir and the degree of Sm/Nd fractionation of this mantle (*5*), which is indicative of the extent of chemical differentiation. The calculated differentiation ages are most accurate using data from the oldest sam-

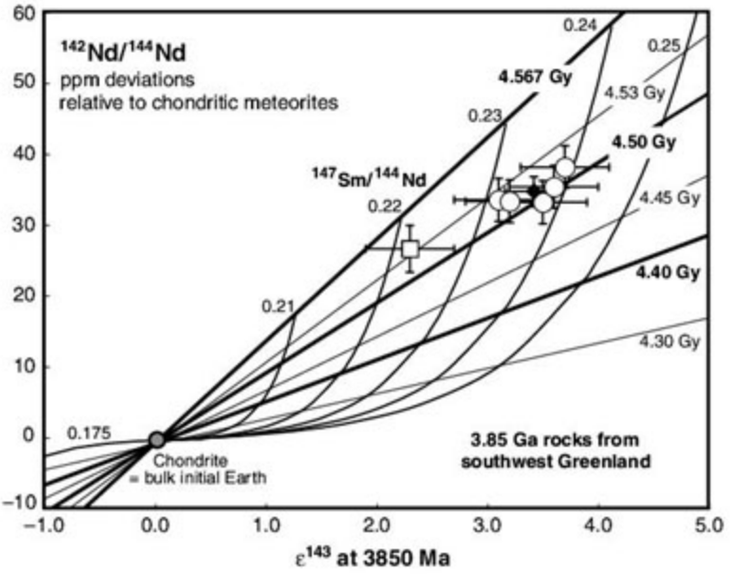

Fig. 1. Two-stage Sm-Nd evolution model (*5*) for the terrestrial mantle starting at the time of solar system origin (T_0 = 4567 Ma) (*30*), with a silicate Earth having a chondritic Sm/Nd ratio and Nd isotopic compositions. The second stage starts at the formation of a Hadean mantle source with high Sm/Nd. This mantle continues to evolve and is ultimately sampled by partial melting to form the ~3.85-Gy-old rocks studied here, which carry and preserve the elevated ^{142}Nd and ε^{143}Nd signatures. The straight lines represent the loci of equal ages for the formation of variable Sm/Nd mantle sources. The curved lines are the loci of increasing ^{147}Sm/^{144}Nd ratios representing varying levels of mantle differentiation. The combined ^{143}Nd and ^{142}Nd data from the oldest (3.85 Gy old), least altered tonalites and amphibolites (circles, with mean indicated by solid diamond) are self-consistent and indicate formation of a chemically fractionated, high Sm/Nd mantle within the first 30 My to 75 My of Earth history. Bulk silicate Earth compositions (*21*); decay equations (*15*); initial ^{146}Sm/^{144}Sm = 0.0075 ± .0025 (*31*). Decay constants: $\lambda_{147} = 6.54 \times 10^{-12}$ yr^{-1} and $\lambda_{146} = 6.74 \times 10^{-9}$ yr^{-1}. Error bars are ± 2 SD external reproducibility (Table 1).

Table 1. Summary of ^{142}Nd and ^{143}Nd isotopic data from two Eoarchean terranes. ^{142}Nd data are presented as the ppm difference from the terrestrial reference, calculated using the average value of terrestrial standards measured during the course of this study. Data sources for ε^{143}Nd(0) (*21*) are given in table S1. The errors on ε^{143}Nd(*t*) are ≤ ±0.5 epsilon units. The ages of the mafic rocks are determined from U-Pb zircon dating of associated cross-cutting felsic rocks and are thus minimums. Complete data sets, analytical methods, and geologic locality and age information are in (*15*).

Sample No.	Age (My)	Lithology	^{142}Nd/^{144}Nd	±2σ	^{142}Nd (ppm)	ε^{143}Nd(0)	ε^{143}Nd(*t*)
		Itsaq complex, West Greenland					
Islands near Nuuk							
G01/113	3849 ± 6	Tonalite	1.1418565	4.2×10^{-6}	15.8	−45.06	+3.1
G93/07	3852 ± 12	Tonalite	1.1418563	2.2×10^{-6}	15.6	−37.73	+3.2
G99/22	3862 ± 16	Tonalite	1.1418561	3.0×10^{-6}	15.5	−36.93	+3.5
G01/36	3849 ± 6	Tonalite	1.1418547	2.8×10^{-6}	14.2		
G97/112	3640 ± 11	Ferrodiorite	1.1418520	2.8×10^{-6}	11.9		+1.7
G97/112	Replicate		1.1418517	2.5×10^{-6}	11.6		
G97/111	3642 ± 3	Augen gneiss	1.1418527	2.4×10^{-6}	12.5		+1.7
JG03/11	>3850	Amphibolite	1.1418586	2.2×10^{-6}	17.6	12.02	+3.6
JG03/12	>3850	Amphibolite	1.1418618	1.0×10^{-6}	20.4	1.68	+3.7
JG03/36	>3850	Amphibolite	1.1418486	3.0×10^{-6}	8.9	−31.52	+2.3
G01/91	>3850	Metagabbro	1.1418509	3.0×10^{-6}	10.9		
Isua supracrustal belt and vicinity							
G06/3.7	3698 ± 8	Tonalite	1.1418544	2.6×10^{-6}	14.0	−51.85	+1.2
JG03/52	>3803 ± 3	Pillow basalt	1.1418526	2.6×10^{-6}	12.4	−6.73	−0.2
JG03/48	>3803 ± 3	Pillow basalt	1.1418605	2.9×10^{-6}	19.3	−31.70	+4.2
G97/98	3795 ± 3	Tonalite	1.1418578	3.1×10^{-6}	16.9	−45.86	+2.1
		Yilgarn craton, Western Australia					
88/28	3731 ± 4	Tonalite	1.1418444	3.2×10^{-6}	5.2	−41.47	+1.7
88/173	3730 ± 5	Tonalite	1.1418438	3.0×10^{-6}	4.6	−48.88	+1.8
Nd standard average (this study); 2σ external precision							
n = 13			1.1418385	4.0×10^{-6}	0.0		

ples, in this case the ~3.85-Gy-old samples from Greenland, because these are less likely to contain mixed-age crustal components. The ^{146}Sm-^{142}Nd scheme requires no corrections for in situ decay in Archean rocks, eliminating a potential source of error, and there is no process that can generate positive ^{142}Nd variations after ^{146}Sm has largely decayed by ~ 4.2 Ga. Alteration or open-system behavior can only move ^{142}Nd signatures toward modern compositions. The samples analyzed here have a wide range of present-day $\varepsilon^{143}Nd = +12$ to -52 (*21*), which after corrections for in situ decay yield a narrow range of initial $\varepsilon^{143}Nd$ (Table 1).

The tonalites and mafic samples indicate similar ages and, assuming the five samples with the highest ^{142}Nd represent the same mantle source, they define a mean mantle differentiation age of 4.51 ± 0.02 Gy (1 SD), which suggests that the Hadean high Sm/Nd mantle formed within the first 35 to 75 My of Earth history (Fig. 1). This is similar to the time of metallic core formation on Earth obtained from the ^{182}Hf-^{182}Hf chronometer ($T_{1/2}$ = 9 My) (*22*). Early massive melting of Earth is predicted in many accretion scenarios [e.g., (*23*)], and these coupled ^{142}Nd -^{143}Nd results provide a temporal linkage between formation of major silicate reservoirs and early catastrophic events during planet formation (*10*). Such differentiations may point to magma ocean scenarios [e.g., (*24*)], whereby distinct chemical domains formed by crystal fractionation in a molten Earth rather than by progressive continental crust extraction over time. The $^{147}Sm/^{144}Nd$ of the Hadean mantle was ≈0.236 (Fig. 1), which is 20% higher than the chondritic (bulk Earth) value of 0.1966 but similar to compositions calculated for lunar highlands crustal rocks (*25*). In contrast to the tonalite suite, ^{142}Nd -^{143}Nd data from 3.7- to 3.8-Gy-old Isua metabasalts show large variations (*6*, *9*, *10*), with many samples falling outside of all possible mantle isochrons generated using two-stage models (fig. S3). This reflects a more complex petrogenesis for these samples [see (*11*, *12*)].

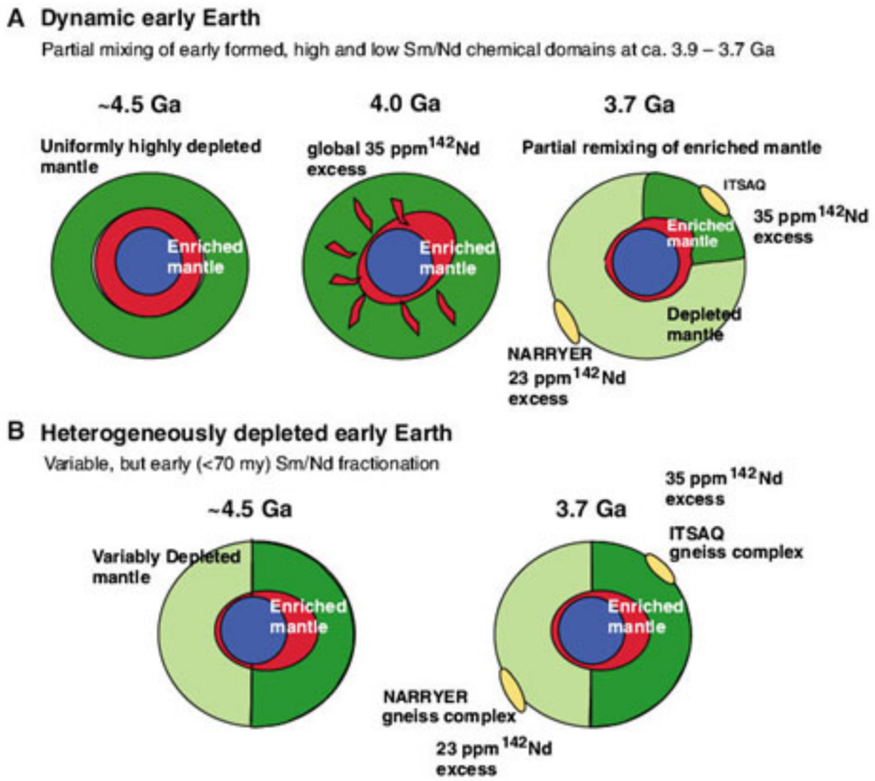

Fig. 2. Two scenarios to account for the distinctive ^{142}Nd signatures of Archean rocks from coeval early crustal terranes. (**A**) Formation of uniform mantle (dark green) with high Sm/Nd early in Earth's history. Most, but not all, of this mantle is subsequently remixed with complementary low Sm/Nd material (red), depicted here as residing in the deep mantle. The Itsaq Complex rocks, southwest Greenland, sample a relict of the early high Sm/Nd domain. The Narryer Gneiss Complex rocks, Western Australia, sample a mantle source with more modest Sm/Nd. (**B**) Early-formed heterogeneous mantle. These chemically distinct mantle source regions persisted for at least 1 Gy, to be sampled by the formation of 3.6- to 3.9-Gy-old Archean rocks in the two regions.

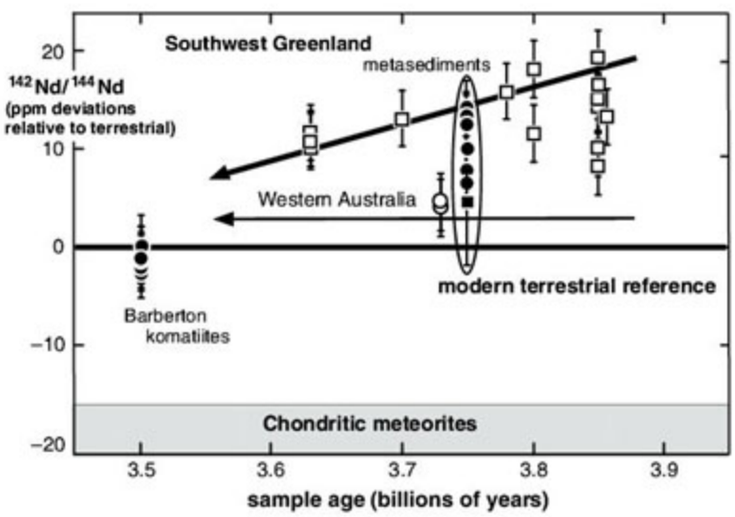

Fig. 3. ^{142}Nd excess (ppm) relative to modern terrestrial compositions as a function of rock crystallization age. Open symbols (this study), with error bars ±3.5 ppm (2 SD). Filled circles (*9*); filled squares (*8*), with errors as reported in each study. The decreasing ^{142}Nd through time suggests progressive remixing of early-formed, highly fractionated mantle sources. The range of data apparent in the mixed provenance metasediments may reflect input from various Archean ^{142}Nd sources (*9*), further supporting the existence of mantle chemical heterogeneity.

What is the fate of the highly depleted Hadean mantle domain? Tracking of ^{142}Nd compositions in West Greenland samples through time shows an apparent decrease in the most positive ^{142}Nd signatures with younger sample crystallization ages (Fig. 3). In contrast, the mantle sampled by the Eoarchean Narryer Complex gneisses and in other somewhat younger Archean regions [i.e., Barberton, South Africa (*9*)] shows minor, or no, ^{142}Nd excess compared with the modern mantle. The trend of decreasing ^{142}Nd in the Itsaq Complex suggests that even the compositions of the oldest samples from 3.85 Ga may already reflect partial destruction of a highly fractionated Hadean mantle domain that formed >4.5 Ga and that the original Sm/Nd may have been even higher, perhaps as

extreme as some portions of the Martian mantle [e.g., (*26*)]. Although the Itsaq-DM seems to have been obliterated, or at least not sampled at present, the source mantle of the Narryer Complex crust persists to the present. These observations require an explanation for the differing behavior of the two depleted mantle components, the Narryer-DM able to retain its identity, despite ongoing mantle dynamics for >4.5 Gy, as compared with the transient Itsaq-DM. If all or much of the mantle was initially as highly fractionated as Itsaq-DM, then why was this mantle only partially, but apparently homogeneously, remixed such that all modern terrestrial rocks yield precisely the same ^{142}Nd, distinct from chondrites? The difference supports models of "hidden reservoirs" where part of the complementary, low Sm/Nd domain is locked in a region of Earth, where it is both never sampled at the surface [e.g., (*27*–*29*)] and isolated from remixing. More speculative suggestions are that part of the low Sm/Nd component may have been lost from Earth during accretion, with the missing material accounting for the present-day high ^{142}Nd, or that Earth accreted with a nonchondritic Sm/Nd ratio. In contrast, the Itsaq-DM mantle source persisted for at least a billion years after its formation, as recorded by compositions of 3.6-Gy-old Greenland samples, but was able to communicate with other less fractionated mantle reservoirs and eventually lost its distinct signature through remixing.

An enduring tenet of geology is that Earth started from a well-mixed homogeneous body and evolved progressively over geologic time to a more differentiated chemical state through observable processes such as plate tectonics and continental crust formation. The ^{142}Nd data presented here, however, provide strong evidence that terrestrial planets such as Earth were affected by non-uniformitarian processes early in their histories, resulting in locally extreme chemical differentiation. Furthermore, some of the chemical effects of these events appear to persist in silicate domains to the present day. Thus, an emerging challenge for understanding the Earth system is determining the relative roles of early planetary processes versus progressive differentiation in shaping Earth's chemical architecture.

References and Notes

1. L. Nyquist, H. Wiesmann, B. Bansal, *Geochim. Cosmochim. Acta* **59**, 2817 (1995).
2. M. Boyet, R. W. Carlson, *Science* **309**, 576 (2005).
3. C. N. Foley *et al.*, *Geochim. Cosmochim. Acta* **69**, 4557 (2005).
4. K. Rankenburg, A. D. Brandon, C. R. Neal, *Science* **312**, 1369 (2006).
5. C. L. Harper, S. B. Jacobsen, *Nature* **360**, 728 (1992).
6. M. Boyet *et al.*, *Earth Planet. Sci. Lett.* **214**, 427 (2003).
7. G. Caro, B. Bourdon, J.-L. Birck, S. Moorbath, *Nature* **423**, 428 (2003).
8. M. Sharma, C. Chen, *Precamb. Res.* **135**, 315 (2004).
9. G. Caro, B. Bourdon, J.-L. Birck, S. Moorbath, *Geochim. Cosmochim. Acta* **70**, 164 (2006).
10. M. Boyet, R. Carlson, *Earth Planet. Sci. Lett.* **250**, 254 (2006).
11. A. Polat, A. W. Hofmann, *Precamb. Res.* **126**, 197 (2003).
12. R. Frei, M. Rosing, T. Waight, D. G. Ulfbeck, *Geochim. Cosmochim. Acta* **66**, 467 (2002).
13. R. Andreasen, M. Sharma, *Science* **314**, 806 (2006).
14. R. W. Carlson, M. Boyet, M. Horan, *Science* **316**, 1175 (2007).
15. Materials and methods are available as supporting material on *Science* Online.
16. A. Nutman, V. McGregor, C. Friend, V. Bennett, P. Kinny, *Precamb. Res.* **78**, 1 (1996).
17. H. Smithies, D. Champion, K. Cassidy, *Precamb. Res.* **127**, 89 (2003).
18. A. Nutman, V. Bennett, C. Friend, K. Horie, H. Hidaka, *Contrib. Mineral. Petrol.* **154**, 385 (2007).
19. A. Nutman, V. Bennett, P. Kinny, R. Price, *Tectonics* **12**, 97 (1993).
20. C. Friend, A. Nutman, *J. Geol. Soc. Lond* **162**, 147 (2005).
21. $\varepsilon^{143}Nd(t) = [(^{143}Nd/^{144}Nd(t)_{sample}/^{143}Nd/^{144}Nd(t)_{CHUR})-1] \times 10^4$, where t refers to the crystallization age of the sample and CHUR is the chondritic reservoir composition used to represent bulk silicate Earth with present-day $^{143}Nd/^{144}Nd = 0.512638$ and $^{147}Sm/^{144}Nd = 0.1966$.
22. S. B. Jacobsen, *Annu. Rev. Earth Planet. Sci.* **33**, 531 (2005).
23. W. B. Tonks, H. J. Melosh, *J. Geophys. Res.* **98**, 5319 (1993).
24. Y. Abe, *Phys. Earth and Planet. Int.* **100**, 27 (1997).
25. M. Boyet, R. Carlson, *Earth Planet. Sci. Lett.* **262**, 505 (2007).
26. L. Borg, D. Draper, *Meteoritics Planet. Sci.* **34**, 439 (2003).
27. C. Chase, P. J. Patchett, *Earth Planet. Sci. Lett.* **91**, 66 (1988).
28. J. Blichert-Toft, F. Albaréde, *Earth Planet. Sci. Lett.* **148**, 243 (1997).
29. I. Tolstikhin, A. W. Hofmann, *Phys. Earth Planet. Int.* **148**, 109 (2005).
30. Y. Amelin *et al.*, *Science* **297**, 1678 (2002).
31. Y. Amelin, A. Ghosh, E. Rotenberg, *Geochim. Cosmochim. Acta* **69**, 505 (2005).

32. Greenland investigations by V.C.B. and A.P.N. were supported by Australian Research Council Discovery grant DP0342794. The manuscript was improved by the extensive comments of two anonymous reviewers and R. Carlson. V.C.B. thanks M. Norman and G. Caro for helpful discussions at various stages of this project.

Supporting Online Material

www.sciencemag.org/cgi/content/full/318/5858/1907/DC1
Materials and Methods
Figs. S1 to S3
Tables S1 to S3
References

31 May 2007; accepted 30 October 2007
10.1126/science.1145928

High-Pressure Creep of Serpentine, Interseismic Deformation, and Initiation of Subduction

Nadege Hilairet,[1]* Bruno Reynard,[1] Yanbin Wang,[2] Isabelle Daniel,[1] Sebastien Merkel,[3] Norimasa Nishiyama,[2]† Sylvain Petitgirard[1]

The supposed low viscosity of serpentine may strongly influence subduction-zone dynamics at all time scales, but until now its role could not be quantified because measurements relevant to intermediate-depth settings were lacking. Deformation experiments on the serpentine antigorite at high pressures and temperatures (1 to 4 gigapascals, 200° to 500°C) showed that the viscosity of serpentine is much lower than that of the major mantle-forming minerals. Regardless of the temperature, low-viscosity serpentinized mantle at the slab surface can localize deformation, impede stress buildup, and limit the downdip propagation of large earthquakes at subduction zones. Antigorite enables viscous relaxation with characteristic times comparable to those of long-term postseismic deformations after large earthquakes and slow earthquakes. Antigorite viscosity is sufficiently low to make serpentinized faults in the oceanic lithosphere a site for subduction initiation.

Subduction zones, in which slabs of oceanic lithosphere sink into the mantle, are active zones where frequent large earthquakes cause considerable human and material damage. Such events are triggered by stress buildup or strain localization, the understanding of which relies on identifying the materials involved and their rheology. On top of slabs of many subduction zones, a layer with low seismic velocity and high Poisson ratio (>0.29) is interpreted as extensively serpentinized mantle material (*1*, *2*), and may accommodate most of the deformation at the slab/mantle wedge interface. Serpentinites form by peridotite hydration either during hydrothermal alteration of the oceanic lithosphere before subduction or by percolation of the fluids released by mineral dehydration within the downgoing slab through the overlying mantle wedge (*3*). The high-pressure variety of serpentine, antigorite, can remain stable down to ~180 km depth in cold subduction zones (*4*). Serpentinites are highly deformed as compared to other exhumed materials in paleosubduction zones (*5*), which points to their crucial mechanical role. The expected low strength or viscosity of serpentinite

[1]Laboratoire des Sciences de la Terre, CNRS, Ecole Normale Supérieure de Lyon, Université Claude Bernard Lyon 1, 46 Allée d'Italie, 69364 Lyon Cedex 07, France. [2]Center for Advanced Radiation Sources, University of Chicago, 5640 South Ellis Avenue, Chicago, IL 60637, USA. [3]Laboratoire de Structure et Propriétés de l'Etat Solide, UMR CNRS 8008, Université des Sciences et Technologies de Lille, 59655 Villeneuve d'Ascq, France.

*To whom correspondence should be addressed. E-mail: nadege.hilairet@ens-lyon.fr

†Present address: Geodynamics Research Center, Ehime University, Japan.

has strong seismic implications because it may govern stress buildup and downdip relaxation over the slab surface, which are critical parameters for earthquake triggering and for the downdip extent of major ruptures (*6*). So far, only viscous relaxation of the anhydrous mantle has been considered a potential trigger of major earthquakes, such as the Tonankai 1944, Nankaido 1946 (*7*), and Alaska 1964 events (*8*). Serpentinites also have global geodynamic importance on the time scale of mantle convection because a serpentinite layer may decouple the mantle wedge from the downgoing slab (*9*). Its presence therefore is a defining condition of the plate tectonic regime on Earth.

The limitations of apparatus have restricted previous high-temperature deformation experiments on serpentinites to pressures below 0.7 GPa (*5*, *9*–*11*). Below the antigorite dehydration temperature (600°C), such low confining pressures favor brittle behavior, with deformation being governed by frictional forces, whereas different deformation mechanisms are to be expected at higher pressures (*11*), as suggested by numerous defects allowing for intracrystalline creep commonly observed in antigorite (*12*). In the absence of high-pressure data, quantifying the role of serpentinite at long and short time scales in subduction zones has remained beyond reach. We performed in situ measurements (*13*) of antigorite flow stress using the recently developed deformation-DIA (D-DIA) apparatus coupled with synchrotron x-ray analysis (*14*) under conditions of low constant strain rates (~10^{-4} to 10^{-6} s^{-1}) and pressure and temperature (*P-T*) of 1 and 4 GPa and 200° to 500°C, respectively; that is, over most of the antigorite stability field (*4*, *15*). We obtained a stress-strain curve for 14 sets of experimental conditions (tables S1 and S2). Strain values $\varepsilon(t)$ were measured on synchrotron x-ray radiographs, and differential stress σ was measured from elastic lattice strains on angle-dispersive x-ray diffraction patterns (*13*, *16*). The stress value taken or extrapolated at 15% axial strain was used arbitrarily as a measure of the ultimate flow stress (table S3). Because sample observation shows features consistent with intracrystalline deformation (*13*), flow stress values were fitted to power-law equations (Table 1), in which the stress exponent depends on the dominant deformation mechanism (dislocation creep, diffusion, etc.), and to an exponential law appropriate for low-temperature creep processes [the Peierls mechanism (*13*)]. The best fit to the present data, at 1 and 4 GPa, was obtained with a single power-law equation that yielded an activation volume of 3.2 ± 0.7 cm^3 mol^{-1}, activation energy of 8.9 ± 5.4 kJ mol^{-1}, and a stress exponent of 3.8 ± 0.8 (Table 1), consistent with deformation by dislocation creep. The decrease of the stress exponent with increasing pressure when fitting data at each pressure independently (*13*) is consistent with the activation of intracrystalline deformation mechanisms at the expense of frictional grain boundary sliding at low confining pressure.

The ductile deformation of antigorite observed above 1 GPa complements observations from previous triaxial experiments, showing brittle behavior of serpentinite below 0.7 GPa and a transition toward a distributed semi-brittle deformation up to 1 GPa (*5*, *11*). If controlled by antigorite, the transition from brittle to ductile creep at the slab interface with either the crust or the mantle wedge should depend mainly on depth, while the thermal structure of the subduction zone exerts only minor effects. In the case of high porosity (microcracks) with reduced effective confining pressure, the transition depth may depend indirectly on temperature through the amount of water released by mineral dehydration.

In order to depict further the potential role of antigorite rheology on wedge dynamics, we calculated a strength profile at a constant strain rate along a slab surface (Fig. 1), assuming a *P-T* profile in a moderately hot subduction zone and considering two extreme cases. In the first model, we assumed a 300-m-thick serpentinite layer formed by hydration above the subducting slab and sheared by 10 cm $year^{-1}$, corresponding to a strain rate of 10^{-10} s^{-1}. Such conditions correspond to those of a subduction zone characterized by strong mechanical coupling or fast postseismic deformation due to sparse serpentinization. In the second case, a 10-km-thick serpentinite layer sheared by 1 mm $year^{-1}$ deforms at a strain rate of 10^{-14} s^{-1}. Such conditions hold for a subduction zone with a layer of extensively serpentinized mantle decoupled from a slowly downgoing slab. These two end-member models indicate that, regardless of strain rate and subduction-zone setting, antigorite is the only mineral among the major phases in the subducting lithosphere and mantle wedge that is capable of yielding by creep at geophysically relevant strain rates and temperatures below 600°C (Fig. 1).

Table 1. Preferred fits to power law $\dot{\varepsilon} = A\sigma^n \exp[-(E_a + PV^*)/(RT)]$ and exponential law $\dot{\varepsilon}_p = A_p \exp[(-E_p/RT)(1 - \frac{\sigma}{\tau})^2]$. Standard errors (1σ) are in parentheses at the right of each parameter. *A* and A_p are material constants, E_a and E_p are activation energies, V^* is activation volume, *n* is a stress exponent, and τ is Peierls stress.

					Power law					
Data used	10^{-1} ln (*A*)			E_a (kJ)			V^* (cm^3)		*n*	R^2
1 and 4 GPa	−8.6	(1.6)		8.9	(5.4)		3.2	(0.7)	3.8 (0.8)	0.89
1 GPa	−12.6	(2.5)		17.6	(6.5)				5.8 (1.3)	0.90
4 GPa	−7.9	(2.8)		16.6	(10.5)				3.4 (1.4)	0.81
					Exponential law					
Data used	τ (GPa)			E_p (kJ)			10^4 A_p			R^2
1 GPa	1.97	(0.36)		59.9	(18.4)		9.8	(2.5)		0.83

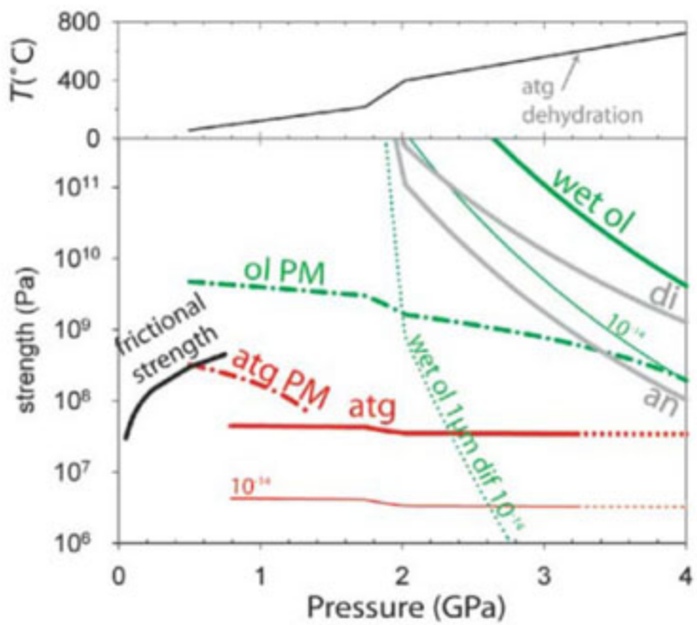

Fig. 1. Strength of antigorite (atg) and other major silicates along a slab surface. Strengths are calculated from deformation laws at a strain rate of 10^{-10} s^{-1} (thick curves) and 10^{-14} s^{-1} (thin curves) along a slab surface *P-T* profile [profile number i50 from (*28*)] (upper graph). The low-temperature dislocation glide Peierls mechanism (PM) (*29*), is the most realistic deformation mechanism for olivine (ol) at these pressure, temperature, and strain-rate conditions. Because the Peierls mechanism cannot be extrapolated to low strain rates, strength can be calculated from the creep law only at 10^{-14} s^{-1}. At 10^{-10} s^{-1}, the transition from frictional behavior according to Byerlee's law (thick black line), and antigorite deforming plastically by the Peierls mechanism, occurs between 0.7 and 1 GPa. Antigorite strength remains at least one order of magnitude lower than that of other major mantle and crust minerals regardless of the deformation mechanism and the strain rate, except for very fine-grained (1 μm) olivine deforming by diffusion creep (dif, dotted curve), the strength of which becomes inferior to that of antigorite before its dehydration at strain rates below ~10^{-12} s^{-1}. Millimeter-sized olivine deforming by diffusion creep yields much higher strength and plots off the graph. The Peierls mechanism is from (*29*) and the wet olivine dislocation creep and diffusion creep from (*30*). di, wet diopside; an, anorthite, dislocation creep laws (*31*).

The exception is fine-grained olivine, which may become weaker than antigorite above 2.5 GPa (Fig. 1). Shear instabilities may, therefore, be reconsidered as a possible mechanism for intermediate-depth seismicity, which may either be related to antigorite dehydration producing very fine-grained olivine or occur within fine-grained partly serpentinized peridotites (*17*).

These deformation experiments provide an upper bound for serpentinite viscosity, because naturally occurring localizations would induce high strain rates and lower the effective viscosity. The values we calculated for effective serpentinite viscosity, ~ 4.10^{19} Pa•s for a strain rate of 10^{-13} s^{-1} (*13*), are of the same orders of magnitude as those used in current numerical models (*18*). Serpentine viscosity as determined by us does not vary much with temperature, which precludes substantial shear heating in a low constant strain-rate system. Our flow law predicts that strain rate, hence viscosity as well, depends nonlinearly on stress. This would enhance positive feedbacks between strain and stress variations, as compared to models using linear stress dependence such as Newtonian rheology (*18*).

Seismologists define three zones downdip along the slab: seismic, transitional (locked during interseismic time), and aseismic. The factors controlling the downdip limit of the seismogenic and locked transitional zones will also govern the downdip propagation of megathrust ruptures, such as the event of 26 December 2004 in Java (*19*). Because serpentinite has a low viscosity, with little pressure and temperature dependence above 1 GPa, the depth at which nonseismogenic creep is possible is governed exclusively by the extent of the serpentinite layer in the subduction zone. This is consistent with observations in Japan, where shallow depths (a maximum of 30 km) of seismogenic zones are associated with Poisson ratios higher than 0.29 (*20*), a strong indication of serpentinization, whereas deeper (50 to 70 km) downdip limits coincide with no indices of serpentinization (*21*). In Sumatra, where no evidence of serpentinization is found, the downdip limit occurs even deeper in the mantle (*22*).

Because of its low viscosity, serpentine can relax stress at rates comparable to those of postseismic and slow seismic deformations. Using a modified Maxwell body with a nonlinear viscous behavior, subject to a permanent deformation ε_0 producing an initial stress $\sigma_0 = \varepsilon_0 E$, where E is the Young modulus (in pascals), the characteristic relaxation time τ_c required to relax half of the initial stress σ_0 is

$$\tau_c = \frac{2^{n-1}-1}{AE(n-1)\sigma_0^{n-1}} \exp\left(\frac{E_a + PV^*}{RT}\right) \quad (1)$$

(*23*), where E_a and V^* are the activation energy and volume, respectively; A and n are material parameters; R is the gas constant; P is the effective confining pressure; and T is the temperature. At temperatures of 200° to 500°C relevant to a slab surface, the relaxation times for antigorite are at least 10 orders of magnitude shorter than those for olivine (Fig. 2). For subduction-zone flow stress estimates up to ~100 MPa (*18*), antigorite relaxation times compare well with characteristic times of co- or postseismic surface deformations such as those measured by geodetic measurements for slow slip events, episodic tremor and slip, silent earthquakes, afterslips, and viscous relaxation (Fig. 2). Viscous relaxation of serpentinite therefore accounts for slow-slip events and for slow earthquakes occurring over periods of a few days to 1 year and which follow a scaling law different from that for regular earthquakes (*24*). These results also suggest that the importance of viscoelastic relaxation processes for triggering large earthquakes in subduction zones over interseismic periods of several years (*25*, *26*) should be reassessed, taking into account the low viscosity of serpentinites measured here. Thus, the triggering of future earthquakes, such as the Tokai event expected in Japan, may depend on serpentinite viscous relaxation (*7*).

Together with a strong stress dependence, the low viscosity of antigorite at *P-T* conditions where other minerals have viscosities orders of magnitude higher confirms that serpentinite is an ideal candidate for strain localization within subduction zones. Moreover, antigorite-bearing serpentinites formed deeply in oceanic transform faults and passive margins may constitute decisive weak zones in the oceanic lithosphere, because their viscosity is lower than the critical value of 10^{20} Pa•s required to initiate subduction (*27*). The present data quantitatively relate viscous deformation of serpentinites to interseismic deformation and slow earthquakes. They should help improve numerical modeling of seismicity and convection in subduction zones.

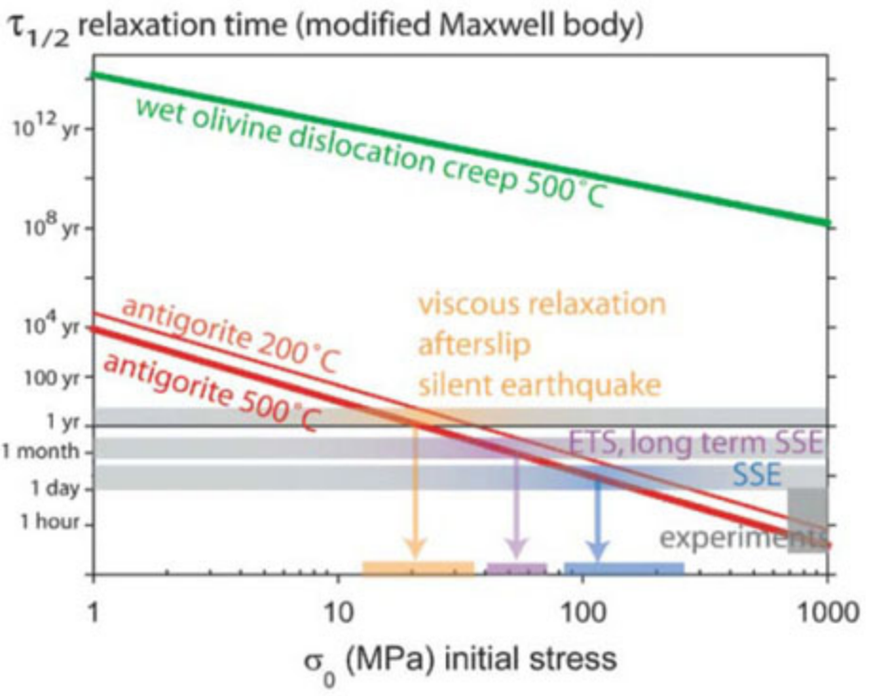

Fig. 2. Maxwell relaxation time for antigorite rheology and post- and slow seismic deformation time scales. $\tau_{1/2}$ is the time calculated (Eq. 1) to relax half of an initial stress σ_0 imposed at $t = 0$ (for instance, by the displacement field of an earthquake occurring close to a serpentinite body), using the antigorite power-law equation at 2 GPa (table S4) and $E = 89$ GPa (*20*). Stress above 20 MPa will be half-relaxed in less than 1 year by antigorite at 500°C (~40 MPa at 200°C), whereas stress relaxation is not possible in wet olivine deforming by dislocation creep (*30*) at these temperatures. Olivine diffusion creep (*30*), not reported here, leads to a constant characteristic relaxation time of ~ 10^7 years. Relaxation of high natural stress by antigorite flow is compatible with the time scales of postseismic deformation after large earthquakes (*7*, *8*, *25*, *26*) and slowslip events or silent earthquakes (*24*). ETS, episodic tremor and slip; SSE, slow slip events.

References and Notes

1. G. A. Abers, *Phys. Earth Planet. Int.* **149**, 7 (2005).
2. H. Kawakatsu, S. Watada, *Science* **316**, 1468 (2007).
3. W. S. Fyfe, A. R. McBirney, *Am. J. Sci.* **275A**, 285 (1975).
4. P. Ulmer, V. Trommsdorf, *Science* **268**, 858 (1995).
5. C. B. Raleigh, M. S. Paterson, *J. Geophys. Res.* **70**, 3965 (1965).
6. S. M. Peacock, R. D. Hyndman, *Geophys. Res. Lett.* **26**, 2517 (1999).
7. P. A. Rydelek, I. S. Sacks, *Earth Planet. Sci. Lett.* **206**, 289 (2003).
8. C. Zweck, J. T. Freymueller, S. C. Cohen, *Phys. Earth Planet. Int.* **132**, 5 (2002).
9. S. A. F. Murrell, I. A. H. Ismail, *Tectonophysics* **31**, 207 (1976).
10. E. H. Rutter, K. H. Brodie, *J. Geophys. Res.* **93**, 4907 (1988).
11. J. Escartin, G. Hirth, B. W. Evans, *J. Geophys. Res.* **102**, 2897 (1997).
12. A.-L. Auzende *et al.*, *Eur. J. Mineral.* **14**, 905 (2002).
13. Materials and methods are available as supporting material on *Science* Online.
14. Y. Wang, W. B. Durham, I. C. Getting, D. J. Weidner, *Rev. Sci. Instrum.* **74**, 3003 (2003).
15. N. Hilairet, I. Daniel, B. Reynard, *Geophys. Res. Lett.* **33**, L02302 (2006).
16. T. Uchida, N. Funamori, T. Yagi, *J. Appl. Phys.* **80**, 739 (1996).

17. J. M. Warren, G. Hirth, *Earth Planet. Sci. Lett.* **248**, 438 (2006).
18. T. V. Gerya, B. Stoeckhert, A. Perchuk, *Tectonics* **21**, 1056 (2002).
19. C. Subarya *et al.*, *Nature* **440**, 46 (2006).
20. N. I. Christensen, *Int. Geol. Rev.* **46**, 795 (2004).
21. T. Seno, *Earth Planet. Sci. Lett.* **231**, 249 (2005).
22. M. Simoes, J. P. Avouac, R. Cattin, P. Henry, *J. Geophys. Res. Solid Earth* **109**, B10402 (2004).
23. D. L. Turcotte, G. Schubert, *Geodynamics* (Cambridge Univ. Press, ed. 2, 2002).
24. S. Ide, G. C. Beroza, D. R. Shelly, T. Uchide, *Nature* **447**, 76 (2007).
25. A. M. Freed, R. Burgmann, *Nature* **430**, 548 (2004).
26. H. Ueda, M. Ohtake, H. Sato, *J. Geophys. Res. Solid Earth* **108**, 2151 (2003).
27. K. Regenauer-Lieb, D. A. Yuen, J. Branlund, *Science* **294**, 578 (2001).
28. J. A. Conder, *Phys. Earth Planet. Int.* **149**, 155 (2005).
29. P. Raterron, Y. Wu, D. J. Weidner, J. Chen, *Phys. Earth Planet. Int.* **145**, 149 (2004).
30. S. Karato, D. C. Rubie, H. Yan, *J. Geophys. Res. Solid Earth* **98**, 9761 (1993).
31. A. Dimanov, G. Dresen, *J. Geophys. Res. Solid Earth* **110**, B07203 (2005).
32. We thank B. Van de Moortèle for the electron microscopy and J. Blichert-Toft, F. Albarède, J. Bass, and the two anonymous reviewers for their suggestions. This work was supported by the Institut National des Sciences de l'Univers (SEDIT program). The experiment was carried out at GeoSoilEnviroCARS (Sector 13) at the Advanced Photon Source (APS), Argonne National Laboratory. Use of the APS was supported by the U.S. Department of Energy (DOE), Office of Science, Office of Basic Energy Sciences, under contract no. DE-AC02-06CH11357. GeoSoilEnviroCARS is supported by NSF–Earth Sciences (grant EAR-0217473), DOE-Geosciences (grant DE-FG02-94ER14466), and the State of Illinois.

Supporting Online Material
www.sciencemag.org/cgi/content/full/318/5858/1910/DC1
Materials and Methods
Figs. S1 to S8
Tables S1 to S3
References

30 July 2007; accepted 7 November 2007
10.1126/science.1148494

A Comprehensive Phylogeny of Beetles Reveals the Evolutionary Origins of a Superradiation

Toby Hunt,[1,2]* Johannes Bergsten,[1,2]* Zuzana Levkanicova,[3] Anna Papadopoulou,[1,2] Oliver St. John,[1,2] Ruth Wild,[1,2] Peter M. Hammond,[1] Dirk Ahrens,[4] Michael Balke,[1,4] Michael S. Caterino,[1,5] Jesús Gómez-Zurita,[1,6] Ignacio Ribera,[7] Timothy G. Barraclough,[2] Milada Bocakova,[8] Ladislav Bocak,[3] Alfried P. Vogler[1,2]†

Beetles represent almost one-fourth of all described species, and knowledge about their relationships and evolution adds to our understanding of biodiversity. We performed a comprehensive phylogenetic analysis of Coleoptera inferred from three genes and nearly 1900 species, representing more than 80% of the world's recognized beetle families. We defined basal relationships in the Polyphaga supergroup, which contains over 300,000 species, and established five families as the earliest branching lineages. By dating the phylogeny, we found that the success of beetles is explained neither by exceptional net diversification rates nor by a predominant role of herbivory and the Cretaceous rise of angiosperms. Instead, the pre-Cretaceous origin of more than 100 present-day lineages suggests that beetle species richness is due to high survival of lineages and sustained diversification in a variety of niches.

The extraordinary diversity of beetles has long fascinated evolutionary biologists (*1*). The strongly sclerotized front wings defining the order Coleoptera (the beetles), which provide protection while retaining the ability of powered flight with the membranous hindwings, may be an evolutionary novelty that promoted extensive diversification (*2*). Beetles appeared around 285 million years ago (Ma) (*2*, *3*), followed by radiations of wood-boring (suborder Archostemata), predacious (Adephaga), and fungivorous (Polyphaga) lineages (*4*) present in the fossil record from the middle Triassic on (*2*, *3*). Their species richness is associated with extreme morphological, ecological, and behavioral diversity (*4*), and diversification of the most species-rich extant lineages may have been driven by co-radiations with angiosperms (*5*) and/or mammals (*6*) and/or geological and climatic change (*7*) occurring since the Cretaceous (145 to 65 Ma).

Studies of phylogenetic relationships within the Coleoptera resulted in a preliminary consensus on the classification, defining 4 suborders, 17 superfamilies, and 168 families (*8*–*10*). However, formal phylogenetic analyses of morphological characters (*11*, *12*) and more recently molecular data (*5*, *13*, *14*) have been limited to subgroups at the family or superfamily level. Because of the sheer size of the group and the complexity of morphological character systems, these analyses have not been applied to the entire order.

We compiled a three gene data matrix providing a complete taxonomic representation for all suborders, series and superfamilies; >80% of recognized families; and >60% of subfamilies (*9*, *10*), which together contain >95% of described beetle species. Sequences for the small subunit ribosomal RNA (18 *S* rRNA) were obtained for 1880 species from de novo sequencing and existing databases. Mitochondrial 16S rRNA (*rrnL*) and cytochrome oxidase subunit I (*cox1*) sequences were added for nearly half of these taxa (table S1) to create a data matrix of rapid, medium, and slowly evolving sequences. Phylogenetic analysis of the combined matrix was performed with a fragment-extension procedure for global sequence alignment followed by tree searches with fast parsimony algorithms (*15*). We tested for long-branch attraction, i.e., the spurious pairing of rapidly evolving lineages, by removing taxa terminal to long branches and assessing trees with a retention index (RI) measure of fit to the traditional classification (table S2) (*15*). The resulting parsimony tree largely agrees with the existing classification at the family and superfamily levels [on average, 95.7% of terminals assigned to a family were recovered as monophyla (table S2)], although our taxon sampling was not comprehensive in some families. Model-based Bayesian methods were applied to a 340-taxon representative subset at the subfamily level.

The trees (Figs. 1 and 2) were rooted with the neuropterid orders, the presumed sister to the Coleoptera (*16*), and recovered the major subdivisions of Adephaga [37,000 known species; posterior probability (*pp*) = 1.0] and Polyphaga (>300,000 species; *pp* = 1.0) as sisters to the Myxophaga (94 species) plus Archostemata (40 species) (*8*). The Adephaga was divided into two clades containing an aquatic (Hydradephaga; diving beetles and whirligig beetles; *pp* = 0.90) and a terrestrial (Geadephaga; ground beetles and tiger beetles; *pp* = 1.0) lineage, supporting a single terrestrial-to-aquatic transition in this suborder (*13*).

In the strongly supported suborder Polyphaga, five families occupied the basal nodes (Figs. 1 and 2) (*pp* = 1.0). These families include the Decliniidae; the Scirtidae, with aquatic larvae; the Derodontidae, an ecologically diverse family from global temperate zones; and the Eucinetidae and the Clambidae. These ancestral five families were previously considered basal Elateriformia (superfamily Scirtoidea), except for Derodontidae,

[1]Department of Entomology, Natural History Museum, Cromwell Road, London SW7 5BD, UK. [2]Department of Biology, Imperial College London, Silwood Park Campus, Ascot SL5 7PY, UK. [3]Department of Zoology, Faculty of Science, Palacky University, tr. Svobody 26, 77146 Olomouc, Czech Republic. [4]Zoologische Staatssammlung München, Münchhausenstrasse 21, 81247 München, Germany. [5]Santa Barbara Museum of Natural History, 2559 Puesta del Sol Road, Santa Barbara, CA 93105–2998, USA. [6]Fisiologia i Biodiversitat Molecular, IBMB-CSIC, Jordi Girona 18-26, 08034 Barcelona, Spain. [7]Departamento de Biodiversidad y Biología Evolutiva, Museo Nacional de Ciencias Naturales, José Gutiérrez Abascal 2, 28006 Madrid, Spain. [8]Department of Biology, Pedagogical Faculty, Palacky University, Purkrabska 2, 77140 Olomouc, Czech Republic.

*These authors contributed equally to the work.
†To whom correspondence should be addressed. E-mail: a.vogler@imperial.ac.uk

which has been associated with Bostrichiformia (*9*, *10*). All five families exhibit archaic morphological features shared only with Archostemata and Adephaga (*8*, *17*). Their basal position was stable (always *pp* = 1.0) (table S3) when trees were rooted with the neuropterid orders or only with Myxophaga or Adephaga as outgroups.

All superfamilies of Polyphaga were previously grouped into five series (*4*, *9*), of which only the Scarabaeiformia (*pp* = 1.0) and the Cucujiformia (*pp* = 1.0) were strongly supported as monophyletic in this study. Staphyliniformia comprised a paraphyletic basal grade, and both Bostrichiformia and Elateriformia were polyphyletic. Relationships among the five series were poorly supported or unresolved in the consensus tree (fig. S1). Nosodendridae, usually included in Bostrichiformia near Derodontidae (*4*, *9*) but recently associated with Scirtoidea on the basis of thoracic characters (*18*), grouped instead with the nonscirtoid Elateriformia, albeit with low support (fig. S1) (*pp* = 0.59).

Within Elateriformia, the superfamilies Buprestoidea (jewel beetles; *pp* = 1.0), Dascilloidea (*pp* = 1.0), and Elateroidea (click beetles and allies; *pp* = 0.72) were supported. Our data showed that Byrrhoidea, sensu Lawrence and Newton (*9*), is paraphyletic, supporting the division of this clade (*8*) into Byrrhoidea (Byrrhidae, moss beetles; *pp* = 1.0) and Dryopoidea (riffle beetles and water pennies). The Cantharoidea (soldier beetles, fireflies, etc.) fell inside the Elateroidea, and our tree supported that bioluminescence arose repeatedly in beetles, in agreement with structural differences in luciferases (*19*). Scarabaeiformia (chafers, stag beetles, and dung beetles; *pp* = 1.0) is thought to be related to the Staphyliniformia (*4*, *14*, *20*). In our trees, it was part of an unresolved paraphyletic Staphyliniformia including the superfamilies Histeroidea (clown beetles; *pp* = 1.0); Hydrophiloidea (*pp* = 1.0), a clade of both Leiodidae and Agyrtidae (*pp* = 1.0); the Staphylinidae (rove beetles including Silphidae and carrion beetles; *pp* = 0.86); and the Hydraenidae as sister (*pp* = 0.74) to the Ptiliidae (featherwing beetles).

The hyperdiverse Cucujiformia, representing more than half of all beetles and 90 families, was strongly supported as monophyletic (Figs. 1 and 2; *pp* = 1.0). Among the seven established superfamilies, the Lymexyloidea (ship-timber beetles) was found near the base of the Tenebrionoidea (30 families; *pp* = 0.76). The Cleroidea (checkered beetles and allies) was monophyletic (*pp* = 0.70) only when including the Biphyllidae plus Byturidae (*pp* = 1.0). The latter two were formerly classified as Cucujoidea, but their association with Cleroidea is supported by genitalic characters (*11*). The Cucujoidea, comprising 34 families, was polyphyletic, but the Cerylonid series (Figs. 1 and 2 and fig. S3) (*pp* = 1.0) consisting of eight families (*21*) was monophyletic. Apart from the Sphindidae (*pp* = 1.0), the remaining cucujoid families formed a monophyletic clade (*pp* = 0.72) together with the species-rich Curculionoidea (weevils and bark beetles; *pp* = 0.73) and Chrysomeloidea (leaf beetles and longhorns).

Once the relationships among coleopteran families and superfamilies were established, we investigated the origins of beetle diversity. Diversification may be driven by feeding strategy, and we tested the hypothesis that feeding on plants (herbivory), and specifically flowering plants (angiosperms), explains the diversity of beetles (*5*). Predominantly herbivorous clades tend to contain

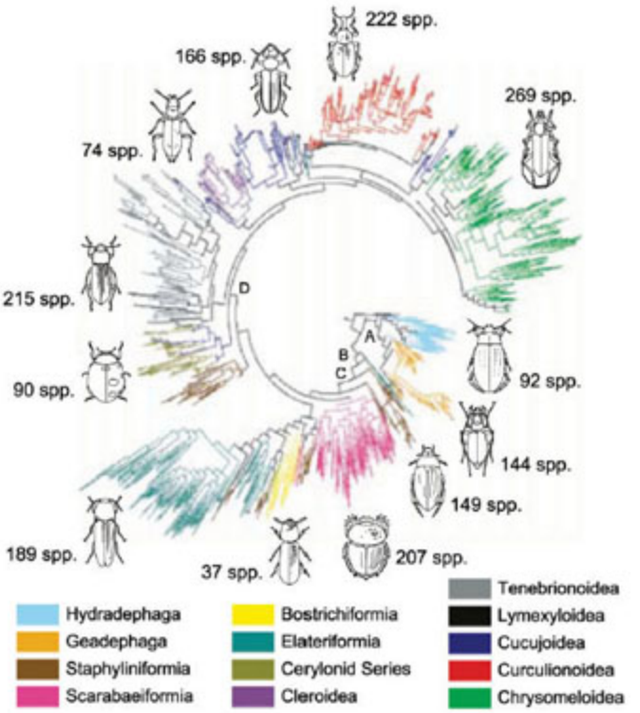

Fig. 1. One of 27 most parsimonious trees obtained from the aligned 1880-taxon matrix. The number of representatives from each major lineage analyzed (in colors) is given. Major clades are denoted by letters: A, Adephaga; B, Polyphaga; C, Polyphaga minus the ancestral five families; and D, Cucujiformia. For full details of the tree, see fig. S4.

Table 1. Comparisons of species richness between clades feeding on living plants and their sister clades with alternative feeding strategies. Restricting the comparisons to those feeding on angiosperms removes contrast 4 and adds two contrasts of angiosperm- versus gymnosperm-feeding lineages within Curculionoidea and two within Chrysomeloidea [table S4; see also (*5*)]. Plant-feeding clades include taxa feeding mainly on rotting vegetation in contrast 7 or in recently dead wood in contrast 8, but probably >70% of species in both clades are herbivorous. Excluding the last two contrasts increases the probability under a Wilcoxon test to $P = 0.28$.

	Plant-feeding	Diet	No. of species	Non–plant-feeding	Diet	No. of species
1	Byturidae	Fruits, flowers	16	Biphyllidae	Fungivorous	195
2	Languriinae	Stem borers	800	Xenoscelinae	Fungivorous, decaying vegetation	100
3	Chrysomeloidea	Herbivorous xylophagous	53,442	Nitidulidae plus Erotylid plus Cucujid series	Mostly fungivorous	7743
4	Curculionoidea	Herbivorous xylophagous	59,340	Brontinae plus Silvaninae plus Priasilphinae	Fungivorous	480
5	Epilachninae	Herbivorous	1051	Coccidulinae plus Chilocorinae plus Scymninae	Predacious	3900
6	Dascillinae	Roots	80	Rhipiceridae	Ectoparasitic on cicadas	57
7	Melolonthinae plus Orphninae plus Rutelinae plus Dynastinae	Herbivorous (and saprophagous)	16,329	Cetoniinae	Saprophagous (detritus)	4121
8	Buprestidae	Xylophagous, herbivorous, roots, leaf miners	14,000	Dryopoidea	Saprophagous, algivorous	3242

more species than nonherbivorous sister clades, but this difference was not significant [Table 1; one-tailed Wilcoxon test on contrasts in log (no. of species), $P = 0.13$] even when we distinguished between angiosperm and gymnosperm feeders ($P = 0.06$) (table S4). Similarly, of 21 significant shifts in diversification rate inferred with a robust equal rates null model (*22*, *23*), only two characterize transitions between angiosperm and gymno-

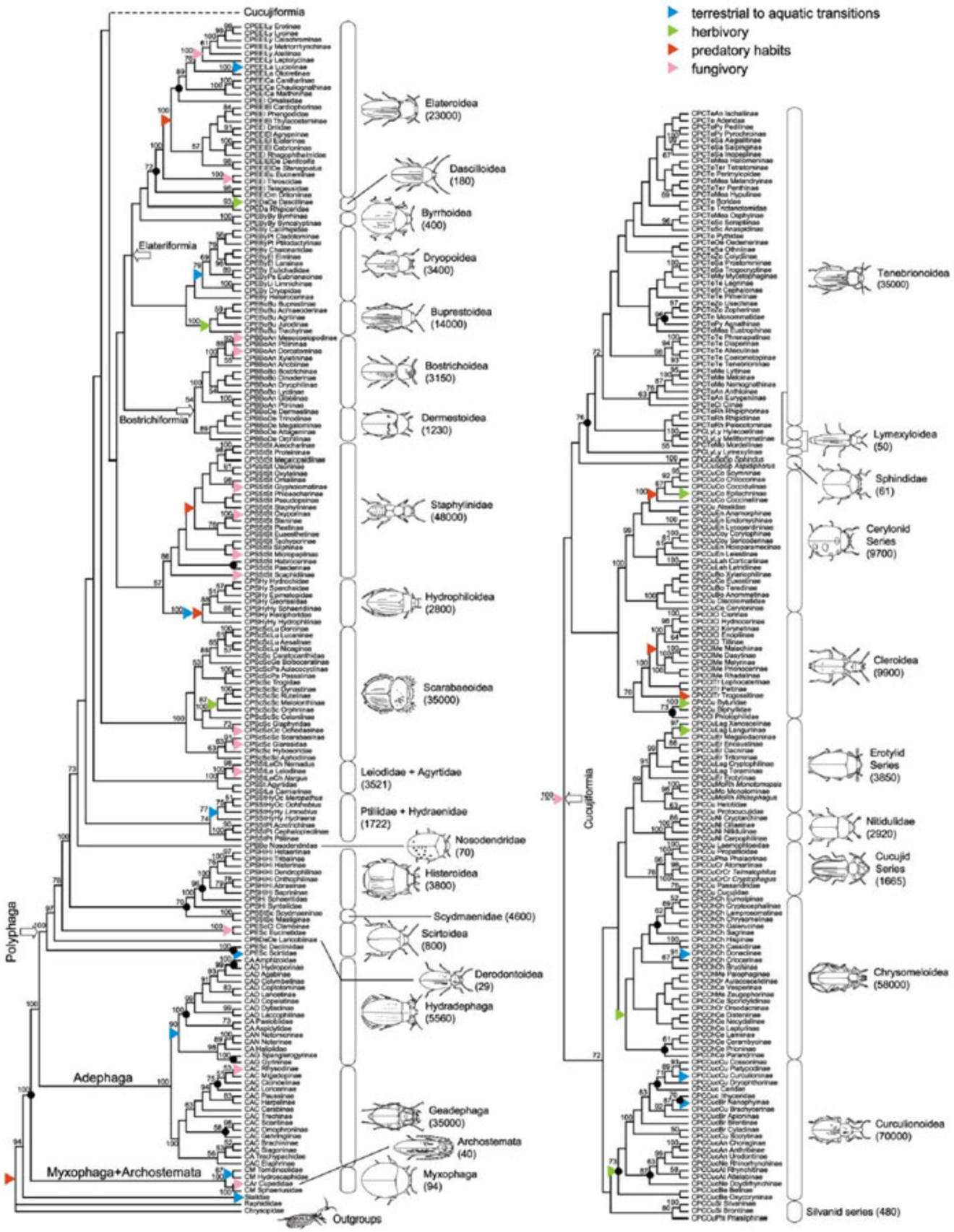

Fig. 2. The phylogeny of Coleoptera at the subfamily level. The tree was selected from the 340-taxon Bayesian analysis based on maximum congruence with the majority-rule consensus (fig. S1). Posterior probability clade support values indicated at nodes >0.5. Approximate known species numbers in terminal taxa are given in parentheses. Black circles mark significant shifts in diversification rate of sister clades (table S5). Colored triangles mark character transitions in lifestyles inferred by parsimony optimization (see figs. S2 and S3 for details).

sperm feeders, whereas the remainder showed no association with transitions to feeding on angiosperms or seed plants (table S5). A significant increase in diversification rate was inferred near the base of the Polyphaga whether herbivorous taxa were included or excluded from the analyses (table S5). Herbivory has played a role in the diversification of some beetle lineages, but the trait per se does not explain why beetles are so diverse.

Fast diversification rates also do not explain beetle diversity. Dating the tree with fossil calibration and penalized likelihood rate-smoothing (Fig. 3 and table S6) (*15*), we estimated net diversification rates across terminal taxa of 0.048 to 0.068 Myear^{-1} (table S7), slightly lower than comparable measures for the angiosperms (0.077 Myear^{-1}) (*24*). However, more than 100 modern beetle lineages were present at the first appearance of crown-group angiosperms dated to <140 Ma on the basis of pollen records (*25*), and less than one-third of extant beetle species are associated with angiosperms (table S8 and fig. S3). Therefore, the extreme diversity of beetles reflects the Jurassic origin of numerous modern lineages, high lineage survival, and the diversification into a wide range of niches, including the utilization of all parts of plants. These switches into new niches occur repeatedly as, for example, the multiple shifts from terrestrial to aquatic habits in the evolutionary history of beetles, which occurred at least 10 times (Fig. 2 and fig. S2).

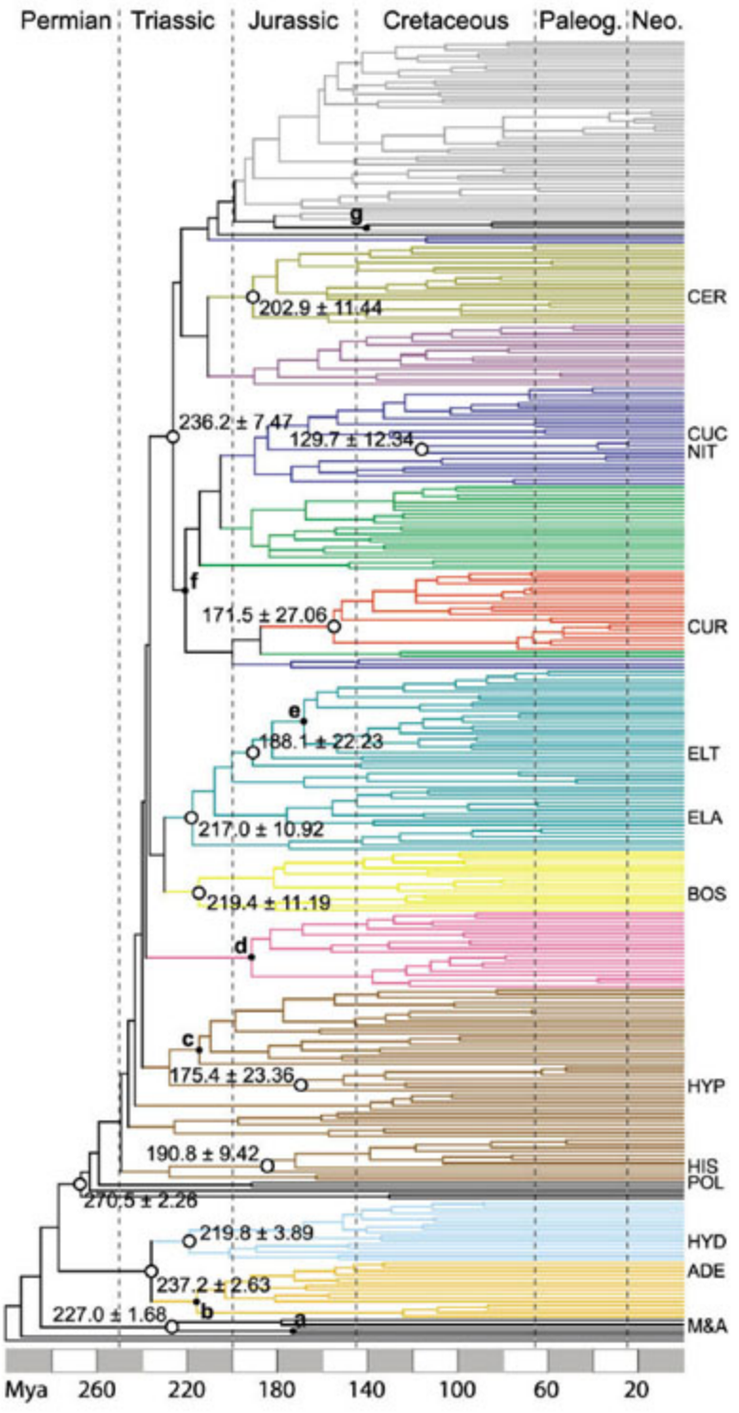

Fig. 3. A dated 340-taxon "all-compatible" consensus tree of Coleoptera from Bayesian analysis was dated with penalized likelihood placing the origin of Coleoptera at 285 Ma (*15*). Estimated number of lineages present at 200 Ma, 36; at 140 Ma, 145; and at 65 Ma, 301 (see also table S7). Colors correspond to the same groups as in Fig. 1. Numbers refer to average ages and 95% confidence intervals (*15*) of selected clades (open circles): CER, Cerylonid series; CUC, Cucujiformia; NIT, Nitidulidae; CUR, Curculionoidea; ELT, Elateroidea; ELA, Elateriformia; BOS, Bostrichiformia; HYP, Hydrophiloidea; HIS, Histeroidea; POL, Polyphaga; HYD, Hydradephaga; ADE, Adephaga; and M&A, Myxophaga and Archostemata. Seven fossil calibration points (table S6) were used to cross-validate rate-smoothing parameters (optimal value = 100) (*15*): point a, Cupedidae; b, *Sogdodromeus* (Geadephaga); c, Staphylinidae; d, *Holcorobeus* (Scarabaeoidea); e, *Elaterophanes* (Elateridae); f, *Cerambycomima* (Chrysomeloidea); and g, *Praemordella* (Mordellidae).

References and Notes

1. S. J. Gould, in *Dinosaurs in a Haystack* (Harmony, New York, 1996), pp. 377–387.
2. R. A. Crowson, *The Biology of Coleoptera* (Academic Press, London, 1981).
3. D. Grimaldi, M. S. Engel, *Evolution of the Insects* (Cambridge Univ. Press, Cambridge, 2005).
4. R. A. Crowson, *Annu. Rev. Entomol.* **5**, 111 (1960).
5. B. D. Farrell, *Science* **281**, 555 (1998).
6. A. L. V. Davis, C. H. Scholtz, T. K. Philips, *J. Biogeogr.* **29**, 1217 (2002).
7. T. L. Erwin, in *Taxonomy, Phylogeny and Zoogeography of Beetles and Ants*, G. E. Ball, Ed. (W. Junk, Dordrecht, Netherlands, 1985), pp. 437–472.
8. R. A. Crowson, *The Natural Classification of the Families of Coleoptera* (Nathaniel Lloyd, London, 1955).
9. J. F. Lawrence, A. F. Newton, in *Biology, Phylogeny, and Classification of Coleoptera: Papers Celebrating the 80th Birthday of Roy A. Crowson*, J. Pakaluk, S. A. Slipinski, Eds. (Museum i Instytut Zoologii PAN, Warzawa, 1995), pp. 779–1066.
10. R. G. Beutel, R. A. B. Leschen, *Coleoptera, Beetles. Volume 1: Morphology and Systematics*, vol. IV of *Handbuch der Zoologie/Handbook of Zoology*, N. P. Kristensen, R. G. Beutel, Eds. (de Gruyter, Berlin, 2005).
11. J. F. Lawrence, A. F. Newton, *Annu. Rev. Ecol. Syst.* **13**, 261 (1982).
12. J. Pakaluk, S. A. Slipinski, Eds., *Biology, Phylogeny, and Classification of Coleoptera: Papers Celebrating the 80th Birthday of Roy A. Crowson* (Muzeum i Instytut Zoologii PAN, Warzawa, 1995).
13. V. L. Shull, A. P. Vogler, M. D. Baker, D. R. Maddison, P. M. Hammond, *Syst. Biol.* **50**, 945 (2001).
14. M. S. Caterino, T. Hunt, A. P. Vogler, *Mol. Phylogenet. Evol.* **34**, 655 (2005).
15. Materials and methods are available as supporting material on *Science* Online.
16. W. C. Wheeler, M. Whiting, Q. D. Wheeler, J. M. Carpenter, *Cladistics* **17**, 113 (2001).
17. J. F. Lawrence, *Spec. Publ. Japan Coleopterological Soc. (Osaka)* **1**, 351 (2001).
18. S. Q. Ge, R. G. Beutel, X. K. Yang, *Syst. Entomol.* **32**, 635 (2007).
19. V. R. Viviani, *Cell. Mol. Life Sci.* **59**, 1833 (2002).
20. J. Kukalova-Peck, J. F. Lawrence, *Can. Entomol.* **125**, 181 (1993).
21. S. A. Slipinski, J. Pakaluk, in *Advances in Coleopterology*, M. Zunino, X. Belles, M. Blas, Eds. (European Association of Coleopterology, Barcelona, 1991), pp. 79–88.
22. T. J. Davies *et al.*, *Proc. Natl. Acad. Sci. U.S.A.* **101**, 1904 (2004).
23. J. B. Slowinski, C. Guyer, *Am. Nat.* **134**, 907 (1989).
24. S. Magallon, M. J. Sanderson, *Evol. Int. J. Org. Evol.* **55**, 1762 (2001).
25. E. M. Friis, K. R. Pedersen, P. R. Crane, *Palaeogeogr. Palaeoclim. Palaeoecol.* **232**, 251 (2006).

26. For collection, identification and information on species counts and life history, we thank R. Booth, M. Barclay, and colleagues from the Czech and Polish entomological community and J. Abbott (Imperial College London) for IT support. Funded by grants from Leverhulme Trust, Natural Environment Research Council (UK), Biotechnology and Biological Sciences Research Council (UK), SysResource (European Commission), Grant Agency of the Czech Republic, Ministry of Education of the Czech Republic, and German Science Association and by a Humboldt Research Fellowship to J.G.-Z. Sequences have been deposited in GenBank with accession numbers given in table S1.

Supporting Online Material

www.sciencemag.org/cgi/content/full/318/5858/1913/DC1
Materials and Methods
Figs. S1 to S5
Tables S1 to S8
References and Notes
Alignment files S1 and S2

25 June 2007; accepted 15 November 2007
10.1126/science.1146954

Induced Pluripotent Stem Cell Lines Derived from Human Somatic Cells

Junying Yu,[1,2]* Maxim A. Vodyanik,[2] Kim Smuga-Otto,[1,2] Jessica Antosiewicz-Bourget,[1,2] Jennifer L. Frane,[1] Shulan Tian,[3] Jeff Nie,[3] Gudrun A. Jonsdottir,[3] Victor Ruotti,[3] Ron Stewart,[3] Igor I. Slukvin,[2,4] James A. Thomson[1,2,5]*

Somatic cell nuclear transfer allows trans-acting factors present in the mammalian oocyte to reprogram somatic cell nuclei to an undifferentiated state. We show that four factors (*OCT4*, *SOX2*, *NANOG*, and *LIN28*) are sufficient to reprogram human somatic cells to pluripotent stem cells that exhibit the essential characteristics of embryonic stem (ES) cells. These induced pluripotent human stem cells have normal karyotypes, express telomerase activity, express cell surface markers and genes that characterize human ES cells, and maintain the developmental potential to differentiate into advanced derivatives of all three primary germ layers. Such induced pluripotent human cell lines should be useful in the production of new disease models and in drug development, as well as for applications in transplantation medicine, once technical limitations (for example, mutation through viral integration) are eliminated.

Mammalian embryogenesis elaborates distinct developmental stages in a strict temporal order. Nonetheless, because development is dictated by epigenetic rather than genetic events, differentiation is, in principle, reversible. The cloning of Dolly demonstrated that nuclei from mammalian differentiated cells can be reprogrammed to an undifferentiated state by trans-acting factors present in the oocyte (*1*), and this discovery led to a search for factors that could mediate similar reprogramming without somatic cell nuclear transfer. Recently, four transcription factors (*Oct4*, *Sox2*, *c-myc*, and *Klf4*) were shown to be sufficient to reprogram mouse fibroblasts to undifferentiated, pluripotent stem cells [termed induced pluripotent stem (iPS) cells] (*2*–*5*). Reprogramming human cells by defined factors would allow the generation of patient-specific pluripotent cell lines without somatic cell nuclear transfer, but the observation that the expression of c-Myc causes death and differentiation of human ES cells suggests that combinations of factors lacking this gene are required to reprogram human cells (*6*). We demonstrate that *OCT4*, *SOX2*, *NANOG*, and *LIN28* are sufficient to reprogram human somatic cells.

Human ES cells can reprogram myeloid precursors through cell fusion (*7*). To identify candidate reprogramming factors, we compiled a list of genes with enriched expression in human ES cells relative to that of myeloid precursors and prioritized the list based on known involvement in the establishment or maintenance of pluripotency (table S1). We then cloned these genes into a lentiviral vector (fig. S1) to screen for combinations of genes that could reprogram the differentiated derivatives of an *OCT4* knock-in human ES cell line generated through homologous recombination (*8*). In this cell line, the expression of neomycin phosphotransferase, which makes cells resistant to geneticin, is driven by an endogenous *OCT4* promoter, a gene that is highly expressed in pluripotent cells but not in differentiated cells. Thus, reprogramming events reactivating the *OCT4* promoter can be recovered by geneticin selection. The first combination of 14 genes that we selected (table S2) directed the reprogramming of adherent cells, which were derived from human ES cell–derived CD45$^+$ hematopoietic cells (*7*, *9*), to geneticin-resistant (OCT4$^+$) colonies with an ES cell morphology (fig. S2A) (*10*). These geneticin-resistant colonies expressed typical human ES cell–specific cell surface markers (fig. S2B) and formed teratomas when injected into immunocompromised severe combined immunodeficient–beige mice (fig. S2C).

By testing subsets of the 14 initial genes, we identified a core set of 4 genes, *OCT4*, *SOX2*, *NANOG*, and *LIN28*, that were capable of reprogramming human ES cell–derived somatic cells with a mesenchymal phenotype (Fig. 1A and fig. S3). Removal of either *OCT4* or *SOX2* from the reprogramming mixture eliminated the appearance of geneticin-resistant (OCT4$^+$) reprogrammed mesenchymal clones (Fig. 1A). *NANOG* showed a beneficial effect in clone recovery from human ES cell–derived mesenchymal cells but was not required for the initial appearance of such clones (Fig. 1A). These results are consistent with cell fusion–mediated reprogramming experiments, where overexpression of Nanog in mouse ES cells resulted in over a 200-fold increase in reprogramming efficiency (*11*). The expression of NANOG also improves the cloning efficiency of human ES cells (*12*) and thus could increase the survival rate of early reprogrammed cells. *LIN28* had a consistent but more modest effect on reprogrammed mesenchymal cell clone recovery (Fig. 1A).

We next tested whether *OCT4*, *SOX2*, *NANOG*, and *LIN28* are sufficient to reprogram

[1]Genome Center of Wisconsin, Madison, WI 53706–1580, USA. [2]Wisconsin National Primate Research Center, University of Wisconsin-Madison, Madison, WI 53715–1299, USA. [3]WiCell Research Institute, Madison, WI 53707–7365, USA. [4]Department of Pathology and Laboratory Medicine, University of Wisconsin-Madison, Madison, WI 53706, USA. [5]Department of Anatomy, University of Wisconsin-Madison, Madison, WI 53706–1509, USA.

*To whom correspondence should be addressed. E-mail: jyu@primate.wisc.edu (J.Y.); thomson@primate.wisc.edu (J.A.T.)

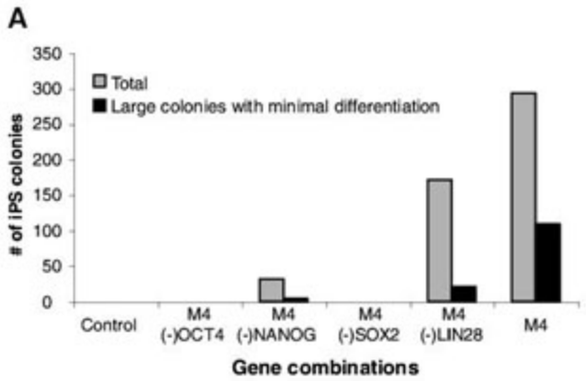

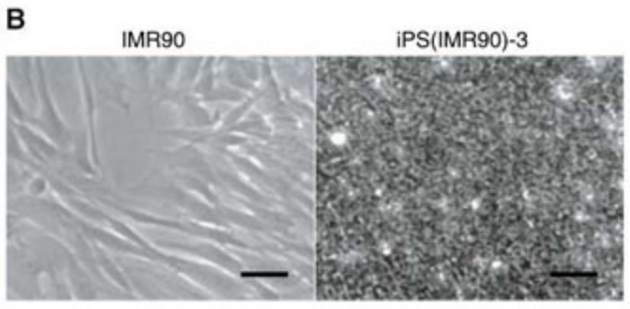

Fig. 1. Optimization of human reprogramming gene combinations with mesenchymal cells derived from human *OCT4* knock-in H1 ES cells. (**A**) Effect of removal of individual genes from the M4 (*OCT4*, *NANOG*, *SOX2*, and *LIN28*) reprogramming mixture. Human iPS colonies were counted on day 15 after lentiviral transduction. Control indicates no transduction or indicates that cells were transduced with *NANOG* only. In three independent experiments with different preparations of mesenchymal cells, individual removal of either *OCT4* or *SOX2* from reprogramming combinations eliminated the appearance of reprogrammed clones, whereas the individual removal of either *NANOG* or *LIN28* reduced the number of reprogrammed clones but did not eliminate such clones entirely. The data presented are from one representative experiment. (**B**) Bright-field images of IMR90 fibroblasts (p18) and iPS(IMR90)-3 (p18+p18), where the first p18 refers to the passage number of IMR90 fibroblasts, and the second p18 means that the reprogrammed clones underwent 18 passages on irradiated mouse embryonic fibroblasts (MEFs). Scale bars, 50 μm.

primary, genetically unmodified, diploid human fibroblasts. We initially chose IMR90 fetal fibroblasts, because these diploid human cells are being extensively characterized by the ENCODE Consortium (*13*), are readily available through the American Type Culture Collection [(ATCC), catalog number CCL-186], and have published DNA fingerprints that allow confirmation of the origin of reprogrammed clones. IMR90 cells also proliferate robustly for more than 20 passages before undergoing senescence but grow slowly in human ES cell culture conditions, a difference that provides a proliferative advantage to reprogrammed clones and aids in their selection by morphological criteria (e.g., compact colonies, high nucleus-to-cytoplasm ratios, and prominent nucleoli) alone (*14*, *15*). IMR90 cells were transduced with a combination of *OCT4*, *SOX2*, *NANOG*, and *LIN28*. Colonies with a human ES cell morphology (iPS colonies) first became visible 12 days after transduction. On day 20, a

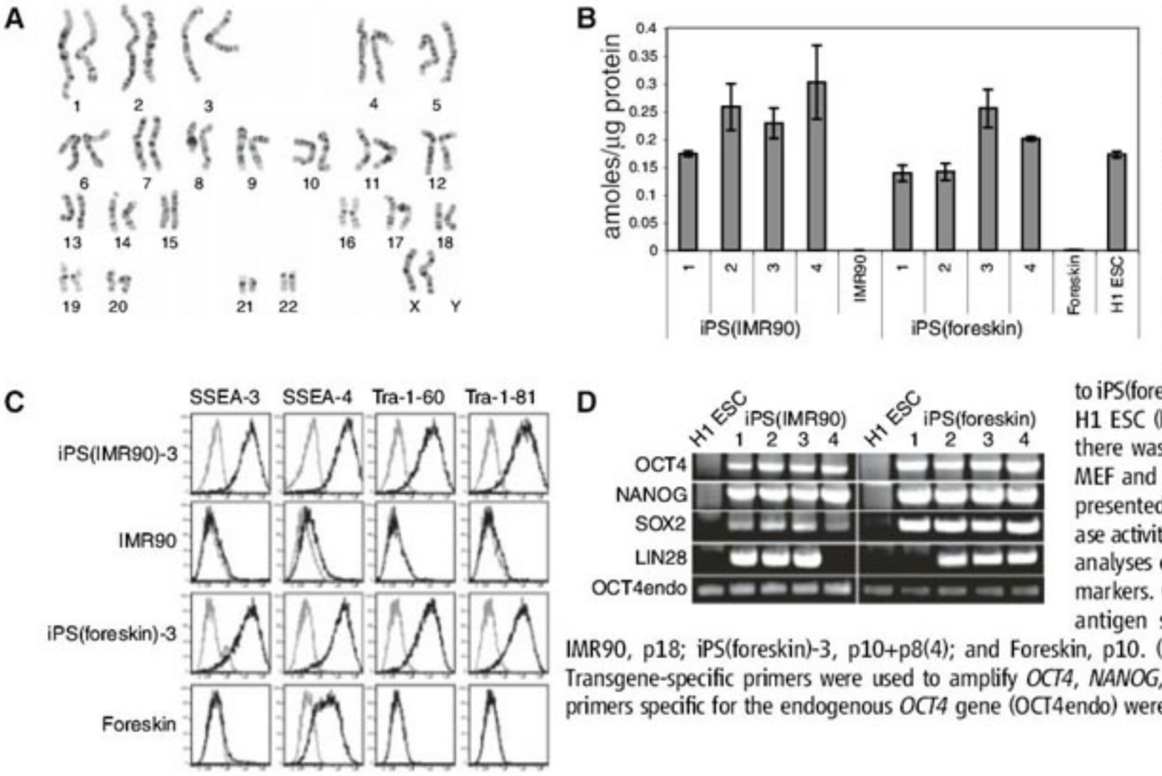

Fig. 2. Reprogramming of IMR90 fibroblasts. (**A**) G-banding chromosome analysis of iPS(IMR90)-3 (p18+p23). (**B**) Telomerase activity is shown for the following: iPS(IMR90)-1 to iPS(IMR90)-4, p18+p22(20) [where p18 refers to the passage number of IMR90 fibroblasts and where p22(20) means that the reprogrammed clones underwent 22 passages, with 2 on MEF and 20 on matrigel in human ES cell culture medium conditioned with MEF (CM)]; IMR90, p18; iPS(foreskin)-1 to iPS(foreskin)-4, p10+p9(5); Foreskin, p10; and H1 ESC (human H1 ES cells), p63(13) [where there was a total of 63 passages, with 50 on MEF and 13 on matrigel in CM]. The data are presented as mean ± SD from three telomerase activity assays. (**C**) Flow cytometry expression analyses of human ES cell-specific cell surface markers. Gray line, isotype control; black line, antigen staining. iPS(IMR90)-3, p18+p5(3); IMR90, p18; iPS(foreskin)-3, p10+p8(4); and Foreskin, p10. (**D**) Provirus integration in iPS cells. Transgene-specific primers were used to amplify *OCT4*, *NANOG*, *SOX2*, and *LIN28* provirus, whereas primers specific for the endogenous *OCT4* gene (OCT4endo) were used as a positive control.

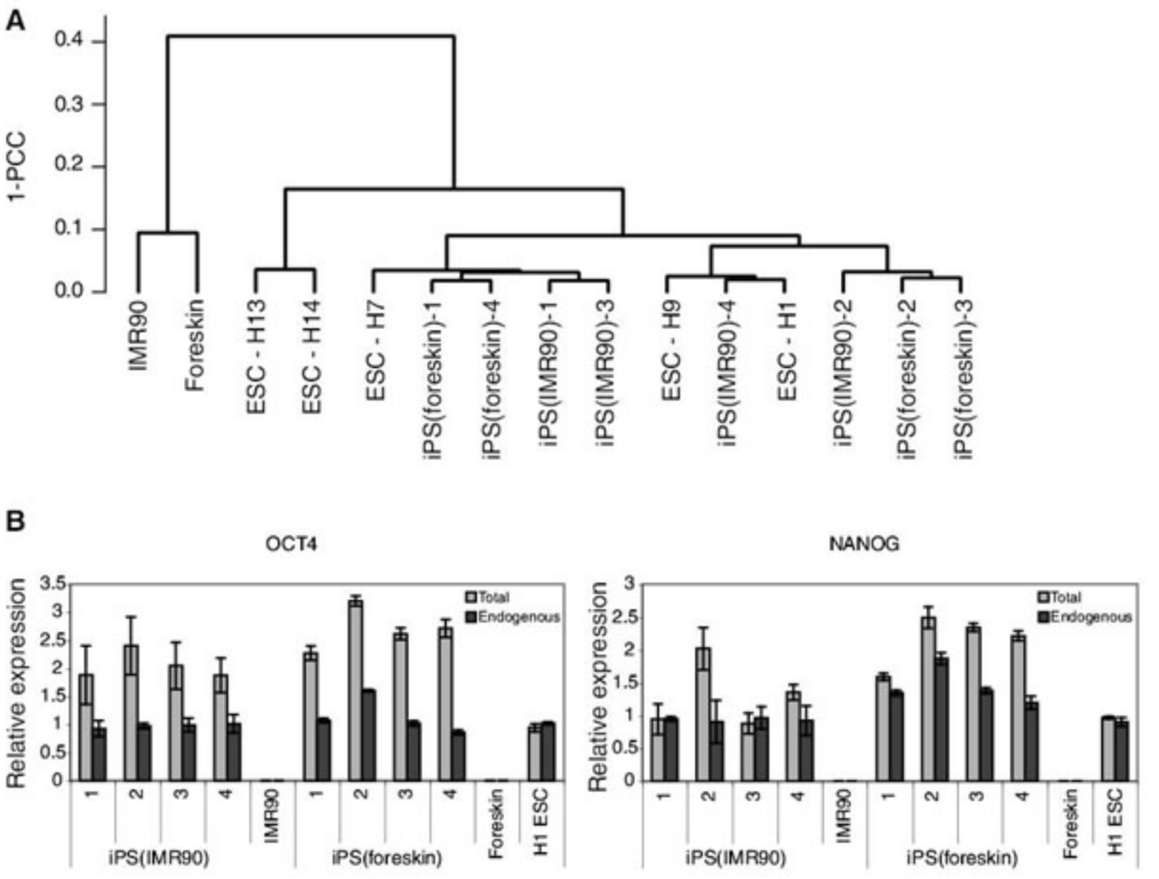

Fig. 3. Global gene expression analyses of iPS cells. (**A**) Pearson correlation analyses of global gene expression (47,759 transcripts) in iPS(IMR90) clones [p18+p6(4)], IMR90 fibroblasts (p19), iPS(foreskin) clones [p10+p7(3)], foreskin fibroblasts (p10), and five human ES cell lines: H1 [p42(12)], H7 [p73(3)], H9 [p50(5)], H13 [p43(5)], and H14 [p61(5)] ES cells (GEO accession number GSE9164). 1-PCC, Pearson correlation coefficient. (**B**) Quantitative reverse transcription–PCR analyses of OCT4 and NANOG expression in iPS(IMR90) [p18+p6(4)] and iPS(foreskin) clones [p10+p7(3)]. IMR90, p19; foreskin fibroblasts, p10; and H1 ESC, p42(12). "Endogenous" indicates that primers were included in the 3′ untranslated region measure expression of the endogenous gene only, whereas "total" indicates that primers in coding regions measure expression of both the endogenous gene and the transgene if present. The data are presented as mean ± SD from three telomerase activity assays.

total of 198 iPS colonies was visible from 0.9 million initial IMR90 cells, whereas no iPS colonies were observed in nontransduced controls. Forty-one iPS colonies were selected, 35 of which were successfully expanded for an additional 3 weeks. Four clones [iPS(IMR90)-1 to iPS(IMR90)-4] with minimal differentiation were selected for continued expansion and detailed analysis.

Each of the four iPS(IMR90) clones had a typical human ES cell morphology (Fig. 1B) and a normal karyotype at both 6 and 17 weeks of culture (Fig. 2A). Each iPS(IMR90) clone expressed telomerase activity (Fig. 2B) and the human ES cell–specific cell surface antigens SSEA-3, SSEA-4, Tra-1-60, and Tra-1-81 (Fig. 2C), whereas the parental IMR90 cells did not. Microarray analyses of gene expression of the four iPS(IMR90) clones confirmed a similarity to five human ES cell lines (H1, H7, H9, H13, and H14) and a dissimilarity to IMR90 cells (Fig. 3, table S3, and fig. S4). Although there was some variation in gene expression between different iPS(IMR90) clones (fig. S5), the variation was actually less than that between different human ES cell lines (Fig. 3A and table S3). For each of the iPS(IMR90) clones, the expression of the endogenous OCT4 and NANOG was at levels similar to that of human ES cells, but the exogenous expression of these genes varied between clones and between genes (Fig. 3B). For *OCT4*, some expression from the transgene was detectable in all of the clones, but for *NANOG*, most of the clones demonstrated minimal exogenous expression, which suggests silencing of the transgene during reprogramming. Analyses of the methylation status of the *OCT4* promoter showed differential methylation between human ES cells and IMR90 cells (fig. S6). All four iPS(IMR90) clones exhibited a demethylation pattern similar to that of human ES cells and distinct from that of the parental IMR90 cells. Both embryoid body (fig. S7) and teratoma formation (Fig. 4) demonstrated that all four of the reprogrammed iPS(IMR90) clones had the developmental potential to give rise to differentiated derivatives of all three primary germ layers. DNA fingerprinting analyses [with short tandem repeat (STR) markers] confirmed that these iPS clones were derived from IMR90 cells and confirmed that they were not from the human ES cell lines that we have in the laboratory (table S4). The STR analysis published on the ATCC website for IMR90 cells used the same primer sets and confirms the identity of the IMR90 cells used for these experiments. The iPS(IMR90) clones were passaged at the same ratio (1:6) and frequency (every 5 days) as human ES cells, had doubling times similar to that of the human H1 ES cell line assessed under the same conditions (table S5), and, as of this writing, have been in continuous culture for 22 weeks with no observed period of replicative crisis. Starting with an initial four wells of a six-well plate of iPS cells (with one clone per well, which is equivalent to about 1 million cells), after 4 weeks of additional culture, 40 total 10-cm dishes (representing about 350 million cells) of the four iPS(IMR90) clones were cryopreserved and confirmed to have normal karyotypes.

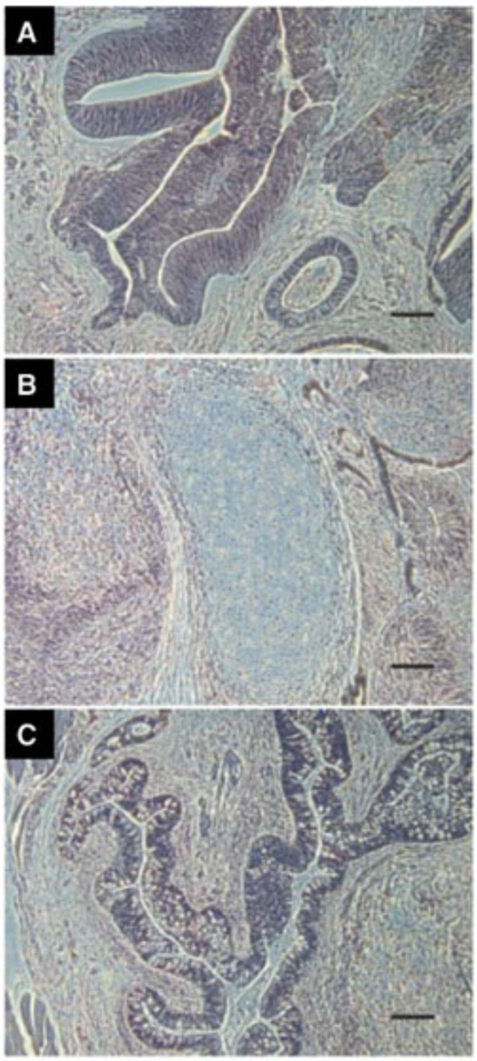

Fig. 4. Pluripotency of iPS(IMR90) cells. Hematoxylin and eosin staining of teratoma sections of iPS(IMR90)-1 (9 weeks after injection). Two six-well plates of iPS(IMR90)-1 cells on MEF (~60 to 70% confluent) were injected into the hind-limb muscle of two mice. Teratomas were obtained from all four iPS(IMR90) clones, injected both at 7 and 15 weeks after initial transduction. The two control mice, each of which were injected with ~12 million IMR90 (p19) fibroblasts, failed to form teratomas. (**A**) Neural tissue (ectoderm); (**B**) cartilage (mesoderm); (**C**) gut epithelium (endoderm). Scale bars, 0.1 mm.

Because IMR90 cells are of fetal origin, we next examined the reprogramming of postnatal fibroblasts. Human newborn foreskin fibroblasts (ATCC, catalog number CRL-2097) were transduced with *OCT4*, *SOX2*, *NANOG*, and *LIN28*. From 0.6 million foreskin fibroblasts, we obtained 57 iPS colonies. No iPS colonies were observed in nontransduced controls. Twenty-seven out of 29 chosen colonies were successfully expanded for three passages, four of which [iPS(foreskin)-1 to iPS(foreskin)-4] were selected for continued expansion and analyses. DNA fingerprinting of the iPS(foreskin) clones matched the fingerprints for the parental fibroblast cell line published on the ATCC website (table S4).

Each of the four iPS(foreskin) clones had a human ES cell morphology (fig. S8A), had a normal karyotype (fig. S8B), and expressed telomerase, cell surface markers, and genes characteristic of human ES cells (Figs. 2 and 3 and fig. S5). Each of the four iPS(foreskin) clones proliferated robustly and, as of this writing, have been in continuous culture for 17 weeks. Each clone demonstrated multilineage differentiation both in embryoid bodies and teratomas (figs. S9 and S10); however, unlike the iPS(IMR90) clones, there was variation between the clones in the lineages, apparent in teratomas examined at 5 weeks. In particular, neural differentiation was common in teratomas from iPS(foreskin) clones 1 and 2 (fig. S9A) but was largely absent in teratomas from iPS(foreskin) clones 3 and 4. Instead, there were multiple foci of columnar epithelial cells reminiscent of primitive ectoderm (fig. S9D). This is consistent with the embryoid body data (fig. S10), where the increase in PAX6 (a neural marker) in iPS(foreskin) clones 3 and 4 was minimal as compared with the other clones, a difference that correlated with a failure to downregulate NANOG and OCT4. A possible explanation for these differences is that specific integration sites in these clones allowed continued high expression of the lentiviral transgenes, partially blocking differentiation.

Polymerase chain reaction (PCR) for the four transgenes revealed that *OCT4*, *SOX2*, and *NANOG* were integrated into all four of the iPS(IMR90) clones and all four of the iPS(foreskin) clones but that *LIN28* was absent from one iPS(IMR90) clone [iPS(IMR90)-4] and from one iPS(foreskin) clone [iPS(foreskin)-1] (Fig. 2D). Thus, although *LIN28* can influence the frequency of reprogramming (Fig. 1A), these results confirm that it is not absolutely required for the initial reprogramming, nor is it subsequently required for the stable expansion of reprogrammed cells.

The human iPS cells described here meet the defining criteria that we originally proposed for human ES cells (*14*), with the notable exception that the iPS cells are not derived from embryos. Similar to human ES cells, human iPS cells should prove useful for studying the development and function of human tissues, for discovering and testing new drugs, and for transplantation medicine. For transplantation therapies based on these cells, with the exception of autoimmune diseases, patient-specific iPS cell lines should largely eliminate the concern of immune rejection. It is important to understand, however, that before the cells can be used in the clinic, additional work is required to avoid vectors that integrate into the genome, potentially introducing mutations at the insertion site. For drug development, human iPS cells should make it easier to generate panels of cell lines that more closely reflect the genetic diversity of a population and should make it possible to generate cell lines from individuals predisposed to specific diseases. Human ES cells remain controversial because their derivation

involves the destruction of human preimplantation embryos, and iPS cells remove this concern. However, further work is needed to determine whether human iPS cells differ in clinically important ways from ES cells.

References and Notes

1. I. Wilmut, A. E. Schnieke, J. McWhir, A. J. Kind, K. H. Campbell, *Nature* **385**, 810 (1997).
2. N. Maherali *et al.*, *Cell Stem Cell* **1**, 55 (2007).
3. K. Okita, T. Ichisaka, S. Yamanaka, *Nature* **448**, 313 (2007).
4. K. Takahashi, S. Yamanaka, *Cell* **126**, 663 (2006).
5. M. Wernig *et al.*, *Nature* **448**, 318 (2007).
6. T. Sumi, N. Tsuneyoshi, N. Nakatsuji, H. Suemori, *Oncogene* **26**, 5564 (2007).
7. J. Yu, M. A. Vodyanik, P. He, I. I. Slukvin, J. A. Thomson, *Stem Cells* **24**, 168 (2006).
8. T. P. Zwaka, J. A. Thomson, *Nat. Biotechnol.* **21**, 319 (2003).
9. M. A. Vodyanik, J. A. Bork, J. A. Thomson, I. I. Slukvin, *Blood* **105**, 617 (2005).
10. Materials and methods are available as supporting material on *Science* Online.
11. J. Silva, I. Chambers, S. Pollard, A. Smith, *Nature* **441**, 997 (2006).
12. H. Darr, Y. Mayshar, N. Benvenisty, *Development* **133**, 1193 (2006).
13. E. Birney *et al.*, *Nature* **447**, 799 (2007).
14. J. A. Thomson *et al.*, *Science* **282**, 1145 (1998).
15. A. Meissner, M. Wernig, R. Jaenisch, *Nat. Biotechnol.* **25**, 1177 (2007).

16. We thank the Charlotte Geyer Foundation for their support. Other funding included NIH grants P51 RR000167 and P20 GM069981. We thank K. J. Heidarsdottir, B. K. Gisladottir, M. Probasco, and C. Glennon for technical assistance, and D. J. Faupel for critical reading of the manuscript. The authors declare competing financial interests. J.A.T. owns stock, serves on the Board of Directors, and serves as Chief Scientific Officer of Cellular Dynamics International and Stem Cell Products. J.A.T. also serves as Scientific Director of the WiCell Research Institute. Microarray data have been deposited in the Gene Expression Omnibus (GEO) database (accession number GSE9164).

Supporting Online Material

www.sciencemag.org/cgi/content/full/1151526/DC1
Materials and Methods
Figs. S1 to S10
Tables S1 to S7
References

9 October 2007; accepted 14 November 2007
Published online 20 November 2007;
10.1126/science.1151526
Include this information when citing this paper.

Treatment of Sickle Cell Anemia Mouse Model with iPS Cells Generated from Autologous Skin

Jacob Hanna,[1] Marius Wernig,[1] Styliani Markoulaki,[1] Chiao-Wang Sun,[2] Alexander Meissner,[1] John P. Cassady,[1,3] Caroline Beard,[1] Tobias Brambrink,[1] Li-Chen Wu,[2] Tim M. Townes,[2]* Rudolf Jaenisch[1,3]*

It has recently been demonstrated that mouse and human fibroblasts can be reprogrammed into an embryonic stem cell–like state by introducing combinations of four transcription factors. However, the therapeutic potential of such induced pluripotent stem (iPS) cells remained undefined. By using a humanized sickle cell anemia mouse model, we show that mice can be rescued after transplantation with hematopoietic progenitors obtained in vitro from autologous iPS cells. This was achieved after correction of the human sickle hemoglobin allele by gene-specific targeting. Our results provide proof of principle for using transcription factor–induced reprogramming combined with gene and cell therapy for disease treatment in mice. The problems associated with using retroviruses and oncogenes for reprogramming need to be resolved before iPS cells can be considered for human therapy.

A major goal of human therapy is to develop methods that allow treatment of patients afflicted with genetic and degenerative disorders with a ready supply of defined transplantable cells. This has raised great interest in embryonic stem (ES) cells, which have the potential to generate all cell types in culture (*1*). ES cell–based therapy, however, would be complicated by immune rejection due to immunological incompatibility between patient and donor cells. As a result, the concept of deriving genetically identical "customized" ES-like cells by somatic cell nuclear transfer (SCNT) using a donor cell from the patient was developed (*2*). This strategy was expected to eliminate the requirement for immune suppression (*3*), but technical and ethical complexities of SCNT impede the practical realization of "therapeutic cloning" (*4*).

In a recent series of studies, mouse and human fibroblasts were reprogrammed in vitro into pluripotent stem cell–like cells (termed "induced pluripotent stem cells," or iPS) through retroviral transduction of combinations of transcription factors (*5*–*9*). This was achieved by selection for reprogrammed cells by reactivation of marked endogenous pluripotency genes Oct4 or Nanog or by subcloning of colonies based on morphological criteria (*5*–*11*). iPS cells derived from mouse and human fibroblasts are highly similar to ES cells by genetic, epigenetic, and developmental criteria. However, it remained to be determined whether mouse iPS cells obtained from adult fibroblasts can serve to restore physiological function of diseased tissues in vivo.

To gain insights into the therapeutic applicability of mouse iPS cells, we evaluated whether hematopoietic progenitors (HPs) could be derived from iPS cells in vitro for subsequent engrafting into adult recipients (*12*). Tail-tip fibroblasts were isolated from a 2-week-old Oct4-Neomycin knock-in mouse (*8*) and a 3-month-old genetically unmodified mouse. Cells were transduced with retroviruses encoding for Oct4, Sox2, Klf4, and c-Myc transcription factors (*13*). Neomycin was added 9 days after infection to fibroblasts derived from Oct4-neo mouse to select for cells that reactivated the endogenous Oct4 gene, a master regulator of pluripotency, and neomycin-resistant colonies were picked on day 20. Transduced fibroblasts from genetically unmodified mice gave rise to colonies that were picked based on morphological criteria (*10*, *11*). Ten out of 12 picked clones eventually generated cell lines with ES-like morphology that expressed ES cell markers AP, SSEA1, and Nanog. Lines designated as ITT026 and ITT4 iPS were randomly chosen from Oct4-Neo and unmodified donor cells, respectively, for further analysis (fig. S1).

Ectopic expression of homeodomain protein HoxB4 in differentiating ES cells has been shown to confer engraftment potential on in vitro–derived hematopoietic cells from ES cells grown in hematopoietic cytokines on the OP9 bone marrow stroma cell line, which has been shown to support hematopoietic differentiation (*12*, *14*). Dissociated embryoid body (EB) differentiated cells generated from V6.5 ES cells and fibroblast-derived ITTO26 and ITT4 iPS cells were infected with Moloney virus encoding green fluorescent protein (GFP)–tagged HoxB4 protein (*12*). Cells expressing CD41 and c-kit antigens (markers of early HPs), as well as markers for myeloid and erythroid differentiation, were detected at similar levels on cells differentiated from the ES and iPS lines (Fig. 1A and fig. S2). Moreover, methylcellulose colony formation assays showed that all samples formed a variety of immature and mature myeloid colonies at comparable frequencies (Fig. 1B and fig. S3). We next transplanted these in vitro–generated HPs into irradiated genetically identical adult C57black6/129Sv F1 recipient mice. HPs from both ES and iPS cells conveyed multilineage reconstitution of recipient mice, as determined by GFP content in peripheral blood for up to 20 weeks, and rescued the mice from lethal irradiation (Fig. 1C). Fluorescence-activated cell sorting (FACS) analysis showed predominant myeloid lineage formation from the transplanted progenitors (fig. S4), consistent with previous studies (*12*, *14*, *15*).

These experiments prompted us to evaluate the therapeutic potential of iPS cells derived from adult fibroblasts of mice afflicted with a genetic disorder of the hematopoietic system. The general therapeutic strategy applied involved (i) reprogramming of mutant donor fibroblasts into iPS cells, (ii) repair of the genetic defect through homologous recom-

[1]The Whitehead Institute for Biomedical Research, Cambridge, MA 02142, USA. [2]Department of Biochemistry and Molecular Genetics, University of Alabama at Birmingham, Schools of Medicine and Dentistry, Birmingham, AL 35294, USA. [3]Massachusetts Institute of Technology, Department of Biology, Cambridge, MA 02142, USA.

*To whom correspondence should be addressed. E-mail: Jaenisch@wi.mit.edu (R.J.); ttownes@uab.edu (T.M.T.)

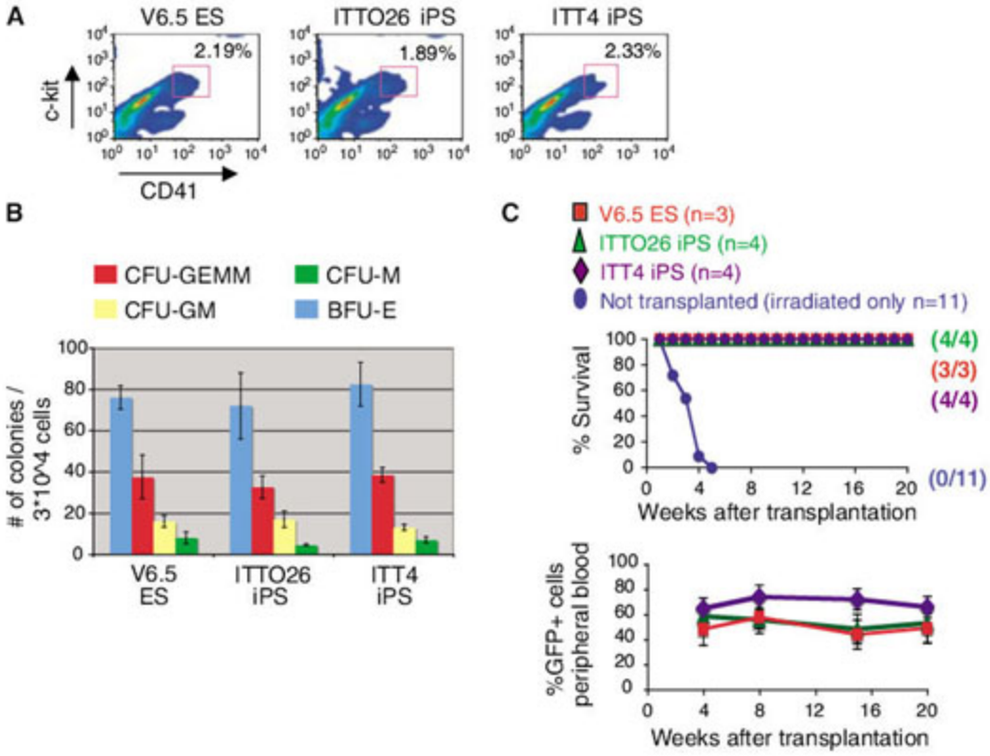

Fig. 1. Hematopoietic reconstitution by iPS cell in vitro–derived HPs. (**A**) FACS analysis of CD41 and c-kit on ES and iPS differentiated cells grown on OP-9 stroma for 6 days. (**B**) Quantitative comparison of various types of hematopoietic colonies obtained in methylcellulose cultures from iPS- and ES-derived differentiated cells grown with myeloid cytokines for 6 days. CFU, colony forming unit; GEMM, granulocyte, erythroid, macrophage, megakaryocyte multilineage; BFU-E, blood forming unit–erythroid; M, monocyte; GM, granulocyte macrophage. One out of two independent experiments is shown. (**C**) Survival curve and the percentage of GFP-positive ES- and IPS-derived HPs in the peripheral blood of transplanted or nontransplanted recipients at indicated time points after transplantation.

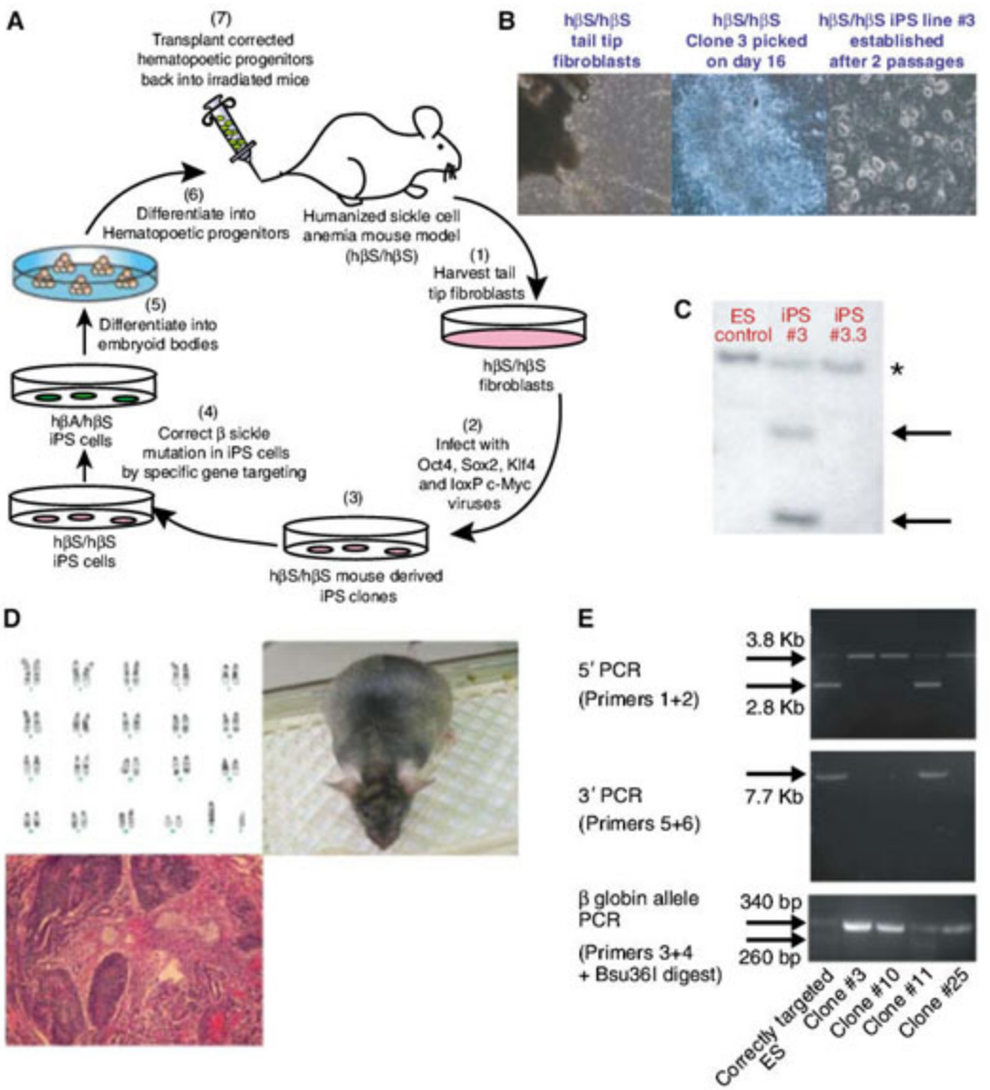

Fig. 2. Derivation of autologous iPS cells from $h\beta^S/h\beta^S$ mice and correction of the sickle allele by gene targeting. (**A**) Scheme for in vitro reprogramming of skin fibroblasts with defined transcription factors combined with gene and cell therapy to correct sickle cell anemia in mice. (**B**) Representative images of various steps of deriving $h\beta^S/h\beta^S$ iPS line #3. (**C**) Southern blot for c-Myc viral integrations in (i) ES cells, (ii) $h\beta^S/h\beta^S$ iPS line #3 and (iii) its derived subclone $h\beta^S/h\beta^S$ iPS #3.3 obtained after infection with adeno-Cre virus and deletion of the viral c-Myc copies. * indicates endogenous c-Myc band. Arrows point to transgenic copies of c-Myc. (**D**) $h\beta^S/h\beta^S$ iPS#3.3 displayed normal karyotype 40XY (upper left), was able to generate viable chimeras (upper right), and formed teratomas (bottom). (**E**) Replacement of the $h\beta^S$ gene with a $h\beta^A$ globin gene in sickle iPS cell line #3.3. Homologous recombinants were identified by PCR to identify correct 5′ and 3′ end replacement. PCR with primers 3 and 4 followed by Bsu36I digestion was used to distinguish $h\beta^S$ and $h\beta^A$ alleles. Correctly targeted clone #11 displayed identical pattern to that previously obtained for correctly targeted ES cell clone.

bination, (iii) in vitro differentiation of repaired iPS cells into HPs, and (iv) transplanting these cells into affected donor mice after irradiation (Fig. 2A).

We chose a humanized knock-in mouse model of sickle cell anemia in which the mouse α-globin genes were replaced with human α-globin genes, and the mouse β-globin genes were replaced with human Aγ and β^S (sickle) globin genes (*16*). Homozygous mice for the human β^S allele remain viable for up to 18 months but develop typical disease symptoms such as severe anemia due to erythrocyte sickling, splenic infarcts, urine concentration defects, and overall poor health (*16*). To conduct this "proof of principle" experiment, we established tail-tip–derived fibroblast cultures from an adult 12-week-old $h\beta^S/h\beta^S$ male and infected the cells with retroviruses encoding for Oct4, Sox2, and Klf4 factors and a lentivirus encoding a 2-lox c-Myc cDNA (Fig. 2B). Twenty-four clones were isolated on day 16 after infection, expanded on feeder cells, and iPS line #3 was randomly selected for further experiments. To reduce the potential risk of tumor formation due to c-Myc transgene expression (*13*), iPS cells were infected with an adenovirus encoding Cre-recombinase to delete the lentivirus-transduced c-Myc copies. One out of 10 iPS subclones (iPS #3.3) had deleted both transduced copies of c-Myc and was used for further experimentation (Fig. 2C). This subcloned cell line stained positive for pluripotency markers, had a normal karyotype, and generated teratomas and chimeras (Fig. 2D, fig. S5, and table S1).

To achieve specific gene correction of the $h\beta^S$ alleles, iPS #3.3 cells were electroporated with a targeting construct containing the human β^A wild-type globin gene (fig. S6) (*16*). Hygromycin- and gancyclovir-resistant cells were screened for correct gene targeting, and one of 72 drug resistant iPS colonies was identified as correctly targeted (clone #11) (Fig. 2E). This result shows that iPS cells can be targeted by homologous recombination at comparable efficiency to that of ES cells (*16*).

We next evaluated whether HPs derived in vitro from corrected iPS cells were able to reconstitute the hematopoietic system of sickle mice and correct their disease phenotype. Three $h\beta^S/h\beta^S$ male mice were irradiated and transplanted with corrected iPS# 3.3.11–derived HPs. All three mice demonstrated stable engraftment based on the presence of GFP+ cells in the peripheral blood for up to 12 weeks after transplantation (Fig. 3A and fig. S7). Further evidence for engraftment was shown by polymerase chain reaction (PCR) analysis of the genomic DNA from peripheral blood of treated and untreated $h\beta^S/h\beta^S$ mice using primers that amplify both $h\beta^S$ and $h\beta^A$ alleles producing 340-bp amplicons. Digestion of the amplicons with Bsu36I restriction enzyme, which cleaves the $h\beta^A$ but not the $h\beta^S$ allele (*16*), showed that DNA from peripheral blood of treated mice carried the specific bands

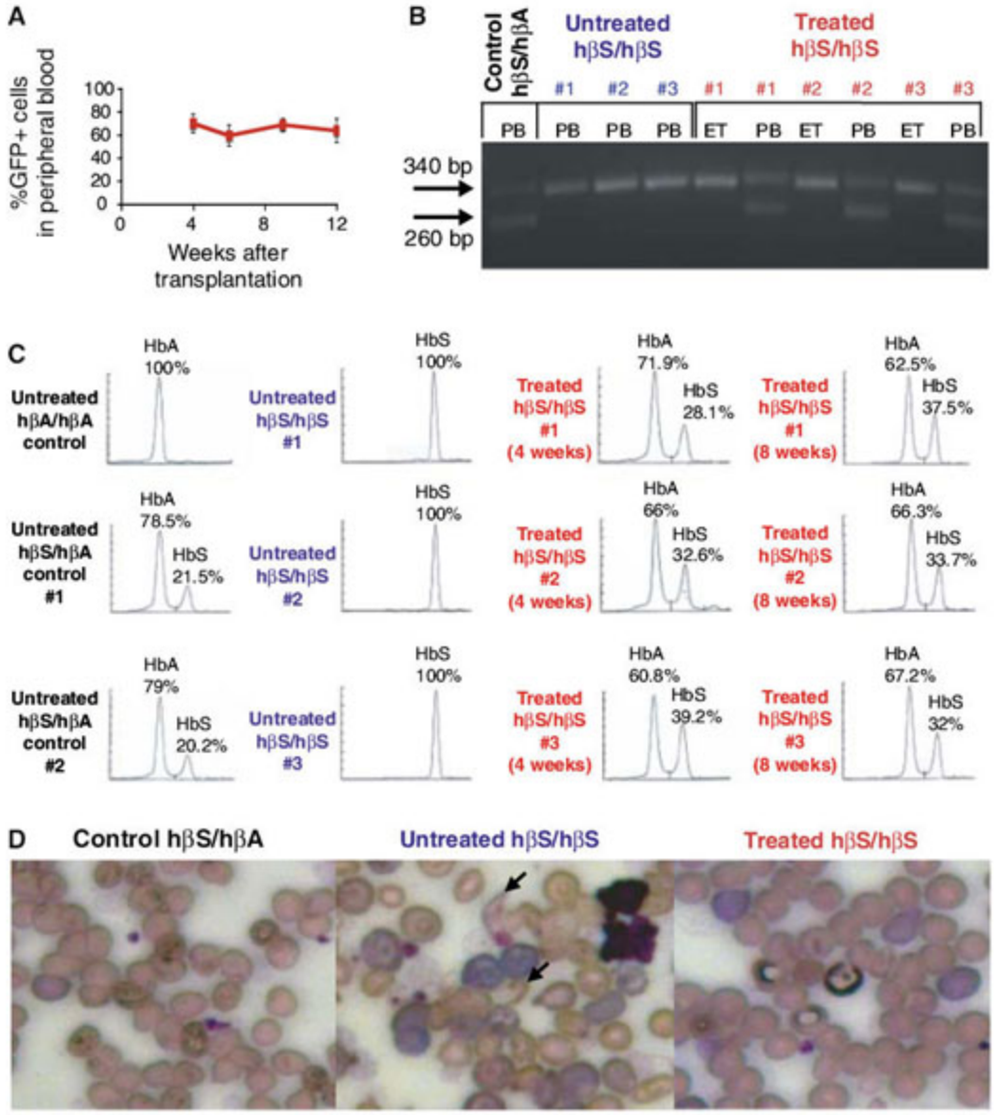

Fig. 3. Correction of sickle cell anemia phenotype by autologous genetically corrected iPS-derived HPs. (**A**) Average GFP+ content in transplanted $h\beta^S/h\beta^S$ recipients at indicated time points after transplantation ($n = 3$). (**B**) Specific detection of cells carrying $h\beta^A$ allele in blood of treated $h\beta^S/h\beta^S$ recipients by PCR in whole peripheral blood (PB) DNA followed by Bsu36I digestion. Ear-tip (ET) fibroblasts from treated $h\beta^S/h\beta^S$ mice were obtained and grown in culture 3 weeks after transplant. (**C**) Electrophoresis detection of human β globin protein in peripheral blood of $h\beta^A/h\beta^A$, $h\beta^A/h\beta^S$, untreated $h\beta^S/h\beta^S$, and treated $h\beta^S/h\beta^S$ mice 4 and 8 weeks after transplant. (**D**) Representative Wright-Giemsa stained blood smears of $h\beta^A/h\beta^S$, treated (8 weeks after transplant), and untreated $h\beta^S/h\beta^S$ mice. Arrows indicate representative sickled deformed erythrocytes.

Table 1. Restitution of disease parameters by corrected IPS-derived HPs. Hematological parameters presented were obtained 8 and 12 weeks after corrective bone marrow transplantation. Parameters for untreated $h\beta^S/h\beta^S$ and $h\beta^A/h\beta^S$ mice are used as controls. Values represent the mean ± SD. Statistical significance was determined for $h\beta^S/h\beta^S$ treated mice compared with untreated $h\beta^S/h\beta^S$ controls; *P* values were calculated using Student's *t* test; $n = 3$ each group. *, $P < 0.01$; **, $P < 0.05$. Weight values were taken from aged matched mouse groups (17 weeks of age). RBC indicates red blood cell count; Hb, hemoglobin; PCV, packed cell volume or hematocrit; RDW, red cell distribution width; MCV, mean corpuscular volume; fl, femoliter.

Mouse group ($n = 3$)	Hb (g/dl)	RBC ($\times 10^6/\mu l$)	PCV (%)	Reticulocytes (%)	RDW (%)	MCV (fl)	Urine concentration (mOsm)	Breaths (per min)	Weight (g)
$h\beta^A/h\beta^S$ control	16.1±1.3	14.7±1.7	55.8±3.1	4.53±0.7	21.9±0.9	39.5±1.1	2378±135	49.6±4.3	28.9±1.2
$h\beta^S/h\beta^S$ untreated	8.86±1.5	6.75±0.2	32.1±5.4	26.8±3.1	29.5±1.58	47.5±1.2	885±149	78.6±9.1	18.9±0.7
$h\beta^S/h\beta^S$ treated (8 weeks)	14.3±0.9*	11.8±0.7*	50.8±6.2*	9.9±2.8*	22.5±1.5*	41.4±3.0**	1827±291*	55.2±6.0*	22.8±1.4**
$h\beta^S/h\beta^S$ treated (12 weeks)	13.63±0.3*	12.62±0.6*	50.0±2.0*	10.0±1.1*	21.5±0.9*	39.7±0.7*	1754±226*	59.2±5.2**	24.1±1.2*

characteristic of the $h\beta^A$ and the $h\beta^S$ alleles (Fig. 3B). DNA samples from control $h\beta^S/h\beta^S$ mice, as well as from ear fibroblasts of treated $h\beta^S/h\beta^S$ mice, did not display any bands corresponding to the $h\beta^A$ allele (Fig. 3B).

Functional correction of the sickle cell defect was evaluated by electrophoresis for human β globin proteins A and S (HbA and HbS) in blood of untreated and treated $h\beta^S/h\beta^S$ mice. Stable and significant detection of HbA protein (mean of 65% versus 0% out of total β globin protein in untreated $h\beta^S/h\beta^S$ mice, $P < 0.01$) (fig. S8) and pronounced reduction in HbS protein 4 and 8 weeks after transplantation were seen in the blood of treated mice (Fig. 3C). Treated $h\beta^S/h\beta^S$ mice had higher levels of HbS than control heterozygous $h\beta^A/h\beta^S$ animals, most likely because only ~70% of the peripheral blood cells were derived from the iPS cells (Fig. 3A).

Morphological analysis of red blood cells (RBCs) in blood smears of untreated $h\beta^S/h\beta^S$ mice demonstrated an abundance of rigid elongated cells, consistent with sickle cell disease, and severe reticulocytosis (Fig. 3D) (*13*). In contrast, blood smears of the treated animals had a lower degree of polychromasia, which is consistent with decreased reticulocyte levels. Also, anisocytosis and poikolocytosis were decreased in treated animals (Fig. 3D). Blood count follow-up tests were performed up to 12 weeks after transplantation. Compared with untreated $h\beta^S/h\beta^S$ mice, the treated animals had marked increases in RBC counts, hemoglobin, and packed cell volume levels (Table 1). Furthermore, $h\beta^S/h\beta^S$ mice showed normalized mean corpuscular volume (MCV) and red cell distribution width (RDW) index values, which are objective parameters for anisocytosis and poikolocytosis (Table 1 and Fig. 3D). An important indicator of sickle cell disease activity and severity is the elevated level of reticulocytes in peripheral blood, which are immature RBCs (*17*), reflecting increased production of RBCs to overcome their chronic loss. Reticulocyte count was dramatically reduced in blood of recipient sickle mice after corrective bone marrow transplantation (Table 1).

Finally, we examined whether the urine concentration defect, which results from RBC sickling in renal tubules and consequent reduction in renal medullary blood flow (*18*, *19*), and the general deteriorated systemic condition reflected by lower body weight and increased breathing (*16*), had been improved. All three pathological features were ameliorated in treated $h\beta^S/h\beta^S$ mice (Table 1). In summary, our results indicate that all hematological and systemic parameters of sickle cell anemia improved substantially and were comparable to those in control mice (Fig. 3 and Table 1). Although none of the mice transplanted with iPS-derived cells showed any evidence of tumor formation, the possibility remains that malignancy may develop at later time points as a result of transgenes encoding oncogenic proteins (*13*).

The ethical debate over "therapeutic cloning," as well as the technical difficulty and inefficiency of the process (*20*), has spurred the quest to achieve reprogramming of somatic cells by defined factors (*5*–*9*, *13*). The recent strategy of deriving iPS cells from genetically unmodified donor cells based on morphological criteria (*10*, *11*), as devised in this study to derive iPS cells from mice with sickle cell anemia, has simplified their potential use for therapeutic application or for studying diseases. The correction of sickle cell anemia described in our experiments indicates that harnessing autologous iPS-derived cells for therapeutic purposes recapitulates several of the promises offered previously by SCNT: (i) no requirement for administration of immunosuppressive drugs to prevent rejection of the unmatched transplanted cells, (ii) the opportunity to repair genetic defects by homologous recombination, and (iii) the opportunity to repeatedly differentiate iPS cells into the desired cell type for continued therapy.

Even though reprogramming of human somatic cells into iPS cells has now been achieved (*6*, *9*), future therapeutic application of iPS cells in humans requires overcoming several obstacles: (i) bypassing the use of harmful oncogenes as part of the reprogramming factors (*13*), (ii) avoiding the use for gene delivery of retroviral vectors that carry the risk of insertional mutagenesis, and (iii) developing robust and reliable differentiation protocols for human iPS cells. Current advances in molecular reprogramming set the stage for devising alternative strategies, such as transient gene expression vectors, engineered membrane-permeable transcription factor proteins, or small molecules that can replace potentially hazardous factors and lessen the risk of cancer associated with the current reprogramming approach.

References and Notes

1. P. H. Lerou, G. Q. Daley, *Blood Rev.* **19**, 321 (2005).
2. R. Jaenisch, *N. Engl. J. Med.* **351**, 2787 (2004).
3. W. M. Rideout 3rd, K. Hochedlinger, M. Kyba, G. Q. Daley, R. Jaenisch, *Cell* **109**, 17 (2002).
4. I. L. Weissman, *Nature* **439**, 145 (2006).
5. N. Maherali *et al.*, *Cell Stem Cell* **1**, 55 (2007).
6. K. Takahashi *et al.*, *Cell* **131**, 861 (2007).
7. K. Takahashi, S. Yamanaka, *Cell* **126**, 663 (2006).
8. M. Wernig *et al.*, *Nature* **448**, 318 (2007).
9. J. Yu *et al.*, *Science*. Published online 20 November 2007; 10.1126/science.1151526.
10. R. Blelloch *et al.*, *Cell Stem Cell* **1**, 245 (2007).
11. A. Meissner, M. Wernig, R. Jaenisch, *Nat. Biotechnol.* **25**, 1177 (2007).
12. M. Kyba, R. C. Perlingeiro, G. Q. Daley, *Cell* **109**, 29 (2002).
13. K. Okita, T. Ichisaka, S. Yamanaka, *Nature* **448**, 313 (2007).
14. S. Eckardt *et al.*, *Genes Dev.* **21**, 409 (2007).
15. Y. Wang, F. Yates, O. Naveiras, P. Ernst, G. Q. Daley, *Proc. Natl. Acad. Sci. U.S.A.* **102**, 19081 (2005).
16. L. C. Wu *et al.*, *Blood* **108**, 1183 (2006).
17. H. F. Bunn, *N. Engl. J. Med.* **337**, 762 (1997).
18. R. Pawliuk *et al.*, *Science* **294**, 2368 (2001).
19. T. M. Ryan, D. J. Ciavatta, T. M. Townes, *Science* **278**, 873 (1997).
20. K. Hochedlinger, R. Jaenisch, *Nature* **441**, 1061 (2006).

21. We would like to thank J. Goldberg, F. Camargo, K. Pawlik, J. Dausmann, K. Velletrie, Y. Lai, and members of the Jaenisch and Townes laboratories for excellent assistance; and K. Humphries and G. Sauvageau for HoxB4 viral constructs. R.J. is supported by NIH grants 5-RO1-HDO45022, 5-R37-CA084198, and 5-RO1-CA087869, and T.M.T. by NIH grant 2-R01-HL057619. J.P.C. is a Howard Hughes Medical Institute Gilliam Fellow. J.H. is a Novartis Fellow of the Helen Hay Whitney Foundation. The authors declare no conflict of interest.

Supporting Online Material

www.sciencemag.org/cgi/content/full/1152092/DC1
Materials and Methods
Figs. S1 to S8
Table S1
References

23 October 2007; accepted 26 November 2007
Published online 6 December 2007;
10.1126/science.1152092
Include this information when citing this paper.

Structure of $G\alpha_q$-p63RhoGEF-RhoA Complex Reveals a Pathway for the Activation of RhoA by GPCRs

Susanne Lutz,[1]* Aruna Shankaranarayanan,[2,3]* Cassandra Coco,[2] Marc Ridilla,[2]† Mark R. Nance,[2] Christiane Vettel,[1] Doris Baltus,[1] Chris R. Evelyn,[4] Richard R. Neubig,[4] Thomas Wieland,[1]‡ John J. G. Tesmer[2,4]‡

The guanine nucleotide exchange factor p63RhoGEF is an effector of the heterotrimeric guanine nucleotide–binding protein (G protein) $G\alpha_q$ and thereby links $G\alpha_q$-coupled receptors (GPCRs) to the activation of the small-molecular-weight G protein RhoA. We determined the crystal structure of the $G\alpha_q$-p63RhoGEF-RhoA complex, detailing the interactions of $G\alpha_q$ with the Dbl and pleckstrin homology (DH and PH) domains of p63RhoGEF. These interactions involve the effector-binding site and the C-terminal region of $G\alpha_q$ and appear to relieve autoinhibition of the catalytic DH domain by the PH domain. Trio, Duet, and p63RhoGEF are shown to constitute a family of $G\alpha_q$ effectors that appear to activate RhoA both in vitro and in intact cells. We propose that this structure represents the crux of an ancient signal transduction pathway that is expected to be important in an array of physiological processes.

Rho guanine nucleotide triphosphatases (GTPases) are peripheral membrane proteins that regulate essential cellular processes, including cell migration, proliferation, and contraction. RhoA, Rac1, and Cdc42 are the best-characterized members of this family, and they control the dynamics of the actin cytoskeleton and also stimulate gene transcription through several transcription factors, such as the serum response factor (SRF) or nuclear factor κB (*1*, *2*). All Rho GTPases cycle between an inactive guanosine diphosphate (GDP)–bound and an active guanosine

triphosphate (GTP)–bound state, a process accelerated by a large family of Rho guanine nucleotide exchange factors (Rho GEFs). Most Rho GEFs contain a catalytic Dbl homology (DH) domain that is immediately followed by a pleckstrin homology (PH) domain (*3*, *4*). In some Rho GEFs, the PH domain appears to autoinhibit the intrinsic GEF activity of the DH domain (*5*–*7*), a constraint that is presumably released upon interaction of the PH domain with membranes or other proteins. One such autoinhibited Rho GEF is p63RhoGEF (*8*–*10*), a RhoA-specific enzyme predominantly expressed in the heart and brain (*11*). p63RhoGEF is directly activated by members of the $G\alpha_q$ subfamily of heterotrimeric guanine nucleotide–binding proteins (G proteins) (*9*, *10*) and thus is regulated by G protein–coupled receptors (GPCRs). In contrast to the $G\alpha_{13}$-regulated p115RhoGEF family (*12*, *13*), p63RhoGEF does not contain a regulator of G protein signaling homology (RH) domain (*8*–*10*) to mediate interaction with $G\alpha_q$.

To define the minimal elements of p63RhoGEF that mediate $G\alpha_q$ activation in vitro, we expressed fragments of p63RhoGEF spanning residues 149 to 477 and 149 to 580 (p63-149-477 and p63-149-580) of the total 580 amino acids in *Escherichia coli* (*14*). The p63-149-477 fragment spans a region similar to that observed in the crystal structure of the Dbl's big sister (Dbs) Rho GEF domain (*15*) (figs. S1 and S2), whereas p63-149-580 spans the entire region previously known to be important for $G\alpha_q$ binding and regulation (*9*). Both fragments possessed only weak GEF activity and stimulated nucleotide exchange on RhoA at less than 1/20th the rate of the isolated DH domain of p63RhoGEF (p63-149-338) (Fig. 1A and table S1). Of these fragments, only the p63-149-580 fragment could bind AlF_4^--activated $G\alpha_{i/q}$ (Fig. 1B, fig. S4, and table S1), a chimera in which the N-terminal helix of $G\alpha_q$ is replaced with that of $G\alpha_i$ (*16*) and that activates p63RhoGEF similarly to wild-type $G\alpha_q$ in cells (fig. S3). To precisely define the $G\alpha_q$-binding core of p63RhoGEF, we tested a series of 72 p63RhoGEF fragments spanning residues 295 to the C terminus for their ability to compete with p63-149-580 for binding $G\alpha_{i/q}$. The minimal fragment required for full inhibition corresponded to p63-295-502 (fig. S5). Like p63-149-580, p63-149-502 had low basal nucleotide exchange activity that could be activated by $G\alpha_{i/q}$ in a saturable manner by up to three- to fourfold (Fig. 1, A and C; fig. S6; and Table 1). These truncations were also functional in human embryonic kidney 293 (HEK293) cells. As with full-length p63RhoGEF (p63-FL), the p63-149-482 and p63-149-502 fragments were immunoprecipitated with the GTP hydrolysis-defective $G\alpha_qRC$

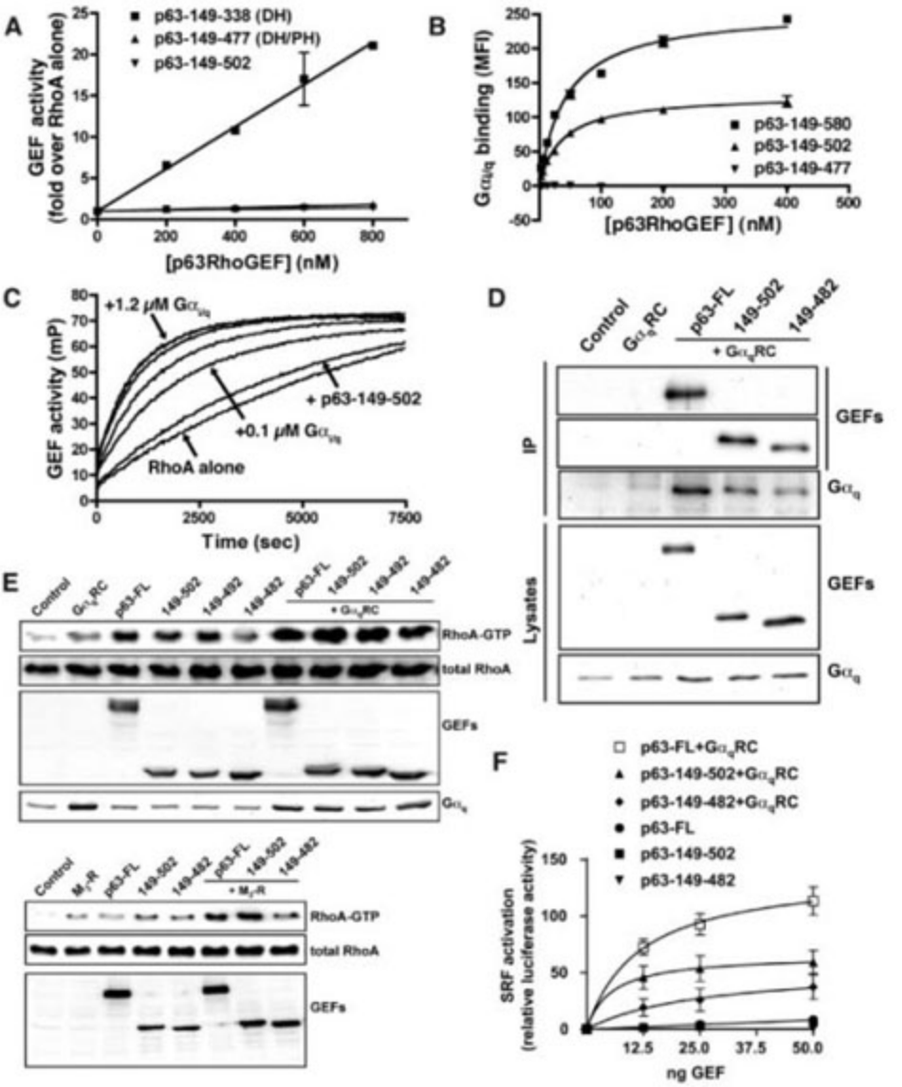

Fig. 1. Identification of the minimal fragment of p63RhoGEF regulated by $G\alpha_q$. (**A**) Basal activity of p63RhoGEF fragments. Activity was monitored by the increase in fluorescence millipolarization (mP) of a fluorescent GTP analog as it bound RhoA. In this experiment, the p63RhoGEF DH domain was 25 and 35 times more effective in activating 2 μM RhoA than were the p63-149-477 and p63-149-502 fragments, respectively. Fold activation is the p63RhoGEF catalyzed nucleotide exchange rate divided by the intrinsic rate of RhoA. (**B**) Equilibrium binding of p63RhoGEF fragments to $G\alpha_{i/q}$. Dissociation constants (K_d's) were determined by an equilibrium-binding flow cytometry protein interaction assay (FCPIA) (*27*) using various concentrations of Alexa Fluor 532–labeled p63RhoGEF fragments. In this experiment, K_d was 43 ± 4 and 36 ± 3 nM for p63-149-580 and p63-149-502, respectively. No binding was observed for p63-149-477. Binding was monitored by the median fluorescence intensity (MFI) and was corrected for nonspecific binding (MFI in the absence of AlF_4^-). (**C**) Stimulation of p63-149-502 by $G\alpha_{i/q}$. Activity was measured as in (A), but with added amounts of $G\alpha_{i/q}$. For fold activation mediated by $G\alpha_{i/q}$, see fig. S6. (**D**) Binding of p63-149-502 to activated $G\alpha_q$ in cell lysates. HEK293 cells were transfected with 1 μg of $G\alpha_qRC$, 1 μg of the respective p63RhoGEF variant plasmid, and up to 2 μg of an empty control vector. Overexpressed fragments were immunoprecipitated with an antibody to c-Myc. Antibodies to c-Myc and $G\alpha_{q/11}$ were used for analysis of precipitated proteins and equal overexpression. (**E**) Activation of RhoA in cells by p63RhoGEF fragments. HEK293 cells were transfected with 1.3 μg of the respective GEF variant plasmid, 0.6 μg of the $G\alpha_qRC$ or M_3-R–encoding plasmid, and up to 2 μg of an empty control vector. Cells overexpressing M_3-R were stimulated for 3 min with 1 mM carbachol. Endogenous RhoA-GTP was detected through its association with the Rho-binding domain of rhotekin. Total RhoA was detected with an antibody to RhoA. (**F**) SRF activation by p63RhoGEF fragments. HEK293 cells were transfected with 12.5 ng of $G\alpha_qRC$ plasmids, up to 50 ng of p63 construct plasmids, and up to 100 ng of an empty control vector as indicated. For expression of SRF-driven firefly luciferase and constitutively expressed renilla luciferase, 21 ng of pSRE.L and 4 ng of pRL.TK were cotransfected. The given values are means ± SE (n = 12 samples) of firefly/renilla luciferase ratios relative to control-transfected cells.

[1]Institute of Experimental and Clinical Pharmacology and Toxicology, Medical Faculty Mannheim, University of Heidelberg, Maybachstrasse 14, D-68169 Mannheim, Germany. [2]Life Sciences Institute, University of Michigan, Ann Arbor, MI 48109–2216, USA. [3]Department of Chemistry and Biochemistry, Institute for Cellular and Molecular Biology, University of Texas at Austin, Austin, TX 78712–0165, USA. [4]Department of Pharmacology, University of Michigan, Ann Arbor, MI 48109–0632, USA.

*These authors contributed equally to this work.
†Present address: Department of Biological Sciences, Purdue University, 915 West State Street, West Lafayette, IN 47907, USA.
‡To whom correspondence should be addressed. E-mail: tesmerjj@umich.edu (J.J.G.T.); thomas.wieland@urz.uni-heidelberg.de (T.W.)

mutant (Fig. 1D). The p63-149-482, p63-149-492, and p63-149-502 fragments also mediated $G\alpha_q$RC- and M_3 muscarinic acetylcholine receptor (M_3-R)–induced activation of RhoA and SRF (Fig. 1, E and F), with p63-149-502 being nearly as effective as wild-type p63RhoGEF.

Table 1. Properties of site-directed mutations of p63RhoGEF. K_i, inhibition constant; NB, no binding.

Protein variant	Fold activation GEF*	$G_{i/q}$ activation†	K_i (nM)‡
p63-149-502 (wild type)	1.4	3.4	29 ± 4
PH domain extension			
F471E	1.3	1.0	NB
A474D	1.2	1.0	NB
L475A	1.2	1.0	NB
P478G	1.3	1.1	NB
I479D	1.2	1.1	NB
Y481A	1.3	3.2	205 ± 52
Q482A	1.2	2.6	157 ± 32
PH domain contacts			
A351K	1.2	3.1	54 ± 1
E385A	1.4	1.2	79 ± 33
Q386A	1.2	1.5	41 ± 10
S415G	1.2	3.6	125 ± 15
DH domain contacts			
R204A	1.2	1.7	66 ± 11
Q212A	1.3	3.2	65 ± 19
W216F	1.4	1.7	76 ± 33
Y220A	1.4	2.3	126 ± 67
R244A	1.3	1.4	72 ± 24
R245A	1.4	1.2	84 ± 19

*Rate of 400 nM p63RhoGEF-catalyzed nucleotide exchange on RhoA divided by the intrinsic rate of RhoA. An average of ≥3 experiments is shown. Standard deviations were <8%. †Fold activation of 400 nM p63RhoGEF mediated by the addition of 800 nM $G\alpha_{i/q}$. An average of ≥3 experiments is shown. Standard deviations were ≤30%. ‡Various concentrations (typically ranging from 0 to 1.8 μM) of the indicated proteins were used to compete with the binding of 100 nM Alexa Fluor 532–labeled p63-149-502 to bead-bound, AlF_4^--activated $G\alpha_{i/q}$. An average of ≥3 experiments is shown (except for A351K, $n = 2$ experiments). A K_d of 50 nM for fluor-labeled p63-149-502 (see table S1) was used to convert median inhibitory concentration values to $K_i \pm$ SD.

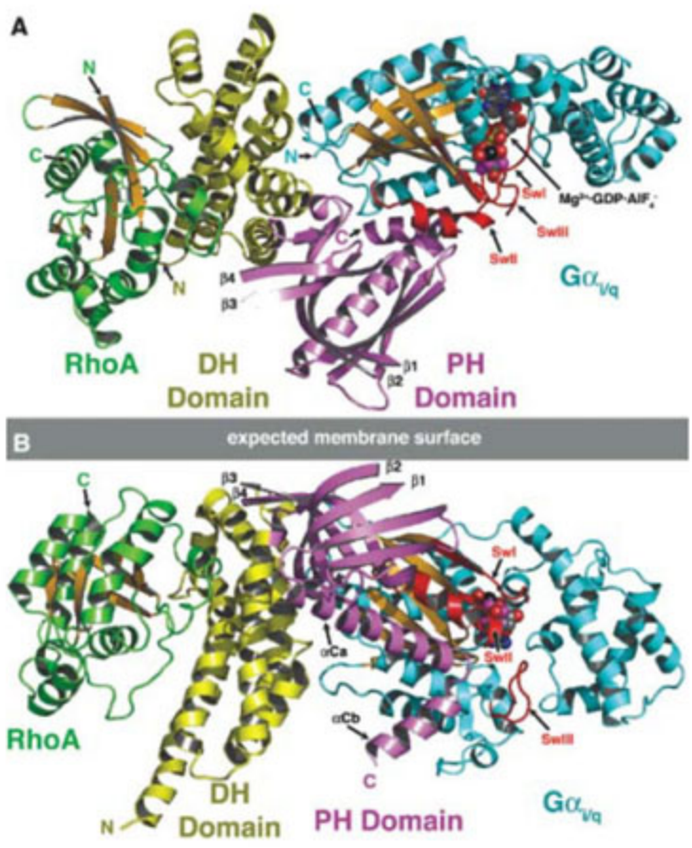

Fig. 2. Crystal structure of the $G\alpha_{i/q}$-p63RhoGEF-RhoA complex. (**A**) $G\alpha_{iq}$ interacts with both the DH and PH domains of p63RhoGEF but not with RhoA. The complex is viewed from the perspective of the expected plane of the plasma membrane. N and C denote the most N- and C-terminal residues observed for each domain. Mg^{2+}·GDP·AlF_4^- is shown as spheres. The three nucleotide-dependent conformational switches of $G\alpha_{iq}$ (SwI, SwII, and SwIII) are red. Two residues of the chimeric N terminus of $G\alpha_{iq}$ are visible and extend toward the membrane surface, consistent with the N-terminal palmitoylation sites of $G\alpha_q$ engaging the lipid bilayer while it is in complex with p63RhoGEF. (**B**) Side view of the $G\alpha_{iq}$-p63RhoGEF-RhoA complex. The PH domain is modeled in its expected orientation at the plasma membrane (*28*), which as a consequence juxtaposes the C-terminal geranylgeranylation site of RhoA with the lipid bilayer.

The molecular basis for the interaction between $G\alpha_q$ and p63RhoGEF was determined by the 3.5 Å crystal structure of p63-149-502 in complex with AlF_4^--activated $G\alpha_{iq}$ and RhoA (Fig. 2, figs. S7 and S8, and table S2). $G\alpha_{iq}$ engages both the DH and PH domains of p63RhoGEF, burying over 3600 $Å^2$ of accessible surface area (Fig. 2), using residues that are highly conserved in the Trio family but not in Dbs (fig. S2). No contacts are formed between $G\alpha_{iq}$ and RhoA. The PH domain of p63RhoGEF interacts with $G\alpha_{iq}$ primarily using a kinked amphipathic helical extension of its PH domain (αCa and αCb helices, residues 471 to 485), which docks into the effector-binding site of $G\alpha_{iq}$ (Fig. 3A). In addition, the α2-β4 and α3-β5 loops of $G\alpha_{iq}$ interact with residues in the 3_{10} helix and the β2-β3 and β4-β5 loops of the p63RhoGEF PH domain (Fig. 3B). The DH domain of p63RhoGEF interacts with the α3-β5 and α4-β6 loops and the C-terminal α5 helix of $G\alpha_{iq}$ on the side of its helical bundle opposite to the RhoA-binding site (Figs. 2 and 3B). The extreme C terminus of $G\alpha_{iq}$ packs against a notch formed by a break in the α2 helix of the DH domain, where the side chain of Tyr^{356} in $G\alpha_{iq}$ forms extensive contacts (Fig. 3B). Thus, the C terminus of Gα can mediate interactions with effectors as well as couple to specific GPCRs (*17*). Overall, the interaction of $G\alpha_{iq}$ with the PH domain of p63RhoGEF is quite similar to the interaction of $G\alpha_{iq}$ with GRK2 (Fig. 4, A and B) (*16*), with the most pronounced difference in $G\alpha_{iq}$ being the conformation of the α2-β4, α3-β5, and α4-β6 loops, which can mold themselves to form high-affinity interactions with at least two distinct effector surfaces. The conserved manner in which the PH domains of p63RhoGEF and GRK2 engage their activated heterotrimeric G protein targets ($G\alpha_{iq}$ and $G\beta\gamma$, respectively) is likewise striking (*18*) (Fig. 4, A and C).

Site-directed mutants of p63-149-502 were produced to test the role of three regions of the $G\alpha_{iq}$-p63RhoGEF interface: the interface of the $G\alpha_{iq}$ effector-binding site with the PH domain extension (Fig. 3A), the interface of the $G\alpha_{iq}$ α2-β4/α3-β5 loops with the remainder of the PH domain, and the interface of the $G\alpha_{iq}$ α3-β5/α5 region with the DH domain (Fig. 3B). Each mutant was tested for intrinsic GEF activity as well as for its ability to bind and be activated by $G\alpha_{iq}$ (Table 1). The alteration of residues in the PH domain extension eliminated $G\alpha_{iq}$ binding and activation, consistent with a recent study (*10*). Mutations in the DH and PH domains of p63RhoGEF exhibited only minimal defects in binding $G\alpha_{iq}$, but some were greatly impaired in $G\alpha_{iq}$ activation (Table 1), including Glu^{385}→Ala^{385} (E385A) (*19*) and Q386A (in the interface with the α2-β4 and α3-β5 loops of $G\alpha_q$); W216F, R244A, and R245A (in the interface with the α3-β5 and α4-β6 loops of $G\alpha_q$); and R204A (in the interface with the α5 C terminus of $G\alpha_q$).

The in vitro activation of p63RhoGEF thus appears to require the interaction of $G\alpha_{iq}$ with both the DH and PH domains (Table 1). We compared

our structure of p63-149-502 to those of the related DH and PH domains of Dbs and the N-terminal set of DH and PH domains of Trio (N-Trio), which are not activated by $G\alpha_q$ (*20*). The DH and PH domains of Dbs and N-Trio interact through conserved residues at their interface and adopt similar conformations in both GTPase-bound and free states (*15*, *20*–*22*). Although residues analogous to these are conserved in p63RhoGEF (fig. S2), the position of the PH domain of $G\alpha_{i/q}$-bound p63RhoGEF is rotated by ~50° around the α6 helix of the DH domain relative to those of Dbs and N-Trio (Fig. 4D). Thus, one way in which $G\alpha_q$ might activate p63RhoGEF is to use its domain-bridging interactions to constrain the otherwise inhibitory PH domain away from the RhoA binding site. In cells, $G\alpha_q$ could regulate p63RhoGEF in additional ways, such as by targeting p63RhoGEF to the plasma membrane, where constraints imposed by the interactions of both proteins with the phospholipid bilayer could in addition optimize the conformation of the DH and PH domains.

We next investigated whether $G\alpha_q$ binds to and stimulates the closely related set of DH and PH domains found in the C terminus of Trio (*23*) and Duet (*24*) (figs. S1 and S2). We constructed variants of Trio and Duet analogous to p63-149-502 (Trio-1894-2232 and Duet-219-558) and demonstrated that these proteins bind and are activated by $G\alpha_{i/q}$ in vitro (Fig. 5, A and B, and table S1). In cells, Trio-1894-2232 and Duet-219-558 co-immunoprecipitated with $G\alpha_q$RC (Fig. 5C), mediated $G\alpha_q$RC- as well as M_3-R–induced activation of RhoA (Fig. 5D and fig. S9), and enhanced $G\alpha_q$RC- as well as M_3-R– or H_1-R–induced activation of SRF, similar to full-length Trio and Duet (Fig. 5E). As in humans (*25*), a splice variant of the *Caenorhabditis elegans* Trio ortholog exists that contains only its C-terminal set of RhoA-specific DH and PH domains (fig. S2). This variant, UNC73 E, is also activated by the constitutively active *C. elegans* ortholog of $G\alpha_q$ and was recently shown to be a critical regulator of neuronal signaling (*26*). Thus, Trio, Duet, and p63RhoGEF define a previously unknown class of $G\alpha_{q/11}$-regulated Rho GEFs in higher vertebrates that diverged from a single ancient *trio* gene.

Our structure of the $G\alpha_{i/q}$-p63RhoGEF-RhoA complex reveals three nodes of a signal transduc-

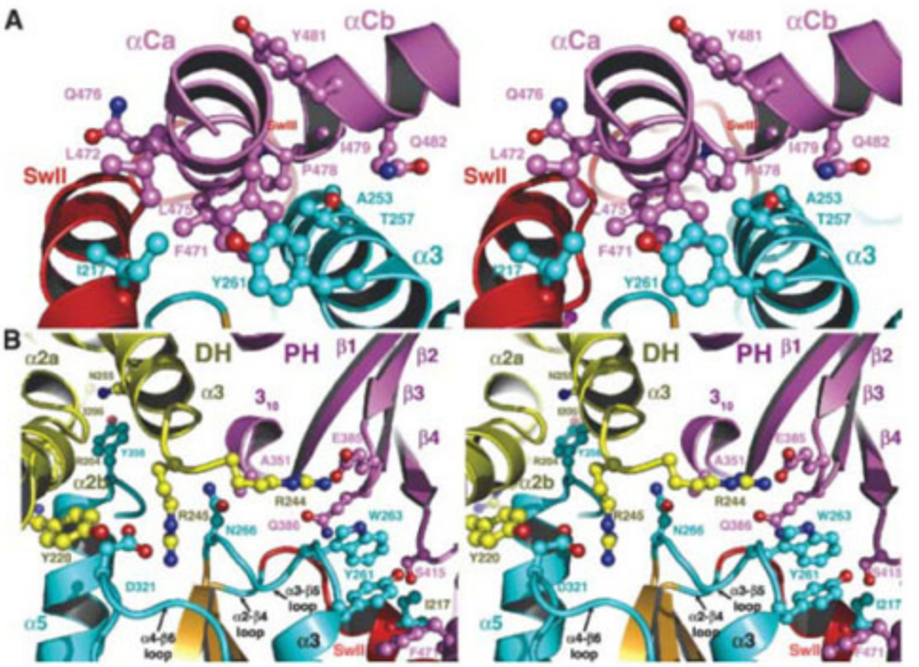

Fig. 3. Stereo views of interfaces of the $G\alpha_{i/q}$·p63RhoGEF complex. (**A**) The interaction of the PH domain extension with the effector-binding site of $G\alpha_{i/q}$. The p63RhoGEF αCa helix kinks at residue 477 to form a ~70° elbow, with the subsequent αCb helix packing against the α3 helix of $G\alpha_{i/q}$. The nonpolar interactions between residues in αCa and the effector-binding site are the most important for high-affinity binding (Table 1). Residues from the PH domain are violet, and those from $G\alpha_{i/q}$ are cyan. (**B**) Interactions of the DH and PH domains with the α-β loops and C terminus of $G\alpha_{i/q}$. The α2-β4 loop of $G\alpha_{i/q}$ appears to stack against an Arg^{244}-Glu^{385} salt bridge that bridges the DH and PH domains. The side chain of $G\alpha_q$-Tyr^{356} at the end of α5 packs against the side of the DH domain, adjacent to p63RhoGEF residues Arg^{204}, Ile^{205}, Gly^{208}, and Asn^{255}.

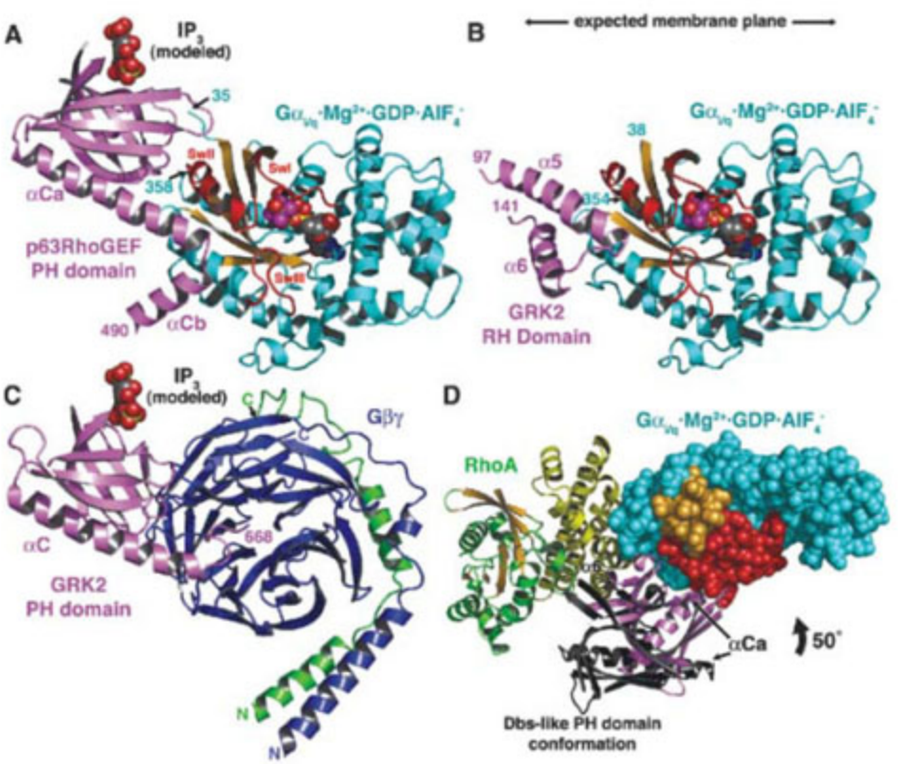

Fig. 4. Emerging themes for protein-protein interactions mediated by $G\alpha_q$ and PH domains and a model for p63RhoGEF activation by $G\alpha_{i/q}$. (**A**) The p63RhoGEF PH domain in complex with $G\alpha_{i/q}$. Inositol 1,4,5-trisphosphate (IP_3) is modeled based on the phospholipase C–γ PH domain·IP_3 complex (*29*) to help define the expected plane of the lipid bilayer. (**B**) GRK2 binds similarly to the $G\alpha_{i/q}$ effector-binding site, using exposed hydrophobic residues in its α5 helix. Only the α5 and α6 helices of the GRK2 RH domain are shown. In both the p63RhoGEF and GRK2 complexes, $G\alpha_{i/q}$ is held in an orientation in which its longest axis is roughly parallel and switch I is held relatively close to the predicted membrane surface (top). In both complexes, the switch I region appears available for the simultaneous binding of regulator of G protein signaling proteins (*30*). (**C**) The GRK2 and p63RhoGEF PH domains engage their protein targets in a similar way, using a C-terminal helical extension and the loops at one edge of the β1-β4 sheet of the PH domain to form an extensive protein interaction site (Fig. 3). (**D**) The DH and PH domains of p63RhoGEF adopt a conformation distinct from that of Dbs (black). The view is the same as in Fig. 2A. The bridging interactions of $G\alpha_{i/q}$ (spheres) appear to rotate the position of the p63RhoGEF PH domain away from the RhoA binding site on the DH domain, along the plane of the membrane surface.

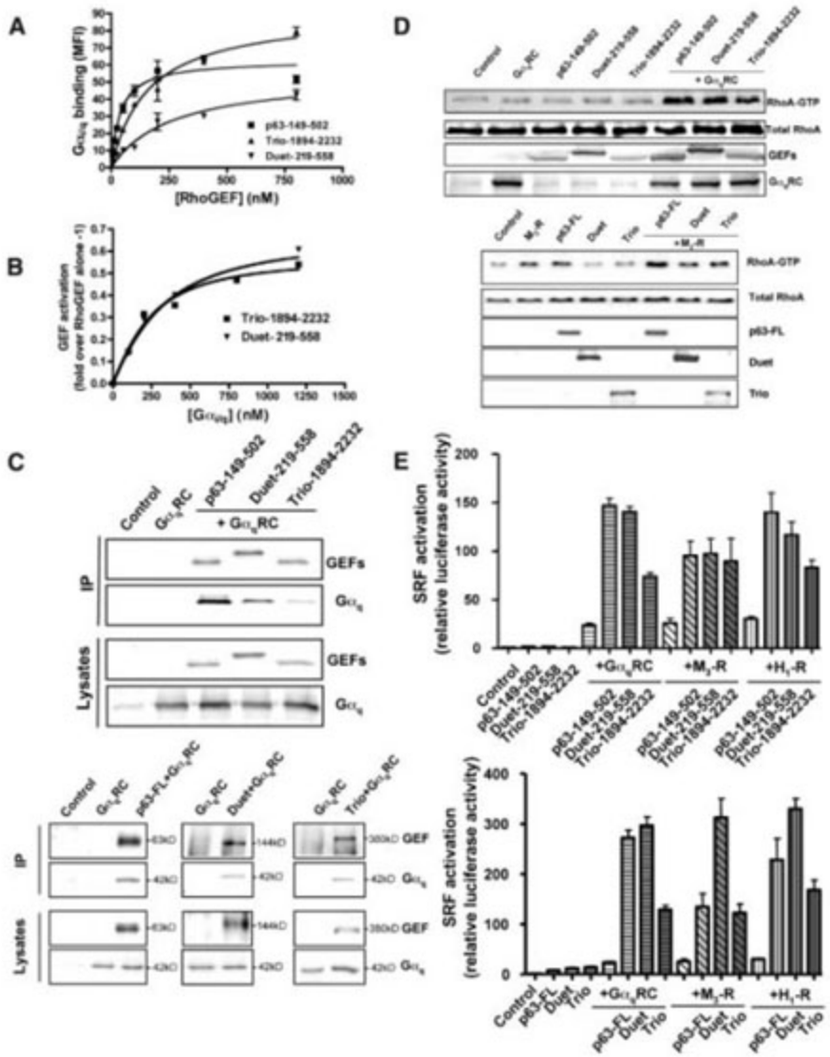

Fig. 5. Regulation of Duet and Trio by $G\alpha_q$. (**A**) Activation-dependent binding of Trio family RhoGEFs to $G\alpha_{i/q}$ measured by FCPIA. In this experiment, K_d = 39 ± 7, 160 ± 23, and 261 ± 61 nM for fluor-labeled p63-149-502, Duet-219-558, and Trio-1894-2232, respectively. (**B**) In vitro activation of Duet-219-558 and Trio-1894-2232 by $G\alpha_{i/q}$. $G\alpha_{i/q}$ activation is plotted as the fold increase over the nucleotide exchange rate catalyzed by 200 nM GEF. (**C**) Interaction of Duet-219-558, Duet-FL, Trio-1894-2232, and Trio-FL with $G\alpha_q$ in cells. HEK293 cells were transfected with 1 μg of $G\alpha_q$RC, 1 μg of truncated GEFs, p63-FL or Duet plasmid, and up to 2 μg of an empty control vector, or alternatively with 4 μg of $G\alpha_q$RC, 4 μg of the Trio plasmid, and up to 8 μg of an empty control vector. Overexpressed p63RhoGEF, Duet, and Trio were immunoprecipitated with antibodies to c-Myc, Flag, and enhanced green fluorescent protein (EGFP), respectively. (**D**) The activation of RhoA in cells by p63-149-502, p63-FL, Duet-219-558, Duet, Trio-1894-2232, and Trio ± $G\alpha_q$RC. RhoA activity in transfected HEK293 cells was determined by binding to Rhotekin (Fig. 1E). Antibodies to c-Myc (p63-FL, truncated GEFs), EGFP (Trio), Flag (Duet), and $G\alpha_{q/11}$ were used to analyze expression. (**E**) The influence of p63-149-502, p63-FL, Duet-219-558, Duet, Trio-1894-2232, and Trio on $G\alpha_q$RC-, or M_3-R– or H_1-R–induced SRF activation. HEK293 cells were transfected with 30 ng of $G\alpha_q$RC, M_3-R, or H_1-R plasmids, 60 ng of the GEF plasmids, and up to 90 ng of an empty control vector as indicated. For expression of SRF-driven firefly luciferase and constitutively expressed renilla luciferase, 21 ng of pSRE.L and 4 ng of pRL.TK were cotransfected. Cells overexpressing M_3-R and H_1-R were stimulated for 24 hours with 1 mM carbachol or 100 μM histamine, respectively. Means ± SE (n = 12 samples) of firefly/renilla luciferase ratios are given.

tion cascade caught in the act of transferring an extracellular signal from heterotrimeric to small-molecular-weight G proteins. The cornerstone of this complex is the PH domain, which engages the DH domain, $G\alpha_{i/q}$, and also probably the membrane using conserved basic residues in its β2 and β4 strands (Fig. 4 and fig. S2). The orientation we predict for $G\alpha_q$ in complex with p63RhoGEF at the membrane appears similar to that predicted for its complex with GRK2-Gβγ (*16*) (Figs. 2B and 4)–one that is dramatically different from the expected orientation for $G\alpha_q$ in the inactive Gαβγ heterotrimer (*17*). These results suggest that a conserved signaling complex is assembled at or near activated G_q-coupled receptors, wherein activated $G\alpha_q$ becomes fixed in orientation with respect to the membrane and serves as a GTP-dependent docking site for structurally diverse effector enzymes.

References and Notes

1. A. B. Jaffe, A. Hall, *Adv. Cancer Res.* **84**, 57 (2002).
2. A. J. Ridley, *Trends Cell Biol.* **16**, 522 (2006).
3. K. L. Rossman, C. J. Der, J. Sondek, *Nat. Rev. Mol. Cell Biol.* **6**, 167 (2005).
4. A. Schmidt, A. Hall, *Genes Dev.* **16**, 1587 (2002).
5. H. C. Welch *et al.*, *Cell* **108**, 809 (2002).
6. B. Das *et al.*, *J. Biol. Chem.* **275**, 15074 (2000).
7. J. M. Bellanger *et al.*, *Biol. Cell* **95**, 625 (2003).
8. S. Lutz *et al.*, *Naunyn Schmiedebergs Arch. Pharmacol.* **369**, 540 (2004).
9. S. Lutz *et al.*, *J. Biol. Chem.* **280**, 11134 (2005).
10. R. J. Rojas *et al.*, *J. Biol. Chem.* **282**, 29201 (2007).
11. M. Souchet *et al.*, *J. Cell Sci.* **115**, 629 (2002).
12. T. Kozasa *et al.*, *Science* **280**, 2109 (1998).
13. Z. Chen, W. D. Singer, P. C. Sternweis, S. R. Sprang, *Nat. Struct. Mol. Biol.* **12**, 191 (2005).
14. Information on materials and methods is available as supporting material on *Science* Online.
15. J. T. Snyder *et al.*, *Nat. Struct. Biol.* **9**, 468 (2002).
16. V. M. Tesmer, T. Kawano, A. Shankaranarayanan, T. Kozasa, J. J. Tesmer, *Science* **310**, 1686 (2005).
17. W. M. Oldham, H. E. Hamm, *Q. Rev. Biophys.* **39**, 117 (2006).
18. D. T. Lodowski, J. A. Pitcher, W. D. Capel, R. J. Lefkowitz, J. J. Tesmer, *Science* **300**, 1256 (2003).
19. Single-letter abbreviations for the amino acid residues are as follows: A, Ala; C, Cys; D, Asp; E, Glu; F, Phe; G, Gly; H, His; I, Ile; K, Lys; L, Leu; M, Met; N, Asn; P, Pro; Q, Gln; R, Arg; S, Ser; T, Thr; V, Val; W, Trp; and Y, Tyr.
20. M. K. Chhatriwala, L. Betts, D. K. Worthylake, J. Sondek, *J. Mol. Biol.* **368**, 1307 (2007).
21. K. R. Skowronek, F. Guo, Y. Zheng, N. Nassar, *J. Biol. Chem.* **279**, 37895 (2004).
22. D. K. Worthylake, K. L. Rossman, J. Sondek, *Structure* **12**, 1079 (2004).
23. A. Debant *et al.*, *Proc. Natl. Acad. Sci. U.S.A.* **93**, 5466 (1996).
24. C. E. McPherson, B. A. Eipper, R. E. Mains, *Gene* **284**, 41 (2002).
25. E. Portales-Casamar, A. Briancon-Marjollet, S. Fromont, R. Triboulet, A. Debant, *Biol. Cell* **98**, 183 (2006).
26. S. Williams *et al.*, *Genes Dev.* **21**, 2731 (2007).
27. D. L. Roman *et al.*, *Mol. Pharmacol.* **71**, 169 (2007).
28. M. A. Lemmon, K. M. Ferguson, *Biochem. Soc. Trans.* **29**, 377 (2001).
29. K. Ferguson, M. Lemmon, J. Schlessinger, P. Sigler, *Cell* **83**, 1037 (1995).
30. J. J. G. Tesmer, D. M. Berman, A. G. Gilman, S. R. Sprang, *Cell* **89**, 251 (1997).

31. We thank V. Tesmer, K.Yoshino, C.-c. Huang, H. Woolls, D. Thal, F. Uhlemann, D. Roman, T. Ferng, C. Brown, J. DelProposto, M. Larsen, and R. Sunahara for assistance. Work was supported by a junior research grant of the Medical Faculty Mannheim (to S.L.), a Midwest Affiliate of the American Heart Association predoctoral fellowship (to A.S.), and NIH grants HL086865 and HL071818 and an American Cancer Society Research Scholar grant (to J.T). The General Medicine and Cancer Institutes Collaborative Access Team has been funded in whole or in part with federal funds from the National Cancer Institute (grant Y1-CO-1020) and the National Institute of General Medical Science (grant Y1-GM-1104). Use of Life Sciences Collaborative Access Team Sector 21 was supported by the Michigan Economic Development Corporation and the Michigan Technology Tri-Corridor (grant 085P1000817). Use of the Advanced Photon Source was supported by the U.S. Department of Energy, Office of Science, Office of Basic Energy Sciences, under contract no. DE-AC02-06CH11357.

Supporting Online Material

www.sciencemag.org/cgi/content/full/318/5858/1923/DC1

Materials and Methods
Figs. S1 to S9
Tables S1 and S2
References

9 July 2007; accepted 31 October 2007
10.1126/science.1147554

Regulation of Replication Fork Progression Through Histone Supply and Demand

Anja Groth,[1] Armelle Corpet,[1] Adam J. L. Cook,[1] Daniele Roche,[1] Jiri Bartek,[2] Jiri Lukas,[2] Geneviève Almouzni[1]*

DNA replication in eukaryotes requires nucleosome disruption ahead of the replication fork and reassembly behind. An unresolved issue concerns how histone dynamics are coordinated with fork progression to maintain chromosomal stability. Here, we characterize a complex in which the human histone chaperone Asf1 and MCM2–7, the putative replicative helicase, are connected through a histone H3-H4 bridge. Depletion of Asf1 by RNA interference impedes DNA unwinding at replication sites, and similar defects arise from overproduction of new histone H3-H4 that compromises Asf1 function. These data link Asf1 chaperone function, histone supply, and replicative unwinding of DNA in chromatin. We propose that Asf1, as a histone acceptor and donor, handles parental and new histones at the replication fork via an Asf1–(H3-H4)–MCM2–7 intermediate and thus provides a means to fine-tune replication fork progression and histone supply and demand.

When one parental nucleosome is disrupted ahead of the moving replication fork, two new nucleosomes, using new and recycled histones, must assemble on the daughter strands to reproduce nucleosomal density (fig. S1A) (*1*). The regulatory link between histone biosynthesis and DNA replication (*2*) ensures the supply of new histones at the global level. However, an additional layer of regulation must be at play locally at individual replication forks to ensure balanced deposition of new and parental histones on the daughter strands. This may involve histone chaperones, such as Asf1 (antisilencing function 1), that can participate in both nucleosome assembly and disassembly (*1*, *3*). Human Asf1a and Asf1b exist in two pools (*4*), a highly mobile (cytosolic) pool that buffers excess soluble histones during replication stress and a salt-extractable pool in nuclear extracts. How the latter relates to other chromatin proteins and contributes to nuclear function remains open.

We isolated and characterized in vivo complexes containing Asf1a or Asf1b, using stable HeLa S3 cell lines expressing tagged Asf1 (e-Asf1) (*5*). Mass spectrometry and Western blotting revealed the presence of Mcm2, 4, 6, and 7 in

[1]Laboratory of Nuclear Dynamics and Genome Plasticity, UMR218 CNRS/Institut Curie, 26 rue d'Ulm, 75248 Paris cedex 05, France. [2]Institute of Cancer Biology and Centre for Genotoxic Stress Research, Danish Cancer Society, Strandboulevarden 49, Copenhagen DK-2100, Denmark.

*To whom correspondence should be addressed. E-mail: Genevieve.Almouzni@curie.fr

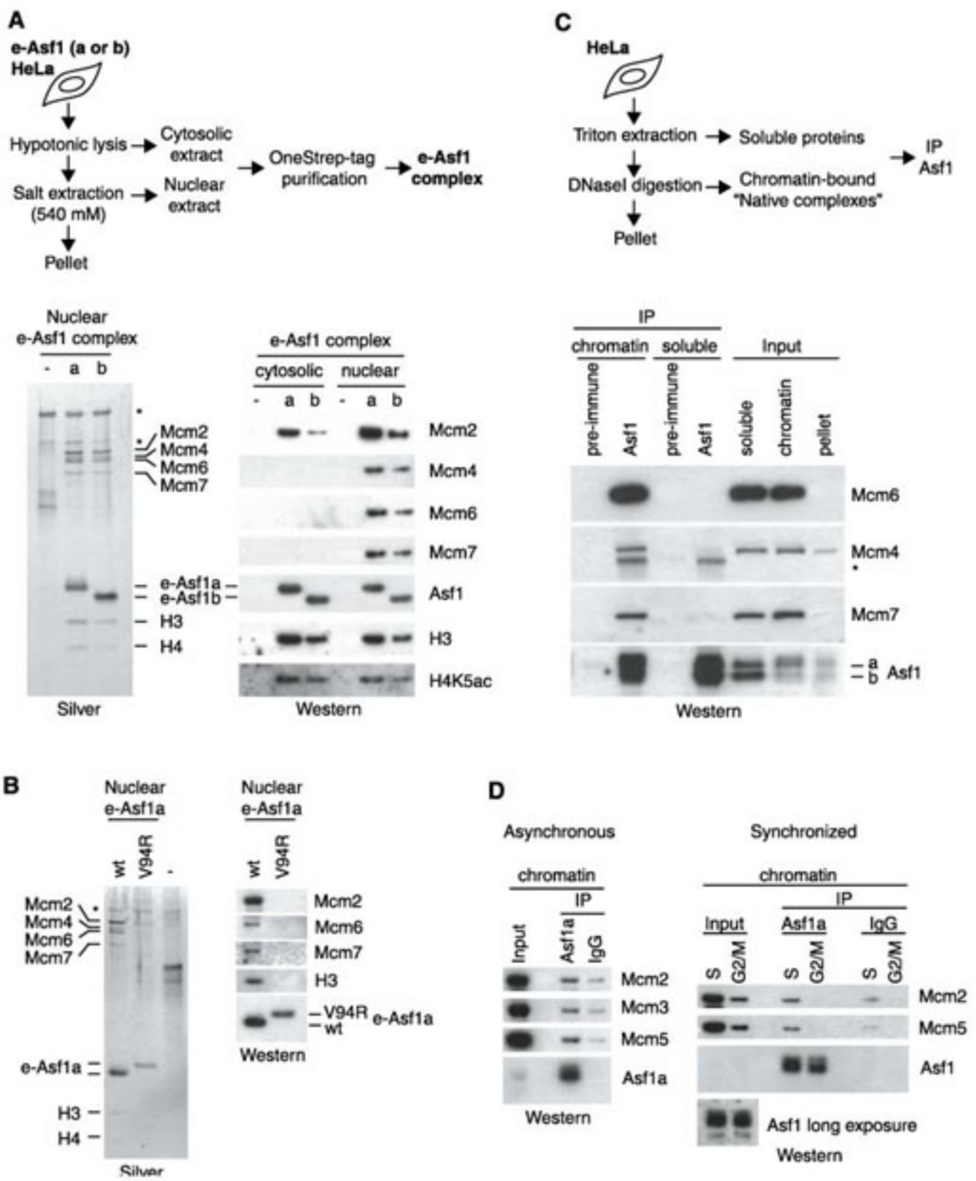

Fig. 1. Characterization of a human Asf1–(H3-H4)–MCM2–7 complex. (**A**) Purification scheme and analysis of e-Asf1 complexes by silver staining (left) and Western blotting (right). Control extract without e-Asf1 (–) was included to identify unspecific proteins (asterisks). (**B**) Silver staining and Western blot analysis of nuclear complexes containing wild-type (wt) or mutant (V94R) e-Asf1a. (**C**) Fractionation scheme and analysis of Asf1 immunoprecipitates (IP) from soluble and chromatin-bound material. The asterisk marks an unspecific band; input is 10% of starting material. (**D**) Analysis of Asf1a immunoprecipitates from asynchronous (left) and synchronized cells (right) (see also fig. S2D). Input is 3% of starting material. Under low-stringency conditions, some MCMs bind unspecifically to control beads.

the nuclear e-Asf1 (a and b) complexes, together with histone H3 and H4 (Fig. 1A and fig. S1B). By comparison, only Mcm2 was associated with cytosolic e-Asf1 (a and b) complexes. Antibodies against Mcm6 coimmunoprecipitated Asf1 and histone H3-H4 from nuclear extracts (fig. S1C), whereas Mcm2, 4, and 7 were retrieved from both cytosolic and nuclear fractions. Given that this set of MCM proteins copurifies on histone H3-H4 columns (*6*), we tested whether Asf1 associates with Mcm2, 4, 6, and 7 through histone H3-H4 by isolating complexes containing e-Asf1a mutated in the histone-binding domain, by replacement of valine at codon 94 with arginine (V94R) (*7*). e-Asf1a V94R did not bind histones H3-H4, as expected, and concomitantly MCMs were lost from the complex (Fig. 1B), which implicated histone H3-H4 in bridging the interaction between Asf1 and MCMs. To further confirm the chromatin link and to avoid the use of salt-extraction, which disrupts MCM2–7 hexamers into subcomplexes (*6*, *8*) (fig. S1C), we used deoxyribonuclease (DNase I)–solubilized chromatin (Fig. 1C and fig. S2A). Again, Mcm2, 4, 6, and 7 coimmunoprecipitated with Asf1 (Fig. 1, C and D), and Mcm6 antibodies retrieved Asf1 (a and b) (fig. S2B). Under these conditions, which preserve the hexameric MCM2–7 complex (*8*) (fig. S2B), Mcm3 and Mcm5 coimmunoprecipitated with Asf1 (Fig. 1D), which was also confirmed by epitope tag purification of e-Asf1 complexes from chromatin (fig. S2C). This interaction on chromatin occurred in S phase (Fig. 1D), which suggested a role in DNA replication.

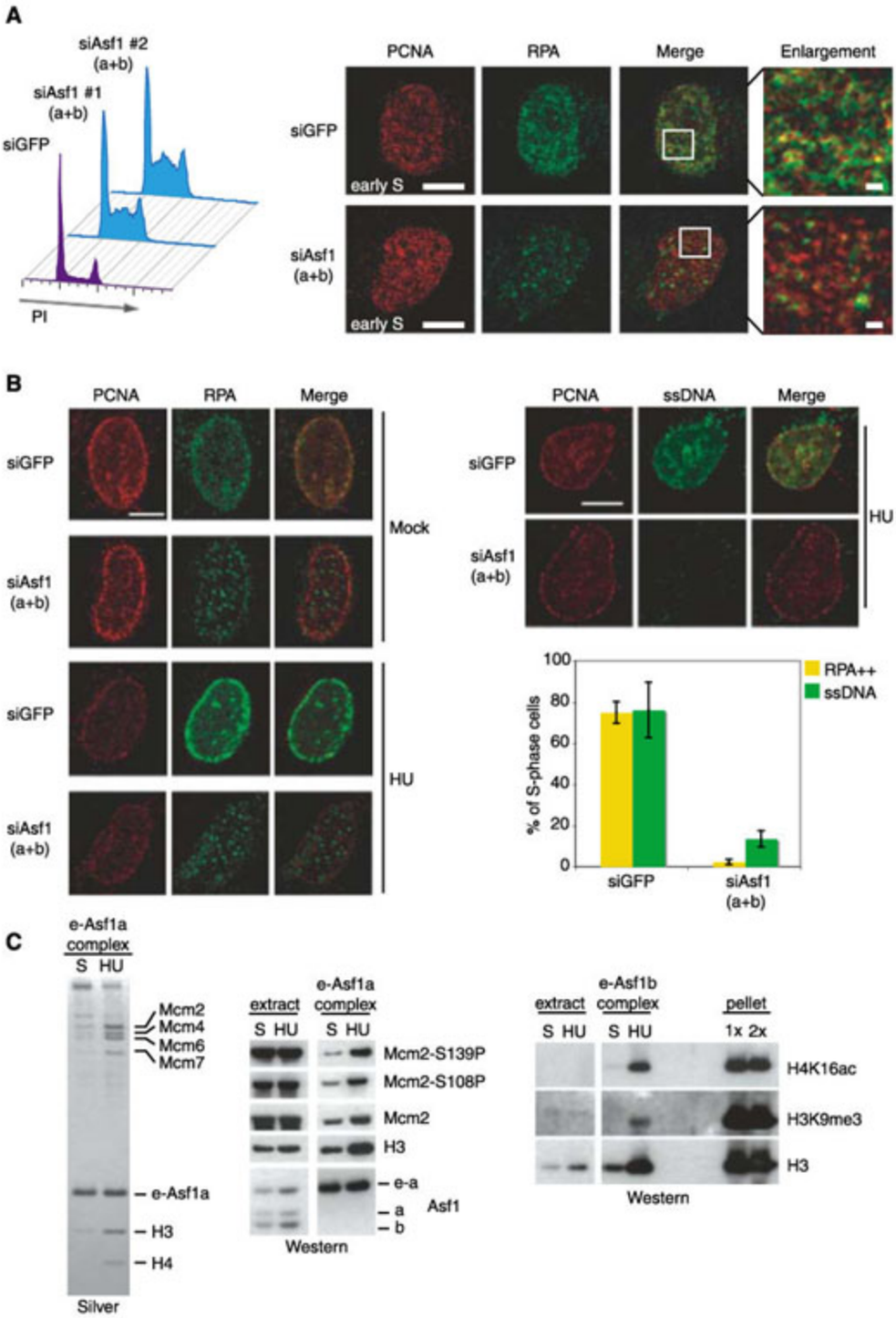

Fig. 2. Asf1 depletion impairs DNA unwinding. (**A**) (Left) Cell cycle profile of U-2-OS cells treated with small interfering RNAs (siRNAs) against Asf1a and Asf1b or control siRNA against GFP (siGFP). (Right) RPA and PCNA replication profiles in preextracted siRNA-treated cells. Images representative of five experiments show early S-phase cells with enlargements (4×). Cells in mid and late S phase showed similar defects (fig. S4A). Scale bars, 10 μm and 1 μm. (**B**) RPA accumulation (left) and ssDNA formation (right) after 1 hour of HU treatment (3 mM). For ssDNA analysis, BrdU was detected without double-stranded DNA (dsDNA) denaturation in cells prelabeled throughout their genome before HU treatment (fig. S6) (*26*). Scale bars, 10 μm. (Lower right) Quantification of PCNA-positive cells with RPA accumulation (yellow) and ssDNA formation (green). Error bars indicate standard deviation in three experiments [$n > 400$ (RPA++), $n > 130$ (ssDNA)]. (**C**) Analysis of nuclear e-Asf1 complexes purified from S-phase cells treated with or without HU, in parallel with nucleosomal histones from pellet material (1× corresponds to same cell numbers as the nuclear extract).

Fig. 2A). Although PCNA patterns were unchanged in Asf1-depleted cells, RPA replication patterns were barely detectable. Some nonextractable RPA localized to bright nuclear foci, which we identified as promyelocytic leukemia (PML) nuclear bodies, clearly distinct from PCNA replication foci (fig. S4B). We verified that Asf1 depletion did not affect RPA expression (fig. S3A) or its ability to bind ssDNA (fig. S5). Thus, absence of RPA replication profiles is consistent with the hypothesis of a helicase defect.

To examine helicase function, we analyzed DNA unwinding in the absence of polymerase progression by treating cells with hydroxyurea (HU) to deplete the nucleotide pool, which inhibits the DNA polymerase and leads to formation of ssDNA (*12*). In *Xenopus*, this response is dependent on MCM2–7 function (*13*). We measured formation of ssDNA ahead of the polymerase by detection of BrdU-substituted DNA and acute accumulation of RPA at replication sites (fig. S6). In control cells treated with HU, 75% of cells in S

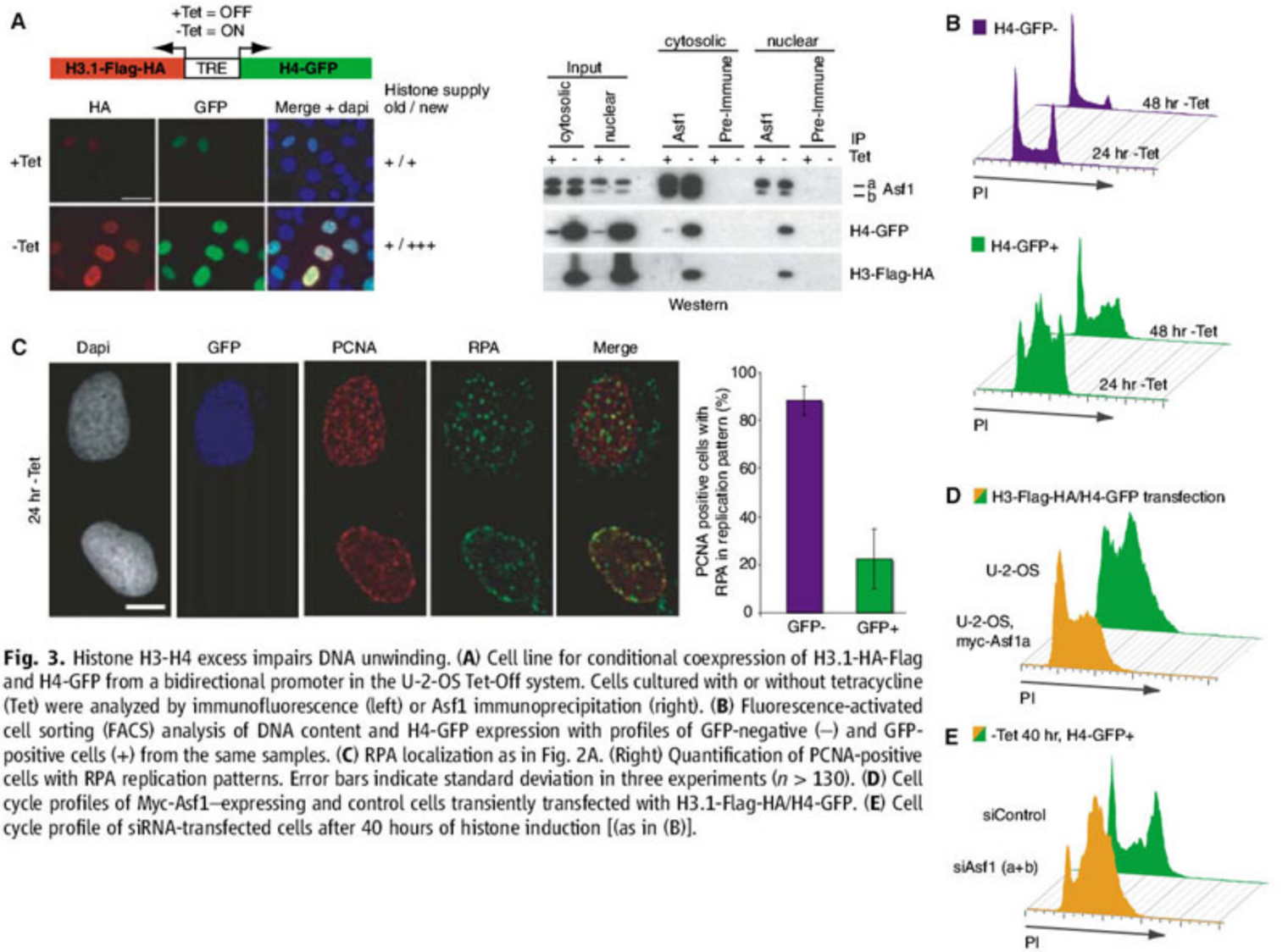

Fig. 3. Histone H3-H4 excess impairs DNA unwinding. (**A**) Cell line for conditional coexpression of H3.1-HA-Flag and H4-GFP from a bidirectional promoter in the U-2-OS Tet-Off system. Cells cultured with or without tetracycline (Tet) were analyzed by immunofluorescence (left) or Asf1 immunoprecipitation (right). (**B**) Fluorescence-activated cell sorting (FACS) analysis of DNA content and H4-GFP expression with profiles of GFP-negative (–) and GFP-positive cells (+) from the same samples. (**C**) RPA localization as in Fig. 2A. (Right) Quantification of PCNA-positive cells with RPA replication patterns. Error bars indicate standard deviation in three experiments ($n > 130$). (**D**) Cell cycle profiles of Myc-Asf1–expressing and control cells transiently transfected with H3.1-Flag-HA/H4-GFP. (**E**) Cell cycle profile of siRNA-transfected cells after 40 hours of histone induction [(as in (B)].

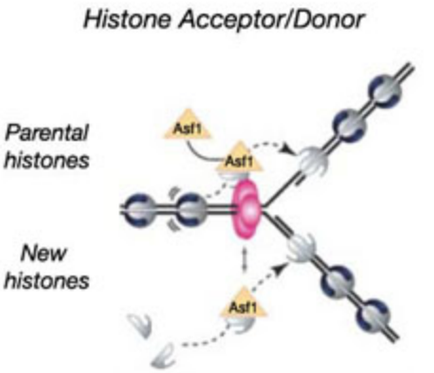

Fig. 4. Model for Asf1 function in replication as a histone acceptor and donor.

phase showed formation of ssDNA and recruitment of RPA to these ssDNA patches at replication sites (Fig. 2B). This response was dramatically reduced when we depleted Asf1 (a and b) (Asf1 knockdown), which indicated that impaired replication reflects a DNA unwinding defect and implied that DNA in chromatin cannot be properly unwound by the replicative helicase. This could reflect a direct effect of Asf1 on DNA unwinding and fork progression or indirect effects, involving DNA damage at the replication fork, replisome collapse, and/or checkpoint signaling. However, we found no evidence of DNA damage or checkpoint activation upon Asf1 knockdown (fig. S7A), and consistently, checkpoint abrogation by caffeine did not rescue the unwinding defect (fig. S7B). Instead, induction of γ-H2AX (phosphorylation of a histone 2A variant) in response to HU treatment was impaired in Asf1-depleted cells (fig. S7D), which was consistent with a role of ssDNA in checkpoint signaling (*12*, *14*). Furthermore, expression and chromatin association of several key replication factors remained unchanged upon Asf1 knockdown (fig. S7C).

To explore whether a direct role of Asf1 in facilitating DNA unwinding could involve interaction with histones and MCM2–7, we followed the Asf1–(H3-H4)–MCM complex when helicase progression is uncoupled from the polymerase. Nuclear Asf1 bound significantly more Mcm2, 4, 6, and 7 and histone H3-H4 in HU-treated cells (Fig. 2C), and within this complex, phosphorylated forms of Mcm2 were prominent [Ser^{108} and Ser^{139}, putative targets of ATR (*15*) and Cdc7-Dbf4 (*16*)], which underlined a connection to replication control. During HU treatment, continued unwinding of nucleosomal DNA ahead of the fork without DNA synthesis creates a situation where displaced parental histones cannot immediately be recycled. The accumulation of Asf1–(H3-H4)–MCM complexes under such conditions suggests that this complex could be an intermediate in parental histone transfer. Within these complexes, we could detect histone modifications, H4 with acetylated lysine 16 (H4K16Ac) and H3 with trimethylated lysine 9 (H3K9me3) (Fig. 2C). This further substantiates our hypothesis, as these chromatin marks are poorly represented on newly synthesized histones (*17*–*19*).

Our results suggest that Asf1 coordinates histone supply (parental and new) with replication fork progression. To manipulate new histone supply, we generated a conditional cell line for coexpression of tagged histone H3.1 and H4 (Fig. 3A). About 50% of the cells expressed H3.1-H4 when tetracycline was removed, and Asf1 bound the exogenous histones (Fig. 3A). After induction, the nonnucleosomal histone pool increased two- to threefold (fig. S8A), a range that is comparable to histone overload during a replication block (*4*). Increasing new histone supply interfered with DNA replication and caused acute accumulation of H3.1-H4 overexpressing cells in S phase [tracked by the green

fluorescent protein (GFP) tag on H4] (Fig. 3B). At later time points, the majority of GFP-positive cells arrested in late S/G_2. We focused on the S-phase defect to address whether H3-H4 excess mimicked Asf1 depletion. The moderate increase in H3-H4 expression did not cause DNA damage monitored by γ-H2AX (fig. S8B). We thus analyzed RPA and PCNA profiles using GFP-negative cells (no H3.1-H4 induction) as an internal control for proper localization (Fig. 3C). Again, as in Asf1-depleted cells, RPA replication patterns in histone-over-expressing cells were barely visible, with some RPA localized to bright nuclear foci mainly corresponding to PML bodies (Fig. 3C and fig. S8D). Furthermore, as for Asf1 knockdown, an excess of new H3-H4 histones impaired ssDNA formation and RPA accumulation at replication sites (fig. S9, A and B), as well as checkpoint activation in response to HU (figs. S9C and S8C). Together, these data indicate that overproduction of histone H3-H4 impairs replication by impeding DNA unwinding. Consistent with the possibility that this results from interference with Asf1 function, we found that ectopic expression of Asf1a partially alleviated the inhibitory effect of histone excess on S-phase progression (Fig. 3D). Moreover, Asf1 depletion aggravated the S-phase defect resulting from histone H3-H4 excess, in that progression into G_2 was delayed even further (Fig. 3E).

Together, our results show that replication fork progression is dependent on the histone H3-H4 chaperone, Asf1, and on an equilibrium between histone supply and demand. This dependency could ensure that replication only proceeds when nucleosomes are being formed behind the fork with a proper balance between new and parental histones H3-H4. In the most parsimonious view, we propose a model (Fig. 4) in which Asf1 uses its properties as a histone acceptor and donor to facilitate unwinding of the parental chromatin template in coordination with nucleosome assembly on daughter strands. Nucleosome disruption during replication fork passage would involve the histone-binding capacity of the MCM2–7 complex and transfer of parental histones to Asf1 through the Asf1–(H3-H4)–MCM intermediate, followed by their deposition onto daughter strands. In parallel, Asf1 would provide the additional complement of histones through its established role as a new histone donor (*4*, *20*, *21*). Asf1 knockdown will impair histone transfer and disruption of parental nucleosomes that thus present an impediment to unwinding and replication fork progression. Similarly, because of the dual function of Asf1, an excess of new histones will not leave Asf1 available for parental transfer, which impairs unwinding. On the basis of structural data (*7*, *22*, *23*), our model implies that parental histones $(H3\text{-}H4)_2$, like new histones (*24*), go through a transient dimeric state during transfer. Furthermore, the MCM–(H3-H4)–Asf1 connection opens new angles to understand MCM2–7 function in chromatin (*25*). In conclusion, having Asf1 deal with both new and parental histones could provide an ideal means to fine-tune de novo deposition and recycling with replication fork progression. By offering a mechanism to coordinate new and parental histones during replication, our model should pave the way to addressing key questions regarding chromatin-based inheritance, including transmission of histone modifications.

References and Notes

1. A. Groth, W. Rocha, A. Verreault, G. Almouzni, *Cell* **128**, 721 (2007).
2. A. Gunjan, J. Paik, A. Verreault, *Biochimie* **87**, 625 (2005).
3. B. Li, M. Carey, J. L. Workman, *Cell* **128**, 707 (2007).
4. A. Groth *et al.*, *Mol. Cell* **17**, 301 (2005).
5. Materials and methods are available as supporting material on *Science* Online.
6. Y. Ishimi, S. Ichinose, A. Omori, K. Sato, H. Kimura, *J. Biol. Chem.* **271**, 24115 (1996).
7. F. Mousson *et al.*, *Proc. Natl. Acad. Sci. U.S.A.* **102**, 5975 (2005).
8. M. Fujita, T. Kiyono, Y. Hayashi, M. Ishibashi, *J. Biol. Chem.* **272**, 10928 (1997).
9. F. Sanematsu *et al.*, *J. Biol. Chem.* **281**, 13817 (2006).
10. L. L. Schulz, J. K. Tyler, *FASEB J.* **20**, 488 (2006).
11. T. S. Takahashi, D. B. Wigley, J. C. Walter, *Trends Biochem. Sci.* **30**, 437 (2005).
12. D. Shechter, V. Costanzo, J. Gautier, *DNA Repair (Amsterdam)* **3**, 901 (2004).
13. M. Pacek, J. C. Walter, *EMBO J.* **23**, 3667 (2004).
14. T. S. Byun, M. Pacek, M. C. Yee, J. C. Walter, K. A. Cimprich, *Genes Dev.* **19**, 1040 (2005).
15. D. Cortez, G. Glick, S. J. Elledge, *Proc. Natl. Acad. Sci. U.S.A.* **101**, 10078 (2004).
16. T. Tsuji, S. B. Ficarro, W. Jiang, *Mol. Biol. Cell* **17**, 4459 (2006).
17. L. J. Benson *et al.*, *J. Biol. Chem.* **281**, 9287 (2006).
18. A. Loyola, T. Bonaldi, D. Roche, A. Imhof, G. Almouzni, *Mol. Cell* **24**, 309 (2006).
19. R. E. Sobel, R. G. Cook, C. A. Perry, A. T. Annunziato, C. D. Allis, *Proc. Natl. Acad. Sci. U.S.A.* **92**, 1237 (1995).
20. J. A. Mello *et al.*, *EMBO Rep.* **3**, 329 (2002).
21. J. K. Tyler *et al.*, *Nature* **402**, 555 (1999).
22. C. M. English, M. W. Adkins, J. J. Carson, M. E. Churchill, J. K. Tyler, *Cell* **127**, 495 (2006).
23. R. Natsume *et al.*, *Nature* **446**, 338 (2007).
24. H. Tagami, D. Ray-Gallet, G. Almouzni, Y. Nakatani, *Cell* **116**, 51 (2004).
25. R. A. Laskey, M. A. Madine, *EMBO Rep.* **4**, 26 (2003).
26. E. Raderschall, E. I. Golub, T. Haaf, *Proc. Natl. Acad. Sci. U.S.A.* **96**, 1921 (1999).

27. We thank P. Le Baccon, W. Faigle, E. Heard, A. Loyola, and A. Probst. Supported by Canceropole, Danish Cancer Society, Danish Research Council, Danish National Research Foundation, Ligue Nationale contre le Cancer, MSM6198959216, NoE Epigenome, and University of Paris 6.

Supporting Online Material

www.sciencemag.org/cgi/content/full/318/5858/1928/DC1
Materials and Methods
Figs. S1 to S9
References

9 August 2007; accepted 1 November 2007
10.1126/science.1148992

Switching from Repression to Activation: MicroRNAs Can Up-Regulate Translation

Shobha Vasudevan, Yingchun Tong, Joan A. Steitz*

AU-rich elements (AREs) and microRNA target sites are conserved sequences in messenger RNA (mRNA) 3′ untranslated regions (3′UTRs) that control gene expression posttranscriptionally. Upon cell cycle arrest, the ARE in tumor necrosis factor–α (TNFα) mRNA is transformed into a translation activation signal, recruiting Argonaute (AGO) and fragile X mental retardation–related protein 1 (FXR1), factors associated with micro-ribonucleoproteins (microRNPs). We show that human microRNA miR369-3 directs association of these proteins with the AREs to activate translation. Furthermore, we document that two well-studied microRNAs—Let-7 and the synthetic microRNA miRcxcr4—likewise induce translation up-regulation of target mRNAs on cell cycle arrest, yet they repress translation in proliferating cells. Thus, activation is a common function of microRNPs on cell cycle arrest. We propose that translation regulation by microRNPs oscillates between repression and activation during the cell cycle.

AU-rich elements (AREs) bind specific proteins to regulate mRNA stability or translation in response to external and internal stimuli (*1*). MicroRNAs are small non-coding RNAs that recruit an Argonaute (AGO) protein complex to a complementary target mRNA, which results in translation repression or degradation of the mRNA (*2*, *3*). We previously demonstrated that the tumor necrosis factor–α (TNFα) ARE can be transformed by serum starvation, which arrests the cell cycle, into a translation activation signal (*4*). AGO2 and fragile X mental retardation–related protein 1 (FXR1) associate with the ARE on translation activation; both proteins are required to increase translation efficiency. Two key questions arose. First, is binding of the AGO2-FXR1 complex, which activates translation, directed by a microRNA complementary to the ARE? Second, can micro-ribonucleoproteins (microRNPs), in general, up-regulate translation under growth-arrest conditions, thereby switching between repressing and activating roles in response to the cell cycle?

A bioinformatic screen identified five microRNAs in miRBASE with seed regions complementary to the TNFα ARE, not including miR16 (*5*) [see supporting online material (SOM) text]. Of these, only human miR369-3 (Fig. 1A and fig. S1) tested positive in the following assays. Its seed sequence potentially forms base pairs with two target sites [seed1 and seed2, shaded in (Fig. 1A)] within the minimal TNFα ARE needed for translation activa-

tion of the luciferase reporter (*4*). We find that expression of miR369-3 in HEK293 cells is reduced in serum-grown cells (Fig. 1B) and that miR369-3 is necessary for translation up-regulation of the ARE reporter. A small interfering RNA (siRNA) directed against the loop region of the miR369-3 precursor (si-pre369) (Fig. 1B and fig. S2) prevented translation (knocked down) up-regulation under serum-starved conditions. When knockdown was followed by rescue with synthetic miR369-3 resistant to the siRNA (Fig. 1C), translation efficiency was increased fivefold. These results indicate that miR369-3 is specifically required directly or indirectly for TNFα ARE–mediated translation activation under growth-arrest conditions.

To test whether translation activation requires formation of base pairs between miR369-3 and the ARE, we used a mutant ARE (mtARE) (*4*) that does not undergo translation up-regulation in either serum condition. We added miR369-3 mutated to restore complementarity (miRmt369-3) (Fig. 1A and fig. S1) and observed that translation is up-regulated only under serum-starved conditions (Fig. 1D). Next, we introduced identical mutations into the ARE at each site complementary to miR369-3's seed region (Fig. 1A and fig. S1) and found that both mtAREseed1 and mtAREseed2 exhibited loss of translation up-regulation, which could be restored by adding increasing amounts of seed-mutated miRseedmt369-3 (Fig. 1E). Because endogenous wild-type miR369-3 is also present, this suggests that both sites are required to form base pairs with miR369-3. Finally, to confirm the involvement of miR369-3, we probed affinity-purified ARE mRNP after formaldehyde cross-linking to preserve in vivo RNP complexes (*4*). Fig. 1F reveals enhanced levels of miR369-3 in the ARE relative to the mtARE-containing complex from serum-starved (–) but not serum-grown (+) cells or when miR369-3 was added to rescue the knockdown of microRNA by si-pre369. Together, these results indicate that miR369-3 associates with the TNFα ARE to up-regulate translation exclusively upon serum starvation by direct base pairing between its seed sequence and complementary ARE regions.

Tethering AGO2 to a reporter mRNA under conditions of serum starvation up-regulates translation (*4*), which suggests that—like miR369-3 recruitment to an ARE (Fig. 1)—other microRNPs might be transformed into activating complexes on cell cycle arrest. This hypothesis was tested by creating a reporter with four artificial 3′UTR target sites (CX) (*6*, *7*) (Fig. 2A). In response to its corresponding synthetic microRNA (miRcxcr4) (*6*, *7*) added exogenously, CX mRNA translation was up-regulated exclusively upon serum starvation (Fig. 2A). No difference in CX translation with or without serum in the absence of added microRNA indicates that the reporter assay behaves comparably under different growing conditions (SOM text). We extended these analyses to high-mobility group A2 (HMGA2) 3′UTR reporter, which contains seven sites for the endogenous Let-7 microRNA, and a matching control with mutated sites (*8*) (Fig. 2B). When HeLa cells were serum-starved, as opposed to grown in the presence of serum (+Snc), HMGA2 translation efficiency increased significantly and was further amplified by addition of

Department of Molecular Biophysics and Biochemistry, Howard Hughes Medical Institute, Yale University School of Medicine, Boyer Center for Molecular Medicine, 295 Congress Avenue, New Haven, CT 06536, USA.

*To whom correspondence should be addressed. E-mail: joan.steitz@yale.edu

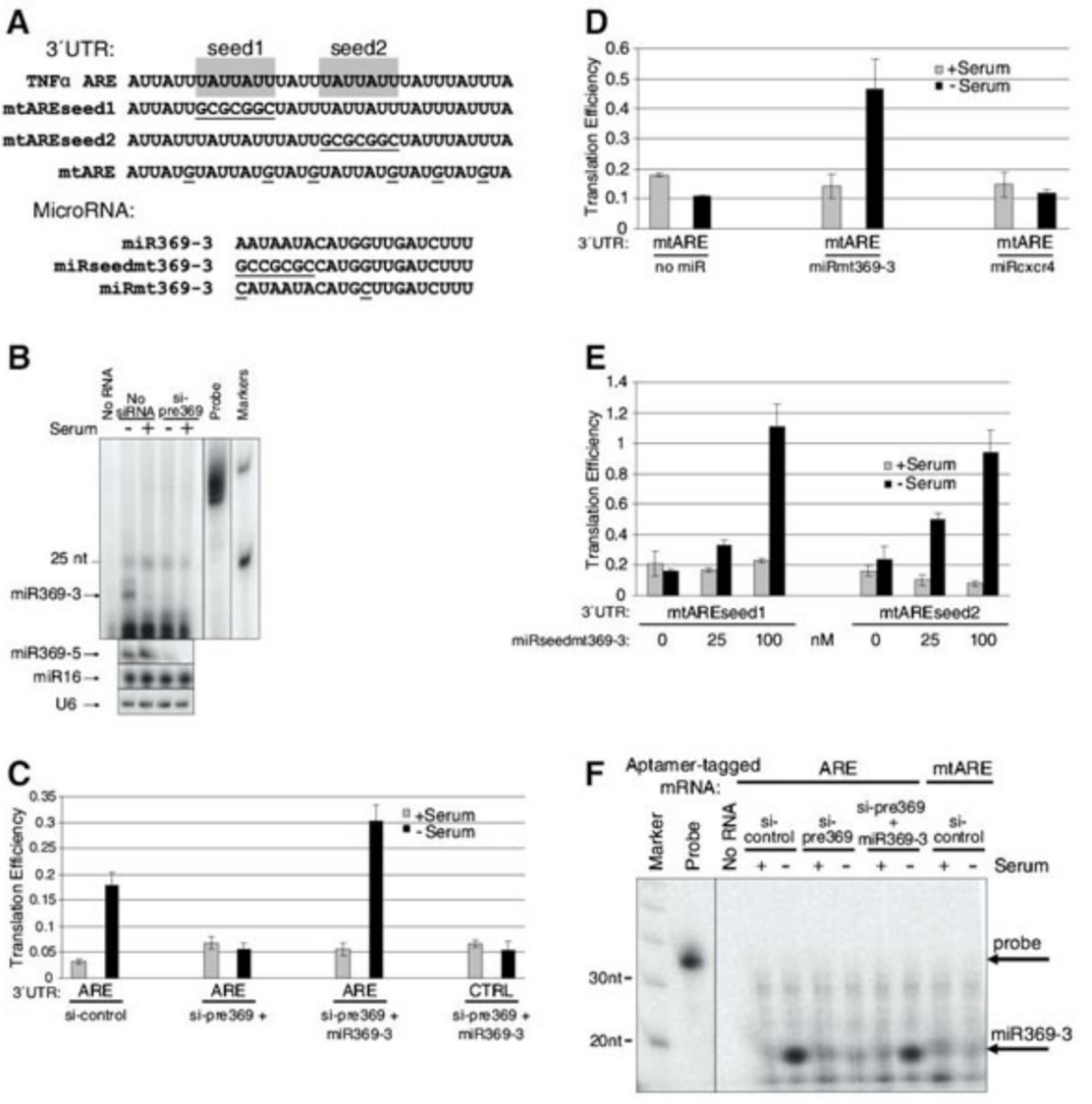

Fig. 1. MiR369-3 is required to activate TNFα ARE reporter translation under growth-arrest conditions. (**A**) 3′UTR sequences of the luciferase reporter: wild-type TNFα ARE and mutants mtAREseed1, mtAREseed2, and mtARE (AUUUAs converted to AUGUAs). MicroRNA sequences: wild-type miR369-3, seed mutant miRseedmtR369-3 (complementary to mtAREseed1 and mtAREseed2), and miRmt369-3 (complementary to mtARE). Target seed regions are shaded; mutations are underlined. (**B**) Ribonuclease protection assay (RPA) for miR369-3 in serum-starved (–) and serum-grown (+) HEK293 cells without or with siRNA treatment against pre-miR369 (si-pre369). MiR369-5 (fig. S2), miR16, and U6 RNA provided controls. (**C**) All translation assays (*4*) used firefly luciferase reporters [here ARE or control (CTRL)]; values were normalized to a *Renilla* cotransfected reporter and to the firefly and *Renilla* mRNA levels to determine translation efficiency (*5*). HEK293 cells grown in serum (+) or without serum (–) were transfected with 50 nM miRcxcr4 (si-control, Fig. 2A), si-pre369 (fig. S2), or si-pre369 plus synthetic miR369-3. (**D**) Translation efficiency of the mtARE reporter without added microRNA or with 50 nM miRmt369-3 or miRcxcr4 control. (**E**) Translation efficiency in serum-grown or -starved cells transfected with either the mtAREseed1 or mtAREseed2 reporter without or with miRseedmt369-3. (C), (D), and (E) show averages from at least three transfections ± standard deviation. (**F**) S1-aptamer–tagged ARE and mtARE reporters were used for in vivo cross-linking–coupled RNP purification (*4*) from HEK293 cells grown in serum under basal translation conditions (+) or serum-starved translation activation conditions (–). MiR369-3 was detected by RPA.

exogenous Let-7 (Fig. 2B). A requirement for microRNA base-pairing was demonstrated using the mutant HMGA2 reporter with and without exogenous complementary mutated Let-7 (Fig. 2B, black bars). Knockdown experiments showed that HMGA2 translation up-regulation is also dependent on the presence of FXR1 and AGO2 (*4*) (Fig. 2C). We conclude that all three microRNAs studied switch to translation activation under growth-arrest conditions.

In both HEK293 and HeLa cells, serum starvation causes translation activation relative to basal levels, which is distinct from alleviating translation repression to restore basal levels. We define basal as the translation efficiency [normalized luciferase activity (see tables S1 to S8)] of reporters that do not contain ARE or of a microRNA-targeted reporter in the absence of the corresponding microRNA (Figs. 1 and 2A), because these values are similar in all tested conditions. Increased translation efficiency is considered activation, whereas translation below this reference level constitutes repression. In serum-grown asynchronous cells, basal translation was observed not only for the ARE, as expected from the lack of miR369-3 (Fig. 1B), but also for the CX reporter in the presence of miRcxcr4 (Fig. 2A, gray bars), which should experience repression according to the literature (*6*). Because translation activation is controlled by the cell cycle (*4*), we reasoned that careful synchronization of the entire cell population might allow translation repression to be better distinguished from basal translation (*5*). Therefore, we subjected HeLa cells to serum starvation followed by release into serum growth conditions for 18 hours, which results in synchronous proliferation (in late S/G_2 phase) (*5*). Translation in these synchronized conditions (+Snc) was significantly repressed (lower than basal translation in asynchronous cells grown in serum by a factor of 3 to 5) for both the ARE reporter and the CX reporter cotransfected with miRcxcr4 (Fig. 2A, striped bars). Synchronization also produced significant repression upon cotransfection of the natural microRNA-targeted HMGA2 3′UTR reporter and exogenous Let-7 or of the mutated HMGA2 reporter and the corresponding mutated Let-7 (Fig. 2B, striped bars) (*8*). Such repressive effects were reproduced with the ARE reporter under synchronized growth; knockdown of the miR369-3 precursor alleviated translation repression, whereas adding back synthetic miR369-3 reversed repression (Fig. 3A, striped bars).

Under synchronized proliferation conditions, tethering λN-tagged AGO2 fusion protein to the 5B box reporter (*4*, *9*) revealed translation repression by a factor of five (Fig. 3B) and a comparable extent of activation (*4*) under growth-arrested conditions, relative to mutant λN-tagged AGO2 proteins (prpΔ and paz10, respectively) (*9*, *10*). The cell cycle regulation of translation was further established by treatment with aphidicolin (which causes G_1 arrest), which led to translation activa-

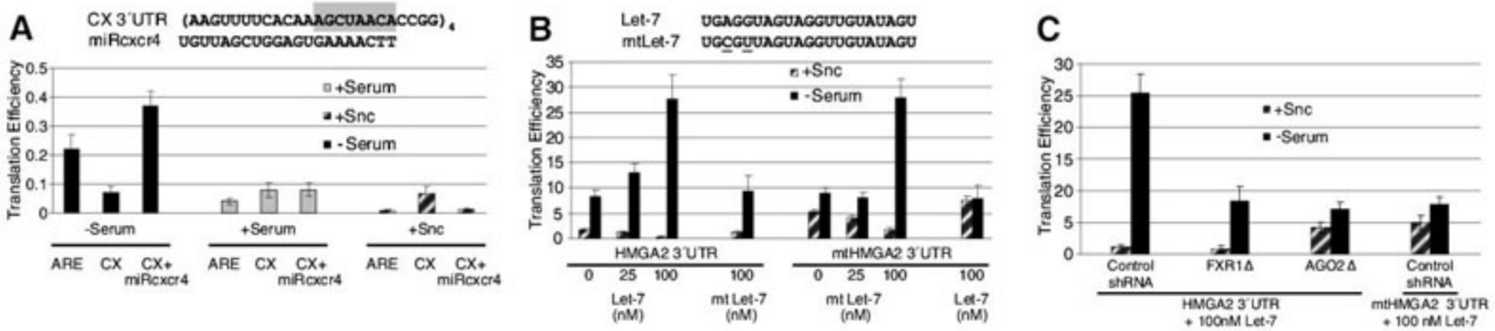

Fig. 2. Two other microRNAs switch from effecting translation activation under cell cycle–arrested conditions to repression in proliferating cells. (**A**) Translation of the ARE or CX reporter, with four tandem copies of the sequence complementary to the artificial cxcr4 target site (*6*, *7*), was assessed as in Fig. 1, C to E, in HeLa cells transfected without or with addition of miRcxcr4 under three different conditions: Black bars are cells grown without serum (translation up-regulation), gray bars are asynchronous cells grown in serum (basal translation) (*4*), and striped bars are serum-grown cells synchronized by release from serum starvation (+Snc) (translation repression). Cells cotransfected with control miRs (mtLet-7) gave results comparable to ARE or CX alone (not shown). (**B**) Translation efficiency in cells transfected with the wild-type HMGA2 3′UTR or mtHMGA2 3′UTR *Renilla* reporter (*8*) without or with increasing concentrations of Let-7 or the compensatory mtLet-7 miRNA (*8*) and under synchronized or serum-starved conditions. (**C**) Translation efficiency of cells transfected as in (B), but with prior RNA interference treatment with short hairpin RNA to knockdown FXR1 or AGO2 as described (*4*). (A), (B), and (C) show averages from at least three transfections ± standard deviation.

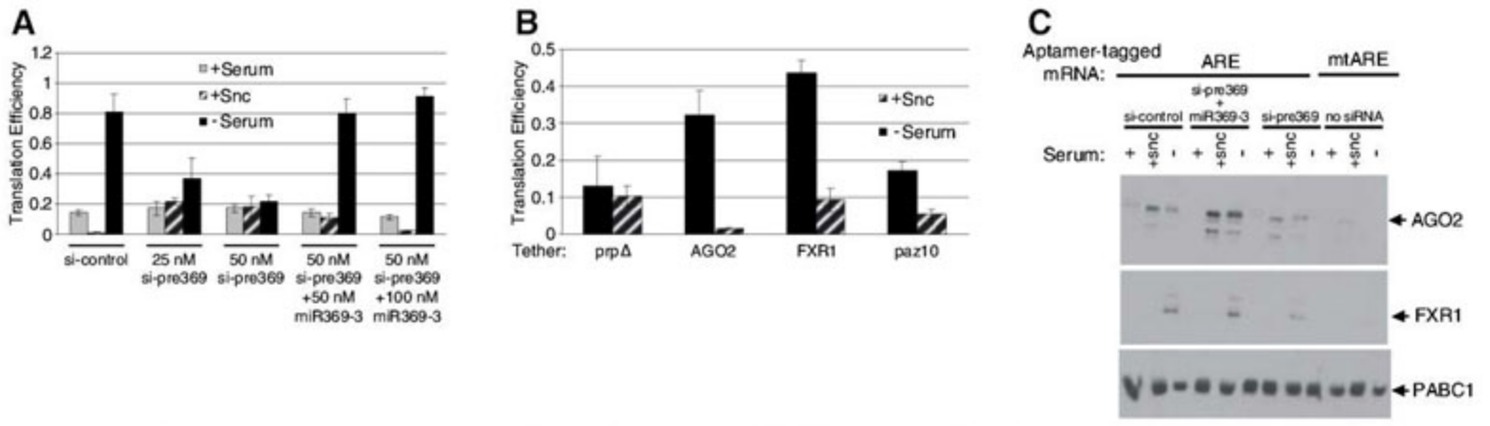

Fig. 3. MicroRNA and protein requirements for translation activation and repression. (**A**) Translation efficiency of cells transfected with the ARE reporter grown under the three conditions described in Fig. 2A, without or with increasing concentrations of si-pre369 and synthetic miR369-3 to rescue the knockdown. (**B**) Translation efficiency in cells cotransfected with the 5B box reporter (*4*) and various λN-tagged proteins: prpΔ (*9*), AGO2, FXR1 (*4*), or paz10 (*10*) under synchronized or serum-starved conditions. (A) and (B) show averages from at least three transfections ± standard deviation. (**C**) Eluates from S1-aptamer–tagged ARE and mtARE reporters after RNP purification (as in Fig. 1F) were subjected to Western analyses for AGO2, FXR1, and PABC1 (as a control). The lower band in the gel probed with antibody against AGO2 is a degradation product. In the three conditions, cellular AGO2 levels are unchanged, and miR369-3 can be immunoprecipitated by AGO2-specific antibody (not shown; see fig. S4 for levels of miR369-3 in synchronized cells). FXR1 usually runs as multiple bands that represent either multiple isoforms or modifications (*4*).

tion, or nocodazole (which arrests cells in G_2/M), which led to translation repression by tethered AGO2 but not by the paz10 or prpΔ mutant AGO protein (fig. S3). Tethering FXR1 failed to cause translation repression (Fig. 3B), possibly because FXR1 is part of the activating but not the repressive AGO2 microRNP. Furthermore, the AGO2 mutant (paz10) that does not bind microRNAs is compromised in translation activation, which indicates a requirement for microRNA binding or that the PAZ-microRNA binding domain has additional roles (*10*).

To confirm that miR369-3 recruits the AGO2-FXR1 complex for translation up-regulation, we performed RNP purification of the aptamer-tagged ARE and mtARE reporters (*4*) from cells transfected with a control siRNA, si-pre369, or si-pre369 with synthetic miR369-3. Control siRNA-treated samples showed the presence of AGO2 and FXR1 (Fig. 3C), in addition to miR369-3 (Fig. 1F), in the ARE complex under serum-starved (–) conditions. Knockdown of miR369-3 production reproducibly reduced AGO2 and FXR1 on the ARE reporter, whereas rescue with synthetic miR369-3 restored AGO2-FXR1 to at least normal levels (Fig. 3C), which correlated with the translation efficiencies seen in Fig. 1C. We conclude that miR369-3 is required for recruitment of the AGO2-FXR1 complex, which activates translation, and that FXR1 is not part of the repressive complex (+Snc lanes in Fig. 3C).

Together our data indicate that microRNA repression is a property of proliferating cells. In the literature, the fold repression by AGO2 or microRNPs fluctuates, depending on the cell line, transfection method, and overall system (*4*, *9*, *11*, *12*). Such variations may reflect differences in the cell cycle state of asynchronous populations and their response to transfection protocols.

We have shown that the TNFα ARE recruits miR369-3 to mediate translation up-regulation in serum-starved conditions and to cause repression in synchronized proliferating cells. Base-pairing of miR369-3 is required to recruit the activating AGO2-FXR1 complex (*4*). The TNFα ARE belongs to an ARE class typified by tandemly repeated AUUUA motifs (*12*, *13*), but it contains three AUUA sequences, two with flanks that allow base-pairing with the seed region of miR369-3 (fig. S1). Both sites shaded in Fig. 1A appear to be required for microRNA-dependent translation activation (Fig. 1E), but their close spacing warrants further investigation (*6*, *14*). Because AREs of the same class resemble each other but have distinct AU-rich sequences, they may recruit different microRNAs, which would explain their highly specific regulated expression patterns (*12*, *13*).

MicroRNAs oscillate between repression and activation in coordination with the cell cycle: In proliferating cells they repress translation, whereas in G_1/G_0 arrest (which often precedes differentiation), they mediate activation. This regulation occurs on at least two levels. First, recruitment of the microRNP reflects both its expression level and its ability to productively interact with mRNA target sites. Second, the AGO2 complex must be subject to modification because tethered AGO2 differentially regulates translation according to cell growth conditions (Fig. 3B and fig. S3). As FXR1 is found exclusively in the activation complex and activation by AGO2 tethering in serum-starved conditions requires FXR1 expression, modifications that switch AGO2 from repressor to activator may alter interactions with FXR1. Such modifications upon serum starvation were suggested by changes in the solubility and subcellular localization of the AGO2-FXR1 complex (*4*). Our findings define a novel role for microRNAs and reveal an unanticipated versatility of microRNP function in response to the cell cycle, with important implications for understanding the contributions of these RNAs to development, differentiation, and carcinogenesis.

References and Notes

1. C. J. Wilusz, M. Wormington, S. W. Peltz, *Nat. Rev. Mol. Cell Biol.* **2**, 237 (2001).
2. M. A. Valencia-Sanchez, J. Liu, G. J. Hannon, R. Parker, *Genes Dev.* **20**, 515 (2006).
3. M. A. Carmell, Z. Xuan, M. Q. Zhang, G. J. Hannon, *Genes Dev.* **16**, 2733 (2002).
4. S. Vasudevan, J. A. Steitz, *Cell* **128**, 1105 (2007).
5. Materials and methods are available as supporting material on *Science* Online.
6. J. G. Doench, P. A. Sharp, *Genes Dev.* **18**, 504 (2004).
7. J. G. Doench, C. P. Petersen, P. A. Sharp, *Genes Dev.* **17**, 438 (2003).
8. C. Mayr, M. T. Hemann, D. P. Bartel, *Science* **315**, 1576 (2007).
9. R. S. Pillai, C. G. Artus, W. Filipowicz, *RNA* **10**, 1518 (2004).
10. J. Liu, M. A. Valencia-Sanchez, G. J. Hannon, R. Parker, *Nat. Cell Biol.* **7**, 719 (2005).
11. J. Liu *et al.*, *Nat. Cell Biol.* **7**, 1261 (2005).
12. C. Y. Chen, A. B. Shyu, *Trends Biochem. Sci.* **20**, 465 (1995).
13. K. S. Khabar, T. Bakheet, B. R. Williams, *Genomics* **85**, 165 (2005).
14. P. Saetrom *et al.*, *Nucleic Acids Res.* **35**, 2333 (2007).

15. This work was supported by NIH grants to J.A.S. and by a Cancer Research Institute postdoctoral fellowship to S.V. J.A.S is an investigator of HHMI. We are grateful to G. Dreyfuss and G. Hannon for sharing reagents. We thank E. Ullu, D. Black, A. Alexandrov, N. Kolev, A. Nag, and K. Tycowski for critical commentary and A. Miccinello for editorial assistance.

Supporting Online Material

www.sciencemag.org/cgi/content/full/1149460/DC1
Materials and Methods
SOM Text
Figs. S1 to S13
Tables S1 to S8
References

20 August 2007; accepted 2 November 2007
Published online 29 November 2007;
10.1126/science.1149460
Include this information when citing this paper.

Rapid Changes in Throughput from Single Motor Cortex Neurons to Muscle Activity

Adam G. Davidson, Vanessa Chan, Ryan O'Dell, Marc H. Schieber*

Motor cortex output is capable of considerable reorganization, which involves modulation of excitability within the cortex. Does such reorganization also involve changes beyond the cortex, at the level of throughput from single motor cortex neurons to muscle activity? We examined such throughput during a paradigm that provided incentive for enhancing functional connectivity from motor cortex neurons to muscles. Short-latency throughput from a recorded neuron to muscle activity not present during some behavioral epochs often appeared during others. Such changes in throughput could not always be attributed to a higher neuron firing rate, to more ongoing muscle activity, or to neuronal synchronization, indicating that reorganization of motor cortex output may involve rapid changes in functional connectivity from single motor cortex neurons to α-motoneuron pools.

In a variety of situations, such as learning new fine motor skills, the human motor cortex can reorganize, increasing output to specific muscles (*1*, *2*). Similarly, in monkeys that have learned movements, the territory from which intracortical microstimulation (ICMS) evokes output to trained muscles expands (*3*), and ICMS triggered from the voluntary discharges of flexion-related neurons can convert local output from excitation of extensor muscles to excitation of flexors (*4*). Does such plasticity of cortical output reflect changes in intracortical excitability exclusively, or can the throughput from single motor cortex neurons to muscles also change rapidly?

In two monkeys, we recorded neurons in the primary motor cortex (M1) hand representation simultaneously with electromyographic (EMG) activity from up to 16 contralateral forearm and hand muscles. Each monkey performed two behavioral tasks: first, a simple hand squeeze task; second, a paradigm that provided incentive for the monkey to increase throughput from M1 neurons to muscles, which we term reinforcement of physiological discharge (RPD). Similar to previous studies (*5*–*7*), in RPD we rewarded the monkey for simultaneous (±6 ms) discharge of (i) spikes from an M1 neuron and (ii) large potentials in the EMG of a selected muscle, termed the RPD muscle. Typically, after recording a neuron during a squeeze task epoch, the same neuron was combined with different RPD muscles in successive epochs. For example, synchronous potentials from a given

neuron and the extensor carpi radialis brevis (ECRB) muscle might be required during one epoch, from the same neuron and the flexor digitorum profundus, radial region (FDPr) muscle during another epoch, and from the neuron and the palmaris longus (PL) muscle during still another.

The effective throughput from a single M1 neuron to a given muscle can be examined in spike-triggered averages (SpikeTAs) of rectified EMG (*8*–*11*). Brief peaks or troughs that follow the aligned spike times represent increased or decreased α-motoneuron discharge probabilities, respectively, reflecting excitatory or inhibitory synaptic input to the motoneuron pool arriving at a fixed latency relative to the neuron spikes. We formed separate SpikeTAs for each neuron-muscle pair during each squeeze or RPD epoch and identified significant peaks or troughs, termed SpikeTA effects, when they typically occur, 6 to 16 ms after the spike triggers (*12*). We chose to analyze both pure postspike effects consistent with monosynaptic input from the M1 neuron to the motoneuron pool and other effects consistent with inputs to the same motoneuron pool from additional neurons synchronized with the recorded M1 trigger neuron (*11*, *13*).

Recordings during at least two epochs of different behaviors (squeeze and/or RPD) were obtained from 67 and 126 neurons in monkeys E and W, respectively, providing a total of 1845 neuron-muscle pairs with satisfactory EMG. For each of these neuron-muscle pairs, we formed a separate SpikeTA for each behavioral epoch. Figure 1 shows such SpikeTAs from a session in which neuron e0035_B was recorded simultaneously with 13 muscles while monkey E performed the squeeze task; this was followed by six RPD epochs, and then the monkey performed the squeeze task again (*14*). Some muscles, such as hypothenar eminence (Hypoth), showed no SpikeTA effects during any epoch. Other muscles, such as ECRB, showed highly significant effects during all eight epochs. We were surprised to find, however, that still other muscles—such as FDPr—showed highly significant effects during some epochs but no effect during other epochs, even though the neuron and the muscle were active concurrently during all epochs.

We selected for the present analysis neuron-muscle pairs that produced a SpikeTA effect in at least one epoch significant at the $P < 0.0001$ level (Wilcoxon signed-rank test). We chose this relatively stringent criterion to provide a high degree of certainty that each of the neuron-muscle pairs selected from the large number examined definitely produced an effect. SpikeTAs for a given neuron-muscle pair in a given epoch then were retained for further analysis only if 4000 or more triggers (neuron spikes discharged during ongoing EMG) were available in that epoch, or if a SpikeTA effect in that epoch was significant at $P < 0.0001$ with fewer than 4000 such triggers. One hundred sixty-five neuron-muscle pairs meeting these criteria were obtained from 28 and 27 neurons in monkeys E and W, respectively.

We classified the SpikeTA effect of each of these 165 neuron-muscle pairs in each behavioral epoch as being highly significant (uncorrected $P < 0.0001$), of intermediate significance ($0.0001 \leq P < 0.05$), or completely absent ($0.05 \leq P$). Of 142 squeeze epoch SpikeTAs, highly significant effects were found in 29 (20%), intermediate effects were found in 37 (26%), and effects were absent in 76 (54%). Of 488 RPD epoch SpikeTAs, highly significant effects were found in 315 (65%), intermediate effects were found in 102 (21%), and effects were absent in 71 (14%). These distributions differed significantly ($X^2 = 112.2$, $P = 0$), indicating that absent effects were more common during squeeze epochs, whereas highly significant SpikeTA effects were more common during RPD epochs. Compared with the squeeze task, RPD increased throughput from M1 neurons to muscles.

To examine whether this increased throughput was selective for the RPD muscle and/or related muscles, we grouped the muscles into forearm flexors, forearm extensors, and intrinsic hand muscles. For each neuron-muscle pair, RPD epochs then were categorized as those in which the RPD muscle was the same muscle as that of the neuron-muscle pair, a muscle of the same group, or a muscle of another group. Of 70 same-muscle RPD epochs, highly significant SpikeTA effects were found in 59, effects of intermediate significance were found in 10, and effects were absent in 1. (Note, however, that we typically chose for RPD a neuron and muscle combination that had shown a SpikeTA effect in online averages during a previous epoch.) Of 182 same-group RPD epochs, highly significant effects were found in 128, intermediate

Departments of Neurology and Neurobiology and Anatomy, University of Rochester School of Medicine and Dentistry, Rochester, NY 14642, USA.

*To whom correspondence should be addressed. E-mail: mhs@cvs.rochester.edu

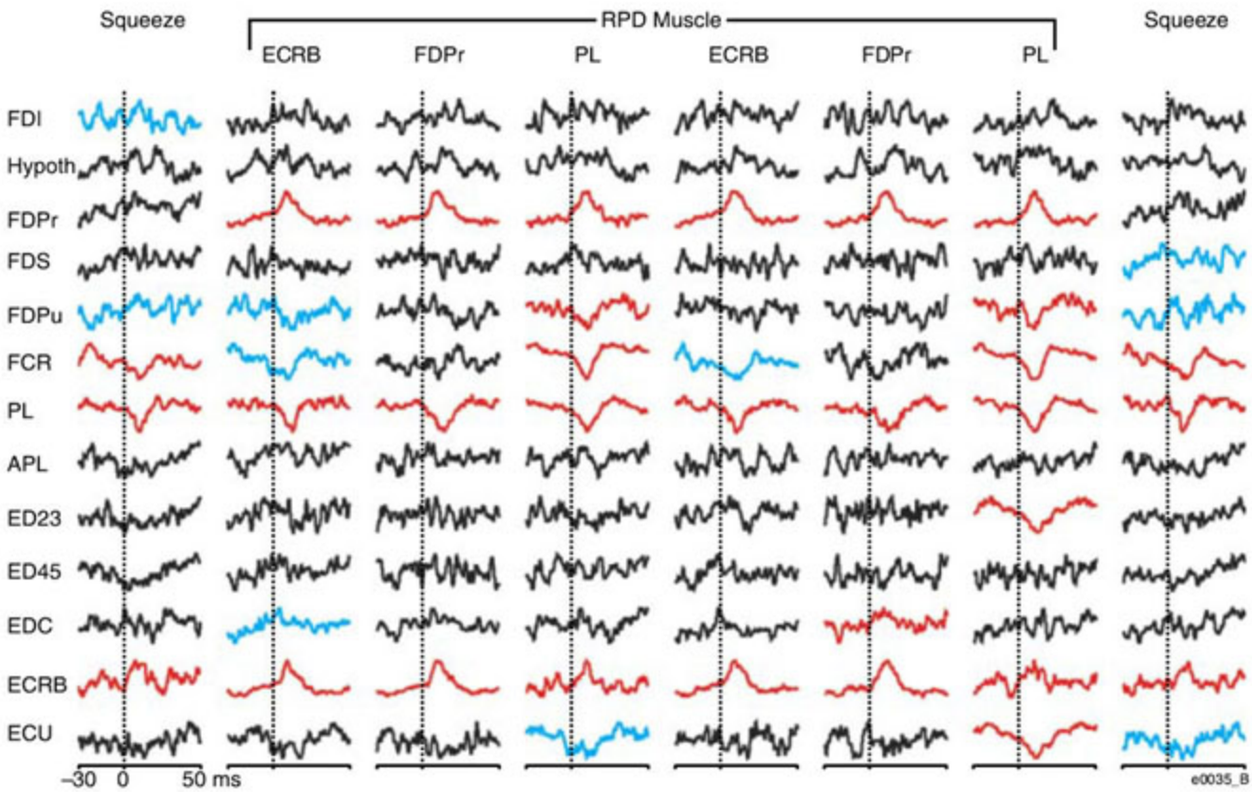

Fig. 1. Spike-triggered averages during eight behavioral epochs. Each column shows averages of rectified EMG from each of 13 muscles (rows) triggered from spikes discharged by neuron e0035_B during one of eight behavioral epochs (*14*). The trigger time is indicated by a vertical line in each column. All SpikeTAs are scaled vertically to fill the same height. SpikeTAs with highly significant effects are shown in red, those with effects of intermediate significance in blue, and those with no significant effect in black. FDI, first dorsal interosseus; Hypoth, hypothenar eminence; FDPr, flexor digitorum profundus, radial region; FDS, flexor digitorum superficialis; FDPu, flexor digitorum profundus, ulnar region; FCR, flexor carpi radialis; PL, palmaris longus; APL, abductor pollicis longus; ED23, extensor digiti secundi et tertii; ED45, extensor digiti quarti et quinti; EDC, extensor digitorum communis; ECRB, extensor carpi radialis brevis; ECU, extensor carpi ulnaris.

effects were found in 31, and effects were absent in 23. Of 236 other-group epochs, highly significant effects were found in 128, intermediate effects were found in 61, and effects were absent in 47. These latter two distributions differed significantly (X^2 = 11.2, $P = 3.7 \times 10^{-3}$), indicating that RPD had more effect on throughput to muscles of the same group than to muscles of other groups. Even other-group RPD epochs showed highly significant SpikeTA effects more commonly than did squeeze epochs ($X^2 = 55.2$, $P = 1.0 \times 10^{-12}$).

Although each of the 165 neuron-muscle pairs was selected because it produced a highly significant SpikeTA effect during at least one epoch, effects were absent in many epochs despite concurrent activity in the neuron and muscle. Epochs with absent effects were less common among neuron-muscle pairs that produced facilitative effects (58 of 131, 44%) than among those that produced suppressive effects (24 of 34, 71%) ($X^2 = 7.5$, $P = 6.3 \times 10^{-3}$). Two mechanisms might explain these absent SpikeTA effects. First, monosynaptic cortico-motoneuronal (CM) excitatory postsynaptic potentials (EPSPs) show facilitation at short interspike intervals (*15*). Consequently, SpikeTAs formed with spikes selected for shorter interspike intervals have larger peaks (*8*, *16*). A SpikeTA effect apparent when the neuron fires at a high rate therefore might disappear when the neuron fires at a lower rate. Second, synaptic input from a given neuron is more likely to recruit motoneurons that already are excited close to threshold by other inputs. Hence, SpikeTAs formed with spikes discharged during periods of higher ongoing EMG activity have larger peaks (*17*). A SpikeTA effect apparent when the level of ongoing EMG activity is high thus might disappear when the level of ongoing EMG is lower.

We therefore selected those 82 neuron-muscle pairs that produced a highly significant effect in one epoch that was absent in another. We then determined whether the neuron firing rate and/or the ongoing EMG each was higher in the epoch with the highly significant effect [multiple fragment approach (*12*), $P < 0.05$, Wilcoxon rank-sum test]. For 34 neuron-muscle pairs, the highly significant effect occurred in an epoch with both higher neuron firing rate and higher EMG (Fig. 2A). For 13 other pairs, only EMG was higher (Fig. 2B), and for 19 other pairs, only neuron firing rate was higher (Fig. 2C). Hence, for the majority (80%) of these 82 neuron-muscle pairs, the highly significant effect occurred in an epoch with higher neuron firing rate and/or higher ongoing EMG compared to the epoch with an absent effect. However, for 16 (20%) of the 82 neuron-muscle pairs, the highly significant effect occurred in an epoch with neither higher neuron firing rate nor higher EMG (Fig. 2D), indicating that additional mechanisms contributed to the presence versus absence of throughput from the M1 neuron to the muscle.

Was the increased throughput mediated in part by synchronization of the M1 trigger neuron with other, unrecorded neurons that also provided input to the same motoneuron pool? SpikeTA effects in which the peak has an onset latency appropriate for the conduction time from M1 to α-motoneurons, and then from motoneurons to their muscle fibers, reflect monosynaptic connections to the motoneuron pool from the M1 trigger neuron, which therefore is termed a CM cell (*8*–*10*, *18*). Their SpikeTA peaks also are expected to be relatively narrow, reflecting the durations of CM EPSPs in motoneurons and the durations of various motor unit action potentials (*19*). However, other SpikeTA effects have onsets that occur too early and/or peaks too wide to have resulted only from the trigger neuron's EPSPs. In such cases, additional neurons that provided synaptic inputs to the same motoneuron pool are thought to have discharged spikes synchronized (± a few ms) with those of the trigger neuron (*11*, *13*).

In Fig. 3, points are plotted at coordinates indicating the onset latency and peak width at half maximum (PWHM) of individual SpikeTA effects. Figure 3A shows highly significant effects overall, Fig. 3B shows effects from neuron-muscle pairs that produced an absent effect in another epoch, and Fig. 3C shows 14 of the 16 effects that were absent in an epoch for which neither neuron firing rate nor ongoing EMG level was lower. (Pretrigger variation prevented our algorithm from accurately measuring onset latency for a few highly significant effects.) Points in the lower left, upper right, and upper left quadrants represent SpikeTA effects that had an early onset (≤5 ms), a wide peak (≥9 ms), or both, respectively, indicative of contributions

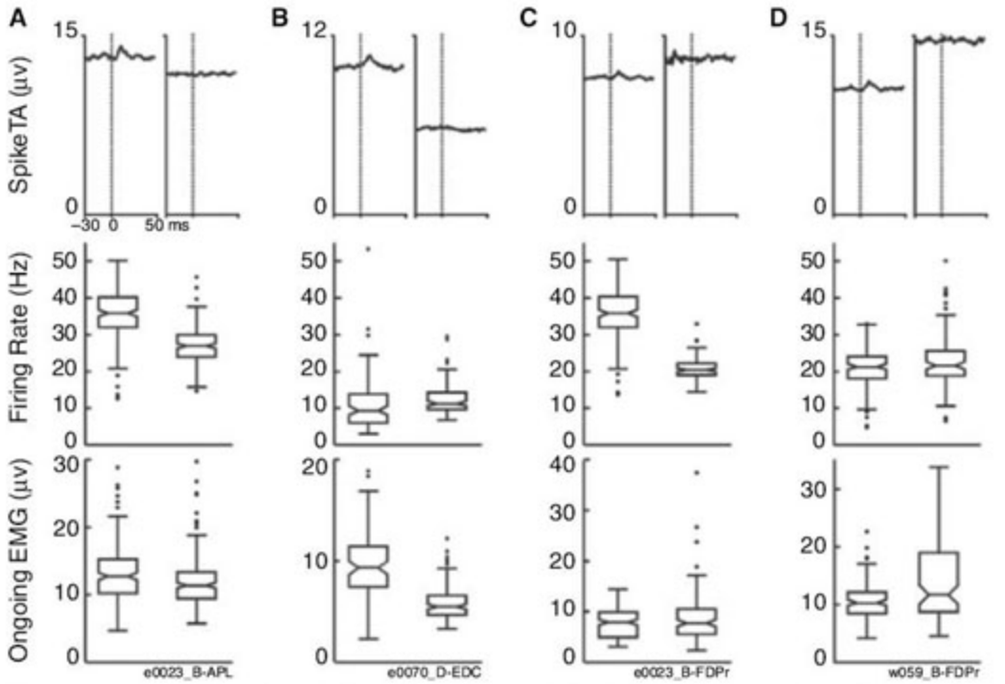

Fig. 2. Neuron-muscle pairs with throughput in some behavioral epochs but not in others. The four neuron-muscle pairs illustrated in (**A** to **D**), respectively, each produced a highly significant SpikeTA effect (top row) in one behavioral epoch (left) but no effect during another epoch (right). The middle and bottom rows show box plots illustrating the distributions (line, median; boxes, 25th to 75th percentile; whiskers, remainder; dots, outliers) of neuron firing rate and ongoing EMG, respectively, during each epoch. Box plots whose notches do not overlap have different medians ($P < 0.05$).

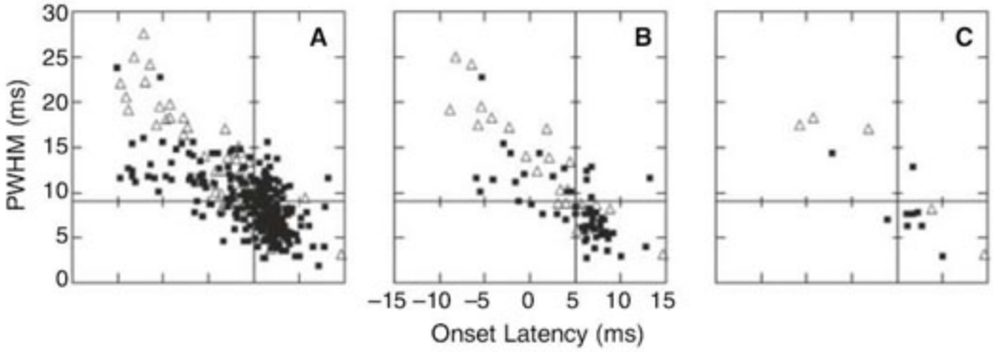

Fig. 3. Temporal characteristics of SpikeTA effects. (**A**) Each highly significant SpikeTA effect is represented by a point (squares, facilitatory; triangles, suppressive) plotted at coordinates indicating its onset latency (abscissa) and PWHM (ordinate). Cross-hairs have been drawn at onset latency = 5 ms and PWHM = 9 ms. (**B**) A similar plot for those neuron-muscle pairs whose SpikeTA effect was absent in another behavioral epoch. (**C**) A similar plot for those neuron-muscle pairs for which neither lower neuron firing rate nor lower ongoing EMG accounted for the absent effect in another epoch.

from neuronal synchrony. Synchrony may have contributed to these effects, and lack of synchrony during another epoch may have resulted in an absent effect [see, however, (*14*)].

Lack of synchrony was unlikely to account for absent effects when the highly significant effects were consistent with monosynaptic connections (onset latency > 5 ms and PWHM < 9 ms, lower right quadrants). Particularly for the eight SpikeTA effects in the lower right quadrant of Fig. 3C (from eight different neurons recorded in eight different sessions, three in monkey E and five in monkey W), the loss of throughput that resulted in absent effects cannot be attributed simply to lower neuron firing rate, lower ongoing EMG, and/or loss of synchronized inputs. Additional factors may have changed the throughput from these M1 neurons to their target muscles.

Although M1 output, particularly that from CM cells, dominates control of distal upper extremity musculature during voluntary activity, our results show that the throughput from individual M1 neurons to muscle activity can be changed rapidly and dramatically. For about half of the neuron-muscle pairs that produced highly significant SpikeTA effects, throughput evident during some behavioral epochs was absent during other epochs. In most cases, differences in intracortical excitability and the resulting changes in excitation of motoneuron pools—reflected by the firing rate of the trigger neuron, the level of ongoing EMG activity, and/or synchrony in the SpikeTA effect—contributed to the presence of effective throughput during some behavioral epochs and not others.

In about 10% (8 of 82) of cases, however, none of these factors could account for the presence versus absence of throughput from the M1 neuron to the muscle's EMG activity. We therefore speculate that three subcortical factors may have contributed as well. First, some SpikeTA effects may be mediated through disynaptic linkages that involve rubrospinal neurons, reticulospinal neurons, or spinal interneurons (*20*–*22*). Such effects may have been blocked during some epochs by inactivity of the interposed neuron. This mechanism seems likely for suppressive effects, all of which are mediated through inhibitory interneurons, and may have contributed to the absence of some facilitative effects as well. Second, single CM cell EPSPs in motoneurons may be relatively small (*23*, *24*). Within motoneuron dendrites, small synaptic inputs may have been amplified by persistent inward currents during some behavioral epochs but not during others (*25*). Third, the synaptic input from an M1 neuron to a motoneuron pool commonly is assumed to remain constant. Although synaptic efficacy might be altered by presynaptic inhibition, available evidence indicates that this mechanism does not affect corticospinal terminals (*26*, *27*). Plastic changes can occur in spinal cord synapses (*28*), however, and dendritic spines have been observed to be remodeled over minutes (*29*). We therefore speculate that the efficacy of CM synapses on motoneurons might have changed in some behavioral epochs. Subcortical factors such as these, which might have played a role in the 10% of cases lacking differences in intracortical excitability, also could have contributed to the rapid change in throughput in many of the other 90%.

Our findings indicate that M1 neurons, even those with relatively direct connections to α-motoneurons, are not always effective in driving their target motoneurons. Rather, throughput can be changed rapidly such that an individual M1 neuron, which is ineffective in eliciting motoneuron discharge during certain motor behaviors, does elicit discharge of the same motoneurons during other behaviors.

References and Notes

1. A. Pascual-Leone, J. Grafman, M. Hallett, *Science* **263**, 1287 (1994).
2. J. Classen, J. Liepert, S. P. Wise, M. Hallett, L. G. Cohen, *J. Neurophysiol.* **79**, 1117 (1998).
3. R. J. Nudo, G. W. Milliken, W. M. Jenkins, M. M. Merzenich, *J. Neurosci.* **16**, 785 (1996).
4. A. Jackson, J. Mavoori, E. E. Fetz, *Nature* **444**, 56 (2006).
5. E. E. Fetz, *Science* **163**, 955 (1969).
6. E. E. Fetz, D. V. Finocchio, *Science* **174**, 431 (1971).
7. E. M. Schmidt, J. S. McIntosh, L. Durelli, M. J. Bak, *Exp. Neurol.* **61**, 349 (1978).
8. E. E. Fetz, P. D. Cheney, *J. Neurophysiol.* **44**, 751 (1980).
9. E. J. Buys, R. N. Lemon, G. W. Mantel, R. B. Muir, *J. Physiol.* **381**, 529 (1986).
10. R. N. Lemon, G. W. Mantel, R. B. Muir, *J. Physiol.* **381**, 497 (1986).
11. M. H. Schieber, G. Rivlis, *J. Neurophysiol.* **94**, 3325 (2005).
12. A. G. Davidson, R. O'Dell, V. Chan, M. H. Schieber, *J. Neurosci. Methods* **163**, 283 (2007).
13. S. N. Baker, R. N. Lemon, *J. Neurophysiol.* **80**, 1391 (1998).
14. Materials and methods are available as supporting material on *Science* Online.
15. R. B. Muir, R. Porter, *J. Physiol.* **228**, 749 (1973).
16. R. N. Lemon, G. W. Mantel, *J. Physiol.* **413**, 351 (1989).
17. K. M. Bennett, R. N. Lemon, *J. Physiol.* **477**, 291 (1994).
18. E. E. Fetz, P. D. Cheney, *J. Physiol. (Paris)* **74**, 239 (1978).
19. S. S. Palmer, E. E. Fetz, *J. Neurophysiol.* **54**, 1194 (1985).
20. A. G. Davidson, M. H. Schieber, J. A. Buford, *J. Neurosci.* **27**, 8053 (2007).
21. E. E. Fetz, S. I. Perlmutter, Y. Prut, K. Seki, S. Votaw, *Brain Res. Brain Res. Rev.* **40**, 53 (2002).
22. K. Mewes, P. D. Cheney, *J. Neurophysiol.* **66**, 1965 (1991).
23. D. G. Lawrence, R. Porter, S. J. Redman, *J. Comp. Neurol.* **232**, 499 (1985).
24. R. Porter, J. Hore, *J. Neurophysiol.* **32**, 443 (1969).
25. C. J. Heckman, R. H. Lee, R. M. Brownstone, *Trends Neurosci.* **26**, 688 (2003).
26. J. Nielsen, N. Petersen, *J. Physiol.* **477**, 47 (1994).
27. A. Jackson, S. N. Baker, E. E. Fetz, *J. Physiol.* **573**, 107 (2006).
28. J. R. Wolpaw, A. M. Tennissen, *Annu. Rev. Neurosci.* **24**, 807 (2001).
29. A. K. Majewska, J. R. Newton, M. Sur, *J. Neurosci.* **26**, 3021 (2006).

30. We thank L. A. Schery and A. Moore for technical assistance and M. Hayles for editorial comments. This work was supported by R01/R37-NS27686.

Supporting Online Material

www.sciencemag.org/cgi/content/full/318/5858/1934/DC1
Materials and Methods
Figs. S1 and S2
Table S1
References

27 August 2007; accepted 16 November 2007
10.1126/science.1149774

Cognitive Recovery in Socially Deprived Young Children: The Bucharest Early Intervention Project

Charles A. Nelson III,[1]* Charles H. Zeanah,[2] Nathan A. Fox,[3] Peter J. Marshall,[4] Anna T. Smyke,[2] Donald Guthrie[5]

In a randomized controlled trial, we compared abandoned children reared in institutions to abandoned children placed in institutions but then moved to foster care. Young children living in institutions were randomly assigned to continued institutional care or to placement in foster care, and their cognitive development was tracked through 54 months of age. The cognitive outcome of children who remained in the institution was markedly below that of never-institutionalized children and children taken out of the institution and placed into foster care. The improved cognitive outcomes we observed at 42 and 54 months were most marked for the youngest children placed in foster care. These results point to the negative sequelae of early institutionalization, suggest a possible sensitive period in cognitive development, and underscore the advantages of family placements for young abandoned children.

For normal development, mammalian brains require an optimal level of environmental input, a so-called "expectable" environment (*1*, *2*). Examples of an expectable environment might include exposure to patterned light information, normal language exposure, and access to responsive caregivers. Unfortunately, not all children are exposed to such environments. Institutional settings vary both within and between countries, but many are characterized by unfavorable caregiver-to-child ratios; highly regimented routines (e.g., all children eat, sleep, and toilet at the same time); impoverished sensory, cognitive, and linguistic stimulation; and unresponsive caregiving practices. These issues af-

[1]Harvard Medical School and Children's Hospital, Boston, MA 02215, USA. [2]Tulane University Health Sciences Center, New Orleans, LA 70112, USA. [3]University of Maryland, College Park, MD 20742, USA. [4]Temple University, Philadelphia, PA 19122, USA. [5]University of California, Los Angeles, CA 90095, USA.

*To whom correspondence should be addressed. E-mail: charles.nelson@childrens.harvard.edu

fecting early development have implications for the millions of children throughout the world who begin their lives in adverse circumstances, such as those who have been maltreated or abandoned or whose parents have died.

Although the effects of early psychosocial deprivation on brain development has been examined extensively in animal models (*3*, *4*), the effects of similar deprivation on humans are less clear. Evidence suggests that children reared in institutions suffer from a variety of neurobiological and behavioral sequelae compared to never-institutionalized children. Children reared in institutions showed reduced metabolic activity in regions of the temporal and frontal cortices (*5*), and cortico-cortico connections between these regions were reduced in number (*6*). In addition, children reared in institutions have shown delays or deviations in a variety of behavioral domains, such as intelligence quotient (IQ), attachment, language, or social-emotional development (*7*–*10*).

This literature on the effects of early institutional care suffers from methodological limitations, particularly selection bias: In nonrandomized studies, a biased sample (e.g., healthier children or more psychologically competent children) may be adopted into families while others remain in institutions. These nonrandom factors make it difficult to attribute differences in behavioral characteristics of children reared in or out of institutional settings to the different environments in which the children were reared.

An additional unanswered question is the importance of timing of environmental enhancement in producing recovery from early deprivation. From the perspectives of both developmental brain plasticity and social policy, a vital question is whether there may be sensitive periods after which recovery becomes significantly more difficult. The Bucharest Early Intervention Project (BEIP) was designed, in part, to address the issue of timing of intervention on remediation of cognitive delay as a result of early deprivation. To address this issue, we designed a randomized controlled trial of foster care versus institutional care for young children who had been abandoned at or shortly after birth and placed in institutions. We avoided the selection bias of previous studies (*11*–*15*) by random assignment of children to the two groups. We assessed the children before the start of intervention, while they were still living in institutions, followed by randomization to continued institutional care or to placement in a foster family and longitudinal follow-up assessments of their cognitive development as assessed by standardized intelligence tests. We also assessed the timing of intervention on this outcome in early childhood.

We assessed three groups of children: an initial group of children abandoned at birth and then studied extensively with a battery of measures. Half of these children were then randomly assigned to foster care (foster care group, FCG) and the other half to continued institutional care (institutional group, IG). A third group consisted of children being reared with their biological families in the greater Bucharest community (never-institutionalized group, NIG).

Participants in institutions comprised 187 children less than 31 months of age and residing in any of the six institutions for young abandoned children in Bucharest, Romania (*16*). These children were initially screened with a pediatric and neurological exam, growth measurements, auditory assessment, and assessment of physical abnormalities. We excluded 51 children from the original sample for medical reasons, including genetic syndromes, frank signs of fetal alcohol syndrome (based largely on facial dysmorphology), and microcephaly (*17*). Thus, the final sample at baseline consisted of 136 children. Weight for age, height for age, weight for height, and head circumference for age were all lower in the IG than in the NIG.

The NIG comprised 80 children who were born at the same maternity hospitals as the institutionalized children. They were recruited from community pediatric clinics, were living with their biological parents, had no history of institutional care, and were matched on age and gender to the institutionalized sample. The final sample of the NIG consisted of 72 children (eight families declined further participation after initial recruitment into the study). All fell within 2 SD of the mean for physical growth (weight, length, and occipitofrontal circumference).

Birth records of the children in institutions were limited, allowing derivation of gestational age data for only 112 children; the length of gestation ranged from 30 to 42 weeks (mean = 37.2 weeks, SD = 2.2 weeks). Birth weight (available for 117 cases) ranged from 900 g to 4150 g (mean = 2767 g, SD = 609 g) and was significantly different from that of the NIG (mean = 3338 g, SD = 467 g), $t(187) = 6.8$, $P < 0.001$.

After initial assessment of all children in both institution and comparison samples, 68 children from the institutions (33 males and 35 females) were randomly assigned to remain in institutional care and were designated the IG (institutional group), and 68 (34 males and 34 females) were randomly assigned to foster care and were designated the FCG (foster care group). Randomization was implemented by assigning each child a number (1 to 136) written on a piece of paper. These papers were then placed in a hat and then drawn from the hat at random. The first number pulled from the hat was assigned to the IG, the next randomly drawn number was assigned to the FCG, and so on, until all children had been assigned to the IG or the FCG. The two sets of twins in the study were each on the same piece of paper and thus placed together.

Because government-sponsored foster care was limited to about one family when our study commenced, we created our own foster care program (*18*, *19*). After extensive advertising followed by screening, we recruited 56 foster families into the project. A total of 46% were single-parent families (widowed, divorced, or never married), and foster care mothers ranged in age from 30 to 66 years (mean = 48 years); all mothers had at least a high school education.

After random assignment, the average age for children at placement in foster care was 21 months. Cognitive development was assessed at

Table 1. DQ and IQ at 42 and 54 months of age.

Evaluation	*N*	Mean DQ and IQ	SD	SE
		IG		
42 months	57	77.1	13.3	1.8
54 months	51	73.3	13.1	1.8
		FCG		
42 months	61	85.7	14.2	1.8
54 months	59	81.0	18.5	2.4
		NIG		
42 months	52	103.4	11.8	1.6
54 months	45	109.3	21.2	3.2

Table 2. DQ and IQ of FCG by entry age group. η indicates effect size in multiples of the pooled standard deviation, and Y is younger than and O is older than age cutoff at entry to foster care.

Age cutoff	42 months (BSID-II)					54 months (WPSSI-R)				
	Y	O	$t(59)$	η	*P*	Y	O	$t(57)$	η	*P*
20 months	93.5	82.6	2.82	0.81	0.007	84.3	79.6	0.87	0.25	0.39
22 months	90.4	83.0	2.01	0.54	0.051	83.2	79.7	0.69	0.19	0.49
24 months	91.5	80.0	3.46	0.89	0.001	85.8	76.4	2.00	0.52	0.05
26 months	90.9	79.1	3.53	0.91	0.001	85.2	75.7	2.01	0.53	0.05
28 months	89.8	78.8	3.14	0.83	0.003	83.4	76.9	1.31	0.35	0.20

Table 3. DQ and IQ of FCG by entry age group.

Age at placement	42 months (BSID-II)				54 months (WPPSI-R)			
	N	Mean	SD	SE	*N*	Mean	SD	SE
0–18 months	14	94.4	11.9	3.2	14	84.8	16.0	4.3
18–24 months	16	89.0	11.3	2.8	15	86.7	14.8	3.8
24–30 months	22	80.1	13.3	2.8	22	78.1	19.5	4.2
30+ months	9	79.7	17.1	5.7	8	71.5	23.8	8.4

baseline (before randomization), 30 months, and 42 months with the Bayley Scales of Infant Development (BSID-II) (*20*) and at 54 months with the Wechsler Preschool Primary Scale of Intelligence (WPPSI-R) (*21*). Both tests were administered by trained and reliable Romanian psychologists. Upon entry into the study, our IG scored below our sample of community children (NIG) on developmental quotient (DQ). The IG also fared worse than the NIG on a variety of other developmental indices (*22*).

The BSID-II measure mental and motor development in infants from 1 to 42 months of age. The test measures a child's level of development in three domains: cognitive, motor, and behavioral. Scores on the mental development index (MDI, a scaled score) of the BSID-II can range from <50 to 150. Children who obtained raw scores that placed their scaled scores below 50 were assigned a numeric MDI score of 49. For our analyses, raw scores were assigned an extrapolated age-equivalent score to allow values <50 when needed (*23*). Thus, DQs were computed for each child [(extrapolated age-equivalent score/chronological age) × 100], allowing inclusion of the entire sample in analyses.

The WPPSI-R consists of 14 subtests that assess intellectual functioning in verbal and performance domains. The verbal section includes such tests as vocabulary, general information, and arithmetic; and the performance section includes such tests as picture completion, copying geometric designs, and using blocks to reproduce designs. Subtest and composite scores represent intellectual functioning in verbal and performance cognitive domains, as well as a child's general intellectual ability (full-scale IQ).

The BSID-II assess a wide range of abilities, focusing on tasks with sensorimotor responses in infancy, whereas the WPPSI-R provides a more focused assessment of children's cognitive abilities by using primarily language-based items. Although test-retest on BSID-II is good, prediction from BSID-II to school IQ is not as strong as prediction from WPPSI-R to later IQ. As a result, one might expect differences in children's performance on the BSID-II versus the WPPSI-R simply because of differences in the nature of the test instruments.

At the outset of our study, we implemented procedures to ensure its ethical integrity. A detailed description of these procedures is included in (*18*), but they are outlined here. First, our study was initiated at the invitation of the then–secretary of state for child protection in Romania and was approved by the local commissions on child protection in Bucharest, the Romanian ministry of health, and, in 2002, by an ad hoc ethics committee comprising appointees from several government and Bucharest University academic departments. It was therefore done with the participation and approval of local authorities. Second, the institutional review boards (IRBs) of the home institutions of the three principal investigators (the University of Minnesota, Tulane University, and the University of Maryland) approved the project. Third, we implemented a policy of noninterference with placement of children in both groups into alternative family care environments, leaving those decisions to Romanian child protection authorities (according to Romanian law). The only exception to the noninterference rule was that we ensured that no child placed in foster care as part of the randomization process would ever be returned to an institution (*18*, *24*–*26*). Fourth, after our preliminary results began to suggest positive benefits of foster care, we held a press conference to announce the results of our investigation. Key ministries in the Romanian government were invited to attend and sent representatives to this meeting. The then–U.S. ambassador to Romania (who was briefed in advance about our findings) gave the opening remarks at the conference. Fifth, although the usefulness of clinical equipoise is controversial among bioethicists (*18*), a reasonable interpretation of clinical equipoise supports the research design in this project. Clinical equipoise is the notion that there must be uncertainty in the expert community about the relative merits of experimental and control interventions such that no subject should be randomized to an intervention known to be inferior to the standard of care (*27*). Because of the uncertainty in the results of prior research, it had not been established unequivocally that foster care was superior to institutionalized care across all domains of functioning, especially with respect to how young children initially placed in institutional care function when placed in foster care as compared with children who remain in the institutional setting. Moreover, at the start of our study there was uncertainty about the relative merits of institutional and foster care in the Romanian child welfare community, with a historical bias in favor of institutional care. Additionally, given that the study was invited by Romanian authorities and conducted there, with the aim of guiding child welfare policy in Romania, it made sense to assess the study in view of the local standard of care, which was institutional care. The study also presented no more than minimal risk to the subjects; specifically, children assigned to the IG continued to receive the same care as if the study had not been conducted, and the measures we used have all been used for many years in developmental science research. Lastly, we were aware from the outset of the policy implications of our work, and as the study progressed we made our results available to government officials and child protection professionals. Indeed, several years after our study began, the Romanian government passed a law that prohibits institutionalizing children less than 2 years old, unless the child is severely handicapped.

Over the course of the study, there were instances of change in actual living arrangements and, in some cases, subject attrition (fig. S1). For example, of the 68 children who composed the IG, only 20 remained in institutions at the 54-month assessment. Seventeen children were lost to attrition. Of these, 9 were adopted or returned to their biological families, and their families decided not to continue participating in the study. Other children who remained in the study changed status: 2 children were adopted, 18 were placed in government foster care (which was not available at the onset of the study), 9 were reintegrated into their biological families, and 2 were placed in families with extended family members. Although some children changed their group assignment, an intent-to-treat approach was followed (*28*, *29*), whereby all analyses we report are based on children's original group assignment. Thus, our findings represent a conservative estimate of the response to intervention.

The first step of our data analysis focused on the randomized trial. Because, at the onset of the study, a number of children (N = 15) were not randomized until after they turned 30 months of age and others (12 children at 29 months and 7 children at 28 months) only shortly before then, we chose to focus our analyses on the later assessments. The NIG is included for reference only and is not included in the statistical analysis (*30*) (tables S1 and S2). Cross-sectional t tests at each time point yielded significant differences between IG and FCG at 42 months (BSID-II), $t(116) = 3.39$ and $P = 0.001$, and at 54 months (WPPSI-R), $t(108) = 2.48$ and $P = 0.015$. The effect size (the difference between means in multiples of standard deviations) was 0.62 at 42 months and 0.47 at 54 months. The primary finding of the randomized trial was that the foster care intervention led to improved cognitive outcomes as assessed by DQ and IQ (Table 1).

We next inquired into possible correlates of this finding within the FCG. We looked at three dichotomous factors: birth weight (above or less than 2500 g), gender, and age at entry to foster care (before or after 24 months of age). Neither birth weight nor gender was significantly associated with DQ or IQ at either 42 or 54 months. To examine the effect of entry age, we used t tests to compare DQ and IQ scores by dichotomized age at entry to foster care (younger than cutoff/older than cutoff) separately for placement cutoffs of 20, 22, 24, 26, and 28 months of age (*31*). Significant differences in 42-month DQ between early and late foster care placement groups existed for all age cutoffs, whereas for 54-month IQ the deflection point appeared to occur at 24 and 26 months (Table 2 and tables S3 and S4). In other words, the assessment at 42 months yielded significant differences in DQ regardless of age of placement, whereas the WPPSI-R data at 54 months suggested that children placed before 2 years of age had the best response to intervention.

In addition, we computed a regression of DQ at 42 months and IQ at 54 months on DQ at entry age. We used slope estimates to show the expected loss of 42- and 54-month DQ and IQ points for each additional month of institutionalization. Results revealed that the cost of remain-

ing in the institution was 0.85 DQ points per month at 42 months ($P < 0.001$) and 0.59 IQ points at 54 months ($P < 0.09$).

Children's scores differed slightly on the BSID-II versus the WPPSI-R exam (Table 2). We attribute this to the different psychometric properties of these instruments as mentioned earlier. As a secondary analysis, we separated the FCG into two groups that experienced similar durations of intervention but that had entered foster care at different ages. One group consisted of those children who entered foster care before 18 months of age ($n = 14$, mean placement age = 12.0 months), and the other group consisted of children entering after 18 months ($n = 47$, mean placement age = 26.6 months). We then chose the measurement occasion that most nearly equated these groups on length of intervention, specifically the 30-month DQ assessment for the earlier entry group and the 42-month assessment for the later entry group. At these assessment points, the mean lengths of time in foster care were 18.2 and 16.1 months respectively, and the mean DQs were 89.6 and 83.1, $t(59) = 1.55$, and $P = 0.13$. Although not statistically significant, we interpret the difference in group means as supporting our general conclusions about the importance of earlier placement age for improved cognitive outcomes.

The above analysis did not possess sensitivity to finer gradations in age of placement, and a tertiary analysis was performed. We divided the FCG into four groups: those placed between 0 and 18 months, those placed between 18 and 24 months, those placed between 24 and 30 months, and those placed after 30 months (Table 3). One-way analyses of variance (ANOVAs) yielded significant differences in DQ and IQ at 42 months ($P = 0.008$) but not at 54 months ($P = 0.20$). At 42 months, the two earlier entry groups (0 to 18 months and 18 to 24 months) are not significantly differ from one another, nor are the two later entry groups, but the two early placement groups (0 to 18 months and 18 to 24 months) are different from the two later placement groups (24 to 30 months and above 30 months). The 54-month data showed the anticipated ordering of means, although there are no significant differences among pairwise comparisons. Taken together, these findings suggest that age of entry into foster care (i.e., the timing of placement) was critical in changing children's cognitive abilities [see Supporting Online Material (SOM) text for additional analyses that address the issue of timing and duration of foster care effects on DQ and IQ at 42 and 54 months].

Because we assessed children before randomization, we are confident that differences that resulted from the foster care intervention reflect true intervention effects rather than differences in sample makeup. Moreover, randomization before intervention addressed concerns about previous studies of adopted children that have the potential of selection bias with regard to who is adopted. Additionally, by randomizing children before intervention we increased the likelihood that unknown prenatal risk factors would be randomly distributed across the intervention and control groups. Lastly, the inclusion of an in-country comparison sample confirmed that our cognitive assessments were valid, given that the DQ and IQ means for the never-institutionalized Romanian children were very similar to the means for typically developing children in populations for which the BSID-II and the WPPSI-R have been standardized.

Three main findings emerge from this study. First, as we have previously reported (*22*), children reared in institutions showed greatly diminished intellectual performance (borderline mental retardation) relative to children reared in their families of origin. Second, as a group, children randomly assigned to foster care experienced significant gains in cognitive function. Lastly, at first glance our findings suggest that there may be a sensitive period spanning the first 2 years of life within which the onset of foster care exerts a maximal effect on cognitive development. However, a closer reading of our analyses suggests a more parsimonious conclusion: That the younger a child is when placed in foster care, the better the outcome. Indeed, there was a continuing "cost" to children who remained in the institution over the course of our study. These results are compatible with the notion of a sensitive period, but discovering whether such a period truly exists or determining the borders that delineate it would likely require a larger sample size with a broader age range at intervention onset.

The results of this study have implications for child welfare because they suggest that placement in families is more advantageous for cognitive development in infants and young children than placement in institutional settings. For countries grappling with how best to care for abandoned, orphaned, and maltreated young children, these findings deserve consideration. The results also indicate that previously institutionalized children's cognitive development benefits most from foster care if placement occurs relatively early in a child's life.

References and Notes

1. J. W. Curtis, C. A. Nelson, in *Resilience and Vulnerability: Adaptation in the Context of Childhood Adversities*, S. Luthar, Ed. (Cambridge Univ. Press, London, 2003), pp. 463–488.
2. J. T. Bruer, W. T. Greenough, in *Critical Thinking About Critical Periods*, D. B. Bailey Jr., J. T. Bruer, J. W. Lichtman, F. J. Symons, Eds. (Brookes, Baltimore, MD, 2001), pp. 209–232.
3. H. F. Harlow, S. J. Suomi, *Proc. Natl. Acad. Sci. U.S.A.* **68**, 1534 (1971).
4. M. M. Sánchez *et al.*, *Dev. Psychopathol.* **13**, 419 (2001).
5. H. T. Chugani *et al.*, *NeuroImage* **14**, 1290 (2001).
6. T. J. Eluvathingal *et al.*, *Pediatrics* **117**, 2093 (2006).
7. M. R. Gunnar, in *Handbook of Developmental Cognitive Neuroscience*, C. A. Nelson, M. Luciana, Eds. (MIT Press, Cambridge, MA, 2001), pp. 617–630.
8. C. H. Zeanah *et al.*, *Dev. Psychopathol.* **15**, 885 (2003).
9. S. J. Morrison, A. Ames, K. Chisholm, *Merrill Palmer Q.* **41**, 411 (1995).
10. M. Rutter *et al.*, *J. Child Psychol. Psychiatry Allied Discip.* **39**, 465 (1998).
11. As a rule, most such studies report that children adopted out of institutions suffer from growth and intellectual delays as well as social-emotional problems. The more time the child spends in an institution before adoption, the more substantial and persistent the developmental delays he or she experiences.
12. D. E. Johnson, in *The Effects of Early Adversity on Neurobehavioral Development*, C. A. Nelson, Ed. (Lawrence Erlbaum, Mahwah, NJ, 2000), vol. 31, pp. 113–162.
13. D. E. Johnson *et al.*, *JAMA* **268**, 3446 (1992).
14. M. L. Rutter, J. M. Kreppner, T. G. O'Connor, *Br. J. Psychiatry* **179**, 97 (2001).
15. C. H. Zeanah, *J. Dev. Behav. Pediatr.* **21**, 230 (2000).
16. There were six institutions for abandoned children in Bucharest, and by drawing on all of them we avoided the possibility that some institutions were better or worse than others. These six institutions were representative of institutions in Romania generally and are comparable to institutions in Eastern European (e.g., Russia and Bulgaria) and some Asian (e.g., China) countries.
17. J. M. Tanner, in *Textbook of Pediatrics*, J. O. Forfar, G. C. Anreil, Eds. (Churchill Livingstone, London, 1973).
18. Materials and methods are available on *Science* Online.
19. C. H. Zeanah, A. T. Smyke, L. Settles, in *Handbook of Early Childhood Development*, K. McCartney, D. Phillips, Eds. (Blackwell, Malden, MA, 2006), pp. 424–454.
20. N. Bayley, *Bayley Scales of Infant Development* (Psychological Corporation, New York, ed. 2, 1993).
21. *Wechsler Preschool and Primary Scale of Intelligence* (Harcourt Assessment, San Antonio, TX, 2000).
22. A. T. Smyke *et al.*, *J. Child Psychol. Psychiatry Allied Discip.* **48**, 210 (2007).
23. J. C. Lindsey, P. Brouwers, *Clin. Neuropharmacol.* **22**, 44 (1999).
24. C. H. Zeanah *et al.*, *Infant Ment. Health J.* **27**, 559 (2006).
25. D. R. Wassenaar, *Infant Ment. Health J.* **27**, 577 (2006).
26. C. H. Zeanah *et al.*, *Infant Ment. Health J.* **27**, 581 (2006).
27. C. Weijer, P. B. Miller, *Nat. Med.* **10**, 570 (2004).
28. By "intent to treat," we mean that the data were analyzed on the basis of the original group assignments to which participants were randomized, even though over the course of the study a given child's group assignment may have changed.
29. R. Little, L. Yau, *Biometrics* **52**, 1324 (1996).
30. We previously reported on the DQ of the IG and NIG at baseline [i.e., DQ of the IG = 74 and DQ of NIG = 103 (*22*)].
31. There were too few children below 18 months or above 28 months contributing data, and thus we were unable to examine timing effects for those younger or older than these ages.

32. The work reported in this manuscript was supported by funds from the John D. and Catherine T. MacArthur Foundation; C.A.N. also acknowledges the generous support of the Richard David Scott endowment. We thank J. Kagan and L. Eisenberg for commenting on an earlier draft of this paper; E. Furtado for manuscript preparation; G. Gordon for assistance in data management; S. Koga for overseeing the project in Romania and for intellectual and personal commitment to the project; D. Johnson for evaluating the children in this project before baseline assessment and for wisdom and guidance throughout the project; H. Woodward and the MacArthur Foundation Research Network on Early Experience and Brain Development for input regarding the conceptualization, design, and implementation of this project; anonymous reviewer no. 6, who provided insightful suggestions for both data analysis and interpretation; F. Miller, G. Fleisher, and J. Kahn for discussion of clinical equipoise; the caregivers and children who participated in this project; the BEIP staff for their tireless work on our behalf; and our many colleagues in Romania who facilitated our work, particularly B. Simion, A. Stanescu, M. Iordachescu, and C. Tabacaru.

Supporting Online Material

www.sciencemag.org/cgi/content/full/318/5858/1937/DC1
Materials and Methods
SOM Text
Fig. S1
Tables S1 to S5
References

17 April 2007; accepted 31 October 2007
10.1126/science.1143921

Benchtop Ultracentrifuge

The Optima MAX-XP benchtop ultracentrifuge delivers fast run times of up to 150,000 rpm (2,500 revolutions per second) and is exceptionally quiet. The new MLA-150 fixed-angle rotor has a low k-factor for rapid separation of small volumes such as subcellular particles, viruses, and proteins. The Optima MAX-XP features redesigned software with significant ease-of-use enhancements. The user interface is intuitive and customizable with control via a full-color touch screen. Optional remote monitoring and control of the system is also available. It is offered with multiple levels of biocontainment and is designed to fit in a standard biosafety hood.

Beckman Coulter For information 714-993-8955 www.beckmancoulter.com

Borosilicate Filter Products

The Robu VitraPOR borosilicate glass filter products offer high chemical resistance, minimal thermal expansion, and high thermal shock resistance. They are suitable for use in chemical, biochemical, pharmaceutical, and laboratory applications. Standard fritted disks are available in rounded shapes from 5 mm to 400 mm diameters. They are also available in precision ground and fused edge configurations. Filter candles are available in cylindrical or conical shapes from 9 mm to 40 mm in diameter. Custom filters can be provided in any shape up to 400 mm, in almost any thickness. Any cylindrical or conical filter candle can be produced to customer design. They are available in porosities ranging from 1 μm to 550 μm.

Andrews Glass Co. For information 800-845-0026 www.andrews-glass.com

GC Column Installation

The Cool-Lock Nut simplifies gas chromatography (GC) column installation and eliminates the need for wrenches and other tools. The low thermal mass design allows the Cool-Lock Nut to cool rapidly, preventing users from burning their fingers during column changes. Other design elements prevent the column from slipping to ensure a more reproducible depth for improved method accuracy. The nut is designed for use with Agilent Technologies' GC instruments and works with all standard GC columns. It is available in both long and short ferrule style dimensions and can be used over and over.

Phenomenex For information 310-212-0555 www.phenomenex.com

Cell Behavior Monitoring

ECIS (electric cell-substrate impedance sensing) measurement non-invasively follows the impedance of cell-coated electrodes in real time without the use of fluorescence or radiolabeled materials. In the past, ECIS researchers were restricted to monitoring cells grown at the base of standard tissue culture wells. Now cells can be grown in special disposable flow arrays, where cells are cultured on the floor of a flow channel that is 44 mm high and 0.5 cm wide. Eight independent measuring electrodes, located along the 5 cm length of the channel, monitor cell behavior and its response to changing flow conditions. The flow array can be used with all ECIS models and fits neatly into the standard array holder. To support this flow array, a complete flow module is designed to interface with the ECIS 1600R and ECIS 1600/800 systems. This module includes a peristaltic pump designed to operate within the high humidity of a tissue culture incubator along with medium reservoirs, a flow equalizer, tubing, fittings, and a start-up supply of flow arrays.

Applied BioPhysics For information 8666-301-3247 www.biophysics.com

Transcription Kit

The AmpliScribe T7-Flash Transcription Kit produces a high yield of RNA from an in vitro transcription reaction in a short time. The 30-minute AmpliScribe T7-Flash reaction produces 160–180 μg of RNA from 1 μg of DNA template—more RNA than some kits produce in two hours. High yields of full-length transcripts are readily obtained from a wide range of DNA template sizes.

Epicentre Biotechnologies For information 800-284-8474 www.EpiBio.com/flash.asp

Gel Permeation Chromatography

The Viscotek Model 350 High Temperature Gel Permeation Chromatography (HT-GPC) System is designed for the characterization of polyolefins and other synthetic polymers that are soluble only at elevated temperatures. The system provides absolute molecular weight without extrapolation or correction, molecular size, and intrinsic viscosity, as well as information on branching, structure, and aggregation in a single experiment. The system can also be configured with an infrared detector for short-chain branching analysis or an ultraviolet/visible detector for copolymer compositional analysis. The system includes a high temperature triple detector array, an automated sample preparation and delivery system, a pulseless isocratic pump, and a degasser. The system combines low-angle light-scattering with viscometry and concentration for complete and comprehensive macromolecular characterization. All detectors reside within a temperature-controlled oven compartment that has space for four analytical GPC columns.

Viscotek Europe For information +44 1344 467180 www.viscotek.com

Fractionation Reagent

Fraction-FOCUS makes use of proven technology to fractionate and concentrate all proteomes into multiple fractions, simplifying two-dimensional maps and enhancing detection of low abundant proteins. There is no detectable loss of total protein during the procedure. At the end of the fractionation, cellular proteins are in one of many fractions. The entire fractionation is carried out in micro-scale. It is compatible with all downstream protein identification techniques.

G-Biosciences/Genotech For information 800-628-7730www.GBiosciences.com

Newly offered instrumentation, apparatus, and laboratory materials of interest to researchers in all disciplines in academic, industrial, and government organizations are featured in this space. Emphasis is given to purpose, chief characteristics, and availability of products and materials. Endorsement by *Science* or AAAS of any products or materials mentioned is not implied. Additional information may be obtained from the manufacturer or supplier.

We've got **Careers** down to a **Science**.

For full advertising details, go to **www.sciencecareers.org** and click on **For Advertisers,** or call one of our representatives.

United States & Canada

E-mail: advertise@sciencecareers.org
Fax: 202-289-6742

IAN KING
Recruitment Sales Manager/
Industry – US & Canada
Phone: 202-326-6528

ALEXIS FLEMING
Northeast Academic
Phone: 202-326-6578

TINA BURKS
Southeast Academic
Phone: 202-326-6577

DARYL ANDERSON
Midwest/Canada Academic
Phone: 202-326-6543

NICHOLAS HINTIBIDZE
West Academic
Phone: 202-326-6533

Europe & International

E-mail: ads@science-int.co.uk
Fax: +44 (0) 1223 326532

TRACY HOLMES Sales Manager
Phone: +44 (0) 1223 326525

ALEX PALMER
Phone: +44 (0) 1223 326527

ALESSANDRA SORGENTE
Phone: +44 (0) 1223 326529

MARIUM HUDDA
Phone: +44 (0) 1223 326517

LOUISE MOORE
Phone: +44 (0) 1223 326528

To subscribe to *Science*:
In US/Canada call 202-326-6417 or 1-800-731-4939
In the rest of the world call +44 (0) 1223-326-515

Science makes every effort to screen its ads for offensive and/or discriminatory language in accordance with US and non-US law. Since we are an international journal, you may see ads from non-US countries that request applications from specific demographic groups. Since US law does not apply to other countries we try to accommodate recruiting practices of other countries. However, we encourage our readers to alert us to any ads that they feel are discriminatory or offensive.

Science Careers
From the journal *Science* AAAS

POSITIONS OPEN

DIRECTOR, SANFORD CHILDREN'S HEALTH RESEARCH CENTER

Sanford Research/University of South Dakota and the Department of Pediatrics of the Sanford School of Medicine of the University of South Dakota (USD) are seeking a vibrant leader to head the new Sanford Children's Health Research Center (SCHRC). An historic $400 million gift by philanthropist **T. Denny Sanford** earlier this year has allowed for expansion of Sanford Research/USD and dynamic development of programs focused on children's health. An additional donation by Mr. Sanford has led to the creation of a two-campus Sanford Children's Health Research Center at the Burnham Institute for Medical Research in La Jolla, California and Sanford Research/USD in Sioux Falls, South Dakota. The collaboration between the two locations will establish the basis of an integrated, world class, academic pediatric research network.

We seek a scientist with a superior record of accomplishment in pediatric research to develop a strategic plan for the new research center and to oversee aggressive development of a comprehensive program of basic and applied research in collaboration with the Burnham site in La Jolla. Within SCHRC, Endowed Pediatric Research Programs in Cancer Biology, Neurosciences, Molecular Cardiology, and Developmental Genetics are planned. A research concentration in one of these areas is preferred. Highly qualified individuals with research interests other than those listed will also be given consideration.

Qualifications include the M.D. and/or Ph.D. degrees, a well-established funding record, and strong leadership qualities. This individual should be capable of qualifying for academic appointment at the rank of **ASSOCIATE or FULL PROFESSOR** in the Department of Pediatrics. A comprehensive compensation package will be tailored to the individual's qualifications. In addition, the individual will receive a package of institutional support including laboratory space and research endowment.

SCHRC will be a central occupant of a new multidisciplinary research building to be constructed. This 18-story, 800,000 square-foot facility will be the center of a new biomedical research park.

Applications should include detailed curriculum vitae, a description of research experience and future plans, and the names and contact information for at least three references.

Application materials should be sent to:

H. Eugene Hoyme, M.D.
Professor and Chair, Department of Pediatrics
Sanford School of Medicine of the University of South Dakota
Chief Pediatric Medical Officer, Sanford Children's Hospital
1305 W. 18th Street, P.O. Box 5039
Sioux Falls, SD 57117-5039
Telephone: 605-333-6447; fax: 605-333-1507
E-mail: hoymeg@sanfordhealth.org

We encourage women and candidates from underrepresented minority groups to apply.

The Department of Cellular Biology at the University of Georgia invites applications for a **LECTURER** for fall 2008. A Ph.D. in a relevant field is required. Responsibilities include teaching anatomy and physiology, together with contributing to the Department's current undergraduate curriculum. Preference will be given to applicants with the demonstrated ability to teach and manage large lecture courses. Applicants should send curriculum vitae, research experience, teaching profile, and three recommendation letters to: **Chair-Lecturer Search, Department of Cellular Biology, 724 Biological Sciences, Athens, GA 30602.** Submit electronic applications to **e-mail: cbsearch@uga.edu.** Applications received by February 4, 2008, will receive full consideration. *The Franklin College of Arts and Sciences, its many units, and the University of Georgia are committed to increasing the diversity of its faculty and students, and sustaining a work and learning environment that is inclusive. The University is an Equal Employment Opportunity/Affirmative Action Institution.*

POSITIONS OPEN

INSTITUT PASTEUR

POSTDOCTORAL FELLOWSHIPS
Institut Pasteur, Paris, France

Founded in 1887 by Louis Pasteur and located in the heart of Paris, the Institut Pasteur is a world-renowned private research organization. The Pasteur Foundation of New York is seeking outstanding fellowship applicants. Candidates may apply to any laboratory within 10 Departments: Cell Biology and Infection, Developmental Biology, Genomes and Genetics, Immunology, Infection and Epidemiology, Microbiology, Neuroscience, Parasitology and Mycology, Structural Biology and Chemistry, and Virology. See website for details. Annual package is $70,000 for three years. This is a biannual call for applicants; see website for deadlines. *U.S. citizenship required.*

E-mail: pasteurus@aol.com. Website: http://www.pasteurfoundation.org.

The Del E. Webb Center for Neuroscience, Aging, and Stem Cell Research (NASCR) of the Burnham Institute for Medical Research (BIMR) seeks independent investigators with strong research programs in stem cell and developmental biology, aging and neurodegenerative disorders, or cardiac and pancreatic/metabolic diseases. Applications using genetic model systems are particularly welcome. Individuals at any career level, including **JUNIOR INVESTIGATORS,** are encouraged to apply. BIMR offers an outstanding interdisciplinary and highly collaborative research environment, supported by a wide range of shared resources, including the La Jolla-Wide Interdisciplinary Neuroscience Center Core Facilities Grant funded by NIH. For more details visit our **websites: http://www.burnham.org/** and **http://www.lajollaneuroscience.org/.** Informal inquiries should be directed to appropriate **NASCR Center Program Directors** (contact information listed on the website). To apply, please submit curriculum vitae and research summary electronically by March 1, 2008 (mail to **e-mail: nascrrecruit@burnham.org).** Candidates should arrange to have at least three letters of reference sent to this e-mail address (preferred) or by regular mail to: **Neuroscience, Aging, and Stem Cell Research Recruitment Committee, c/o Stuart A. Lipton, M.D., Ph.D., Scientific Director, NASCR Center, Burnham Institute for Medical Research, 10901 North Torrey Pines Road, La Jolla, CA 92037.** *Equal Opportunity Employer/Affirmative Action.*

The Department of Physiology and Biophysics at the University of Alabama at Birmingham (UAB) invites applications for a tenure-track or tenured faculty position. UAB is a leading research university ranked among the top public universities in NIH funding. We are seeking a dynamic Investigator/Educator to complement the existing strengths of our Department (see our **website: http://www.physiology.uab.edu).** Applicants with expertise in cell signaling and/or cancer biology are especially encouraged to apply. The successful candidate will have an M.D. or Ph.D. in a biomedical science, a strong publication record, a commitment to teaching, and excellent funding potential. Salary and rank **(ASSISTANT, ASSOCIATE, or FULL PROFESSOR)** will be commensurate with experience. Competitive startup funds and generous laboratory space will be offered. Please send curriculum vitae, statement of research plans, and three references to: **Dr. Kevin L. Kirk, Department of Physiology and Biophysics, University of Alabama at Birmingham, 1918 University Boulevard, MCLM 982, Birmingham AL 35294-0005** or by **e-mail: klkirk@uab.edu.** *The University of Alabama at Birmingham is an Affirmative Action/Equal Opportunity Employer.*

THE CHINESE UNIVERSITY OF HONG KONG

Applications are invited for:-

Department of Physics

Assistant Professor

(Ref. 07/267(665)/2)

Applications are invited for an assistant professorship in physics and materials science. Applicants should have a relevant PhD degree with postdoctoral research experience. A demonstrated record of research accomplishments is highly preferred. The appointee is expected to develop his/her independent research programme and show strong leadership. Appointment will normally be made on contract basis for up to three years initially, leading to longer-term appointment or substantiation later subject to performance and mutual agreement. Applications will be accepted until the post is filled. [Monthly salary range: HK$45,580 to HK$58,025; approximate exchange rate in December 2007: US$1=HK$7.8]

Salary and Fringe Benefits
Salary will be highly competitive, commensurate with qualifications and experience. The University offers a comprehensive fringe benefit package, including medical care, plus a contract-end gratuity for an appointment of two years or longer, and housing benefits for eligible appointees.

Further information about the University and the general terms of service for appointments is available at *http://www.cuhk.edu.hk/personnel*. The terms mentioned herein are for reference only and are subject to revision by the University.

Application Procedure
Please send full resume, copies of academic credentials, a publication list and/or abstracts of selected published papers (if any), together with names, addresses and fax numbers/e-mail addresses of three referees to whom the applicants' consent has been given for their providing references (unless otherwise specified), to Professor Hai-Qing Lin, Chairman, Department of Physics, The Chinese University of Hong Kong, Shatin, Hong Kong (Fax: (852) 2603 5204). The Personal Information Collection Statement will be provided upon request. Please quote the reference number and mark "Application - Confidential" on cover.

Postdoctoral Position
Biological/Organic Chemistry

The Bioscience Division of Los Alamos National Laboratory strives to build a strong scientific and technological base for addressing the complex problems of infectious diseases. In this position, you will join an interdisciplinary team of cell biologists, biochemists, and immunologists working to develop novel detection and surveillance systems against biothreat agents. We are seeking an outstanding candidate with an excellent publication record. Mandatory requirements include a Ph.D. (received within the past 5 years); a foundation in molecular and cellular biology and bioorganic chemistry; expertise in two or more of the following: mammalian and bacterial cell culture, design, synthesis and analysis of biologically relevant molecules, and combinatorial libraries. A publication record demonstrating one or more of these skills. Experience in a BSL 2 laboratory is preferred, as is a background working at the interface of host/pathogen biology and drug delivery systems, and expertise in bacterial diseases and biofilm research. Starting salary is commensurate with background and experience with generous medical, vision and dental benefits.

For a full job description and to apply, refer online at:
http://www.hr.lanl.gov/JobListing/index.aspx?JobType=Postdoc
referencing Job# 213698, as well as submit CV; statement of research, outreach, and career goals; reprints of publications; university transcripts; and three letters of recommendation with contact information, to: **Dr. Rashi Iyer, Biosciences Division, M888, Los Alamos National Laboratory, Los Alamos, NM 87544; E-mail: rashi@lanl.gov. Web site: http://ext.lanl.gov.** EOE

Los Alamos
NATIONAL LABORATORY

www.lanl.gov/jobs

TWO TENURE TRACK POSITIONS
NEUROSCIENCE

The Department of Psychology, Hunter College (CUNY) invites applications for two faculty positions in Neuroscience (tenure track) to begin fall, 2008. The department currently offers training in Neuroscience at the undergraduate, Master's and doctoral level to an urban ethnically diverse student population at a public university. The senior position (associate/ full professor) requires a candidate with an internationally recognized research program, a history of substantial external funding, and the ability to provide leadership in the expansion of an interdisciplinary doctoral program in Neuroscience. An emphasis on behavioral and/or functional processes and mechanisms in animals or humans is desirable.

For the junior position (assistant or associate professor) we are seeking a neuroethologist/neurophysiologist with a research focus on the analysis of neural mechanisms underlying behavior. Postdoctoral research experience and a demonstrated potential to obtain external funding are important criteria as is the ability to develop interdisciplinary collaborations and contribute to the strengthening of undergraduate training in neuroscience.

Applications should include a cover letter, CV, statement of research objectives and names and contact information of three or more academic references. Please send applications to: **Gordon Barr, Ph.D., Acting Chair of Psychology, Hunter College, 695 Park Avenue, 611 North, New York, NY 10065.**

HUNTER
The City University of New York

EEO/AA/ADA/IRCA employer.

INVEST IN CUNY

Tenure-Track Faculty Position
in Science Education
in the Department of Biology

The Department of Biological Sciences at the California State University, Chico invites applications for a full-time, tenure-track faculty position at the level of **ASSISTANT** or **ASSOCIATE PROFESSOR** in science education to begin Fall 2008. Applicants must have a Doctorate in a biological science or science education with at least a Master's degree or equivalent in biology. Postdoctoral experience is desired. Teaching responsibilities include introductory and upper-division biology courses and general education courses for non-majors. Candidates must have a record of research in biology (education) and will be expected to establish an active research program in biology education and seek extramural funding. Masters and undergraduate student participation in the research program is expected.

All applicants must complete the Application for Academic Employment Form, which is available on-line at **http://www.csuchico.edu/hr/Forms/VPHR-FacultyEmplApp.doc** and a resume, a 1-page narrative describing your evidence of quality teaching, a statement of plans for scholarly activity in biology education, preferably as pdf documents; unofficial graduate and undergraduate transcripts, and three current letters of recommendation to: **Biology Education Search, Dr. Ailsie McEnteggart, Biology Chair, California State University, Chico, Chico CA 95929-0515**. Review will begin **January 14, 2008**. Applications completed after that date may be considered. Application materials submitted electronically must be in PDF format. For full announcement and description of science education opportunities at CSU, Chico, please see: **http://csucareers.calstate.edu**. For disability-related accommodations, call **530-898-6192**.

CSU, Chico is an EOE/AA/ADA Employer and only employs individuals lawfully authorized to work in the United States.

Children's Hospital Boston

Harvard Medical School

Assistant/Associate Professor
Division of Genetics, Department of Medicine

Applications are invited for a tenure-track Assistant/Associate Professor position in the Division of Genetics in the Department of Medicine at Children's Hospital Boston. We seek an outstanding MD and/or MD/PhD scientist who will establish a vigorous basic science or translational research program with relevance to developmental biology and developmental disorders of childhood. The successful candidate will have modern laboratory space located in the new Children's Hospital Center for Life Science Building that will open in the spring of 2008. Joint appointments in the Program in Genomics at Children's Hospital, and the Broad Institute of MIT and Harvard may be available for appropriate applicants. The Division resides within a very strong research community in genetics, developmental biology and related disciplines throughout the Harvard Longwood Medical Area and the investigator will hold both Children's Hospital Boston and Harvard Medical School faculty appointments.

Please submit a current CV, a 2- or 3-page description of research interests and directions, and three to five reference letters. Materials should be sent via e-mail by **March 1, 2008** to: **geneticssearch@childrens.harvard.edu**. For questions, please contact **Marcy Belliveau** at **617-355-3480**.

We particularly encourage applications from women and minority candidates. Equal Opportunity/Affirmative Action Employer.

Bioenergy- and Bioproducts-Related Microbiology Faculty Positions: Michigan State University

The Department of Microbiology and Molecular Genetics at Michigan State University (MSU) seeks applications for two academic-year, tenure-track, junior- or senior-level faculty positions in bioenergy and bioproducts-related microbiology. Requirements include a doctoral degree in microbiology or a related discipline, at least two years of postdoctoral research experience, and a strong record of research accomplishment in addressing fundamental questions of microbial diversity, genetics, genomics, metabolism and/or physiology. Examples of possible research areas include, but are not limited to, the ecology and physiology of biomass conversion, metabolic analysis, and systems biology approaches. The successful applicants will join colleagues associated with the DOE-funded Great Lakes Bioenergy Research Center, the Center for Microbial Ecology, and the Microbial Systems Sciences Group. Responsibilities include developing an independent, externally funded research program with national visibility and teaching within our graduate, professional, and/or undergraduate programs. The offer will include a competitive startup package and a laboratory within our new state-of-the-art research building.

Applicants should submit a letter of application, curriculum vitae including complete publication list, statement of research goals, copies of pertinent reprints and contact information (address, e-mail, and phone) for three referees to: **Bioenergy Microbiology Search Committee, Department of Microbiology and Molecular Genetics, 2209 Biomedical and Physical Sciences Building, Michigan State University, East Lansing, MI 48824** (web: mmg.msu.edu). Electronic submissions to **MMGCHAIR@MSU.EDU** in pdf format are preferred. Review of applications will begin by **January 31, 2008** and will continue until the positions are filled.

Michigan State University is an Affirmative Action/ Equal Opportunity Employer.

UNIVERSITY OF MASSACHUSETTS MEDICAL SCHOOL

Director, Program in RNAi Therapeutics

Director, Program in Gene Therapy

The University of Massachusetts Medical School is searching for two senior leaders to direct new programs in RNAi Therapeutics and in Gene Therapy. Both programs will be permanently housed in a state-of-the-art new research building with sufficient space and funding to support a substantial number of new faculty hires. Although administratively separate, it is expected that the two programs will have common interests and work closely together. The two programs will capitalize upon and enhance the Medical Schools existing strengths in RNA biology and RNAi research, and be an integral part of ongoing clinical translational efforts including an active clinical gene therapy trial program.

Successful applicants will be leaders in their respective fields with nationally and internationally recognized active research programs, and have the vision and ability to recruit a cohort of equally outstanding faculty. Both programs will play pivotal roles in the development of the UMass Advanced Therapeutics Cluster, a key component of Commonwealth of Massachusetts Life Sciences Initiative. The two programs will also be an important component of the University's clinical and translational science award (CTSA) application.

Applicants should send a curriculum vitae and cover letter briefly outlining their interest in the position to:

Dr. Michael R. Green
Chair, Search Committee
Program in Gene Function and Expression
University of Massachusetts Medical School
Lazare Research Building
364 Plantation St., Room 628
Worcester, MA 01605

or electronically to **michael.green@umassmed.edu**

The University of Massachusetts Medical School is an Equal Opportunity/Affirmative Action Employer.

THE UNIVERSITY OF SOUTHERN MISSISSIPPI DEPARTMENT OF BIOLOGICAL SCIENCES TENURE-TRACK FACULTY POSITION IN BIOLOGICAL SCIENCES/GENOMICS

The University of Southern Mississippi Department of Biological Sciences invites applications for a tenure-track assistant professor position studying fundamental questions at the genomic, proteomic or bioinformatic levels. This position complements an ongoing search for an additional faculty position in bioinformatics/computational biology (**http://www.usm.edu/biology/positions**). The department is particularly interested in applicants with interests and experience in biomedical-related research. The successful applicant will join a growing, interdisciplinary, research-intensive department and will have the opportunity to interact with the state-wide, NIH-funded Mississippi Functional Genomics Network (**http://mfgn.usm.edu/**) at the research or administrative levels. The applicant will also have an opportunity to interact with the Mississippi Computational Biology Consortium (**http://mcbc.usm.edu/mcbc/**).

The University, a Carnegie High Research Activity Institution with 15,000 students, is located in Hattiesburg, near the resort areas of the Gulf Coast. Hattiesburg is the medical, commercial and cultural center of south Mississippi and is renowned for safe, affordable living and abundant outdoor recreational activities. The Department of Biological Sciences (**http://www.usm.edu/biology/**) is comprised of twenty-nine faculty and offers BS, MS and Ph.D. degrees. Over 60 graduate students currently pursue MS and Ph.D. degrees.

The successful candidate will be expected to establish an active, extramurally funded research program, mentor graduate students and participate in undergraduate and graduate teaching in his or her area of expertise. Postdoctoral research experience is required. Laboratory and office space as well as a generous start-up package will be provided. Applicants should submit a letter of application, curriculum vitae, statement of research plans, copies of pertinent reprints and three letters of reference to **Glen Shearer, Bioinformatics Search Committee, Dept. of Biological Sciences, The University of Southern Mississippi, 118 College Drive #5018, Hattiesburg, MS 39406-0001**. Electronic submission preferred (**glen.shearer@usm.edu**). Review of applications will begin on **15 January 2008** and continue until the position is filled.

The University of Southern Mississippi is an Affirmative Action/ Equal Opportunity Employer.

National Institute for Basic Biology, Okazaki, Japan

Professorships/Associate Professorship

The National Institute for Basic Biology (NIBB) in Okazaki, Japan, invites applications from outstanding candidates for four professorships and one associate professorship.

Since it was founded on the recommendation of the Science Council of Japan in 1977, the NIBB has functioned as a national center for biological sciences. Its research activities are among the highest ranked within the field in Japan, as judged by measures such as citations per paper. To assist in its efforts, the NIBB recruits exceptional scientists not only from Japan but also from around the world.

We are seeking to appoint candidates with the high potential to become international leaders in any area within the field of basic biology. We welcome applications from candidates of all nationalities with excellent research records and fluency in either Japanese or English.

For more information, please visit the website at **<http://www.nibb.ac.jp/profapplication/>**.

To apply, please submit your curriculum vitae, brief summaries of your research accomplishments and future research plans (each within 800 words), two letters of recommendation, and reprints of representative work, which must be received no later than January 21, 2008. E-mail applications are also accepted (see the website above for more details).

Inquiries should be addressed to:
Tetsuo Yamamori,
Professor,
Division of Brain Biology,
National Institute for Basic Biology,
38 Myodaijicho,
Okazaki 444-8585,
Japan
Tel/Fax: 81-564-55-7615

National Central University

Faculty positions for Life Sciences

The Department of Life Sciences at the NCU is seeking candidates for several tenure track faculty positions. The duty of these positions will include research and teaching in selected postgraduate as well as undergraduate subjects. Qualified candidates should have a Ph.D. degree in life sciences-related fields and at least two years of postdoctoral training. Persons with an outstanding record of academic and scholarly accomplishment in life sciences are encouraged to apply. The deadline for application is February 15, 2008.

Please send by mail a letter of intent, curriculum vitae with publication lists, reprints of 1-3 representative publications, a brief of research and teaching proposal, and three recommendation letters to:

Dr. Wei-Hsin Sun
Chairman of Recruitment Committee
Department of Life Sciences
National Central University
No.300, Jhongda Rd
Jhongli City, 32054, Taiwan
E-mail: weihsin@cc.ncu.edu.tw
Fax: 886-3-4228482

VICE CHANCELLOR FOR RESEARCH UNIVERSITY OF MISSOURI - COLUMBIA

The University of Missouri-Columbia (MU) is seeking a scholar and administrator of national prominence for the position of Vice Chancellor for Research. The position is responsible for leadership and administration of research and technology development. The Vice Chancellor provides leadership for infrastructure and incentives that will enable faculty to achieve eminence in their research and scholarly goals. Responsibilities include administration of: (1) the Division of Sponsored Programs; (2) programs to generate increased funding and to diversify sources of funding; (3) a strategic plan that enables the University to excel in identified areas of current or emerging research strength; (4) MU's research initiatives at national institutes and foundations; (5) nine research centers and Office of Research operations with over 700 staff; (6) the University's responsibilities for compliance with Federal regulations and other legal restrictions on research; and (7) the MU Technology Management and Industry Relations Program. The Vice Chancellor is a key member of both the Chancellor's and Provost's staffs.

The successful candidate will have a terminal degree. In addition to an exemplary record of research, the person will have proven experience with national, state and private funding sources. Proven administrative and budgetary experience, good interpersonal skills, strong public speaking abilities, and a commitment to collegial, creative leadership in a highly diverse university system are expected.

The University of Missouri-Columbia was established in 1839 as the first public university west of the Mississippi River. It is the flagship of the University of Missouri System and is one of the most comprehensive and diverse universities in the United States. MU is a research extensive institution, a land-grant university, and a member of AAU. It offers baccalaureate, masters, first professional and doctoral degree programs. The University has a vital campus life with faculty and over 28,000 students dedicated to excellence in teaching and research. MU is situated in the attractive community of Columbia and ranked as one of the five most livable cities in the United States. Based on data from the National Science Foundation, MU ranks No. 2 among all institutions in the Association of American Universities in growth of federal research funding from 1995 to 2005. In fiscal year 2006, MU spent $215.2 million in research and development, royalties and patent applications have doubled in the past year, and a technology business incubator is currently being built. In the humanities, MU holds a large number of national awards and fellowships from public and private agencies. Visit the University of Missouri-Columbia's website at **www.missouri.edu**.

How to Apply: Nominations, applications, and inquiries will be treated in strict confidence. Please send all correspondence and applications to: **Dean Carolyn Herrington and Chair/Division Director Gerald Hazelbauer, co-chairs, Search Committee, Vice Chancellor for Research, c/o Office of the Provost, University of Missouri-Columbia, 114A Jesse Hall, Columbia, MO 65211**. Electronic submission is encouraged and may be forwarded to: **researchvicechansearch@missouri.edu**.

Applicants please submit: a detailed curriculum vitae; addresses, email addresses, and telephone numbers for three references; and a two- to three-page personal statement of the applicant's research leadership philosophy. References will not be contacted until advanced stages of screening, and candidates will receive prior notification.

Formal review of applications and nominations will begin **February 4, 2008**, and the search will continue until the position is filled. Please contact the chairs of the Search Committee (via **Linda Cook** at **573/882-0159**; **cookl@missouri.edu**) with questions.

The University of Missouri System is an Equal Opportunity/ Affirmative Action institution and is nondiscriminatory relative to race, religion, color, national origin, sex, sexual orientation, age, disability or status as a Vietnam-era veteran. The University of Missouri is in compliance with Title VI of the Civil Rights Act of 1964, Title IX of the Education Amendment of 1972, Section 504 of the Rehabilitation Act of 1973, and the Americans with Disabilities Act of 1990.

ASSISTANT PROFESSOR, TENURE-TRACK
Geomicrobiology/Molecular Biogeochemistry - #07920

Located in Ithaca, N.Y., Cornell University is a bold, innovative, inclusive and dynamic teaching and research university where staff, faculty, and students alike are challenged to make an enduring contribution to the betterment of humanity.

The Department of Microbiology in the College of Agriculture and Life Sciences at Cornell University invites candidates with outstanding records of achievement to apply for this position, which is on an academic year basis. Development of a leading research program (60% effort) supported by external funding is expected. We are interested particularly in candidates conducting cross-disciplinary research that spans frontiers in both the biogeosciences and molecular microbiology. Research skills may include fundamentals in microbial physiology or molecular biology, biogeochemistry, metagenomics and/or nanoscience. The appointee will participate (40% effort) in both graduate- and undergraduate-level courses related to environmental biogeochemistry and microbiology. Cross-disciplinary and interdepartmental research and teaching will be encouraged. In addition to close associations with colleagues in the Microbiology Department **(see http://www.micro.cornell.edu/cals/micro/faculty/index.cfm)** and the broader graduate field of Microbiology, Cornell offers an innovative array of collaborative research opportunities - especially with scientists in biogeochemistry, ecology, evolutionary biology, and earth sciences. Established interdisciplinary Cornell programs include: the New Life Sciences Initiative, the Nanobiotechnology Center, the Cornell Center for Materials Research, and the Biogeochemistry and Biocomplexity Initiative.

Qualifications: Ph.D. in Microbiology, Geosciences, Microbial Ecology, or a closely related area. Postdoctoral experience is strongly preferred. Demonstrated research and teaching ability is essential. We are interested particularly in candidates conducting cross-disciplinary research that spans frontiers in both the biogeosciences and molecular microbiology. Research skills may include fundamentals in microbial physiology or molecular biology, biogeochemistry, metagenomics and/or nanoscience. A competitive salary and fringe benefits are offered, commensurate with background and experience.

Applications: Applicants should submit (i) a letter of application, (ii) a curriculum vitae, (iii) a statement of current and future research interests, (iv) a statement of teaching goals, and (v) names plus contact information for three referees willing to send letters upon request to:

Chair, Geomicrobiology Search Committee
Department of Microbiology, Wing Hall
Cornell University
Ithaca, NY 14853-8101

For electronic submissions, place "***Geomicrobiology Application***" in the subject heading and send via e-mail to **PLL2@cornell.edu**. Applications will be reviewed starting on February 1, 2008, and continue until a successful applicant is identified. The appointment should begin August 25, 2008, or as negotiated.

Cornell University
Cornell University is an Affirmative Action/ Equal Opportunity Employer and Educator.

http://chronicle.com/jobs/profiles/2377.htm

THE HONG KONG UNIVERSITY OF SCIENCE AND TECHNOLOGY
DEPARTMENT OF BIOLOGY
Faculty Positions

Applications are invited for tenure-track positions at the levels of Assistant or Associate Professor, specifically in the areas of molecular and cellular biology using well-defined plant or animal model systems. Applicants of other disciplines of biology will also be considered. HKUST is a publicly-funded research university with strong graduate programs. The Department of Biology is a dynamic department with well-equipped modern facilities and has active research programs in cell, molecular, developmental, cancer, plant, marine and environmental biology. Information about the Department can be obtained from http://www.ust.hk/~webbo/.

Applicants must have a PhD degree, postdoctoral experience and the ability to establish independent research programs. Teaching responsibilities include undergraduate and graduate courses. Starting salary will be commensurate with qualifications and experience. Initial appointment will normally be on a three-year contract. A gratuity will be payable upon successful completion of contract. Re-appointment will be subject to mutual agreement. Fringe benefits including medical/dental benefits, annual leave and housing will be provided where applicable.

Applications indicating areas applied for, together with a curriculum vitae, a short statement on research interests and the names and addresses of 3 referees should be sent to: **The Chair of Recruitment Committee, Department of Biology, The Hong Kong University of Science and Technology, Clear Water Bay, Hong Kong (E-mail: bovacant@ust.hk) before 29 February 2008.**

(Information provided by applicants will be used for recruitment and other employment-related purposes.)

Georgia Institute of Technology | EMORY UNIVERSITY SCHOOL OF MEDICINE

Georgia Tech and Emory
Joint Biomedical Engineering Department

The Wallace H. Coulter Department of Biomedical Engineering at Georgia Tech and Emory University, a joint department between Georgia Tech's College of Engineering and Emory University's School of Medicine, invites nominations and applications for tenure track faculty positions at all levels: assistant, associate and full professor. We seek innovative, collegial individuals to enhance and contribute to ongoing research initiatives in the following research focus areas: molecular/optical imaging, systems biology, bionanotechnology, and vaccine development with applications in cancer and infectious diseases. For information on our research areas please see Research Overviews on our website: **www.bme.gatech.edu**.

Candidates most hold a doctoral degree in biomedical engineering/ science or a related discipline. Candidates should have the ability to develop a funded research program and to participate in teaching and advising in our undergraduate and graduate programs. Candidates meeting these minimum requirements are encouraged to submit a: (1) letter of application, (2) curriculum vitae, (3) statement of research interests and their relationship to the aforementioned thrusts, (4) statement of teaching interests and their relationship to the Coulter Department's educational programs and (5) three letters of reference to the department chair via the BME online application system.

To apply visit: **http://www.bme.gatech.edu/welcome/jobs.shtml**.

Application deadline: March 1, 2008

Applications from women and underrepresented minorities are encouraged. Georgia Tech is an Affirmative Action/Equal Employment Opportunity Employer.